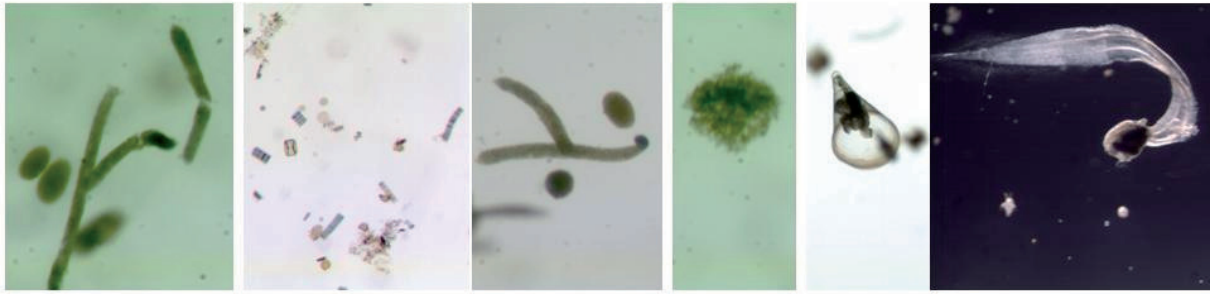


Flux and modification of sinking particles: Three field studies in the Southern Ocean



Dissertation

zur Erlangung des akademischen Grades eines Doktors in den
Naturwissenschaften
– Dr. rer. nat. –

vorgelegt von:

Friederike Ebersbach
Möckernstraße 47
28201 Bremen

Bremen, 1. November 2010



Die vorliegende Arbeit wurde in der Zeit von Mai 2007 bis Oktober 2010 an der Universität Bremen durchgeführt. Die Untersuchungen fanden am Alfred-Wegener-Institut für Polar- und Meeresforschung in Bremerhaven (Deutschland) und am Antarctic Climate and Ecosystems Cooperative Research Centre in Hobart, Tasmanien (Australien) statt.

Gutachter:

1. Gutachter: Prof. Dr. Dieter Wolf-Gladrow
2. Gutachter: Prof. Dr. Ulrich Bathmann

weitere Prüfer:

Prof. Dr. Kai Bischof
Dr. Eva-Maria Nöthig

weitere Mitglieder des Prüfungsausschusses:

Isabelle Schulz
Sina Wolzenburg

Tag des Promotionskolloquiums: **13. Dezember 2010**

Danksagung

Diese Arbeit hätte ohne die Hilfe vieler verschiedener Leute nicht entstehen können und allen, die mich darin unterstützt haben, gilt mein Dank.

Besonders bedanken möchte ich mich bei meinen beiden Gutachtern, Dieter Wolf-Gladrow und Uli Bathmann, für die Zeit und die fachliche Unterstützung, die sie meiner Doktorarbeit gewährt haben. Ergiebige Diskussion über forschungsspezifische Fragestellungen, wie auch lange Gespräche nicht-wissenschaftlicher Natur trugen erheblich zum Erfolg dieser Arbeit bei. Ebenso danke ich den weiteren Mitgliedern des Prüfungsausschusses, dass sie sich Zeit für mich nehmen.

Ich danke Evi Nöthig, Uta Passow und Christina De La Rocha dafür, mich jeweils ein Stück des Weges zur Fertigstellung dieser Arbeit betreuend begleitet zu haben. Philipp Assmy hat mir ausführlich und geduldig auf viele Fragen geantwortet und das danke ich ihm sehr.

Der Arbeitsgruppe Biogeochemie des AWI danke ich für die gute Arbeitsatmosphäre, wozu die nette Bürogemeinschaft mit Scarlett ihren Teil beitrug. Die Unterstützung in Laborfragen durch die Technischen Assistentinnen war hervorragend und ich bedanke mich bei den geduligen Helferinnen. Außerdem sind die vielen Diskussionen mit Doktoranden und Diplomanden zu erwähnen, die so manch beflügelnde Idee hervorbrachte.

Ich möchte Victor Smetacek und dem gesamten LOHAFEX-Team für dieses spannende Projekt danken, sowie der Crew von Polarstern für eine außergewöhnliche und unvergessliche Fahrt.

Ganz besonders möchte ich mich bei Tom Trull bedanken, der im Jahre 2005 während meines einjährigen Aufenthaltes in seiner Arbeitsgruppe ‚CO₂ group‘ am ACE CRC in Hobart, Tasmanien, mein Interesse für die genaue Untersuchung von absinkendem partikulären Material im Ozean überhaupt erst geweckt hat. Ihm verdanke ich nicht nur, dass mich dieser Forschungsschwerpunkt in den Bann geschlagen hat, sondern auch viel Wissen auf diesem Gebiet, vor allem bei der praktischen Anwendung an Bord. Die andauernde Kooperation im Laufe meiner Doktorarbeit sowie die erneute mehrmonatige Aufnahme in seiner Arbeitsgruppe in Hobart, haben meine Arbeit enorm bereichert.

Viele weitere Menschen standen mir in der Zeit meiner Arbeit hilfreich zur Seite, all Jene einzeln zu nennen, würde diesen Rahmen sprengen. Daher danke ich stellvertretend denen, die in der Endphase (meist spontan) ein Ohr für das eine oder andere Anliegen von mir hatten, Daniela, Andi und Stefan.

Desweiteren danke ich der Graduiertenschule GLOMAR der Universität Bremen für die großzügige Förderung durch ein Stipendium, ohne die ich diese Doktorarbeit nicht hätte durchführen können, und für die tatkräftige Unterstützung bei jeglichen die Arbeit betreffenden Angelegenheiten. Das Netzwerk, das durch den guten Zusammenhalt innerhalb der GLOMAR-Doktoranden bestand, konnte mich das eine ums andere Mal stärken.

Was wäre die Arbeit ohne Freunde? Ich bin sehr froh, durch meine Arbeit gute und enge Freundschaften geknüpft haben zu dürfen, die über diese Zeit hinaus bestehen sollen. Auch den Freundeskreisen danke ich, die außerhalb der Arbeit bereits bestanden oder neu hinzugekommen sind, und die Zeit nach wie vor überdauern.

Der Sport als bester Ausgleich zur Denkarbeit hat mich über so manche anstrengende Phase hinweggerettet, ob laufen, schwimmen, klettern oder reiten. Hiermit danke ich ganz

speziell meinen Kletterfreunden und -freundinnen, die so ziemlich jede meiner Stimmungen mitgemacht haben und mich in den allermeisten Fällen aufmuntern konnten.

Sehr am Herzen liegt es mir, mich bei meiner Familie zu bedanken. Sie hat mir immer den Rücken freigehalten und war für mich da, wenn ich sie brauchte. Meinem Bruder danke ich, meiner Schwester danke ich dafür, dass sie genau so ist, wie sie ist, und meinen Eltern danke ich besonders für ihr Vertrauen.

Zuletzt möchte ich Stefan danken – ohne ihn wäre ich nicht die, die ich bin.

Table of contents

I. Summary	1
I.1 Zusammenfassung	3
I.2 Summary	7
II. General Introduction	9
II.1 The role of carbon in the ocean.....	11
II.2 The role of iron in the ocean	17
II.3 Export of organic matter to depth	20
II.4 Techniques to study vertical flux.....	25
II.5 Aims of the thesis.....	30
III. Manuscripts	33
III.1 List of Manuscripts and declaration of own contribution	35
III.2 Manuscript 1	37
III.3 Manuscript 2	63
III.4 Manuscript 3	113
III.5 Manuscript 4	145
IV. Synthesis and future perspectives	189
IV.1 Synthesis.....	191
IV.2 Conclusions	201
IV.3 Future perspectives.....	204
References.....	207
Eidesstattliche Erklärung.....	217
Appendix 1	219

I. Summary

I.1 Zusammenfassung

Die Ozeanoberfläche ist mit dem tiefen Ozean durch absinkende Partikel verbunden, die Kohlenstoff in die Tiefe transportieren. Der abwärts gerichtete Export biogener Partikel verteilt Kohlenstoff und Nährstoffe im Ozean und spielt eine wichtige Rolle bei der Kontrolle des atmosphärischen CO₂-Gehalts (Volk und Hoffert 1985). Dieser Transportmechanismus ist als Biologische Pumpe bekannt (Volk und Hoffert 1985; De La Rocha 2007). Ihre Stärke hängt unter anderem von der Primärproduktion (PP) und dem Exportfluss im oberen Ozean ab (De La Rocha 2007). Nur ein kleiner Anteil (0.1-8.8%) des durch Photosynthese in der Euphotischen Zone (der sonnendurchschienenen Schicht) geformten organischen Materials erreicht den Meeresboden (Lutz et al. 2002). Die große Mehrheit der absinkenden Partikel wird recycelt, z.B. veratmet, zersetzt oder gefressen – und die Effektivität der Biologischen Pumpe bestimmt den Anteil des primär produzierten Materials, der in die Tiefe abgelagert wird (De La Rocha 2007). Die Modifikation des partikulären Materials passiert größtenteils in der Mesopelagischen Zone, die direkt unterhalb der Euphotischen Zone anschließt und bis in 1000 m Tiefe reicht (Boyd and Trull 2007). Die Mechanismen, die die Veränderung der absinkenden Partikel beeinflussen, sind kaum im Detail bekannt, aber sie sind essentiell, um Exportflussprozesse und die Sequenzierung von Kohlenstoff in der Tiefe zu verstehen.

Diese Dissertation führt weitere Entwicklungen einer neuen Technik zur Untersuchung intakter absinkender Partikel ein, um Rückschlüsse auf den Exportfluss (basierend auf einzelnen Partikeln) ziehen zu können. In drei Feldstudien werden diese Daten mit Exportflussdaten verglichen, die mit anderen Methoden erzielt wurden. Die Feldstudien fanden in verschiedenen Regionen des Südlichen Ozeans statt. Im Fokus jeder Studie standen die Untersuchung der absinkenden Partikel und die Identifikation der den Exportfluss bestimmenden Prozesse.

Obwohl Bulksedimentfallen üblicherweise benutzt werden, um die biogeochemische Flusszusammensetzung zu untersuchen, sind sie nur begrenzt geeignet, die ursprüngliche Form des partikulären Materials zu erhalten (z.B. Asper 1987; Gardner 2000). Daher bieten frei treibende Sedimentfallen, die mit Polyacrylamid-Gel (PA-Gel) bestückt sind, großes Potential, die Flussstruktur zu untersuchen (**Manuskript 1**). Erfolgreiche Beispiele des Gebrauchs dieser Gel-Fallen werden in **Appendix 1, Manuskript 1, 2 und 3** vorgestellt, und die durch unpassendes Fallendesign entstehenden Probleme werden in **Manuskript 1 und 4** demonstriert.

I. Zusammenfassung

Das SAZ-Sense Projekt fand im Südlichen Ozean südlich von Australien statt und erforschte zwei Stationen in der Subantarktischen Zone (SAZ) und eine Station in der Polarfrontzone (PFZ) (Griffiths et al. in prep.). Innerhalb der SAZ wurden zwei gegensätzliche Stationen untersucht: Die Station mit der höheren PP zeigt niedrigere Exportflüsse (von Fäzies dominiert), und die Station mit der geringeren PP verzeichnete hohe Exportflüsse (vorrangig Fäzies und zu einem kleineren Anteil auch Phyto-Detritus-Aggregate; **Manuskript 2**). Die PFZ-Station war durch die geringste Oberflächen-PP innerhalb von SAZ-Sense und mittlere Exportflüsse (kleine Kotballen und Ketten stark verkieselter Diatomeen) charakterisiert (**Manuskript 2**). Die absinkenden Partikel wurden aufgrund der guten Erhaltung in PA-Gelen unterschieden, die es ermöglicht, einzelne unversehrte Partikel zu identifizieren. Die Größenordnung des auf den PA-Gelen basierenden Kohlenstoffflusses stimmte mit biogeochemischen Daten überein, die von Bulkproben zweier anderer frei treibender Sedimentfallen bestimmt wurden. Die insgesamt auftretende Dominanz von Fäzies war mit den hohen Fraßraten während SAZ-Sense konsistent (**Manuskript 2**).

KEOPS (KErguelen Ocean and Plateau compared Study) wurde im Indischen Sektor des Südlichen Ozeans durchgeführt und erforschte den Ursprung erhöhter Phytoplanktonbiomasse in natürlich eisengedüngten Wassern über dem Kerguelenplateau im Vergleich mit umgebendem HNLC-Wasser (Blain et al. 2007). Beruhend auf in Gel-Fallen gesammelten absinkenden Partikeln, wurden die Merkmale des partikularen Flusses einer Station mit hoher Biomasse über dem zentralen Plateau und einer Station mit moderater Biomasse an dessen Peripherie erkundet (**Appendix 1**). Aggregate aus Fäzies waren an beiden Stationen am häufigsten. Daten des Unterwasser-Video-,Profilers‘ (UVP) lassen erkennen, dass der Anteil großer Partikel mit der Tiefe zunimmt, was die Relevanz von Fraßaktivität und der daraus folgenden Neuzusammensetzung des absinkenden Materials bestärkt. Außerdem wurde klar, dass die Größenordnung des Exportflusses über dem Plateau entschieden höher war als außerhalb des Plateaus, obwohl die Effektivität des Kohlenstoffexports außerhalb des Plateaus größer war.

Das Eisendüngungsexperiment LOHAFEX fand im Atlantischen Sektor des Südlichen Ozeans statt und untersuchte eine Phytoplanktonblüte, die durch Eisenzugabe hervorgerufen wurde (Smetacek und Naqvi 2010). Das einzellige Plankton, das mit dichte-neutralen PELAGRA-Fallen gesammelt wurde, zeigte einen geringen Diatomeenfluss (**Manuskript 4**). Stattdessen bestand der Fluss von unizellularem Planktonkohlenstoff (UCP) aus Dinoflagellaten, Flagellaten, kokkenähnlichen Zellen (2 μm groß) und zu einem geringen Anteil auch aus Diatomeen; der Gesamtkohlenstofffluss war gering (**Manuskript 4**). Der

I. Zusammenfassung

relativ kleine Anteil von UCP bei gleichzeitig großer Bedeutung von Fäzies in Bezug auf den POC-Fluss deutet darauf hin, dass die Struktur der Gemeinschaft innerhalb der LOHAFEX-Blüte als ein Recyclingsystem beschrieben werden kann (**Manuskript 4**).

Zusammenfassend wird deutlich, dass sich die hier präsentierte neue Methode der Gel-Fallen (**Manuskript 1**) als ein angemessener, nutzbringender Ansatz bewiesen hat, absinkende Partikel zu sammeln und zu untersuchen (**Manuskript 2, 3, 4 Appendix 1**). Außerdem habe ich gezeigt, dass die Identifizierung des partikulären Flusses wertvolle Details über die Zusammensetzung des Flusses und die Prozesse liefert, die den Exportfluss in drei verschiedenen Regionen des Südlichen Ozeans bestimmen.

I.2 Summary

The surface ocean is coupled with the deep ocean via sinking particles that transport carbon to depth. The downward export of biogenic particles redistributes carbon and nutrients in the ocean and plays a significant role in controlling atmospheric CO₂ levels (Volk and Hoffert 1985). This transport mechanism is known as the biological pump (Volk and Hoffert 1985; De La Rocha 2007). The strength of the biological pump depends on factors such as surface primary production (PP) and export flux in the upper ocean (De La Rocha 2007). Only a small amount (0.1-8.8%) of the organic material being formed in the euphotic zone (the sunlit surface layer) through photosynthesis reaches the seafloor (Lutz et al. 2002). The vast majority of the sinking particles is recycled, e.g. respired, degraded or grazed upon – and the efficiency of the biological pump determines the fraction of primarily produced material settling to depth (De La Rocha 2007). Most of the modification of the particulate matter occurs in the mesopelagic zone, which adjoins beneath the euphotic layer and reaches down to 1000 m (Boyd and Trull 2007). However, the mechanisms influencing alteration of sinking particles are not known in detail, but they are essential to understand export flux processes and the sequestration of carbon at depth.

This thesis introduces further developments of a novel technique to examine intact sinking particles making it possible to draw conclusions on export fluxes on the base of individual particles. In three field studies, these data were compared to export flux data received with other sampling technologies. The field studies took place in different regions of the Southern Ocean. The focus of all studies was to investigate sinking particles and identify export driving processes.

Although bulk sediment samples are commonly used for studying the biogeochemical flux composition, they are limited in terms of preserving the original forms of particulate matter (e.g. Asper 1987; Gardner 2000). Hence, free-floating sediment traps equipped with polyacrylamide gels (PA gels) provide great potential to examine flux structure (**Manuscript 1**). Successful examples of using these gels trap are given in **Appendix 1**, **Manuscript 1**, **2** and **3**, and the problems that might arise due to unsuitable trap design are demonstrated in **Manuscript 1** and **4**.

The SAZ-Sense project was situated in the Southern Ocean south of Australia and studied two sites in the Subantarctic Zone (SAZ) and one site in the Polar Frontal Zone (PFZ) (Griffiths et al. in prep.). Within the SAZ, two contrasting sites in terms of surface biomass accumulation and export fluxes were investigated: The site with higher PP showed lower

I. Summary

export fluxes (dominated by faecal material), and the site with lower PP had high export fluxes (mainly faecal material and to a small extent also of phyto-detritus aggregates; **Manuscript 2**). The PFZ site was characterised by the lowest surface PP within SAZ-Sense and intermediate export flux (small faecal pellets and chains of heavily silicified diatoms; **Manuscript 2**). The sinking particles were distinguished because of their good preservation in PA gels, which allows identifying intact individual particles. The magnitude of the PA gel based carbon flux agreed with biogeochemical data obtained from bulk samples of two other free-floating sediment traps (**Manuscript 2**). The overall dominance of faecal material was consistent with the high grazing rates detected during the SAZ-Sense study (**Manuscript 2**).

KEOPS (Kerguelen Ocean and Plateau compared Study) was carried out in the Indian Sector of the Southern Ocean and examined the origin of elevated phytoplankton biomass in naturally iron-fertilised waters over the Kerguelen Plateau in comparison to surrounding HNLC-waters (Blain et al. 2007). Based on sinking particles collected with gel traps the characteristics of the particulate flux of a high biomass site over the central plateau and a moderate biomass site at its periphery were ascertained (**Appendix 1**). Aggregates of faecal material were most abundant at both sites. Data from the underwater video profiler (UVP) revealed that the fraction of large particles increased with depth, supporting the relevance of grazing and subsequent repackaging of the sinking material (**Manuscript 3**). Furthermore, it became evident that the magnitude of export flux over the plateau is much higher than off the plateau despite the fact that the efficiency of carbon export is higher off the plateau (**Manuscript 3**).

The iron fertilisation experiment LOHAFEX was carried out in the Atlantic Section of the Southern Ocean and investigated a phytoplankton bloom that was induced by iron addition (Smetacek and Naqvi 2010). The unicellular plankton collected with neutrally buoyant PELAGRA traps displayed low diatom flux (**Manuscript 4**). Instead, unicellular plankton carbon (UCP) flux was provided by dinoflagellates, flagellates, coccoid cells (2 μm in size) and to a small extent diatoms; overall C flux was low (**Manuscript 4**). Whereas the fraction of UCP was relatively small, faecal material was highly important with regard to POC flux. This indicates that community structure within the LOHAFEX bloom can be described as a recycling system.

In conclusion, the presented novel technique of using gel traps has proved to be a valuable, good approach to collect and investigate sinking particles. Moreover, I showed that the identification of the particulate flux provides valuable details on flux composition and export flux determining processes in three different regions of the Southern Ocean.

II. General Introduction

II. General Introduction

II.1 The role of carbon in the oceans

In the oceans, carbon is essential for life of any form. It enters the ocean as CO_2 at the surface, where equilibrium between atmospheric (gaseous) CO_2 and aqueous (dissolved) CO_2 is established through a steady exchange. In the oceans, CO_2 exists as free CO_2 , as bicarbonate (HCO_3^-) and as carbonate ion (CO_3^{2-}). Different phytoplankton species use different CO_2 sources for primary production (PP), but they all need sunlight as energy source. Thus, in the euphotic zone (the sunlit layer of the ocean) biomass is formed by primary producers and the dissolved inorganic carbon (DIC) is converted into organic carbon.

This organic material is now part of the production and recycling system of carbon in the water column where it is passed on into the food web. Only a small fraction of the carbon that entered the ocean at its surface settles down to the seafloor as particulate matter. During this transit through the water column particles undergo changes in form and composition. However, little is known about modification processes of sinking particles.

The amount of particulate organic carbon (POC) that reaches the deep ocean varies between 0.1 and 8.8% of PP (Lutz et al. 2002). The surface ocean, where CO_2 is taken up by phytoplankton, is coupled with the deep ocean (>1000 m), where some of this carbon is sequestered through the ‘biological pump’. This pump is essential to flux dynamics in the mesopelagic zone (100-1000 m), which is also called the ‘twilight zone’ as it is located directly underneath the euphotic zone. In order to better understand the mechanisms determining the ocean’s uptake of CO_2 and the subsequent burial of carbon in the deep sea this study will focus on export processes with a special emphasis on particulate fluxes in the mesopelagic zone (e.g. Boyd and Trull 2007).

II. General Introduction

Table 1. Nomenclature of abbreviations used in this thesis.

CO ₂	carbon dioxide
HCO ₃ ⁻	bicarbonate
CO ₃ ²⁻	carbonate ion
DIC	dissolved inorganic carbon
DOC	dissolved organic carbon
POC	particulate organic carbon
BSi	biogenic silica
UPC	unicellular plankton carbon
OM	organic matter
TEP	transparent exopolymer particle
PP	primary production
NP	new production
RP	regenerated production
NCP	net community production
HNLC	High-Nitrate-Low-Chlorophyll
Fe	iron
<i>D</i>	organic matter decomposition rate (d ⁻¹)
<i>W</i>	particle sinking rate (m d ⁻¹)
<i>r</i>	radius (m)
<i>g</i>	acceleration due to gravity (m s ⁻²)
$\Delta\rho$	density difference (g m ⁻³)
μ	dynamic viscosity of seawater (Pa s)
<i>z</i>	depth (m or km)
<i>z</i> ₀	depth of the euphotic zone (km)
<i>C</i> _{flux}	sinking flux of POC (mmol C m ⁻² d ⁻¹ or mg C m ⁻² d ⁻¹)
<i>C</i> _{prod}	primary production (mmol C m ⁻² d ⁻¹ or mg C m ⁻² d ⁻¹)
<i>C</i> _{export}	export production (mmol C m ⁻² d ⁻¹ or mg C m ⁻² d ⁻¹)
<i>p</i>	partition coefficient
<i>b</i> ₁ and <i>b</i> ₂	<i>D</i> / <i>W</i> (m ⁻¹)
UVP	underwater video profiler
NBST	neutrally buoyant sediment trap
SAZ	Subantarctic Zone
PFZ	Polar Frontal Zone
SEM	scanning electron microscopy
AUV	autonomous underwater vehicle
SANT	Subantarctic Water Ring Province

II. General Introduction

The biological pump—At the ocean's surface organic matter (OM) is formed through photosynthesis by taking up CO_2 from the atmosphere (**Fig. 1**), leading to the utilisation of nutrients and solar energy by primary producers. The availability of macro nutrients (nitrate, phosphate and silicic acid) and micro nutrients (such as iron and zinc) therefore has to be adequate for build-up of biomass. With respect to nutrient supply, new production (NP) is distinguished from regenerated production (RP). NP is defined as phytoplankton production, derived from nutrients having their origin outside the euphotic zone (supplied by upwelling, atmospheric deposition or nitrogen fixation), while regenerated production is based on nutrients recycled within the euphotic zone (Dugdale and Goering 1967). Net PP (NPP) is the sum of new and regenerated PP minus the energy that is used for respiration.

The build-up of OM is therefore indirectly responsible for a drawdown of atmospheric CO_2 by the ocean (Volk and Hoffert 1985). This carbon then reaches the ocean's interior imbedded in marine particles which consist of POC and biominerals (**Fig. 1**). Part of this OM is further transported to depths by different mechanisms, such as the solubility pump, the soft-tissue pump and the carbonate pump (Volk and Hoffert 1985). The solubility pump is driven by the differences of CO_2 solubility in warm and cold water, such as surface water and deep-water. This pump is only active in Polar Regions, where it is fuelled by the increased CO_2 solubility of downwelling cold water. It is called the physical pump, which differentiates it from the soft-tissue and carbonate pump (Volk and Hoffert 1985). These two pumps arise

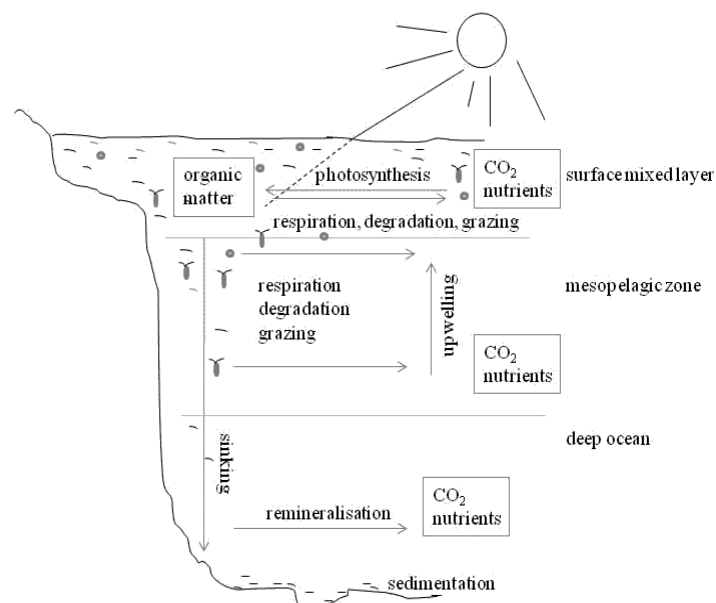


Fig. 1. A simplified view of the biological pump: Surface mixed layer, mesopelagic zone and deep ocean are connected through several cycles. The major direction of transport is from the surface into the deep, although recycling occurs at any depth, and only a small amount of primarily produced matter is deposited at the sea floor.

II. General Introduction

from biological fluxes of organic material and calcium carbonate (CaCO_3) and are referred to as biological pump (Volk and Hoffert 1985; Ducklow et al. 2001; De La Rocha 2007). These transport mechanisms apply for both pools, for particulate organic material (POM) as well as for dissolved organic material (DOM).

The strength and efficiency of the biological pump is determined by several factors, such as production of OM and biominerals at the surface, settling of particulate material into the deep and remineralisation of these particles (De La Rocha 2007). The appearance of particles formed at the surface is influenced predominantly by the plankton community in the upper layer. On the one hand, phytoplankton composition regulates the original material, which can vary from small picoplankton to large diatom cells, whereas, on the other hand, OM provided by primary producers can be mediated by zooplankton. The particles supplying the pool of potentially exported material can therefore either be amorphous and fluffy (e.g. phyto-detritus) or compact and dense (e.g. faecal pellets) or anything in between (e.g. coagulation of faecal matter and/or aggregates of phytoplankton material) (compare also II.3.). If they survive bacterial degradation or zooplankton and chemical dissolution on their way to depth, the sinking particles might reach the bottom of the ocean and be buried or consumed by organisms living at the seafloor. This certainly depends on their sinking velocity (w), which according to Stokes law (equation (1)) depends on particle size (of the radius r) and density ($\Delta\rho$ as density difference between particle and seawater):

$$W = \frac{2gr^2(\Delta\rho)}{9\mu} \quad (1)$$

with g being the acceleration due to gravity and μ the dynamic viscosity of seawater. Large particles may sink at faster rates than smaller ones. However, this can be reversed by taking into account their morphology because large particles might be very fluffy and less dense, while small particles may be more compact and denser. Beside particle creation due to plankton interactions, mineral availability also affects particle characteristics as they might increase particle density (compare also II.3.).

The strength and efficiency of the biological pump depends on many more factors, such as the level of photosynthetic production and nutrient limitation, the amount of zooplankton grazing and the degree of oxidative mineralisation at different depths in the water column, followed by aggregation and settling. Thus, it is indispensable to examine the complex system of biogeochemical cycles in the ocean including its interactions in order to receive a better picture of processes such as the biological pump. This was one of the major reasons for creating JGOFS, the Joint Global Ocean Flux Studies (see below).

II. General Introduction

Carbon cycle in the ocean—It was only in the 1980s when the term ‘biogeochemical cycles’ became familiar among scientists as they tried to describe the complex set of coupled processes involved in global change to policy makers. In 1987, JGOFS was approved as a Large Scale Ocean Project by the Scientific Committee on Oceanic Research (SCOR). The JGOFS program was developed creating a long term study that encompasses the world’s oceans with international participation. The goals of JGOFS included the need ‘To determine on a global scale the processes controlling the time varying fluxes of carbon and associated biogenic elements in the ocean...’, and ‘To develop the capability to predict on a global scale the response of oceanic biogeochemical processes to anthropogenic perturbations, in particular those related to climate change’ (SCOR 1990).

One of the initiatives of JGOFS was AESOPS (Antarctic Environment and Southern Ocean Study), which focussed on two distinct regions: the Ross-Sea continental shelf and the southwest Pacific Sector of the Southern Ocean (Smith et al. 2000). Some of the AESOPS results will be discussed in more detail in II.3. In the Atlantic Sector of the Southern Ocean, JGOFS projects were conducted by POLARSTERN (e.g. Dubischar and Bathmann 2002; Rutgers van der Loeff et al. 1997; 2002). For a review of Southern Ocean JGOFS see Bathmann et al. (2000).

Knowledge on biogeochemical cycles and interaction between particular processes has increased enormously in the last 30 years. But some uncertainty, for instance on feedback mechanisms between rising CO₂-levels in the atmosphere and ocean uptake of CO₂, is left and the debate about global change is ongoing. The beginning of interactions between science and policy in the 1980s was followed by numerous meetings, workshops and conferences. The International Panel for Climate Change (IPCC) was established in 1988. The 4th and most recent IPCC Assessment report, which is a result of a joined work program by the international science community, was published in 2007 and has been widely discussed. Minor differences of opinions and some uncertainties notwithstanding the overall picture of the global carbon cycle is becoming clearer (**Fig. 2**). However, the role of anthropogenic input and its relevance for global change is much less apparent and still heavily under debate.

II. General Introduction

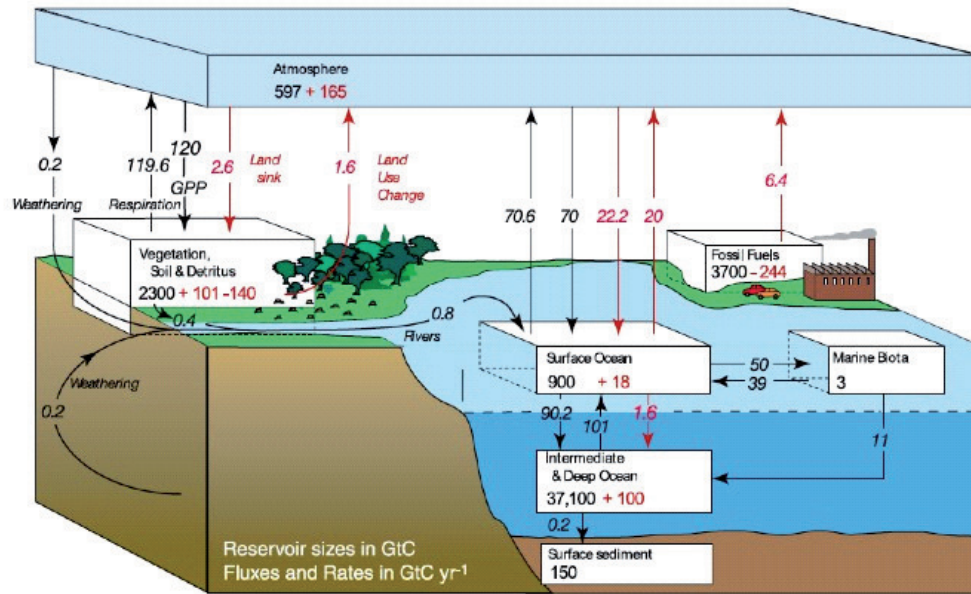


Fig. 2. The global carbon cycle for the 1990s (IPCC report, 2007). Numbers in black show reservoirs and fluxes prior to the industrial revolution and red numbers indicate anthropogenic input (data from Sabine et al. 2004; Sarmiento and Gruber 2006). GPP is annual gross (terrestrial) primary production.

Beside the land biosphere, the oceans make up for the largest carbon reservoir: they have taken up more than 100 Gt C since the industrial revolution as a result of the unbalanced CO₂ fluxes between ocean and atmosphere (Fig. 2). Had the ocean not acted as a carbon sink, CO₂ level increase in the atmosphere from pre-industrial times (value of 180 ppm) until today would have been about three times higher (Sabine et al. 2004).

Marine productivity accounts for roughly half the global PP with the other half being provided by the terrestrial biosphere (Fig. 2). However, within different marine ecosystems and throughout different ocean basins, neither the PP nor the efficiency of the biological pump and the subsequent export fluxes are in the same range.

One third of the global oceans are characterised as so called High-Nitrate-Low-Chlorophyll (HNLC) areas (i.e. areas with marginal productivity). Despite high nitrate levels, PP in HNLC-waters is comparably low. Large areas of the Southern Ocean, the equatorial Pacific and the northern North Pacific Ocean are affected by this phenomenon. It became obvious that in these regions the biological pump is not operating at its full capacity. Another factor limiting build-up of biomass (i.e. being essential to PP) besides macro nutrients are micro nutrients (compare II.1). It was therefore suggested that micro nutrients, in particular iron, might be limiting for phytoplankton growth rates in HNLC-areas (Martin et al. 1991).

II. General Introduction

II.2 The role of iron in the oceans

In the late 1980s the trace metal iron (Fe) came into focus as the limiting factor for PP in HNLC areas (Martin and Gordon 1988; Martin et al. 1989). As postulated by Martin (1990) atmospheric Fe input via dust was much higher during the last glacial maximum, coinciding with increased PP in vast regions of the ocean, more efficient CO₂ uptake by phytoplankton and consequently lower CO₂ levels in the atmosphere. The so-called ‘iron hypothesis’ has since been investigated in HNLC-waters, with bottle experiments as well as iron-fertilisation experiments (for areas up to 300 km²) and modelling studies (see Boyd et al. (2007) for a recent review).

Since the beginning of the 1990s several mesoscale iron addition experiments were performed in waters from Equatorial to Polar Regions (**Table 2**), and have verified that iron enrichment enhances PP (de Baar et al. 2005; Boyd et al. 2007). In spite of biomass accumulation at the surface and CO₂ uptake of the growing phytoplankton community, the response of export fluxes is less clear (Boyd et al. 2007). Thus, it is not proved that iron induced blooms transport CO₂ to depth when these blooms decline. This topic is still heavily under debate (Buesseler et al. 2008). Iron fertilisation has been proposed as one way to sequester carbon and thus counteract the rising atmospheric CO₂ levels due to human impact (Smetacek and Naqvi 2008), but has also been strongly disapproved (Chisholm et al. 2001). However, the scientific as well as political interest has attributed a lot of effort to studying iron limitation in-situ in the last 20 years by conducting multiple iron enrichment experiments in different parts of the Ocean (**Table 2**).

Table 2. List of conducted iron fertilisation experiments performed in different ocean basins (see Footnotes for explanations of abbreviations); modified after Boyd et al. (2007).

Year	Study	Region
1993	IronEX I	open equatorial Pacific Ocean, south of Galapagos Islands
1995	IronEX II	open equatorial Pacific Ocean (multiple iron addition)
1999	SOIREE	Pacific sector of the Southern Ocean
2000	EisenEx	Atlantic sector of the Southern Ocean
2001	SEEDS I	Northwest Pacific
2002	SOFEX-S, SOFEX-N	Southern Ocean southeast of New Zealand, South and North
2002	SERIES	Northeast Pacific (Subarctic)
2004	EIFEX	Atlantic sector of the Southern Ocean
2004	SEEDS II	Northwest Pacific
2008	LOHAFEX	Atlantic sector of the Southern Ocean

Explanation of abbreviations: IronEx (I andII): Iron Enrichment Experiment; SOIREE: Southern Ocean Iron Release Experiment; EisenEx: Iron Experiment; SEEDS (I and II): Subarctic Pacific Iron Experiment for Ecosystem Dynamics Study; SOFEX: Southern Ocean Iron Experiment; SERIES: Subarctic Ecosystem Response Iron Enrichment Study; EIFEX: European Iron Fertilisation Experiment, LOHAFEX: Iron (‘Loha’ is hindi for iron) Fertilisation Experiment

II. General Introduction

This study focuses mainly on the Southern Ocean and therefore only experiments that took place in this region (plus the two initial experiments that demonstrated feasibility) are discussed in more detail. The phenomenon of natural iron fertilisation will be considered as well – again concentrating on Southern Ocean sites.

Iron fertilisation experiments—In fall 1993, shortly after the ‘iron hypothesis’ was established (Martin 1990), the first iron fertilisation experiment IronEx I was conducted in HNLC-waters of the open equatorial Pacific Ocean near the Galapagos Islands (Martin et al. 1994, Coale et al. 1996a, 1998). The results demonstrated a direct and unequivocal biological response to added iron: PP and Chla increased, biomass levels in all classes counted were higher than in the non-fertilised surrounding waters and there was evidence for increased grazing (Martin et al. 1994). During IronEx II, where multiple iron addition was performed in waters somewhat west to the IronEx I side, massive blooms were produced and a large drawdown in atmospheric CO₂ and nutrients was detected (Coale et al. 1996a). Furthermore, the results indicated that iron enrichment favours diatoms – which are known to be the main driver of POC export to depth in vast areas of the ocean. Taking into consideration that most HNLC areas are situated in the Southern Ocean where diatoms also are a key species in regard to PP and export fluxes, similar experiments in these regions were a desideratum (Coale et al. 1996a).

In late austral summer 1999, the meso-scale Southern Ocean Iron RElease Experiment (SOIREE) took place in the Pacific sector of the Southern Ocean in a HNLC area and examined a diatom bloom responding to iron addition (Boyd et al. 2000). Despite increased growth rates and a shift towards larger cells IN-patch (with iron addition), no increasing export in comparison to OUT-patch stations (without iron addition) was observed with sediment traps deployed at 110 and 310 m, respectively (Boyd et al. 2000; Trull and Armand 2001; Trull et al. 2001; Waite and Nodder 2001). The positive response of the phytoplankton community to iron addition but the absence of enhanced export during this first iron enrichment experiment in the Southern Ocean was motivation to investigate other regions of the Southern Ocean. The goal of the Southern Ocean Iron Enrichment Experiment SOFeX, which was conducted south of New Zealand in austral summer 2002, was to compare two different regimes in regard to iron fertilisations: SOFeX-North was characterised by high nitrate and low silicic acid and SOFeX-South by high nitrate and high silicic acid (Coale et al. 2004; Buesseler et al. 2004). Although PP in the north was dominated by nonsilicious phytoplankton, export fluxes increased (in both patches, SOFeX-North and –South) after iron addition (Coale et al. 2004). This indicated that iron-limited carbon removal from these waters played a strong role (Coale et al. 2004).

II. General Introduction

Moreover, three iron enrichment experiments conducted by the Alfred Wegener Institute for Polar and Marine Research (AWI, Bremerhaven, Germany) with RV Polarstern were performed in the Atlantic Sector of the Southern Ocean: EisenEx in spring 2000 (Assmy et al. 2007), the European Iron Fertilisation Experiment (EIFeX) in summer 2004 (Bathmann 2005) and LOHAFEX in summer 2008 (see Manuscript 4 and Chapter III). During EisenEx a strong species-specific response of the iron induced diatom bloom was observed, but the fate of the EisenEx bloom is not known (Assmy et al. 2007). The EIFeX bloom showed a decline at the end (Hoffmann et al. 2006) which was followed by a sinking event that was detected in the water column as well as in the sediments (Peeken et al. 2006; Smetacek et al. in prep.). So far, this experiment was the only one to observe enhanced export fluxes to depths associated with iron addition. Due to ship time constraints it was only possible to partially investigate the fate of these two stimulated bloom before their final decline. That is why LOHAFEX, a third iron enrichment experiment, was designed to allow for a complete examination of the senescent bloom (<http://www.awi.de/en/home/lohafex/>).

Natural iron fertilisation—Beside atmospheric input in form of dust it has also been observed that surface water plumes off islands can be enriched in Fe (e.g. Martin et al. 1994) or that upwelling water can have an impact on Fe levels (e.g. Coale et al. 1996b). In the Southern Ocean, albeit being the largest HNLC area, several mechanisms such as upwelling of iron-rich deep water, lateral advection of Fe from the continental shelf or the release of dissolved Fe from ice melting can account for natural iron fertilisation (e.g. Karl et al. 1991; Ishii et al. 1998). For instance, it has been documented that phytoplankton blooms do occur in the vicinity of islands (Sullivan et al. 1993; Tyrell et al. 2005). Two studies on continuously occurring natural iron fertilisation were performed in the Indian Sector of the Southern Ocean: the CROZet natural iron bloom and EXport experiment (CROZEX) in austral spring to summer 2004/2005 (Pollard et al. 2007) and the Kerguelen Ocean and Plateau compared Study (KEOPS) in austral summer 2005 (Blain et al. 2007). The naturally occurring bloom off the Kerguelen Island was found to be contingent on persistent iron fertilisation but its duration was due to the concomitant supply of macronutrients from surrounding waters and from below (Blain et al. 2007). Within this bloom, a smaller increase in export flux than in PP was observed (Blain et al. 2007, Trull et al. 2001). This may partly reflect greater biomass accumulation over the plateau but also stronger recycling (Trull et al. 2001), which is consistent with the faecal material dominated particle flux (Appendix 1). During KEOPS, the surface phytoplankton community was dominated by diatoms (Armand et al. 2008), which stands in contrast to CROZEX, where silicic acid concentrations were limiting diatom growth

II. General Introduction

in some regions of the bloom (Poulton et al. 2007). Accordingly, phytoplankton community structure showed significant differences within the iron stimulated bloom during CROZEX and was dominated by *Phaeocystis antarctica* in regions of low silicic acid concentrations (Poulton et al. 2007). Carbon export deeper in the water column revealed association with biomass accumulation at the surface (Marsh et al. 2007) and Pollard et al. (2007) postulated that deep POC export was clearly linked to Fe-fertilised productivity at the surface.

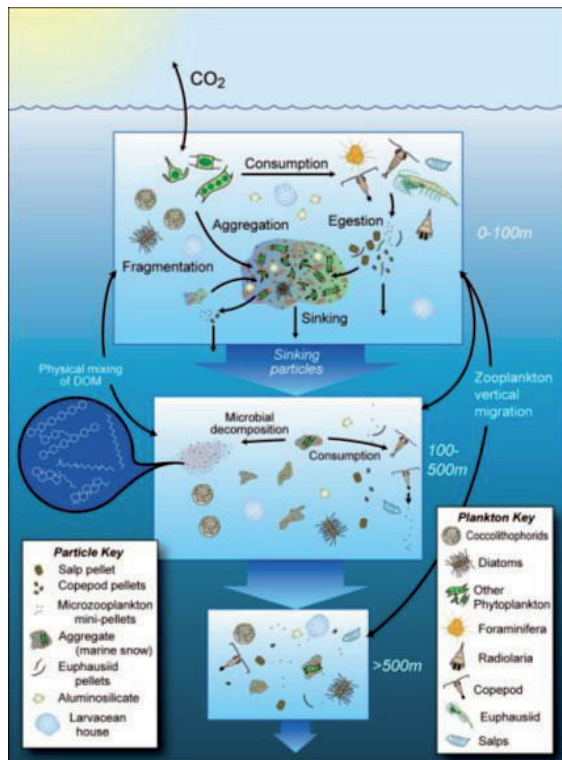


Fig. 3. Pathways of particle formation and processes that are important for particle transport to depth (http://cafethorium.whoi.edu/website/images/tzex_img1.jpg). In the upper layer, particles can form via aggregation and/or ingestion by zooplankton. These particles are then either transported downwards or degraded by bacteria and/or zooplankton or fragmented. The major mechanisms important for transport to depth are passive sinking, physical mixing of POM and POM and active transport by zooplankton vertical migration.

II.3 Export of organic matter to depth

In the ocean, particles such as phyto-detritus or faecal pellets can be formed in the entire water column: at the surface (mainly regulated through PP), in the mesopelagic and deep ocean as well as on the seafloor (Fig. 3). During their transit towards depth, particles are very likely altered and thus undergo changes in terms of size, shape and composition (e.g. Iversen et al. 2010). Particles leaving the sunlit surface layer can appear in various forms (Fig. 3). Therefore, they are variably prone to either sinking or being recycled and may change their forms during passage through the water column (e.g. Iversen and Ploug 2010; Iversen et al. 2010). Modification of the sinking particles at depth generally plays an important role as most of the flux attenuation occurs in the mesopelagic zone, but the processes being responsible for these dynamics are only poorly understood (Boyd and Trull 2007).

II. General Introduction

Character of the vertical flux of organic matter—Although the shapes of particulate matter vary enormously (Fig. 4), particles are commonly divided into fragile marine snow and more compact faecal pellets (compare review of Turner (2002)). Faecal pellets can originate from different zooplankton species and thus differ considerably in shape and size (Fig. 4). However, they have always been discerned from marine snow particles (Fig. 4), which are characterised as being larger than 0.5 mm and are very various in shape and appearance (Alldredge 1992). Recently it became evident that even much smaller particles are playing an important role for the vertical export (e.g. Guidi et al. 2008; Stemmann et al. 2008). Observations of in-situ images from particulate flux in the upper 200 m revealed that the particle assemblage is covering a size range from 3.5 to 2000 μm (Stemmann et al. 2008). This indicates that beside the relatively large marine snow particles and faecal pellets, small particles such as fractions of larger particles (for instance resulting from degradation processes) have to be taken into consideration to understand flux dynamics.

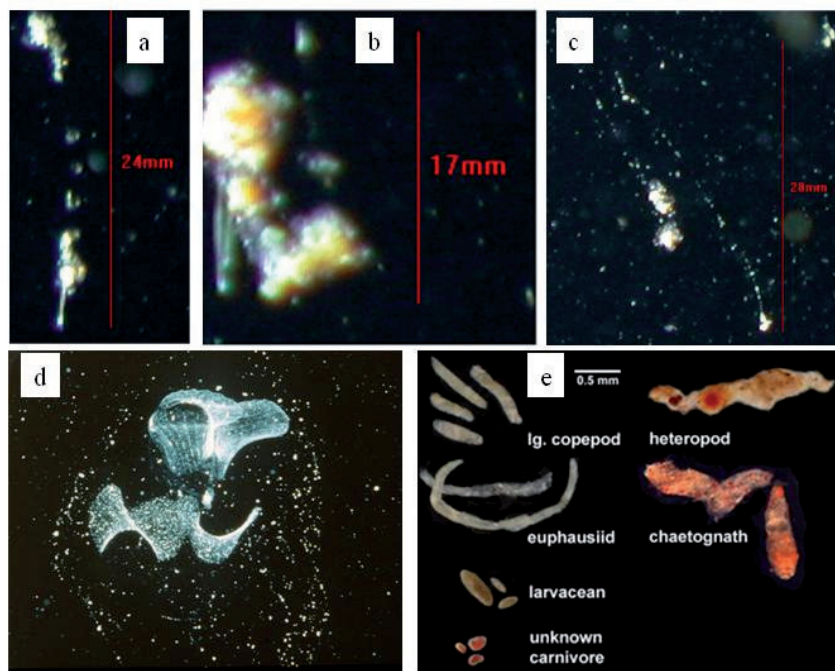


Fig. 4. Different forms of in-situ sinking particles: Marine snow in the in the water column off the coast of Mauritania at 54 m (a and b) and at 28 m depth (c) displaying the fragile structure of these particles (courtesy of N. Nowald), mucus feeding structure demonstrating the variable shape of marine snow (Robison et al. 2005), and different types of faecal pellets (courtesy of D. Steinberg).

Nonetheless, marine snow sized particles (>0.5 mm) are the key drivers for export flux in large areas of the ocean due to their high abundance and relatively high carbon content (e.g. Allredge and Silver 1988; Alldredge and Gotschalk 1989; Silver and Gowing 1991). During

II. General Introduction

the past few decades a whole range of terms was used to describe sinking particles being in general referred to as marine snow: ‘flocs’ (Pomeroy and Deibel 1980; Hill 1998), ‘flakes’ (Alldredge and Youngbluth 1985; Shanks and Trent 1980) or organic aggregates of faecal origin (Waite et al. 2005). Kiorboe (2001) proposed to distinguish between aggregates that were formed via physical coagulation or through zooplankton-mediated aggregation. In general, two pathways to create marine snow are postulated – they are either produced by zooplankton or by coagulation of smaller particles (Alldredge 1992). Examples for the second pathway are the rare events of mass sinking of phytoplankton blooms that might lead to a downward flux of coagulated phytoplankton cells (see review of Beaulieu (2002) and references therein). More recently Lam and Bishop (2007) suggested a separation into ‘more tightly packed faecal pellets’ and ‘looser and less dense aggregates of faecal matter and marine snow’. However, it makes sense to adhere to the concept of marine snow and faeces in general.

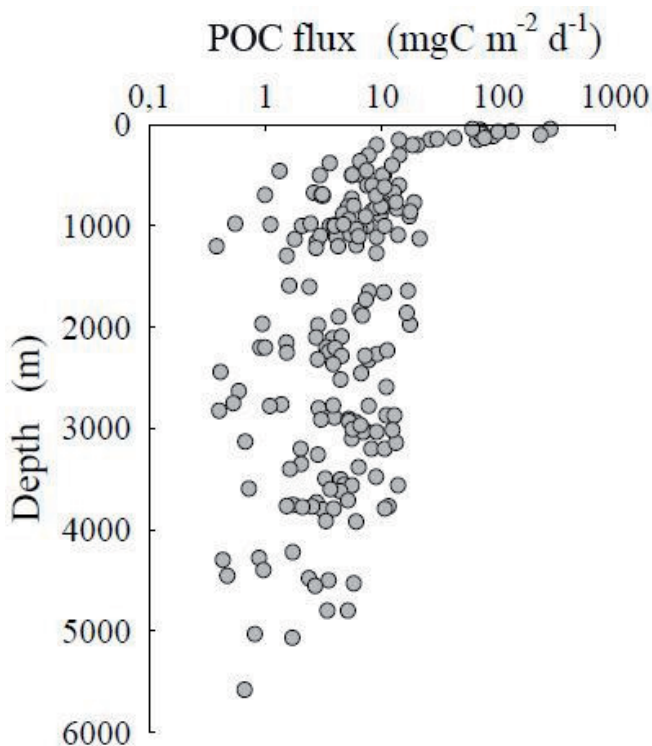


Fig. 5. POC flux attenuation with depth (adapted from De La Rocha 2007).

Attenuation with depth—Less than half the particulate matter produced in the surface layer survives transit through the mesopelagic zone and only a small amount reaches the deep ocean and sediments (Boyd and Trull (2007) and references therein), as shown in **Fig. 5**. A common approach of estimating POC flux at depth is using an empirical relationship between

II. General Introduction

surface POC and either surface PP (Suess 1980) or export flux (Martin et al. 1987), as depicted in equation (2) or (3), respectively:

$$C_{\text{flux}}(z) = \frac{C_{\text{prod}}}{(0.0238z+0.212)} \quad (2)$$

$$C_{\text{flux}}(z) = C_{\text{export}} \left(\frac{z}{z_0} \right)^{-0.858} \quad (3)$$

POC flux (C_{flux}) at depth z (in km) is defined as a function of PP of organic carbon in surface waters or POC export from the base of the euphotic zone (z_0 (in km)). In many areas, POC flux cannot solely be predicted based on PP values (e.g. Bishop 1989; Boyd and Newton 1995; Lampitt and Antia 1997), indicating that the magnitude of PP may not be the most important factor in determining flux to depths (Boyd and Newton 1999). Buesseler (1998) claimed that varying food web dynamics and species assemblages, rather than higher PP at the surface, may lead to an increasing flux to depth. Thus, surface PP and export from the euphotic zone are decoupled in most cases (Buesseler 1998; Boyd and Newton 1995, 1999). In conclusion, variations in POC flux into the deep ocean cannot be described by variability in PP or export from the surface layer alone (Lutz et al. 2002).

Lutz et al. (2002) also stated that constant power law relationships (such as equation (3)) generally overestimate deep water POC fluxes and hence underestimate particle retention in the water column. Instead, they recommend using a region-specific empirical flux algorithm (equation (4), modified after Andersson et al. (2004)), where POC flux (C_{flux}) at depth z (in m) is partitioned into a pool of fresh, labile POC degrading rapidly relative to its sinking rate ($(1-p)e^{-b_1z}$) and a pool of rapidly sinking or very refractory POC without significant decomposition during transit to depth (pe^{-b_2z}). The two relationships for D/W are b_1 and b_2 , where D is the organic matter decomposition rate (d^{-1}) and W the particle sinking rate ($m d^{-1}$).

$$C_{\text{flux}}(z) = C_{\text{flux}_0} [(1-p)e^{-b_1z} + pe^{-b_2z}] \quad (4)$$

Based on the comparison of PP and flux dynamics in the water column (from surface traps and moored sediment traps at depth), it became obvious that conditions and forcings that serve to create and attenuate variability in flux are concentrated within 1000 m below the euphotic zone (e.g. Honjo 1996; Buessler 1998; Lutz et al. 2002). A compilation of AESOPS surveys (see II.1) suggests that in the mesopelagic zone up to 90% of surface POC are remineralised in the Southern Ocean (Honjo et al. 2000), whereas below 1000 m changes in POC fluxes are not significant (Nelson et al. 2002).

II. General Introduction

Regional variability on the Example of the Southern Ocean—In the global ocean, the fraction of NPP that is sinking out of the surface ocean (POC surface export flux) generally ranges between 2 and 20%, with values reaching 50% in some regions (Boyd and Trull (2007) and references therein). The fraction that sinks beyond 1000 m ranges from 6 to 25% (Berelson 2001; Francois et al. 2002; Martin et al. 1987).

Compilations of trap data showed that the annual average POC export to the deep ocean varies more than 10-fold globally (see Boyd and Trull (2007) and references therein). Fischer et al. (2000) for instance reported POC fluxes at 1000 m that ranged from $0.01 \text{ g m}^{-2} \text{ y}^{-1}$ in the Northwest Weddell Sea to $5.15 \text{ g m}^{-2} \text{ y}^{-1}$ at Cape Blanc. In the Southern Ocean, POC export at 1000 m can range from 0.01 to $2.53 \text{ g m}^{-2} \text{ y}^{-1}$, with fluxes at the Polar Front being the highest (Fischer et al. 2000). This coincides with relatively uniform POC fluxes of $1.7\text{--}2.3 \text{ g m}^{-2} \text{ y}^{-1}$ at 1000 m depth within the Polar Frontal Zone (PFZ) and the Antarctic Zone (Honjo et al. 2000) and POC fluxes at the same depth between 1.7 and $2.5 \text{ g m}^{-2} \text{ y}^{-1}$, in the Ross Gyre and PFZ or Antarctic Circumpolar Current (Nelson et al. 2002). Within the Atlantic Sector of the Southern Ocean POC fluxes between 800 and 1600 m are in the range of 0.03 and $5.13 \text{ g m}^{-2} \text{ y}^{-1}$ (Antia et al. 2001). According to Boyd and Trull (2007) remineralisation length scales in the Southern Ocean may differ from those in other regions. Generally, the Southern Ocean might be primarily affected by seasonal and interannual variability, rather than being characterised by any regime of high or low export efficiency (Lampitt and Antia 1997).

Although the Southern Ocean is one of the oceans which has been studied the least, several data sets on surface conditions and flux rates (including PP, surface POC export flux and deep POC export flux) exist and demonstrate the specifics of this ocean basin. These characteristics allow the Southern Ocean to be distinguished from other regions of the world's oceans in many respects. Deep surface mixed layers and only moderate seasonal warming and stratification are characteristic for the open Southern Ocean (e.g. Trull et al. 2001). Compared to lower latitudes POC surface export fluxes at 100 m are relatively high in the Southern Ocean with 30-50% of NPP (e.g. Buesseler, 1998; Nelson et al. 2002; Pondaven et al. 2000). Buesseler et al. (2001) therefore concluded that the Southern Ocean is characterised by one of the most efficient biological pumps. This is also in agreement with the findings of several other studies showing that high surface POC export fluxes are not necessarily associated with high PP but could also follow moderate phytoplankton biomass accumulation at the surface (e.g. Rutgers van der Loeff et al. 1997) like it is characteristic for parts of the Southern Ocean.

II. General Introduction

However, especially in the Southern Ocean the POC surface export flux is positively correlated to degradation rates in the mesopelagic zone (Berelson 2001). This means that high POC surface export often translates into strong modification processes of the sinking particle assemblage in the mesopelagic zone. Furthermore, it has been validated in previous studies that remineralisation rates in the mesopelagic zone of the Southern Ocean are very high (e.g. Berelson 2001; Buesseler et al. 2001; Fischer et al. 2000; Honjo et al. 2000, Nelson et al. 2002). However, the responsible processes were not known in detail (Boyd and Trull 2007; Buesseler and Boyd 2009).

The role of minerals—For the deep flux of particulate matter, relatively constant ratios of around 5% POC of the total flux were recorded using a compilation of deep sediment traps (Armstrong et al. 2002). CaCO_3 and POC fluxes appear to be strongly correlated, with the correlation between opal and POC being significant as well, but somewhat less pronounced (Francois et al. 2002; Klaas and Archer 2002). In conclusion, it has been suggested that minerals, such as CaCO_3 , opal or clay may act as ‘ballast’ and thus drive the vertical export of POC (Armstrong et al. 2002; Francois et al. 2002; Klaas and Archer 2002).

The reasons for this observation might be a protection mechanism of minerals against degradation of organic matter or the effect of increasing sinking velocities due to higher density (ballast) and it was postulated that minerals have a certain carrying capacity for POC (Armstrong et al., 2002; Francois et al. 2002; Klaas and Archer 2002). Alternatively, the cause for this correlation could be vice versa: on its way to depth POC scavenges particles that are too small to sink on their own (Honjo 1982; Passow 2004). From this perspective the 5% ratio reflects the capacity of POC to carrying minerals as shown by laboratory experiments (Passow and De La Rocha 2006). A third possibility is that there is no direct connection between POC and mineral flux despite the correlation (De La Rocha and Passow 2007).

II.4 Techniques to study vertical particle flux

In order to study particle fluxes a variety of tools are used, depending on the particular scope of the research question. These include for example sediment traps of different designs, pumping and/or filtration systems that transport water including its particulate load to the surface, optical methods such as camera systems, profilers or floats and remote sensing, and,

II. General Introduction

last but not least, the classical approach of collecting sinking particles ‘by hand’ via SCUBA diving.

Filtration systems—Pumps and filtration units have been widely used to collect large volumes of water and separate the particles therein by size (e.g. Abramson et al. 2010; Bishop et al. 1985; Lam and Bishop 2007; Waite et al. 2005). One example is the multiple unit large volume in-situ filtration system (MULVFS; Bishop et al. 1985; Lam and Bishop 2007), which allows biogeochemical investigations of two particle size classes (separated by a 51 μm filter). Furthermore, the collection of POM and DOM using pump systems offers the possibility to investigate sinking particles and dissolved material simultaneously, and hence to gain insights on dynamics between the particulate and dissolved pool (Abramson et al. 2010; Waite et al. 2005). This is of particular interest for understanding the underlying transition processes important for formation and degradation of POM, which can have an impact on export flux (compare also II.2 and II.3).

Optical methods—Technologies based on purely optic measurements overcome the disadvantage of filtration systems, which are likely to damage particle structure through high pressure. As optics are designed to trace particles without interacting with them, they are considered to deliver a realistic view of in-situ particle flux. From the first cameras used in the 1980’s (e.g. Honjo et al. 1984; Asper 1987) until today’s underwater camera systems (e.g. Guidi et al. 2008; Stemmann et al. 2008) technologies have improved immensely. Technologies like the marine survey camera (Honjo et al. 1984), the marine flux camera (Asper 1987), the Underwater Video profiler (UVP) in the first generation (Gorsky et al. 1992), the Marine Snow Profiler (MSP, Lampitt et al. 1993), the Particle Camera (ParCa, Ratmeyer and Wefer 1996) generated astonishing images that helped improving to understand particle dynamics. Only recently, the development of optic and in-situ imaging techniques made recordings of the complete particle size spectra feasible: the newest UVP generation can handle $> 90 \mu\text{m} - 2 \text{ cm}$ (Gorsky et al. 2000, Guidi et al. 2008; Stemmann et al. 2008).

Remote sensing—The just mentioned techniques, however, only create a snap-shot of the global ocean at one specific time on a small regional basis – mainly depending on ship time. The aim to collect data on wider spatial and temporal scales was partially satisfied by remote sensing. Although this satellite-based technique only observes the ocean’s surface and hence does not supply information on fluxes in the water column, it is a powerful tool for gaining consistent time-series of surface PP, which can be of importance for flux studies because it is indirectly related to export processes (Trull and Boyd 2007).

II. General Introduction

The Coastal Zone Colour Scanner (CZCS), which was the first radiometer launched and operated from 1978 to 1986, demonstrated that near-surface Chla measurement was feasible over long periods and large areas (Longhurst et al. 1995). Today, for instance, the Sea-viewing Wide Field-of-view Sensor (Sea WiFS) continuously provides surface Chla data (O'Reilly et al. 1998) and POC distribution (Allison et al. 2010) of most parts of the global ocean. The Moderate Resolution Imaging Spectroradiometer (MODIS) is also a prevalent satellite based sensor that delivers ocean wide data on, amongst others, surface Chla, sea surface temperature and sea surface height (<http://modis.gsfc.nasa.gov/>). Global Chla-maps played a major role in discovering the HNLC areas such as large parts of the Southern Ocean. Nevertheless, remote sensing suffers from one large disadvantage: cloud cover inhibits operation, which is a major concern in the Southern Ocean.

Floats—ARGO (Array for Real-time Geostrophic Oceanography) floats, a measuring system covering large areas of the ocean independent of ship time and cloud cover are beneficial for ocean wide observations. Moreover, they are programmed to dive to 2000 m depth collecting depth profiles (in contrast to being restricted to the surface) and send their data to a satellite when they surface (once every 10 days). Starting in 2000 the international program ARGO deployed about 3000 long-lived autonomous profiling floats – for temperature, salinity and mid-depth circulation – (<http://www-argo.ucsd.edu/>).

The Carbon Explorer, a faster derivative of the ARGO-style float has been equipped to measure POC, describing the vertical structure of the water column and co-locating multiple measurements using physical and bio-optical sensors (Bishop et al. 2002; 2004). Even though it is not capable of measuring particle fluxes (Bishop et al. 2002) and it thus has limited applicability for process flux studies, it provides valuable additional information on POC distribution over wide depth ranges that can be referred to for comparison.

Gliders, autonomously diving and slowly moving platforms for measurements, belong to the newest developments of oceanographic instruments. In principle they are ARGO floats with small wings and a compass, which can be steered (in contrast to ARGO-floats that are floating with ocean currents). Travelling for several months over distances of several thousand kilometres, gliders continuously perform measurements along their characteristic zigzag dive path (from the surface down to up to 1000 m depth). When they are at the surface they sent their data to a satellite through which they can also be reprogrammed (<http://www.ifm-geomar.de/index.php?id=1241&L=1>).

Sediment traps—Although the above mentioned tools are subtle and beneficial for their specific task, they all suffer from one major disadvantage: they do not return intact sinking

II. General Introduction

particles. Sediment traps offer the possibility to directly collect and examine sinking particles even though several problems are known to influence the reliability of sediment trap records (for a recent review see Buesseler et al. (2007) and references therein). It has been challenged whether or not particles settle vertically and whether or not different techniques (including differently designed traps, time scale and oceanographic setting) are comparable. In particular, two issues have to be considered: i) the aspect of quantitatively exact collection, and ii) the representative character of the collected material.

As for i) geometry of the trap and deployment conditions play an important role in trap efficiency. It has been suggested to use cylindrical traps with aspect ratios of 3-5 (e.g. Gardner 1980a/b; Hargrave and Burns 1979) – generating a tranquil zone at the bottom of the trap, which is essential for collecting sinking particles (Gardner 1980a/b). Hydrodynamic effects, such as current velocities which can create turbulence, might result in a tilt of the trap and are likely to lead to under- or overcollection (Gardner 1985). In order to reduce hydrodynamic biases, free-floating sediment traps that are coupled with the water motion – in contrast to moored sediment traps – were considered to be favourable (Staresinic et al. 1978). Although a perfect coupling is virtually impossible (Gardner 1985), the development of neutrally buoyant sediment traps (NBSTs) has been recommended as a step forward (Gardner 2000). They present the least biased form of sediment traps in terms of hydrodynamics as they are free vehicles that flow with the current and thus minimise internal flow (Valdes and Price 2000). This technology has been approved in comparison with free-floating sediment traps (Stanley et al. 2004). Beside the cylindrical NBSTs (e.g. Buesseler et al. 2000; Stanley et al. 2004; Valdes and Price 2000), a trap design with funnel shaped collection devices was also used successfully (Lampitt et al. 2008). Apart from the hydrodynamic bias, swimmers (metazoan zooplankton and occasionally small fish that are thought to actively enter the trap) can have a strong impact on collection efficiency (see review and comment from Lee et al. (1988)). Their uninvited presence in sediment traps can either account for additional mass (mainly in poisoned traps) or reduce the collected material through flux feeding (compare Lee et al. (1988) and references therein). The development of the Intended Rotating Sphere (IRS) trap was an improvement to avoid swimmer (Peterson et al. 1993; 2005). In addition, swimmer picking is a common and essential way to correct for introduced errors (see Buesseler et al. 2007 for recommendations).

Concerning ii), swimmers also have a large effect as they can alter particle forms via ingestion and/or disaggregation (Lee et al. 1988 and references therein). Furthermore, swimmers can alter particle shape, size and composition through their swimming behaviour

II. General Introduction

(Dilling and Alldredge 2001; Goldthwait et al. 2004). Another point is the disintegration of marine snow by the collection devices of the sediment traps (Gardner 1985). Due to shear motion in the vicinity of the deployed sediment trap the fragile material might easily be destroyed during collection making it difficult to determine the original shape of the sinking particles. Already at the very beginning of sediment trap studies the validity of collected material was doubted: Within the trap new aggregates may potentially be formed from particles that sank into it (as observed with a camera attached to a sediment trap by Asper (1987)). Another concern for particle preservation within the trap is the effect of processes such as chemical solution and/or bacterial degradation of the collected material (compare Gardner (2000) and references therein).

II. General Introduction

II.5 Aims of the thesis

The main focus of this thesis is to investigate particle flux in the mesopelagic zone by introducing free-floating gel traps and to compare results of this novel technique with other sampling technologies as they were assessed in three different regions of the Southern Ocean.

The following hypotheses will be tested in this study:

I Structure and composition of sinking particles provide information on the mechanisms of particle flux and modification.

II Free-floating gel traps are well suited to collect intact sinking particles.

III Different magnitude and composition of biogenic particle fluxes in different regions of the Southern Ocean can be categorised as biogeochemical provinces.

Much is known about processes at the surface ocean, where DIC is converted into organic carbon through photosynthesis, leading to a build-up of biomass. It is also known that only a small amount of carbon that is fixed during PP settles at the seafloor where it is buried for thousands of years and that the biological pump can act as a mechanism to transport carbon to depths. Taking into consideration that the vast majority of the initially produced POC is lost during transit through the water column, it becomes clear that processes which determine the efficiency of the biological pump are essential to understand flux dynamics in the oceans. Due to most of the flux modification occurring in the mesopelagic zone, it is necessary to ask the question of what is happening to sinking particles within this zone. In order to address this question, a technique is required that allows studying the flux on the base of individual particles.

The aim of this study is to test a novel technique, consisting of the combination of free-floating sediment traps and polyacrylamide gels (PA gels), which will be referred to as gel traps. Beside other tools such as ‘normal’ free-floating sediment traps, NBSTs and camera systems, these gel traps were used to investigate different areas of the Southern Ocean. Being a large sink of atmospheric CO₂, the Southern Ocean is of particular interest to understanding export flux processes. Due to the importance of the mesopelagic zone in terms of flux alteration, I will focus on processes within the mesopelagic zone in three parts of the Southern Ocean.

II. General Introduction

The following specific questions were addressed:

- 1) Can polyacrylamide gels capture the forms of individual sinking particles in a way that allows conclusions to be drawn on flux dynamics?
- 2) How do particle fluxes differ between two regions of the Southern Ocean south of Australia, where different surface plankton communities are present?
- 3) Are the processes in naturally iron fertilised waters on the Kerguelen Plateau in the Indian Sector of the Southern Ocean mirrored in sizes and forms of the sinking particle assemblage in comparison to surrounding waters?
- 4) What is the fate of unicellular plankton during an iron fertilisation experiment in the Atlantic Sector of the Southern Ocean – recycling or sinking?

Question 1 will be answered in **Manuscript 1**, which is a method script that is introducing gel traps as a technique to examine particulate flux on the base of individual sinking particles. Furthermore, it demonstrates the advantages over traditional sediment traps and shows its limitations in regard to compatibility of trap and gel container where the sample is collected in.

The second question is addressed in **Manuscript 2**, presenting a field study in the Southern Ocean south of Australia. During this project three sites (P1, P2, and P3) were studied in two different regions (SAZ and PFZ). **Manuscript 2** is focusing on a comparison of particulate export within the sites and is based on data received from three different sediment trap types, one of which were gel traps as described in **Manuscript 1**.

Manuscript 3 and **Appendix 1** are dealing with question 3. In **Appendix 1** the results of export fluxes determined with gel traps in an area of natural iron fertilisation and surrounding HNLC-waters in the Indian Sector of the Southern Ocean are presented. **Manuscript 3** compares these gel trap based fluxes with particle fluxes received from an underwater camera system.

Question 4 is discussed in **Manuscript 4** that reports on the composition of export fluxes following an iron fertilisation experiment, which was conducted in the Atlantic Sector of the Southern Ocean. Flux data were mainly obtained from NBST bulk samples, and to a minor extent also from NBST PA gels.

Each of these manuscripts (**Manuscript 1-4**, **Appendix 1**) is organised as a scientific paper, with a separate introduction, result and discussion section. Chapter VI provides a synthesis by placing the main conclusions of the manuscripts in a broader context, thus outlining suggestions for future research.

III. Manuscripts

III. List of Manuscripts

III.1 List of Manuscripts and declaration of own contribution

Manuscript 1:

A unique opportunity to study intact marine particles: The combination of Polyacrylamide gels and sediment traps (F. Ebersbach, T. W. Trull, D. M. Davies, C. Moy)

The method was tested by me in the laboratory at the ACE CRC in Hobart, TAS, Australia (with the help of technicians). I performed all necessary steps to accomplish the described method – the combination of Polyacrylamide (PA) gels and sediment traps – in the laboratory at ACE CRC and at the AWI, and I successfully applied it during three cruises in the Southern Ocean and North-West Pacific. The manuscript was primarily written by me.

Based on the plan to conduct some additional laboratory tests on buffers and means of preservation that will be conducted beginning 2011 by my Co-Authors T. Trull and D. Davies, we decided to postpone submission of the manuscript to *Limnology and Oceanography: Methods* until then. The manuscript would benefit from these further improvements of the technique.

Manuscript 2:

Controls on mesopelagic particle fluxes in the Sub-Antarctic and Polar Frontal Zones in the Southern Ocean south of Australia in summer – perspectives from free-drifting sediment traps (F. Ebersbach, T.W. Trull, D. M. Davies, S. G. Bray)

All data that are related to the gel method were obtained by me (including several steps between image analysis and conversion into carbon flux). I made the calculations for Tables 1, 6 – 8 and Fig. 5 – 9.

The manuscript was predominantly written by me and I also dealt with the two reviews.

On 30 June, the manuscript was accepted by *Deep-Sea Research II*.

Manuscript 3:

Optical imaging of mesopelagic particles indicates deep carbon flux beneath a natural iron fertilized bloom in the Southern Ocean

(M.J. Jouandet, T. W. Trull, M. Picharel, F. Ebersbach, L. Stemann, S. Blain)

III. List of Manuscripts

I provided one of the two data sets that are presented (compare also Appendix 1). Furthermore, I was involved in discussing the two approaches of obtaining particulate export flux rates and contributed to writing the manuscript.

After considering comments of two reviewers the manuscript was re-submitted to *Limnology and Oceanography* on 25 October 2010.

Manuscript 4:

Sedimentation patterns of phyto- and protozooplankton during the iron fertilisation experiment LOHAFEX in the Southern Ocean

(F. Ebersbach, P. Assmy, E. Nöthig)

This manuscript is entirely based on my own work: participation in the cruise and sample collection on board, microscopic work and analysis in the laboratory (TEP) at AWI, carbon flux estimates and data interpretation.

I wrote the manuscript and plan to submit it to *Journal of Marine Systems*. Due to an overview paper on LOHAFEX being in preparation, I did not intend to anticipate any general conclusions and thus restricted this manuscript to my own data.

Appendix 1:

Ebersbach, F., Trull, T., 2008. Sinking particle properties from polyacrylamide gels during the Kerguelen Ocean and Plateau compared Study (KEOPS): Zooplankton control of carbon export in an area of persistent natural iron inputs in the Southern Ocean. *Limnology and Oceanography* 53 (1), 212-224.

This paper was written by T. Trull and me together as outcome of my stay within his working group and my successful participation in the KEOPS cruise. Moreover, this work provided the basic ideas for the concept for this thesis.

The manuscript was published in January 2008 in *Limnology and Oceanography*.

Manuscript 1

A unique opportunity to study intact sinking particles: The combination of Polyacrylamide gels and sediment traps

F. Ebersbach¹, T.W. Trull^{2,3,4}, D.M. Davies², C. Moy²

(order needs to be discussed prior to submission)

1 International Graduate School for Marine Science (GLOMAR), University of Bremen, and Alfred Wegener Institute for Polar and Marine Research, Am Handelshafen 12, 27570 Bremerhaven, Germany

friederike.ebersbach@awi.de

2 Antarctic Climate and Ecosystems Cooperative Research Centre, Hobart, 7001, Australia

3 Centre for Australian Weather and Climate Research, a partnership of the Bureau of Meteorology and the Commonwealth Scientific and Industrial Research Organisation, Hobart, 7001, Australia

4 Institute for Marine and Antarctic Studies, University of Tasmania, Hobart, 7001, Australia

(Draft September 2010 – in preparation for L&O: Methods)

Acknowledgements

This work received support from the Australian Government Cooperative Research Centre Program. This research was in part supported by the Australian Government Cooperative Research Centres Programme through the Antarctic Climate and Ecosystems CRC (ACE CRC), Australian Antarctic Science projects #2720 and #1156, the Australian Antarctic Division, CSIRO Marine and Atmospheric Research, the US National Science Foundation (VERTIGO Award #0301139), the French-Australian Science and Technology Program (Award #FR040170), the Australian Antarctic Science Program (AAS#1156) and the Captain and Crew of RSV Aurora Australis. F.E. was supported by the German Science Foundation (DFG) through the Excellence Initiative in the frame of the International Graduate School for Marine Science (GLOMAR) of the University of Bremen.

Abstract

Identifying the character of sinking particles is essential to the evaluation of ecosystem controls on particle export, yet most sediment trap studies collect sinking particles into tubes or cups that allow the particles to clump together. This makes the identification of particle characteristics as they existed in the water column difficult and subject to biases. Placing a layer of transparent viscous water-soluble gel of polyacrylamide into sediment traps keeps particles isolated from each other and allows the characterization of their sizes, shapes, and individual origins. This technique was introduced more than 30 years ago (Jannasch et al. 1980) but has not been widely applied or described in detail in an easily available article. As a stimulus to its use, and with an emphasis on open ocean applications, we present simple recipes for gel preparation, deployment, recovery, and processing for microscopic image analysis. We also describe a few useful methodological modifications and indicate avenues for further development.

Introduction

Only a small amount of particulate organic carbon (POC), the material produced in the euphotic zone of the ocean's surface waters, reaches the sea floor via the biological pump (Volk and Hoffert 1985). The vast majority (80-98%) of the sinking particles is recycled in the water column, with most alteration taking place in the mesopelagic zone, the so called 'twilight zone', which adjoins underneath the euphotic layer and reaches down to 1000 m (e.g. Boyd and Trull 2007; Buesseler and Boyd 2009). Various particle sources lead to the formation of different types of sinking particles, collectively referred to as marine snow (Alldredge 1992). Aggregation of phytoplankton results in fluffy material, whereas fecal pellets are compact "packaged" particles. Degradation processes, such as bacterial solubilization (e.g. Bidle and Azam 1999; Iversen et al. 2010) or biological mediation (e.g. Noji et al. 1991; Dilling and Alldredge 2000), act as particle sinks. Grazing repackages particles demonstrating the complexity of interactions in terms of food-web structure. Particle composition, however, provides insights into food-web dynamics and underlying processes that occur in the mesopelagic zone.

In the past decades, POC fluxes have been investigated with different types of sediment traps (see Buesseler et al. 2007a for a recent review) or filtration units (e.g. Lam and Bishop 2007), but the sampling procedure can strongly impair shape and structure of the collected material. This problem is particularly important in the assessment of the hypothesized dominant role of aggregates in modulating export (e.g. Boyd and Newton 1995; 1999; Michaels and Silver 1988; Riebesell and Wolf-Gladrow 1992), because it is difficult if not impossible to tell whether the aggregates recovered in traps formed in the ocean or in the trap. Optical methods utilizing camera systems (e.g. Asper 1987; Stemmann et al. 2008; Guidi et al. 2008) or sensor floats (e.g. Bishop et al. 2002) provide powerful means to investigate particle fluxes over a wide depths range, but do not return material to the surface. Albeit offering the possibility to collect intact particles, the "classic attempt" of scuba-diving (e.g. Alldredge and Silver 1988) is depth limited.

The overall goal is to collect sinking particles in a way that is representative of the in-situ flux, and in a way that facilitates the optical and chemical characterization of their forms. The use of polyacrylamide gel (PA gel) in sediment traps was first introduced in an attempt to obtain a flux time series by Jannasch et al. (1980) and rediscovered by Lundsgard (1995), who deployed sediment traps with PA gels to study flux characteristics by keeping particles separated as they settle into the gel. Recently, PA gels have been used successfully in sediment traps to enable characterization of fragile particles, including studies in coastal (e.g. Kiorboe et al. 1994; Lundsgard et al. 1999; Waite et al. 2005) and open ocean settings (e.g. Ebersbach and Trull 2008; Ebersbach et al. 2010; Jackson et al. 2005; Waite and Nodder 2001; Waite et al. 2000) or to validate model estimates (e.g. Boyd et al. 2002; Jackson et al. 2005). This perspective affects the design of the sediment trap deployment system, the deployment duration, and the choice of the receiving gel (density, viscosity, incorporation of poison). The advantage over previously used methods is that the collected material is preserved as well

separated, individual particles retaining their delicate form by virtue of the gentle deceleration as they settle in the graded viscosity gel.

Our approach of studying particle flux with PA gels on free-floating sediment traps combines the benefits of both collection and preservation of marine snow particles and the unique possibility to investigate POC flux on the basis of individual particles. The traps can easily be deployed at depths of 1000 m and deeper offering the opportunity to study the entire mesopelagic zone.

Materials and Procedures

The method for collecting intact sinking particles in PA gels consists of the following Steps: (i) the PA gels are prepared in an onshore laboratory, (ii) the PA gels are installed in the gel traps and the brine (see below for properties) decanted onto them at sea prior to deployment, (iii) the sediment traps (referred to as gel traps) are deployed, (iv) the gel traps are recovered and overlying brine is drained, (v) low-magnification microscopy of the PA gels completed promptly on board, and (vi) high-magnification microscopy is carried out onshore.

Design of the gel trap—To deploy a gel trap, several aspects have to be taken into consideration: the design of the sampling device, the matching of the trap to the gel container (see below for details), and the position of the gel trap in the water column. It is well known that the design of the sediment trap has a large impact on collecting sinking particles (e.g. Gardner 2000; Buesseler et al. 2007a). The trap design is a plain cylinder of appropriate aspect ratio (see Assessment for further discussion) with no baffle, a base with a stopcock, and fittings that allow it to be clamped to a cable (Fig. 1). It is essential that the gel container diameter be matched to that of the cylinder to reduce particle and wall interactions. Fig. 2 illustrates that the gel completely covers the trap base. Gel containers were made from 500 ml Nalgene straight-side, wide-mouth polycarbonate containers, modified by replacing the bottoms with an optically clear polycarbonate base for optimal illumination and photo-microscopy. The containers have air-tight screw top lids for long-term storage.

PA gel preparation in the laboratory—The acrylamide monomer is a potent neurotoxin and carcinogen (refer to the appropriate material safety data sheets for this and the TEMED and persulfate). No specific precautions are necessary for the resultant polymer. In order to prepare the brine, seawater with salinity similar to the site of deployment was filtered through 2 quartz filters (nominal pore size 0.8 μm) and the salinity of the filtered seawater (FSW) adjusted to 50 psu by the addition of 15 g L⁻¹ of sodium chloride. Brine is used to ensure that the gel is sufficiently dense to remain at the bottom of the container when deployed. The brine can be buffered by the addition of sodium tetraborate (see Table 1 for chemicals and quantities), which has proved essential for preserving calcareous material; this is an important improvement over previous methods. Although gels have been observed to preserve organic particles, addition of mercuric chloride (30 mg L⁻¹) can be made at this point (see Assessment for details). The FSW brine is then degassed by boiling for one hour and cooled afterwards while flushing

III. Manuscript 1

with nitrogen to ensure complete removal of oxygen which would otherwise destroy the free radical sulfate ions that initiate the formation of linear polyacrylamide. The nitrogen flush can be stopped once the TEMED catalyst has been added. The polymerization reaction is exothermic and hence the reactants should be kept cool in an ice bath.

40% acrylamide solution is mixed into the FSW brine and while the solution is stirred continuously, ammonium persulfate (initiator) is added. Once completely dissolved, the nitrogen flush is stopped and TEMED (catalyst) is gradually added while stirring gently with a glass rod. The PA gel will immediately start to thicken and the reaction is complete within a day. Tiny air bubbles that might form in the solution during the reaction will disperse within a few days. After the polymerization is finished, the PA gel can be transferred into the gel containers to form a 4 cm thick layer. The PA gel can be stored at ambient temperature in a sealed container indefinitely.

Preparation of gel trap and PA gel onboard—At least one day before deploying the trap, the PA gel is moistened with a few mL of FSW brine taking care not to disturb the gel and then closing the gel container. This procedure allows the top layer of the PA gel to soften, thus creating a viscosity gradient that will gently decelerate the sinking particles and protect their fragile shapes as they enter the gel. Immediately prior to deployment, the gel container and trap are assembled and additional brine is decanted on top of the PA gel (a depth of 10 – 15 cm) to ensure a smooth viscosity gradient between the softened gel surface and seawater. The higher density prevents washing out of the sample. Finally, the gel trap is filled with FSW taking care to not disturb the density gradient. The trap opening is kept covered until its clamped to the cable and about to be immersed.

Deployment and recovery of the gel traps—The free-floating sediment trap array is shown in Fig. 1. The spacing of several trap tubes at various depths (100 to 150 m apart) allows comparison of the collected particle flux over a wide depth range. During deployment and recovery it is important to keep the traps vertical because tilting might lead to an outflow of the PA gel or destruction of the fragile material within it. The potential hazard of contamination with particles from the surface layer or the atmosphere is minimized through fast and efficient deployment and recovery. Usually, the gel traps are deployed for 24 hours (see Assessment for further discussion).

Sample treatment, storage and further processing—Immediately after recovery, the tubes are clamped vertically in a rack and drained carefully by opening the bottom stopcock. This reduces the risk of surface particles entering the trap during recovery and settling in the gel. However, the drainage has to be carried out slowly enough to minimize turbulence in the vicinity of the PA gel, which would disturb the collected material. Once the PA gels are drained, the gel containers can be taken out of the tube and the remaining overlying brine is carefully removed with a 50 mL plastic syringe equipped with a short length of fine-bore tubing which allows seawater to be removed but offers too much resistance if it contacts the viscous gel. Hence, any particles or swimmers that might originate from the surface layer (where it may have entered the trap tube during recovery) are eliminated. The sealed gel

III. Manuscript 1

containers are stored at 4°C and can be kept for several months. It is also possible to freeze the samples. Further means of preservation are discussed in the Assessment section.

Microscopic examination—Immediately following recovery, particles were examined in dark-field transmitted light with a Zeiss Stemi 2000 CS stereo-microscope coupled to a Leica DFC280 1.5 megapixel camera, with live recording to Leica Firecam software on an Apple Powerbook G4 computer. The PA gels were photographed under low magnification (6.5 to 50x) against an etched-glass grid of 36 cells (12.5x14 mm each cell) on board (compare Ebersbach and Trull 2008) capturing the delicate forms of the particles while fresh and insuring against unforeseen degradation problems or loss. High magnification microscopy is conducted onshore (see Fig. 3).

Assessment

We want to emphasize the power of this technique to study downward particle flux as a main contributor to the biological pump. The improvements and changes in the method, as compared to previously applied approaches, are summarized in Table 2 and will be clarified below.

Gel properties—In general, we follow the method of Lundsgard (1995) to prepare our PA gels. We modified the PA gel density by increasing the amount of acrylamide from 8% to 16%, which results in a more viscous gel described by Jannasch et al. (1980) as having the consistency of cold honey. This prevents particles from sinking through the gel and flattening or becoming clumps and suspends the sinking material within the topmost centimeter of the PA gel keeping them within the narrow depth of field of the microscope as opposed to letting it settle to the bottom prior to microscopic investigations (Lundsgaard et al. 1999). A sufficient gel thickness of around 4 cm is advisable as particles may eventually (after many months) reach the bottom of the gel container (this is discussed in more detail below).

Despite its toxic ingredients and the health hazards that arise during the procedure of polymerizing the acrylamide (see Materials and Procedures) the polymer end product is non-toxic and suits our application. We attempted to avoid the toxic preliminary steps by making the gels from powdered PA that would not have posed a health issue. Not surprisingly, a PA gel based on the monomer-free recipe is easily soluble in FSW, it dissolves immediately and hence is unsuitable. Other materials, such as Ficoll, Carboxy-methyl cellulose or other substrates like resins could be looked at as an alternative approach. A major consideration is to produce an optically clear substance thus we conclude that the benefits of PA gels prepared as described justify the additional precautions.

Modifications of gel trap design—The cylindrical trap design minimizes impacts with the collected material (Fig. 2) and has widely been used in the past (e.g. Lundsgaard et al. 1999; Waite and Nodder 2001; Waite et al. 2000) and to further minimize contact with particles we deliberately did not include a baffle at the mouth. The accuracy of fit of the gel in the trap tube (Fig. 2) is essential for the quantitative catch of the material and largely improves the reliability of the gel technique because it not

III. Manuscript 1

only minimizes contact with trap wall but also representatively samples the POC flux for different particles. Earlier approaches were focused on only observing the particles: Waite et al. (2000), for instance, found a lot of individual sinking diatoms and aggregates which would hardly have been recognizable in a bulk sample. Our modification provides the possibility of comparing PA gel based POC fluxes with POC flux estimates from sediment trap bulk samples and camera systems (Ebersbach and Trull 2008; Ebersbach et al. 2010; Jouandet et al. *subm.*).

The advantage of using free-floating surface-tethered sediment traps (as shown in Fig. 1) is that they are coupled to water motion and thus reduce hydrodynamic biases (e.g. Gardner 2000). Neutrally buoyant sediment traps (NBSTs), which drift freely and are coupled to water motion, are even less biased by hydrodynamic effects (Gardner 2000; Buesseler et al. 2007a). Unfortunately, our field tests of the neutrally buoyant funnel-shaped PELAGRA trap (Lampit et al. 2008) equipped with PA gels were not successful. The potential sources of several interferences for sinking particles are shown in Fig. 4. Firstly, when rolling along the funnel's side during collection, particles very likely interfere with the wall (and get damaged) or/and with each other (and break, collide, clump together and form "artificial aggregates"). Thus, these disturbances might bias the original shapes of the material before it leaves the sampling funnel at the bottom. Secondly, the bottom funnel opening is narrower than the gel surface causing the particles to concentrate in one area of the gel. Furthermore, small-scale motion in the vicinity of the opening might create turbulence which can again have an impact on particle structure. Thus, material settling into the PA gel is probably heavily affected by physical stress. The non-uniform distribution of collected material from a two days deployment of a PA gel with a PELAGRA trap (Fig. 5) demonstrates that the impact on particle forms impedes the advantages of PA gels making them incompatible with the PELAGRA traps. Because these particles have been altered by their contact with the funnel (Fig. 5), funnel traps are not as reliable as cylindrical traps to obtain particles in the forms that they exist in the sea and a promising future direction could be cylindrical NBSTs equipped with PA gels (McDonnell and Buesseler 2010).

Deployment and recovery of the gel trap—Apart from the trap's design to ensure successful sampling, the "load" of the PA gel is also important for further investigation. We aim for a gel with evenly distributed and separated particles, thus allowing identification of individual particles under the microscope (Fig. 6a shows a perfect example). Particle coverage can easily be regulated via deployment time – the longer the trap is left in the water collecting material, the more will settle into the gel, and vice versa. A deployment time of 24 hours was successful in several studies (e.g. Ebersbach and Trull 2008; Ebersbach et al. 2010). Of course, productivity of the study area also plays an important role and has to be considered – the higher the flux the shorter a deployment. Although deployment time (Lamborg et al. 2008) and seasonal background (Buesseler et al. 2007b) were similar for these two studies, the amount of material collected in PA gels was very different at the two contrasting sites (*pers. observation F. Ebersbach*). While the PA gels from the low productive waters were nearly empty, the gels from the area of high productivity were almost overloaded (Fig. 6c and d).

III. Manuscript 1

The former were difficult to analyze because the trapped few particles may not be representative, whereas the latter made it almost impossible to distinguish individual particles. As for the operations onboard it is self evident that a careful handling is necessary to minimize biases, such as the collection of surface particles during recovery (as presented in Fig. 6b).

Particle size and composition from PA gels—Ship movement becomes the biggest restriction for microscopic investigations of viscous PA gels on board. However, low-magnification microscopy on board and successive image analysis (Ebersbach and Trull 2008) provide the data on fresh particle size spectra (Ebersbach and Trull 2008; Ebersbach et al. 2010; Jackson et al. 2005). Any detailed investigation of the particles themselves requires high magnification microscopy to be carried out in a laboratory onshore. Because of the three-dimensional nature of the particles, confocal microscopy remains an excellent approach to assessing densities of picoplankton and larger phytoplankton in three dimensions within particles, and the change in these densities with depth (Waite et al. 2000).

Means of preservation—Ideally a means of preservation would halt further sinking of the particles into the PA gel, stop bacterial growth and prevent the dissolution of calcareous material. The PA gels have been observed microscopically to act as a preservative in themselves which is why Jannasch et al. (1980) did not use a preservative but they suggested that traditional poisons could be compatible. They also proposed freezing the PA gel for storage, and our laboratory tests confirm that freezing and thawing doesn't impair gel properties. Freezing stops bacterial degradation, keeps the particle structure within the gel, and prevents particles from further sinking. For short-term (<1 month) transits from a research vessel to shore, refrigeration has been seen to be adequate to preserve particle integrity (Waite et al., 2000), and poses fewer risks to any whole organisms embedded in particles. We found that high concentrations of mercuric chloride (HgCl_2), a common preservative and fixative in sediment trap work, produced an unacceptably cloudy gel but at lower concentrations (30 mg L^{-1}) the PA gel was unaffected. Lundsgaard (1995) successfully used formalin with a PA gel as an alternative to freezing. So far, we relied on the preserving potential of PA gels as such (as it is entirely anoxic) and did not use extra means of fixation (e.g. Ebersbach and Trull 2008; Ebersbach et al. 2010). The addition of a borate buffer (Table 1) to maintain the pH above 9 preventing dissolution is an important modification and successfully preserves all particles long term.

The collected material might possibly settle to the bottom of the gel container, although it might take several months. Other than freezing the PA gel, this could be stopped with chemical post recovery hardening. When a PA gel simply dries out on the air, it shrinks and affects embedded particles, and the hardened gel is full of tiny air bubbles disturbing its optical clear properties. We found no other means of hardening the PA gel.

Discussion and Recommendation

The method described here offers the unique opportunity to study particle flux in a way that is predominant over so far existing methods, like “normal” sediment traps, filtration units, or camera systems: it retrieves intact sinking particles to the surface. The deployment of our free-floating sediment traps equipped with a PA gel (as shown in Fig. 1) easily provides means of collecting material over a wide depths range – from surface layers down to 1000 m (deeper deployment seem possible if adequate equipment is available). By using gel equipped free-floating sediment traps, sinking particles are collected in-situ in the water column, and brought to the surface in a PA gel. The gels can be scanned at sea and investigated in detail in the laboratory onshore. Therewith, our method overcomes the disadvantage of pure optical methods (where images of the sinking material are recorded in-situ but particles are not retained).

In comparison to “normal” sediment traps, our PA gel traps exhibit following advantages:

- (i) PA gels form optically clear, thermally stable solutions in either fresh or seawater. Due to the transparency of the gel, the particles can be studied in detail under the microscope without removal.
- (ii) The PA gels are chemically stable and can be prepared months in advance. Gel filled containers (ready for deployment) can easily be shipped to the study area. The gel samples (after a successful deployment) can also be stored and transported during the next couple of months.
- (iii) The polymeric nature of the PA gels limits unwanted colligative effects, such as changes in ionic strength or osmotic pressure, so that they do not provoke cell lysis or mineral precipitation and the use of a buffer prevents dissolution of calcareous particles.
- (iv) The PA gels offer sufficient viscosity to isolate individual particles. Provided the gels are prepared with a viscosity gradient at the surface they even allow very fine features to be recovered intact.
- (v) Because of the lack of particle perturbation, the gels allow the estimation of particle size distributions using optical methods and image analysis.
- (vi) The matrix of the gels permits the use of biochemical techniques for the study of particles, such as application of stains.

The use of PA gels allows the identification of individual particles and subsequent separation into particle groups, such as different types of fecal pellets and aggregates (Ebersbach and Trull 2008; Ebersbach et al. 2010). In addition, image analysis allows particle size distributions of the sedimenting material to be generated (Jackson et al. 2005) such that particle flux data can be compared in detail with models and predictions (Boyd et al., 2002). The fact that carbon flux can be estimated independently for each group, gives insights into changes of particle composition with depths and their

III. Manuscript 1

contribution to overall POC flux. This, in turns, is evident for the impact of food-web dynamics. Therefore, we recommend using PA gels at the least as an additional tool when deploying “normal” sediment traps in order to validate assumptions made on downward particle flux. Moreover, we advise the use of free-floating sediment traps as they are a powerful tool to avoid hydrodynamic effects during collection of sinking material. Given the key benefits of the PA gels (i to vi, see above) a deployment with NBSTs promises to reveal further insights into particle flux (Mc Donell and Buesseler 2010).

References

- Allredge, A. L. 1992. Marine Snow in Oceanic Cycling, p. 139-147. In W. Nierenberg [ed.], Encyclopedia of Earth System Science. Academic Press.
- Allredge, A. L., and M. W. Silver. 1988. Characteristics, Dynamics and Significance of Marine Snow. Progress Oceanography **20**: 41-82.
- Asper, V. L. 1987. Measuring the flux and sinking speed of marine snow aggregates. Deep Sea Research **34**: 1-17.
- Bidle, K. D., and F. Azam. 1999. Accelerated dissolution of diatom silica by marine bacterial assemblages. Nature **397**: 508-512.
- Bishop, J. K. B., R. E. Davis, and J. T. Sherman. 2002. Robotic Observations of Dust Storm Enhancement of Carbon Biomass in the North Pacific. Science **298**: 817-821.
- Boyd, P. W., G. A. Jackson, and A. M. Waite. 2002. Are mesoscale perturbation experiments in polar waters prone to physical artefacts? Evidence from algal aggregation modelling studies. Geophysical Research Letters **29**: 36 31-34.
- Boyd, P. W., and P. Newton. 1995. Evidence of the potential influence of planktonic community structure on the interannual variability of particulate organic carbon flux. Deep Sea Research Part I: Oceanographic Research Papers **42**: 619-639.
- Boyd, P. W., and P. P. Newton. 1999. Does planktonic community structure determine downward particulate organic carbon flux in different oceanic provinces? Deep Sea Research Part I: Oceanographic Research Papers **46**: 63-91.
- Boyd, P. W., and T. W. Trull. 2007. Understanding the export of biogenic particles in oceanic waters: Is there consensus? Progress In Oceanography **72**: 276-312.
- Buesseler, K. O. and others 2007a. An assessment of the use of sediment traps for estimating upper ocean particle fluxes. Journal of Marine Research **65**: 345-416.
- Buesseler, K. O., and P. W. Boyd. 2009. Shedding light on processes that control particle export and flux attenuation in the twilight zone of the open ocean. Limnology and Oceanography **54**: 1210-1232.
- Buesseler, K. O. and others 2007b. Revisiting Carbon Flux Through the Ocean's Twilight Zone. Science **316**: 567-570.
- Dilling, L., and A. L. Allredge. 2000. Fragmentation of marine snow by swimming macrozooplankton: A new process impacting carbon cycling in the sea. Deep Sea Research Part I: Oceanographic Research Papers **47**: 1227-1245.
- Ebersbach, F., and T. Trull. 2008. Sinking particle properties from polyacrylamide gels during the Kerguelen Ocean and Plateau compared Study (KEOPS): Zooplankton control of carbon export in an area of persistent natural iron inputs in the Southern Ocean. Limnology and Oceanography **53**: 212-224.
- Ebersbach, F., T. W. Trull, D. M. Davies, and S. G. Bray. 2010. Controls on mesopelagic particle fluxes in the Sub-Antarctic and Polar Frontal Zones in the Southern Ocean south of Australia in summer - perspectives from free-drifting sediment traps. Deep-Sea Research II. in press.
- Gardner, W. D. 2000. Sediment trap sampling in surface waters, p. 240-280. In R. Hanson, H. Ducklow and J. Field [eds.], The Changing Ocean Carbon Cycle, A midterm synthesis of the Joint Global Ocean Flux Study. Cambridge University Press.
- Guidi, L., G. A. Jackson, L. Stemann, J. C. Miquel, M. Picheral, and G. Gorsky. 2008. Relationship between particle size distribution and flux in the mesopelagic zone. Deep Sea Research Part I: Oceanographic Research Papers **55**: 1364-1374.
- Iversen, M. H., N. Nowald, H. Ploug, G. A. Jackson, and G. Fischer. 2010. High resolution profiles of vertical particulate organic matter export off Cape Blanc, Mauritania: Degradation processes and ballasting effects. Deep-Sea Research I **57**: 771-784.
- Jackson, G. A., A. M. Waite, and P. W. Boyd. 2005. Role of algal aggregation in vertical carbon export during SOIREE and in other low biomass environments. Geophysical Research Letters **32**: 1-4.
- Jannasch, H. W., O. C. Zafiriou, and J. W. Farrington. 1980. A sequencing sediment trap for time-series studies of fragile particles. Limnology and Oceanography **25**: 939-943.

III. Manuscript 1

- Jouandet, M.-P. and others 2010. Optical imaging of mesopelagic particles indicates deep carbon flux beneath a natural iron fertilized bloom in the Southern Ocean. *Limnology and Oceanography*. subm.
- Kiorboe, T., C. Lundsgaard, M. Olesen, and J. L. S. Hansen. 1994. Aggregation and sedimentation processes during a spring phytoplankton bloom: A field experiment to test coagulation theory. *Journal of Marine Research* **52**: 297-323.
- Lam, P. J., and J. K. B. Bishop. 2007. High biomass, low export regimes in the Southern Ocean. *Deep Sea Research II* **54**: 601-638.
- Lamborg, C. H. and others 2008. The flux of bio- and lithogenic material associated with sinking particles in the mesopelagic 'twilight zone' of the northwest and North Central Pacific Ocean. *Deep Sea Research II* **55**: 1540-1562.
- Lampitt, R. S. and others 2008. Particle export from the euphotic zone: Estimates using a novel drifting sediment trap, 234Th and new production. *Deep Sea Research Part I: Oceanographic Research Papers* **55**: 1484-1502.
- Lundsgaard, C. 1995. Use of high viscosity medium in studies of aggregates. In S. Floderus, A.-S. Heiskanen, M. Oleson and P. Wassmann [eds.], *Sediment trap studies in the Nordic Countries, 3. Proceeding of the Symposium on Seasonal Dynamics of Planktonic Ecosystems and Sedimentation in Coastal Nordic Waters*. Numi Print.
- Lundsgaard, C., M. Olesen, M. Reigstad, and K. Olli. 1999. Sources of settling material: aggregation and zooplankton mediated fluxes in the Gulf of Riga. *Journal of Marine Systems* **23**: 197-210.
- McDonnell, A. M. P., and K. O. Buesseler. 2010. Variability in the average sinking velocities of marine particles. *Limnology and Oceanography*. in press.
- Michaels, A. F., and M. W. Silver. 1988. Primary production, sinking fluxes and the microbial food web. *Deep Sea Research Part A. Oceanographic Research Papers* **35**: 473-490.
- Noji, T. T., K. W. Estep, F. Macintyre, and F. Norrbin. 1991. Image analysis of faecal material grazed upon by three species of copepods: Evidence for coprophagy, coprophagy, and coprophagy. *Journal of the Marine Biological Association of the United Kingdom* **71**: 465-480.
- Riebesell, U., and D. Wolf-Gladrow. 1992. The relationship between physical aggregation of phytoplankton and particle flux: a numerical model. *Deep-Sea Research* **39**: 1085-1102.
- Stemann, L. and others 2008. Volume distribution for particles between 3.5 to 2000µm in the upper 200 m region of the South Pacific Gyre. *Biogeosciences* **5**: 299-310.
- Volk, T., and M. I. Hoffert. 1985. Ocean carbon pumps: analysis of relative strengths and efficiencies in ocean-driven atmospheric CO₂ changes. *Geophysical Monographs* **32**: 99-110.
- Waite, A. M., Ö. Gustafsson, O. Lindahl, and P. Tiselius. 2005. Linking ecosystem dynamics and biogeochemistry: Sinking fractionation of organic carbon in a Swedish fjord. *Limnology and Oceanography* **50**: 658-671.
- Waite, A. M., and S. D. Nodder. 2001. The effect of in situ iron addition on the sinking rates and export flux of Southern Ocean diatoms. *Deep-Sea Research II* **48**: 2635-2654.
- Waite, A. M., K. A. Safi, J. A. Hall, and S. D. Nodder. 2000. Mass sedimentation of picoplankton embedded in organic aggregates. *Limnology and Oceanography* **45**: 87-97.

Figure captions

Fig. 1. Free-floating surface-tethered sediment trap deployment system with motion damping elastic bungee. In addition to the ARGOS beacon, the surface float was fitted with a strobe light and radar reflector to aid recovery. The long pick-up line makes grappling from large ships relatively easy and allows the trap to be brought to the stern of the ship and then onboard with minimal disturbance of the PA gels. The cylindrical traps (see Fig. 2 for a detailed drawing) were secured directly to the wire with bulldog clamps.

Fig. 2. Cylindrical trap and gel container: Detailed diagram of the deployment system of the PA gel. The gel completely covers the trap base within a tight-fitting inner container, which is retrieved by removing the base after slowing draining the overlying fluid through the valve. The optically clear polycarbonate bottom of the gel container is essential for optimal particle visualisation. No baffle is used to avoid unwanted influences on particle forms. In the trap the gel is overlain by brine that forms a viscosity gradient between gel and seawater and also acts to retard fluid motions in the trap.

Fig. 3. High resolution images of PA gels deployed in the Southern Ocean during a bloom situation. The fine structures of fragile particles, the intact fecal pellet and the diatom chains are nicely preserved and illustrate the power of PA gels in terms of collecting individual particles separated from each other and undisturbed. Scale bar: 1 mm.

Fig. 4.

The PELAGRA trap, a neutrally buoyant sediment trap where the material is collected with non-symmetric funnels (0.1156 m²) and concentrated into screwed-on 500 mL cups (see Lampitt et al. 2008 for details). The diagram shows the combination of PELAGRA and a gel container filled with PA gel. A deployment of PA gels can only be successful if inter particle and wall interactions are minimal, and in the diagram several potentially hindering zones are indicated: particles might collide, stick together or break when rolling down the funnel's side or get damaged by small-scale turbulence when leaving the funnel. Furthermore, the small bottom opening in comparison to the PA gel area affects particle distribution across the gel (see Fig. 5).

Fig. 5. Compilation of a PA gel deployed with a PELAGRA trap (compare Fig. 4). The uneven distribution of collected material demonstrates the interference of trap design in terms of preserving the in-situ particle flux (a funnel shaped sediment trap in particular). One reason for the tail-like alignment of the collected material within the gel may be that collided and clumped-up particles reach the gel as bulk instead of remaining individual particles when leaving the funnel opening. Clearly, the fragile

structures of sinking particles have been disrupted. Moreover, the annular accumulation of material in the gel has been caused by the smaller exit funnel diameter.

Fig. 6. Examples of particles collected in PA gels. Samples a) and b) are from a Southern Ocean site, c) and d) from the Northwest Pacific (deployment was during a summer bloom in each case); depicted is one grid cell (1.25×1.4 cm) of a PA gel. Scale bar: 1 cm. a) represents the perfect distribution of material from a 24 h deployment (at 100 m, unpoisoned) showing that individual particles are collected separated from each other, b) illustrates the results of a gel trap recovery (unpoisoned) from 200 m that included dragging through the surface layer (and probably collected many individual phytoplankton cells and chains meanwhile) for more than 30 min (Ebersbach and Trull 2008), c) and d) show nearly overloaded PA after three day deployments at 150 m (note the negligible difference in particle preservation between the unpoisoned PA gel (c) and the poisoned PA gel (d) – taking into consideration that images were taken immediately after recovery).

Fig. 1.

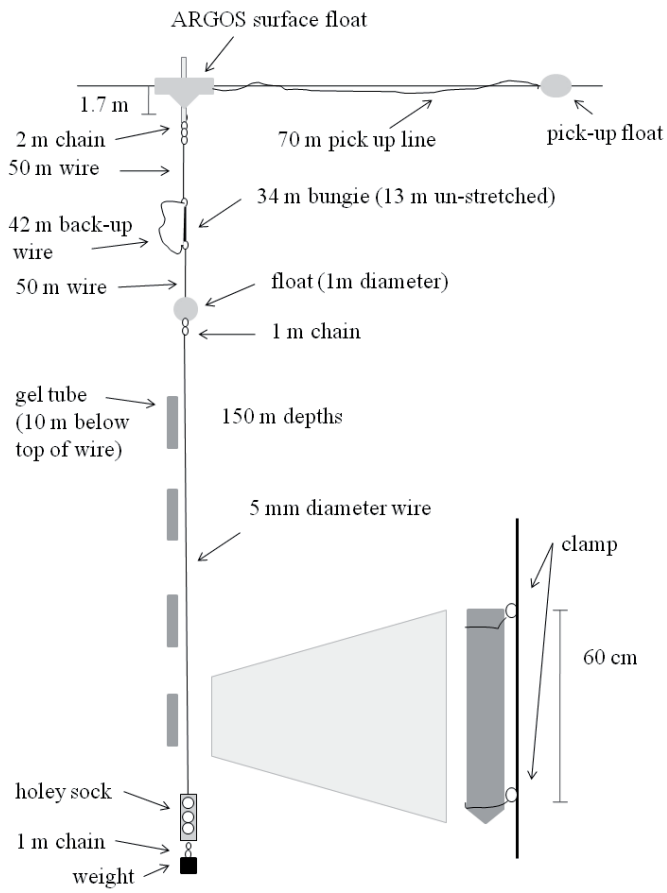


Fig. 2.

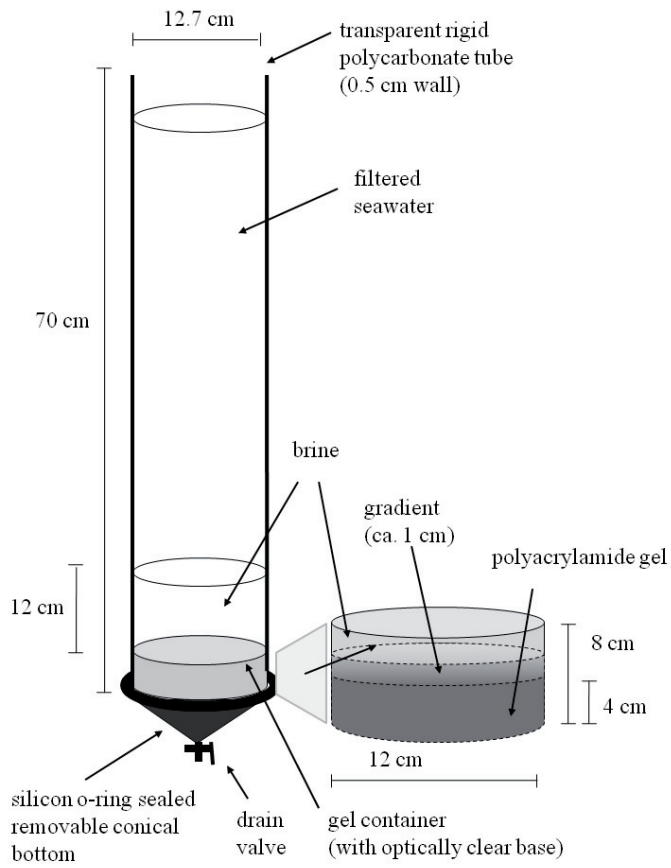


Fig. 3.

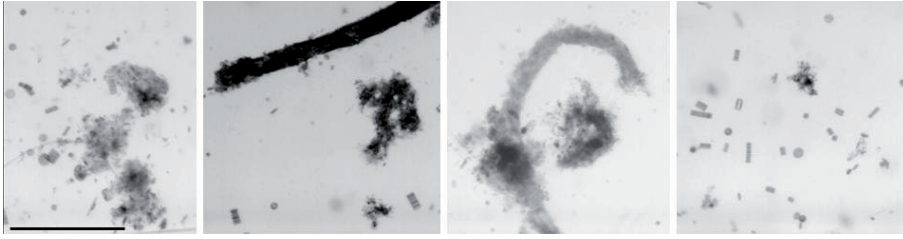


Fig. 4.

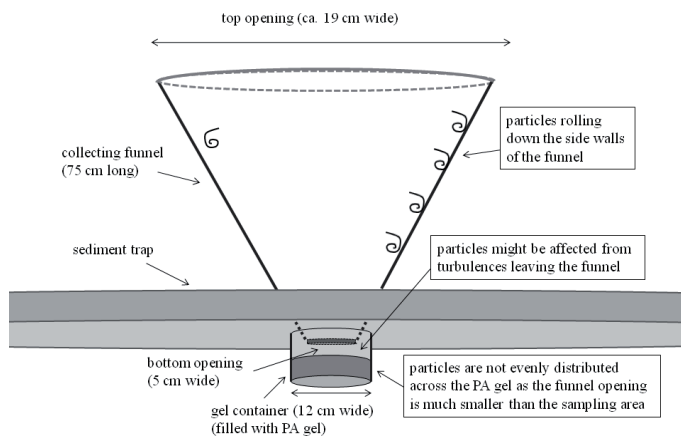


Fig. 5.

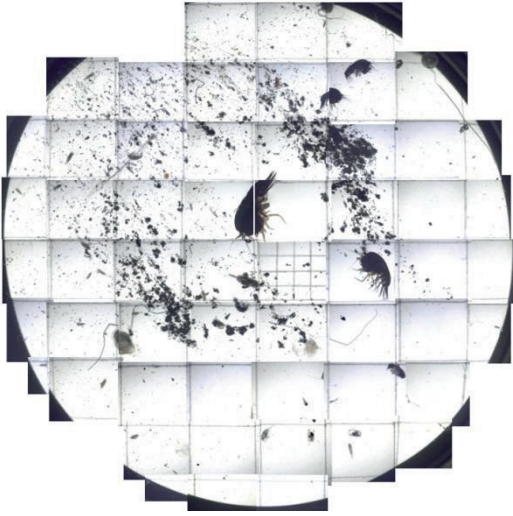
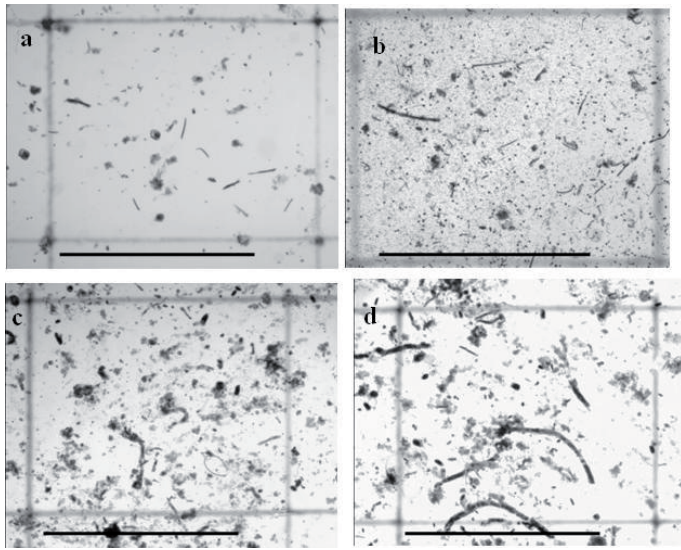


Fig. 6.



Tables

Table 1. Ingredients for 1 L 16% PA gel sufficient for five traps equipped with gel containers as shown in Fig. 2. Note: ¹ the addition of buffer ($\text{Na}_2\text{B}_4\text{O}_7 \times 10 \text{H}_2\text{O}$) is recommended but not required to prepare a PA, and ² the preservative (HgCl_2) should only be used if long term preservation is needed (compare Assessment for a detailed discussion).

Quantity	Reagent
600 mL	Medium (e.g. FSW)
15 g	Sodium chloride (NaCl)
400 mL	Acrylamide solution (40%)
4 g	Ammonium persulfate
4 mL	N,N,N',N'-tetramethylethylenediamine (TEMED)
1 g	Sodium tetraborate hydrate ($\text{Na}_2\text{B}_4\text{O}_7 \times 10 \text{H}_2\text{O}$) ¹
30 mg	Mercuric chloride (HgCl_2) ²

III. Manuscript 1

Table 2. Differences in the application of the PA gel methods in regard to sediment trap deployment systems, positioning of the PA gel during deployment and PA gel properties.

PA gel properties	PA gel deployment device	Sediment trap design	Reference
8, 12 or 15% PA	directly in the trap (sampling jar)	Multiple-sampling sequential trap (cylindrical trap unit (76 × 25 cm) and a sample-concentrating funnel (70° cone)	Jannasch et al. 1980
8% PA	Plastic petri dish (PA gel surface smaller than collection area of the trap)	Moored cylindrical trap (inside diameter: 5.2 and 7.2 cm, aspect ratios > 6)	Kiorboe et al. 1994; Lundgaard 1995; Lundsgaard et al. 1999
8% PA	Plastic petri dish (see above)	Free-floating cylindrical trap (inner diameter: 7.39 cm, aspect ratios > 8)	Waite and Nodder 2001, Waite et al. 2000; Jackson et al. 2005
8% PA	Plastic petri dish (see above)	Moored cylindrical trap (55 × 8 cm tubes)	Waite et al. 2005
16% PA	Gel container (modified polycarbonate jars with optical clear bottom)	Free-floating cylindrical trap (70 × 12 cm tubes)	Ebersbach and Trull 2008; Ebersbach et al. 2010; Jouandet et al. subm.

Manuscript 2

Controls on mesopelagic particle fluxes in the Sub-Antarctic and Polar Frontal Zones in the Southern Ocean south of Australia in summer – perspectives from free-drifting sediment traps

Friederike Ebersbach^{1,2}, Thomas W. Trull^{2,3,4}, Diana M. Davies² and Stephen G. Bray²

1 International Graduate School for Marine Science (GLOMAR), University of Bremen, and Alfred Wegener Institute for Polar and Marine Research, Am Handelshafen 12, 27570 Bremerhaven, Germany

friederike.ebersbach@awi.de

2 Antarctic Climate and Ecosystems Cooperative Research Centre, Hobart, 7001, Australia

3 Centre for Australian Weather and Climate Research, a partnership of the Bureau of Meteorology and the Commonwealth Scientific and Industrial Research Organisation, Hobart, 7001, Australia

4 Institute for Marine and Antarctic Studies, University of Tasmania, Hobart, 7001, Australia

(Manuscript accepted in Deep-Sea Research on 30 June 2010)

Abstract

The SAZ-Sense project examined ecosystem controls on Southern Ocean carbon export during austral summer (January – February 2007) at three locations: P1 in the low biomass Subantarctic Zone (SAZ) west of Tasmania, P3 in a region of elevated biomass in the SAZ east of Tasmania fuelled by enhanced iron supply, and P2 in High-Nutrient/Low Chlorophyll (HNLC) Polar Frontal Zone (PFZ) waters south of P1 and P3. Sinking particles were collected using: i) a cylindrical time-series (PPS3/3) trap for bulk geochemical fluxes, ii) indented rotating sphere (IRS) traps operated as in-situ settling columns to determine the flux distribution across sinking-rate fractions, and iii) cylindrical traps filled with polyacrylamide gels to obtain intact particles for image analysis.

Particulate organic carbon (POC) flux at 150 m (PPS3/3 trap) was highest at P1, lower at P2, and lowest at P3 (3.3 ± 1.8 , 2.1 ± 0.9 , and 0.9 ± 0.4 mmol m² d⁻¹, respectively). Biogenic silica (BSi) flux was very low in the SAZ (0.2 ± 0.2 and 0.02 ± 0.005 mmol m⁻² d⁻¹ at P1 and P3, respectively) and much higher in the PFZ (2.3 ± 0.5 mmol m² d⁻¹ at P2). Hence, the high biomass site P3 did not exhibit a correspondingly high flux of either POC or BSi. Separation of sinking-rate fractions with the IRS traps (at 170 and 320 m depth) was only successful at the PFZ site P2, where a relatively uniform distribution of flux was observed with ~ 1/3 of the POC sinking faster than 100 m d⁻¹ and 1/3 sinking slower than 10 m d⁻¹.

Analysis of thousands of particles collected with the gel traps (at 140, 190, 240, and 290 m depth) enabled us to identify 5 different categories: fluff-aggregates (low-density porous or amorphous aggregates), faecal-aggregates (denser aggregates composed of different types of particles), cylindrical and ovoid faecal pellets, and isolated phyto-cells (chains and single cells). Faecal-aggregates dominated the flux at all sites, and were larger in size at P1 in comparison to P3. The PFZ site P2 differed strongly from both SAZ sites in having a much higher abundance of diatoms and relatively small-sized faecal-aggregates. Overall, the particle images suggest that grazing was an important influence on vertical export at all three sites, with differences in the extents of large aggregate formation and direct diatom export further influencing the differences among the sites.

1. Introduction

The downward transfer of particulate organic carbon within the sea by biological processes, known as the biological pump, had a strong influence in maintaining low pre-industrial atmospheric CO₂ levels (Volk and Hoffert, 1985). Its response to industrial CO₂ emissions is uncertain, and is expected to be relatively moderate, but merits consideration in assessing the magnitude of emissions reductions required for stabilization of atmospheric CO₂ (Falkowski et al., 2000; Matear and Hirst, 1999; Sarmiento and Le Quéré, 1996). The overall strength of the biological pump can be thought of as consisting of 3 steps: i) primary production of organic matter by photosynthesis, ii) export of a fraction of this production from the euphotic zone as sinking particles, and iii) attenuation of this sinking flux by mesopelagic processes that limit the depth to which it is transferred and thus the duration over which it remains isolated from the atmosphere. Each of these steps exhibits similar variance and thus has similar potential importance in the control of the pump efficiency (Boyd and Trull, 2007; Kwon et al., 2009), but the factors controlling these steps are still under debate (Boyd and Trull, 2007; Buesseler and Boyd, 2009).

Attempts to predict the organic carbon export flux from primary production or phytoplankton biomass accumulation have not been very successful, because primary and export production are often decoupled by other aspects of ecosystem structure (e.g. Bishop, 1989; Boyd and Newton, 1995; 1999; Buesseler 1991; Buesseler and Boyd, 2009). Of particular interest is determining the conditions under which phytoplankton can be directly exported via physical flocculation and sinking, without passing through higher trophic levels that engender respiration losses of POC (Alldredge and Jackson, 1995; Michaels and Silver, 1988; Turner 2002).

Globally distributed deep ocean sediment trap programs have revealed some of the factors that correlate with high POC flux, including the presence of ballast minerals (primarily autochthonous biogenic carbonates and silica, and secondarily allochthonous lithogenic particles) and the occurrence of strong seasonality (Armstrong et al., 2002; Francois et al., 2002; Klaas and Archer, 2002; Lampitt and Antia, 1997; Lutz et al., 2002; 2007). But the importance of minerals is less clear at mesopelagic depths, where POC dominates particle contents to a much greater degree, particle size and porosity are strong influences on sinking rates (Alldredge, 1998; Alldredge and Gotschalk, 1988; De La Rocha and Passow, 2007; Passow, 2004; Stemmann et al., 2004), and where the vast majority of flux attenuation occurs (Buesseler et al., 2007a; Martin et al., 1987).

In this context of uncertainty regarding the controls on particle export and attenuation, particularly at mesopelagic depths, methods that directly examine the forms and compositions of sinking particles are useful. In this study, we used three different types of mesopelagic free-drifting sediment traps to determine i) POC and mineral ballast fluxes, ii) particle sinking rates, and iii) particle sizes and shapes. These methods let us examine several currently debated aspects of the controls on POC flux, including the roles of phytoplankton flocs, zooplankton faecal pellets, ballast minerals, and particle aggregation processes.

2. Material and Methods

2.1 Study area

The SAZ-Sense study took place in the Australian sector of the Southern Ocean and was carried out during midsummer (17th January – 20th February 2007). Three process stations were studied in detail: P1 in the SAZ west of Tasmania, P3 in the SAZ east of Tasmania and P2 in the PFZ further south (Fig. 1), with a much more limited set of measurements carried out at intervening transect stations (see Griffith et al., this issue, for an overview). This paper focuses exclusively on the process stations, which were each occupied for approximately 6 days. Sites P1 and P2 have been examined previously, including a process study (overview in Trull et al., 2001a), but this was the first process study at P3.

Site P1 is representative of a large proportion of the circumpolar SAZ, in terms of exhibiting iron limitation, seasonally low silicate levels, non-limiting nitrate and phosphate levels, low to moderate biomass throughout much of the year, and a mixed phytoplankton community that includes cyanobacteria, coccolithophores, small diatoms, and flagellates (Rintoul and Trull, 2001; Sedwick et al., 1999; 2008; Trull et al., 2001b; Wang et al., 2003). Site P2 is also representative of circumpolar conditions for the PFZ. It has very low dissolved iron levels, non-limiting macro-nutrient concentrations year-round, lower biomass with a pronounced summer maximum, and a phytoplankton community dominated by diatoms. These differences in surface water communities are also reflected in the composition of sinking particles reaching the deep sea, with carbonates dominating sediment trap collections at P1 and silica dominating P2 (Trull et al., 2001b).

Site P3 differs from the circumpolar conditions that prevail at P1 and P2, in that it receives inputs of southward flowing oligotrophic waters from eddies generated by the East Australian Current – an influence that has been increasing strongly in recent decades (Hill et al., 2008). Increased iron supply is observed in this region of the SAZ (Bowie et al., 2009), as are surface biomass levels as observed by satellite remote sensing (Mongin et al., this issue). Thus, this site offers the opportunity to observe the response of export to natural iron inputs to the Subantarctic Zone, which can be compared to other Southern Ocean natural iron fertilisation studies such as CROZEX (Pollard et al., 2007) and KEOPS (Blain et al., 2007).

In the absence of sustained observations, the main indication of the seasonal context of the SAZ-Sense study comes from satellite observations. Ocean colour observations show the development of seasonal blooms with biomass accumulation starting in December 2006 at P1 and P2, and in February 2007 at P3 (Mongin et al., this issue). Based on those satellite ocean colour observations, the bloom at P3 was still growing, while the peak at P1 was already over and at P2 the bloom was strongly declining. Prior to the cruise, surface Chl *a* levels based on SeaWiFS images were highest at P3, somewhat lower at P1 and lowest at P2 (~ 0.4, ~ 0.3, and ~ 0.25 mg m⁻³, respectively; Mongin et al., this issue).

III. Manuscript 2

The SAZ-Sense ship-board observations provide further detail of the oceanographic conditions (for an overview, see Griffiths et al., this issue), including the vertical water column structure and associated biomass distributions. P1 had the shallowest mixed layer (41 ± 18 m), P2 had the deepest mixed layer (53 ± 6 m), and P3 was characterised by a deep mixed layer (79 ± 2 m) and a secondary shallower stratification (16 ± 2 m) (Table 1). The euphotic depth was shallowest at P3 (47 ± 13 m), and at a comparable depth range at P1 and P2 (61 ± 5 and 76 ± 14 m, respectively; Table 1). During the study surface Chl a and surface POC were highest at P3, followed by P1 and P2 (Table 1). In keeping with the mixed layer and euphotic zone depth variations, in the SAZ (P1 and P3) the biomass maxima were shallower than at P2 in the PFZ (Fig. 2; Table 1). This correlation of shallow mixed layers with high biomass concentrations led to roughly similar standing stocks of Chl a and POC (integrated over depth) at all 3 sites (Table 1). Primary production estimated from tracer incubation experiments exhibited strong variability at site P1 and similar values to P3, with somewhat lower values at the PFZ site P2 (Table 1). Low f-ratios (< 0.3) at all stations indicate that regenerated production dominated over new production (Cavagna et al. this issue; Table 1). Similarly, net community production estimates from O₂/Ar supersaturations indicated higher values in the SAZ than the PFZ (Cassar et al., 2010).

There was some evidence for varying bottom-up controls on phytoplankton production among the three sites. At all three process stations mixed layer nitrate and phosphate were sufficient to not limit phytoplankton growth (nitrate: 5.5, 24.3, and 5.0 μM , phosphate: 0.22, 1.58, and 0.52 μM , at P1, P2, and P3 respectively) but silicate concentrations were low enough to affect diatom growth (0.29, 0.77, and 0.71 μM , at P1, P2, and P3 respectively, Griffiths et al., this issue). At P1, Fv/Fm values were low (< 0.5 , Cheah et al., this issue; Petrou et al., this issue), and primary production was likely to have been limited by Fe, and possibly also silicic acid. At P2, Fv/Fm values were higher (0.58), but iron/phosphate ratios were suggestive of iron limitation (Lannuzel et al. this issue), and the deep mixed layer suggestive of light limitation (Doblin et al., this issue). At P3, there was no indication of Fe limitation from iron/phosphate ratios or Fv/Fm values (0.58; Cheah et al., this issue; Petrou et al., this issue; Lannuzel et al., this issue).

Plankton communities also differed among the three sites in several ways. In the SAZ (P1 and P3) the biomass generally consisted of non-diatoms (de Salas et al., this issue), although at P1 beside nanoflagellates a lightly silicified *Thalassiosira* sp. was also abundant. P3 was dominated by cyanobacteria and heterotrophic dinoflagellates (de Salas et al., this issue). At the PFZ site P2 a deep chlorophyll maximum occurred just below the euphotic depth but above the mixed layer (compare Table 1, Fig. 2 and Westwood et al., this issue) and was characterised mainly of heavily silicified diatoms and nanoflagellates (de Salas et al., this issue). Bacterial and viral abundances were higher in the SAZ than the PFZ and highest at P3 (Evans et al., this issue). There were no mesozooplankton population studies carried out during SAZ-Sense, but grazing clearance rates from deckboard

incubations suggest high micro-zooplankton grazing pressure, sufficient to remove 82, 67, and 42% of primary production at P1, P3, and P2 respectively (Pearce et al., this issue).

2.2 Collection of sinking particles using free-drifting sediment traps

Three types of sediment traps were deployed, on separate arrays, as detailed in Table 2. All three arrays were similar in their overall design and consisted of a surface float beneath which the respective traps were suspended by an elastic link that dampens wave motions. Details of the array design and evidence of its ability to isolate wave motions during rough weather are available in Trull et al. (2008), although the SAZ-Sense deployments differed slightly by not including drogues at depth, because the traps themselves act in this capacity. Weather conditions for the P1 and P2 deployments were rough, although more benign at P3. Pressure sensors mounted on the deepest trap on each array indicated that the traps remained at fixed depth, within the ~ 4 m, 5 minute resolution of the pressure sensor records. Drift of the traps was slow ($< 10 \text{ cm s}^{-1}$) at P1 and P3 in the SAZ, and higher at P2 in the Antarctic Circumpolar Current (up to 23 cm s^{-1}). These drift rates were similar to water velocities estimated from the shipboard acoustic Doppler current meter, and suggest very low water velocities relative to the traps (of the order of a few cm s^{-1}), and thus large hydrodynamic artefacts in the particle collections were not expected (Buesseler et al., 2007b).

To obtain bulk component fluxes (particulate organic carbon, biogenic silica, and biogenic carbonates), we deployed at each station a single cylindrical trap with an internal conical funnel at its base (Technicap, La Turbie, France, model PPS3/3) at 150 m depth with a collection area of 0.125 m^2 that collected samples into a carousel of 12 cups over a period of 6 days. All cups were filled with brine with salinity of ~ 52 psu, made by freezing filtered ($0.2 \mu\text{m}$ pore size) surface seawater. Some cups were also preserved with mercuric chloride (1 g L^{-1}) as a biocide (Table 3). Most cups were analysed for component fluxes, with some cups used separately for trace metal studies (no poison added).

To estimate particle sinking rates, we deployed at each station two indented rotating sphere (IRS) traps (described in detail by Peterson et al., 2005; Peterson et al., 2009; Trull et al., 2008) at 170 and 320 m depth on a second separate array. The IRS traps (Prime Focus, Inc. Seattle, WA, USA), have cylindrical tubes (0.018 m^2 collection area) that collect particles onto dimpled spheres, which then rotate to transfer the particles into a settling tube for separation into 11 fractions based on their sinking velocities (as listed in Table 4). The sum of these fractions also provides a measurement of the total flux. The IRS traps collected particles for a total of 5 days. As in previous deployments, we programmed the IRS traps to collect the 11th sample in a way that checks the functioning of the trap (Trull et al., 2008), and filled the cups with the same brine and mercuric chloride concentrations as for the PPS3/3 trap.

To collect intact particles for optical examination of their sizes and shapes, we deployed four individual cylindrical polyacrylamide gel traps. The gel traps had a collection area of 0.011 m^2 and were deployed along a third separate array at each station at 140, 190, 240 and 290 m depths. To avoid

overloading the gels with particles, these deployments were limited to a single day, during the first day of the deployments of the PPS3/3 and IRS traps. The preparation of the polyacrylamide traps and subsequent processing has been previously described (Ebersbach and Trull, 2008).

2.3 Sample Analyses

2.3.1 Chemical analysis

The PPS3/3 trap samples were washed through a 350 μm screen to remove zooplankton, using 0.8 μm pore size GF/F filtered seawater, and the fraction passing the screen was collected by low vacuum filtration onto 25 mm diameter 1 μm pore size silver membrane filters (Sterlitech, Concord, MA, USA). The IRS trap samples were filtered in the same way without previous screening (the IRS ball greatly reduces swimmer contamination), although swimmers (zooplankton) were subsequently removed from the filters using forceps. For both the IRS and PPS3/3 trap samples, the filters (after being dried in a clean oven at 60° C) were sub-sampled in a flow-bench with a 5 mm diameter pre-cleaned stainless steel punch to provide aliquots for biogenic silica by alkaline digestion and spectrometry. The PPS3/3 trap sample filters were then punched for POC and PON analyses by catalytic combustion elemental analysis after de-carbonation (20 μL of 2 M HCl followed by drying at 60 °C for 48 hrs) and the remainder of the filter was used for PIC determination by acidification in a closed module and coulometric CO₂ titration. The IRS trap filters were encapsulated and de-carbonated with no further sub-sampling before elemental analysis because of the very small amount of material collected. Methods are detailed in Trull et al. (2008). Sub-sampling introduces variability of 10-20% from inhomogeneous filter coverage that well exceeds the analytical uncertainties of these methods (Trull et al., 2008).

2.3.2 Particle properties from the polyacrylamide gels

Immediately after recovery, the gel cups were removed from the tubes. Within a few hours of recovery the gels were photographed under low magnification (6.5 to 50) against an etched-glass grid of 36 cells (12.5 \times 14 mm each). Gels were stored at 2°C until further investigations in the laboratory onshore. The low magnification images were processed using image analysis software to obtain statistics of particle abundances and forms (Ebersbach and Trull, 2008). We divided the particles into 5 classes of particles: fluff-aggregates, faecal-aggregates, phyto-cells, cylindrical faecal pellets, and ovoid faecal pellets (see Table 5, Fig. 3). Assuming that particles were more or less evenly distributed over the gel surface, 10 grid cells per gel were analysed (16.8 cm², which corresponds to one fifth of the collection area) and projected to the gel area.

To allow size comparisons for particles of different shapes, we calculated equivalent spherical diameters (esd) from the observed areas ($\text{esd} = 2(\text{area}/\pi)^{0.5}$). We set a minimum particle size for analysis of 0.001 mm² (36 μm esd), because few particles were smaller than this, and because this ensured that gel thickness and refractive index variations were not mis-interpreted as ‘particles’. For each particle type, volumes were estimated from the imaged areas using the geometric approximations

given in Ebersbach and Trull (2008), i.e. aggregates and phyto-cells were regarded as spheres, cylindrical pellets as cylinders, and ovoid pellets as ellipsoids.

To convert volume flux into carbon flux, we adopted carbon contents of $0.057 \text{ mg C mm}^{-3}$ for faecal pellets (Gonzalez and Smetacek, 1994), and applied the parameterisation for carbon conversion factors used in our previous work (Ebersbach and Trull, 2008). That formulation is based on the fractal decrease of carbon contents with size observed for large coastal marine snow aggregates (Alldredge, 1998), but scaled to match up with solid geometry estimates for phytoplankton at lower sizes, where extrapolation of the large aggregate results would yield unrealistically high carbon contents. This scaled coastal aggregate relationship yields values ranging from $0.014 \text{ mg C mm}^{-3}$ for small aggregates (0.004 mm^3) to $0.0015 \text{ mg C mm}^{-3}$ for very large aggregates (10 mm^3). Because the phyto-cells were mostly provided by diatoms we used a power-law relation compiled for extant diatoms: $\log_{10} C = \log_{10} a + b * \log_{10} V$ (with C = carbon content in mg per cell and V = cell volume in mm^3 , estimated from images (see above)), with $\log_{10} a = -0.541$ and $b = 0.881$ (Menden-Deuer and Lessard, 2000). This results in carbon contents that range from 0.035 to $0.016 \text{ mg C mm}^{-3}$ for our smallest ($36 \mu\text{m esd}$) to largest ($300 \mu\text{m esd}$) diatoms. For comparison we also calculated POC fluxes using a new algorithm based on correlating suspended particle size distributions with deep ocean sediment trap fluxes (Guidi et al., 2008). The correlation reflects the combined influence of particle size on POC content and on sinking rate, and separating out the sinking rate dependence leads to a POC content as a function of size that can be applied to our gel trap particles ($\text{POC} = 0.38 \text{ esd}^{2.55}$; with POC in mg m^{-3} for esd in mm). This yields slightly lower POC fluxes at P1 and P2, and slightly higher estimates at P3 than our algorithm, but does not change the relative values of the fluxes among the three process stations.

3. Results

3.1 Geochemical fluxes from the PPS3/3 and IRS traps

3.1.1. Flux magnitudes

POC fluxes at 150 m depth collected by the PPS3/3 trap were approximately three, two and one thousand $\mu\text{mol m}^{-2} \text{ d}^{-1}$ at process stations P1, P2, and P3 respectively (Table 3). At each station, the POC flux varied by a factor of 3 across the individual 12-hour samples. This variability was not correlated with the time of collection (day versus night), or with the presence or absence of poison in the trap cups. All the flux samples had POC/PON ratios close to the canonical Redfield ratio for phytoplankton of 6.6, with the exception of sample 12 from process station P1 with a POC/PON of 2.6 despite displaying no conspicuous difference in its macroscopic character. PIC fluxes were about one magnitude lower than POC fluxes and decreased more strongly from P1 to P2 to P3 whereby the POC/PIC ratio at P3 was twice as high as at P1 and P2 (Table 3).

Biogenic silica fluxes varied more strongly between stations than those of POC, with the highest flux occurring in the PFZ (averaging ca. two thousand $\mu\text{mol Si m}^{-2} \text{ d}^{-1}$ at P2), much lower

fluxes in the western SAZ and lowest values in the eastern SAZ (less than one tenth and one hundredth of the PFZ flux at P1 and P3, respectively). The high BSi flux at P2 was not accompanied by high POC, and this site exhibited the lowest, POC/BSi ratio (Table 3). The low surface silicate at all sites (Cavagna et al., this issue) together with high BSi fluxes at P2 underline the importance of silicate and therefore diatoms for export controls at the PFZ-site. In contrast, the low BSi fluxes and high POC/BSi ratios at the SAZ-sites P1 and P3 suggests that diatoms were not important for POC flux in the SAZ, where CaCO_3 dominated biogenic mineral fluxes (Table 3). As for POC, BSi fluxes among the individual cups varied strongly, ~2-fold at P2 and P3, and more than 10-fold at P1, and no correlations of BSi flux with time of collection or use of poison were evident.

The IRS trap total fluxes (obtained by summing all sinking-rate fractions; Table 4) gave similar POC and BSi fluxes at 170 m depth to those obtained with the much larger diameter PPS3/3 trap at 150 m depth. This provides considerable encouragement that the fluxes were not strongly biased by flow past the traps, because this hydrodynamic bias is thought to vary strongly with trap diameter (Gust and Kozerski, 2000). It also suggests that potential biases from zooplankton entering the traps were accounted for, given that sieving of zooplankton from the poisoned and un-poisoned PPS3/3 trap cups gave similar results to the IRS trap in which zooplankton were excluded by the indented rotating sphere and direct removal using forceps.

3.1.2. Fluxes as a function of sinking rates from the IRS traps

Technical problems precluded deployment of the IRS traps at P1, and the low flux at P3 only allowed estimation of the total flux by combining the fractions (Table 4). Thus, separation of the particle flux into different sinking-rate fractions was only possible at P2, where sufficient material was obtained in all 11 sinking rate fractions to allow analysis of POC and BSi for both the 170 and 320 m depth traps (but not PON or PIC; Table 4). These data suggest that the POC (and BSi) flux was relatively evenly spread across the full range of sinking-rate fractions (with each containing 11% or less of the flux), but with somewhat higher fluxes in two fractions – a relatively fast sinking fraction (the 410-850 m d^{-1} fraction in the 170 m trap, and the 205-410 m d^{-1} fraction in the 320 m trap) and a relatively slow sinking fraction (the 2.3-26 m d^{-1} fraction at both depths). For the 170 m depth trap, this fast fraction contained 17% of the POC flux, and the slow fraction 28% of the POC flux. For the 320 m depth trap, the respective contributions were somewhat smaller (12 and 15% respectively), but still stood out as the two largest fractions.

3.2 Particle characteristics from the gel traps

3.2.1 Classification of sinking particles

The single day deployments of the gels yielded even coverage of particles across the gel surfaces, and sparse, well separated particle distributions optimal for image analysis. Different particle types were identifiable (Fig. 3, Table 5), including diatoms (mainly as chains but also a few individual cells), intact faecal pellets, and aggregates of these and other more amorphous materials. Within the faecal pellets cylindrical and ovoid pellets were distinguished. A wide range of aggregates was present

(Fig. 4 and 5) and reflects the large variety of components that account for marine snow (Alldredge and Gotschalk, 1990). A minority of the aggregates appeared to be rather fluffy and will be referred to as fluff-aggregates. The others are either more compact or seem to be composed of smaller particles and will be referred to as faecal-aggregates (Table 5, Fig. 3).

3.2.2 General characteristics of the particle fluxes

Small particles were most abundant at every site, with numerical fluxes dropping by 4 orders of magnitude as size (esd) increased from 0.01 to 0.1 cm (Fig. 6). Nonetheless, the volume and carbon fluxes were mainly carried by mid-sized and larger particles (esd of 0.05 and 0.1 cm; Fig. 7 and 8). The carbon flux was dominated by slightly smaller particles than the volume flux (compare Fig. 7 and 8), because the larger particles were assumed to have lower carbon densities (see Methods section 2.3.2). The overall importance of the large particles in controlling the carbon flux is emphasised by the cumulative carbon flux (Fig. 9). It clearly shows that the large particles that only make up 5-10% of the numerical flux provide more than half of the carbon flux.

3.2.3. Differences in particle flux characteristics among the sites

Total volume flux of particles from the gel traps was highest at P1, followed by P2 and P3 (Table 6). The carbon fluxes calculated from the images showed the same trend, $P1 > P2 > P3$, and decreased from around 10000 to 600 $\mu\text{mol C m}^{-2} \text{d}^{-1}$ (Table 7). The sites also differed in the number and the nature of the particles observed. In terms of particle numbers, P2 had the highest flux, followed by P1 and P3 (Table 6). This was due to the very large number of very small particles (mainly phytoplankton cells) at P2 (Table 6, Fig. 6). The larger, flux-dominating particles were predominantly faecal-aggregates at all sites, followed by large cylindrical faecal pellets, with rarer occurrences of ovoid faecal pellets (as is apparent from the images in Fig. 4 and quantified in Table 6). Fluff-aggregates did not play a large role at any of the sites (Tables 6, 7), although it is of course possible that fluffy material, such as phyto-detritus or feeding structures, were included within some of the less tightly packed faecal-aggregates. Particle composition at P3 was similar to P1 in being dominated by faecal-aggregates and having a dearth of phyto-cells, but the dominance of the faecal-aggregates is somewhat reduced by the presence of cylindrical faecal pellets (Table 7).

The sizes of the particles within the different particle classes also varied among the sites. The faecal-aggregates were largest at P1, where their volumes were almost twice that of the faecal-aggregates at P2 and P3 (Table 9). Fluff-aggregates were four to ten times smaller than faecal-aggregates; they were larger at P2 than P1, and absent at P3. The largest cylindrical pellets were found at P3, followed by P1 (half the volume or length) and then P2 (circa one order of magnitude smaller). Pellets at P2 were somewhat wider (lower aspect ratios) than at P1 and P3. Within the category of ovoid faecal pellets, at least two size classes can be distinguished (see particles labelled e, h, and i in Fig. 3) and at P1 more of the larger ones were found (Table 8). Phyto-cells did not differ appreciably in size between the sites.

3.3 Variations of flux and particle composition with depth

A decrease of the POC flux with increasing depth (from 170 to 320 m) was recognisable in the IRS traps at P2 and P3: by almost half at P2, and even more strongly to one fifth at P3 (Table 4). The greater depth resolution of the gels as compared to the IRS traps (Table 2) gives further insights into the flux variation with depth. In particular, the shallowest gel trap revealed distinct differences among the stations. At the SAZ-sites P1 and P3, the flux at 140 m was lower than the flux at 190 m, which then decreased slightly by 290 m. Whereas P2 (PFZ) showed a relatively high flux at 140 m in comparison to 190 m and then a continuous strong decrease with depth.

Except at the shallowest depths at P1, the total volume flux decreased with increasing depths (Fig. 7, Table 6). In regard to total carbon flux, variations with depth were complex (Fig. 8, Table 7). At P2 the faecal-aggregate fluxes, and thus the carbon fluxes, dropped by one half from the surface to 290 m depth, whereas at P1 and P3 changes in the faecal-aggregate and carbon fluxes were much less pronounced (Table 7). At P2, where phyto-cells were important, their carbon flux declined with depth. For the faecal pellets no trends with depth were recognisable.

4. Discussion

4.1 Overview

We first discuss the sediment trap results, beginning with technical aspects of trap function, followed by comparisons of the flux magnitudes for the different trap types and the 3 process stations (section 4.2). Next we examine the particle characteristics as observed in the gel traps (section 4.3). Finally, we consider the probable ecosystem controls on the particle fluxes, including comparing the SAZ-Sense results to other studies (section 4.4).

4.2 Vertical export determined by sediment traps

4.2.1 Functioning of the sediment traps

Hydrodynamic effects can impair trapping efficiency (e.g. Gust and Kozerski, 2000; Buesseler et al., 2007b), but because of the very low relative water velocities for all three sediment trap types (see section 2.2), this influence is likely to have been minimal. This view is corroborated by the even coverage of particles across the surface of the gels, and the fine structures preserved within them. It also appears that the entry of zooplankton into the traps is unlikely to have strongly biased the flux results for two reasons: i) the PPS3/3 results were indistinguishable between poisoned and unpoisoned cups, and ii) the total fluxes from the IRS trap with its zooplankton excluding indented rotating sphere, were only slightly lower than the fluxes from the open-mouthed PPS3/3 trap, and within the uncertainties defined by the standard deviations of the individual cups (Table 3 and 4).

The fidelity of the separation of the sinking particles by settling speed by the IRS trap requires careful evaluation. Ideally, when operated in sinking-rate mode, it transfers particles from the indented-rotating-sphere into the settling tube, where they enter successive cups in the carousel

III. Manuscript 2

according to their sinking rates (Peterson et al., 2005). For the IRS rotation interval and carousel cycle duration of 6 hours used here, this results in fractions with sinking rates ranging from $>850 \text{ m d}^{-1}$ to $\sim 2.3 \text{ m d}^{-1}$ (Table 3). The effectiveness of this separation requires evaluation. A particular concern is the possibility that very slow-sinking particles remain in the funnel beyond the duration of a full carousel rotation (6 hours in this study and our previous work; Trull et al., 2008), and are thus transferred into the subsequent cycle where they could be erroneously collected into the carousel fractions that collect faster sinking particles. Programming the collection interval of the last cup in the cycle (#11) to have the same one minute duration as the first cup in the subsequent cycle (#1) provides some quality control on this issue (Trull et al. 2008).

As shown in Table 3, for the IRS trap at P2, the POC flux collected in the 11th cup at 170 m and 320 m depths were similar and these amounts are only slightly less than the POC fluxes collected by the first cups for these traps. This suggests that carry-over was significant. If so, the fluxes observed in the other cups should be reduced for this contribution. For example, the flux to each cup could be considered to represent the sum of the contribution from the most recent IRS rotation and a background of a steady flux of slow sinking particles (Armstrong et al., 2009). However, there are aspects of the flux distribution over the 11 fractions that suggest that this is an over-simplification. The POC flux per cup duration for many sinking rate fractions is less than the POC flux to the 11th cups (e.g. cups 6-10 for both the 170 and 320 m deployments). Indeed, the POC flux per cup duration for the 11th cups is much larger than that for the preceding 10th cups. This suggests that the high fluxes per cup duration in the 11th cups may be induced by the carousel rotation, perhaps by causing particles that have accumulated at the mouth of the cup to enter the cup. In our previous work, we found large colonial radiolaria in the 11th cups, and attributed the high fluxes per cup duration to their unusual presence (Trull et al., 2008). These or other unusual organisms were not discernable in the present study, but the material in the 11th cups had high POC/BSi ratios in comparison to the preceding 10th cups, suggesting that the material entering the 11th cups was different in character. One way to rationalise these results is to consider that very slowly sinking material has not completely left the settling tube within six hours, and the motion of the carousel as it turns to cup #11 and then again to cup #1 causes some or all of this material to be moved further along the settling tube and into the cups. Thus the carry-over quantity to subsequent cups would be an aliquot related to the carousel motion, rather than a steady background flux. In other words, correction for carry-over should be equal to (or less than) the 11th cup fluxes, rather than depending on the duration that the cups were open.

Correcting for carry-over in this way does not change the overall character of the distribution of POC flux across the sinking-rate fractions, rather it emphasises the initial perspective from the uncorrected data – that the flux is spread across the full range of sinking fractions, but with an elevated flux from two classes of particles – a relatively fast sinking fraction, and a very slow sinking fraction (see corrected flux values in Table 4).

4.2.2 Flux characteristics of the three sites

In terms of POC flux, the same sequence was observed for all the trap types deployed ($P1 > P2 > P3$), although the flux estimates vary in magnitude for the different trap types (Tables 3, 4 and 7). In comparison to the PPS3/3 and IRS traps, which tend to be similar, the gel traps gave the highest POC flux values for each site, and also a wider range in relative fluxes among the sites than for the measured POC fluxes in the PPS3/3 and IRS traps. The POC fluxes from PPS3/3 and IRS traps were determined directly via geochemical analysis, while the gel trap flux estimates were based on converting particle volume as identified through microscopic observations into units of carbon (see section 2.3.2). Because most of the flux is carried by faecal-aggregates at all three sites, it is likely that the conversion factor for this particle type is the cause of this difference. The fact that the faecal-aggregates are somewhat inhomogeneous as they might originate from processed material (see section 4.3) supports this conclusion. At P3 where faecal-aggregates contribute much less to total volume flux due to their overall smaller size and numbers (Table 6 and 8), their relative contribution to POC flux is still similar to the other stations (Table 7) suggesting that carbon content of the larger faecal-aggregates might be overestimated. This perspective is consistent with the small differences between our estimates and those obtained with the algorithm from Guidi et al. (2008). At P1, where large faecal-aggregates were dominant, our POC flux was higher than that from the Guidi algorithm, as it was to a lesser degree at P2. At P3, in contrast, our flux appears to be underestimated, which might be explained by the high abundance of small and relatively compact particles.

The complex flux variations with depth as estimated from the gel traps (see section 3.3) could be affected by small scale variations in time and space (notice also the relatively high standard deviation of up to 1/3 of the mean for POC flux with PP3/3 traps; Table 3). In addition they could reflect the introduction of biases from the volume-to-carbon algorithms used in estimates from the gel traps (discussed above).

Furthermore, when comparing fluxes among the three sites, we have to keep in mind, that the collected material is derived from the mesopelagic (see Table 2 for trap deployment depths). The largest flux attenuation is often found higher up in the water column (for instance at the pycnocline at 50-60 depths (Reigstad et al., 2008)). Since the euphotic depth was between 34 and 90 m (Table 1) during this study, the sinking particles underwent heavy processing before they reached the traps (140 m or deeper; Table 2). Certainly, some of the particulate matter was remineralised between the base of the mixed layer and 140 m (Cassar et al., 2010). Thus the collected particles represent the mesopelagic flux and differ considerably from surface particles leaving the euphotic zone.

4.3 Composition of particles

The particle categories identified from the gel traps (see 3.2.1, Fig. 3 and Table 5) provide some insights into the forms of the sinking material during SAZ-Sense. However, it is important to keep in mind that inferences based on these observations are uncertain because the formation pathways remain unknown. For example, since marine snow aggregates capture surrounding particles

III. Manuscript 2

as they travel through the water column (Alldredge and Silver, 1988) the identification of the collected material cannot necessarily identify the ecological pathways that initiated vertical export. Bacterial degradation may also have altered particle composition and shape (Azam, 1998). Moreover, the sinking particles collected at 140 m depth or deeper (Table 2) have already left the euphotic zone, where most of the flux alteration occurred.

Based on their structural appearance the aggregates were separated into fluff-aggregates and faecal-aggregates (Fig. 3, Table 5). Different fluff-aggregates resembled different types of aggregates found during earlier studies and might possibly include phyto-detritus, flocculent faecal pellets or larvacean houses (e.g. Fowler and Knauer, 1986; Alldredge and Silver, 1988; Alldredge and Gotschalk, 1989). Microscopic observations reveal that most of the faecal-aggregates were composed of smaller particles with distinct cylindrical and ovoid shapes resembling individual faecal pellets, or at least tightly packed and optically opaque sub-units similar to those detected by Alldredge and Gotschalk (1990). However, within this particle type a large variety of shapes and forms occurred (Fig. 4 and 5): some were relatively compact and consisted of agglomerated faecal pellets, while others contained less distinct material, such as loose faecal matter, phyto detritus, or feeding structures or exopolymeric polysaccharide particles. Our observations are very similar to particles collected from the PFZ south of New Zealand using large volume in-situ filtration system (MULVFS) by Lam and Bishop (2007), who found intact faecal pellets as well as aggregates of faecal matter and marine snow. They concluded that the material was heavily processed by zooplankton – a view which we share based on our observations of large numbers of aggregates containing at least some faecal matter. Wexels Riser et al. (2008) studied the vertical flux regulation by zooplankton in the northern Barents Sea, where the importance of faecal pellets in terms of carbon flux below the euphotic layer was decreasing. They proposed that faecal pellets were transferred into unidentifiable organic matter that is to a large extent faecal pellet derived – which resembles our faecal-aggregates. Since the particles of this class vary a lot, their origin might be due to several different formation pathways. In addition to direct faecal material production as a result of grazing, it is likely that the sinking material underwent other processes, such as fragmentation of particles into smaller ones (Dilling and Alldredge, 2000; Noji et al., 1991). According to Dilling and Alldredge (2000) large zooplankton such as euphausiids are capable of fragmenting marine snow and Noji et al. (1991) observed copepods breaking up faecal pellets. This could explain some of the large size range and variety in shapes within the faecal-aggregates. Unfortunately, zooplankton data from SAZ-Sense are not available for comparison. But the faecal pellets as preserved in the gels and divided into cylindrical and ovoid pellets provide some indication of probable taxa (Fig. 3). The cylindrical faecal pellets were probably derived from copepods and euphausiids, and the ovoid faecal pellets may originate from small copepods or larvaceans (Gonzalez, 1992; Turner, 2002; Wilson et al., 2008; Wexels Riser et al., 2008).

Phyto-cells were most important at the diatom dominated PFZ site P2 (Table 6 and 7), where they were collected as chains and rarely also as individual cells (Fig. 6). These highly silicified diatom

species (e.g. *Fragilariopsis kerguelensis*; de Salas et al., this issue) might have entered the gel trap individually, or within aggregates which then fell apart in the traps. Since diatom aggregates have been collected in previous studies (e.g. Waite and Nodder, 2001; Waite et al. 2005), it is quite possible that our phyto-cells reached the traps within fluff- or faecal-aggregates. Indeed, our images of PFZ particles (Fig. 5) were very similar to those of Waite et al. (2005) for aggregates in the SAZ east of New Zealand.

4.4 Ecosystem controls on the flux

4.4.1 Influence of particle types on vertical export

Gross primary production (GPP) and net primary production (NPP) at P1 were about twice as high as at P3 and three times higher than at P2 (Table 1). At P1 and P2 POC fluxes were approximately one magnitude lower than GPP, and at P3 almost two magnitudes. Considering these variations among all three sites implies that primary production and carbon flux were not coupled in a linear way (Table 1). This is consistent with the perspective developed in earlier work. Boyd and Newton (1995; 1999) suggested that details of ecosystem structure are as influential as primary production in the control of export. The particles identified in the gel traps make clear that zooplankton were an important regulator of export throughout the study region, contributing strongly to the flux either as faecal pellets or faecal-aggregates (Fig 4 and 5). This is in agreement with the estimated high importance of grazing from shipboard incubation experiments which suggested that, in the eastern and western SAZ, grazing removed on average 67 and 82% of the primary production, respectively (Pearce et al.; this issue). The smaller and more compact faecal-aggregates at P2 and P3, in comparison to the larger and fluffier faecal-aggregates at P1 (Table 8, Fig. 5), suggests that the impact of grazing is more pronounced in the eastern SAZ and the PFZ. This is supported by the relatively large contribution of faecal pellets to the flux in the eastern SAZ (Table 7). In contrast, the higher abundance of fluff-aggregates and the somewhat looser appearance of the faecal-aggregates in the western SAZ suggest the possible importance of different processes in the water column, e.g. coagulation of phytoplankton and formation of phyto-detritus. Nevertheless, hardly any unprocessed phytoplankton material was found in the traps (Fig. 4 and 5). This in part probably reflects the distance between the biomass distributions in shallow mixed layers and the traps (Fig. 2, Table 9), and emphasises the point that we measured mesopelagic fluxes (compare also section 4.2.2), for which considerable degradation had already occurred during the transit out of the mixed layer and into the traps.

4.4.2 Impact of particle sizes and structure on sinking rates and export

According to Stokes law for spherical particle settling ($w_s = (g \cdot \Delta\rho \cdot d^2) / (18 \cdot \eta)$), the settling velocity, w_s , is proportional to excess density above seawater, $\Delta\rho$, to the square of the particle size, d , and inversely proportional to the viscosity of the surrounding seawater, η . Particle size presumably influenced individual particle sinking rates, because particle size varied more than an order of magnitude (Figure 7), although median particle size varied by less than 50% among the sites (Table 8)

III. Manuscript 2

so that the influence of size on total flux may not have been particularly strong. Particle excess density (partly controlled by porosity) may have been more important than size in terms of sinking rates, and thus in terms of degradation prior to reaching the traps, given the variations between tightly packed and more fluffy or amorphous faecal-aggregates (Fig. 4 and 5). This may have contributed to the high flux attenuation with depth that was found at P2. Regarding the ballasting effect, the presence of calcium carbonate and silica minerals have been demonstrated to influence POC export to traps in the ocean interior (Armstrong et al., 2002; Francois et al., 2002; Klaas and Archer, 2002), although their role may be less relevant closer to the ocean surface (Passow, 2004; Trull et al., 2008). Therefore, the highest CaCO_3 flux at P1 might have enhanced export as previously suggested for this region (Cardinal et al., 2005).

Biogenic silica only played a role at P2 (Table 3) and indicates the importance of diatoms for the export in the PFZ. However, the evenly distributed BSi content over particles sinking at different rates as obtained from the IRS trap (Table 4) does not support the view that the mineral had the dominant impact on settling rates of the sinking material. This would agree with the finding that the slow sinking and the fast sinking fraction at P2 (see 3.1.2 and Table 4) appear to be composed of similar chemical composition as far as POC and BSi are concerned. In general, POC/BSi ratios show no clear trend as a function of sinking rate across all the fractions. This suggests that sinking rates did not depend strongly on mineral ballast contents (this perspective is likely to extend to all mineral contents, given that PIC contents at P2 were very low, less than 10 % of BSi contents (Table 3) and based on historical data (Trull et al., 2001b), lithogenic fluxes at this site were probably also very low). However, material without BSi, may have sunk extremely slowly. This is consistent with the very high POC/BSi ratios in cup 11 for the fraction sinking at less than 2.3 m d^{-1} in the IRS traps (Table 4).

The PFZ site P2 also shows the strongest attenuation with depth (Table 9). This might result from the high abundance of small particles (Table 8, Fig. 4 and 5) that could possibly be too small to sink, as generally for the same particle type sinking rates decrease with decreasing particle size (Alldredge and Gotschalk, 1988; Ploug et al., 2008). Therefore both phyto-cells and tiny faecal-aggregates could contribute to the slow sinking fraction ($2.3\text{-}6 \text{ m d}^{-1}$) as collected in the IRS trap (Table 4). The fast sinking fraction ($410\text{-}850 \text{ m d}^{-1}$) may contain larger faecal-aggregates and/or faecal pellets.

BSi export was high in the PFZ (P2), but low in the SAZ (P1 and P3). In agreement with literature (e.g. Cardinal et al., 2005), fluxes of BSi and POC were strongly decoupled at P2, and thus POC to biomineral ratios were high in the SAZ and low in the PFZ. Based on the finding of many empty diatoms in the gels (mainly *Fragilariopsis kerguelensis*, Fig. 5), this might be a mechanism for the downwards transport of silicate at this site.

4.4.3 Estimates of export efficiency

Export-ratios (e-ratios; e-ratio = POC/NPP (Table 9) based on NPP from Cavagna et al., (this issue) and POC as collected in the traps (Table 3, 4, 7) were generally low: on average 0.13, 0.19 and 0.02 at P1, P2 and P3, respectively (Table 9). Sequence and magnitudes coincide with the e-ratio calculations based on export production estimated from ²³⁴Th water column inventories from Jacquet et al. (this issue), who concluded that low export efficiency in the more productive eastern SAZ (P3) – in contrast to the higher export in the less productive western SAZ (P1) – was somewhat unexpected. The high e-ratios at P2 may mirror the higher export efficiency due to the post bloom situation or the impact of large diatoms on carbon flux as suggested by Boyd and Newton (1995). The observation that export at P3 was least efficient despite highest primary production (Table 9) coincides with relatively small faecal-aggregates (Fig. 4 and 5, Table 8) and low ballast mineral content, suggesting that slow sinking may have influenced export flux. The distance between the shallow mixed layers, where biomass production and export occurred, and the deeper mesopelagic traps influences our ability to assign the cause of the variations in the trap-based e-ratios among the sites. In particular, the greater distance at P3 than at P1 and P2 (Figure 2) may have contributed to its lower apparent e-ratio.

Because export efficiency may of course vary seasonally (Wassmann, 1990; Honjo, 1996), it is important to take the seasonal context of the study into account. According to Mongin et al. (this issue), the bloom in the western SAZ (P1) had not reached its peak. The large amount of relatively unprocessed and fresh material at P1 (see 4.4.1; Fig. 4 and 5), supports the idea that we encountered a growing bloom. In the eastern SAZ (P3) the blooming event occurred over a longer time period without a distinct peak prior to the cruise, and in the PFZ (P2) the peak biomass period had already passed (Mongin et al., this issue). This is in agreement with the more compact (and more processed) particles at these sites (P2 and P3) if we assume that phytoplankton has been grazed down and zooplankton mediated particles were produced. The large number of empty diatoms in the gel traps at the P2 site (Fig. 5, Table 6) could be a result of bloom senescence at the sampling time.

Recently, the term high biomass, low export condition (HBLE) has been suggested for settings like we found at P1 (Lam and Bishop, 2007). According to these authors the most important factors determining POC export during the Southern Ocean Iron Experiment (SOFeX) were biological processes that affected the fragmentation and remineralisation of large particles – coinciding with the view that faecal-aggregates usually are the main contributors to POC flux as previous studies have indicated (e.g. Bishop et al., 1977; 1987). This is in agreement with the dominance of more or less heavily processed particles (faecal-aggregates) during SAZ-Sense and also agrees with many other studies in Polar regions (e.g. Blain et al., 2007; Pollard et al., 2007; Wassmann et al., 2008).

The results of the project ‘Carbon flux and ecosystem feed back in the northern Barents Sea in an era of climate change’ (CABANERA; Wassmann et al., 2008) indicate that vertical carbon export was mainly driven by grazing and pelagic retention (Reigstad et al., 2008) and the production of fast sinking faecal pellets (Wexels Riser et al., 2008). This coincides with results from the Kerguelen

III. Manuscript 2

Ocean and Plateau compared Study (KEOPS) that was carried out in PFZ waters (Blain et al., 2007), where most of the particle flux originated from faecal matter (Ebersbach and Trull, 2008). Similar to our dominating faecal-aggregates, KEOPS reported on aggregates of faecal matter that were responsible for downward POC export. A comparison of flux spectra from SAZ-Sense (Fig. 6) and KEOPS (Ebersbach and Trull, 2008) validates this. Compared with particle distribution during KEOPS, the PFZ site P2 shows a slight shift towards smaller particles. The SAZ sites differ somewhat from each other: at P3 the range of particle sizes lies in the average distribution found during KEOPS, but large particles are not present at all, and at P1 the trend is somewhat shifted towards larger particles. Overall, the generally similar characteristics at KEOPS and SAZ-Sense indicate similar export mechanisms.

In contrast, POC export during the Southern Ocean Iron Release Experiment SOIREE, that took place under similar conditions (HNLC and iron fertilised waters; Boyd et al., 2000) was driven by phyto-detrital aggregates (Waite and Nodder, 2001). Jackson et al. (2005) compared measured particle fluxes from SOIREE with model estimates and yielded number flux spectra, which resemble our particle distribution in regard to overall trends. However, the SOIREE particles in total were much smaller (as small as 0.8 μm in diameter), the abundance of the 10 μm sized particles (our smallest) was about one magnitude higher and the decrease towards larger particles was less steep (for the 0.4 cm size class the difference exceeds two magnitudes), suggesting that during SOIREE the flux was carried by larger particles. This agrees with the dominance of large marine-snow aggregates entirely composed of diatoms observed in SOIREE gels (Waite and Nodder, 2001) and is in opposite to the more tightly packed faecal-aggregates responsible for POC flux during SAZ-Sense. Marine-snow aggregates have also been observed in many other studies, where aggregation of phytoplankton was pre-dominant (e.g. Alldredge and Gottschalk, 1989; Passow et al., 1994; Waite et al., 2005; Pollard et al., 2007; Salter et al., 2007). The CROZet natural iron bloom and EXport experiment (CROZEX), for instance, also suggests an important role for the direct export of a diverse range of diatoms (Salter et al., 2007).

Thus, the different export mechanisms and the subsequently different particle regimes highlight the importance of studying flux composition in detail. As shown by various studies on particle size distribution in different regions of the ocean (e.g. Ebersbach and Trull, 2008; Jackson et al., 2005; Guidi et al., 2008; Stemmann et al., 2008; Jouandet et al., 2010), the approach of determining particle size spectra provides insights in the context of carbon transport from the surface ocean into the mesopelagic zone. This is an important step towards prediction of carbon flux in response to changing environments.

5. Conclusions

The overall results are a clear reminder that simple indices, such as satellite estimates of phytoplankton biomass, are a poor guide to ecosystem function in general, or to export production specifically. The elevated biomass observed at P3, which is present throughout the year as indicated by satellite remote sensing (Mongin et al., this issue), was not accompanied by elevated primary or new production, and did not translate into increased sinking flux, at least not during the short shipboard observational period reported here. This provides a cautionary note, as have other studies of natural iron fertilisation (Pollard et al., 2007; Blain et al., 2007), about the effectiveness of iron inputs (which were elevated at the P3 site; Bowie et al., 2009) to increase biological pump strength. The clear influence of zooplankton grazing in the control of particle production and export observed via the use of the polyacrylamide gel traps emphasises the influence of higher trophic levels on biological pump responses to stimulation of photosynthesis. This perspective, known as the ecumenical iron hypothesis, considers the impact of grazers on primary production in iron-limited ecosystems (Cullen, 1995; Morel et al., 1991). It was originally formulated based on general ecological principles, and has less commonly been directly demonstrated. The combination of three trap types to obtain geochemical flux measurements, particle sinking rate estimates, and images of intact particles is powerful and will benefit other studies in the future.

Acknowledgements

This research was in part supported by the Australian Government Cooperative Research Centres Programme through the Antarctic Climate and Ecosystems CRC (ACE CRC), Australian Antarctic Science projects #2720 and #1156, the Australian Antarctic Division, CSIRO Marine and Atmospheric Research, and the captain and crew of RSV Aurora Australis. The NERC Earth Observation Data Acquisition and Analysis Service (NEODAAS) supplied data for the ocean color image provided by the Plymouth Marine Laboratory. The Institut National des Sciences de l'Univers (INSU, France) provided the PPS3/3 trap, and F. Dehair (Vrije Universiteit Brussel, Belgium) provided one IRS trap. Thanks to D. McLaughlin (moorings preparation), C. Moy (gel preparation), M. Rosenberg (assistance with trap deployments), C. Bloomfield (biogenic silica analysis), and T. Rodemann (UTAS Central Science Laboratory, elemental analysis). U. Passow, U. Bathmann, E. Nöthig, C. Klaas, D. Wolf-Gladrow and B. Griffiths are thanked for thoughtful discussions, as are two anonymous reviewers who helped to improve the manuscript. F. Ebersbach was funded by GLOMAR (PhD scholarship).

References

- Allredge, A.L., 1998. The carbon, nitrogen and mass content of marine snow as a function of aggregate size. *Deep-Sea Research I* 45, 529-541.
- Allredge, A.L., Gotschalk, C., 1988. In situ settling behaviour of marine snow. *Limnology and Oceanography* 33 (3), 330-351.
- Allredge, A.L., Gotschalk, C., 1989. Direct observations of the mass flocculation of diatom blooms: characteristics, settling velocities and formation of diatom aggregates. *Deep-Sea Research* 36 (2), 159-171.
- Allredge, A.L., Gotschalk, C., 1990. The relative contribution of marine snow of different origins to biological processes in coastal waters. *Continental Shelf Research* 10 (1), 41-58.
- Allredge, A.L., Jackson, G.A., 1995. Aggregation in marine systems. *Deep-Sea Research II* 42, 1-7.
- Allredge, A.L., Silver, M.W., 1988. Characteristics, Dynamics and Significance of Marine Snow. *Progress in Oceanography* 20, 41-82.
- Armstrong, R.A., Lee, C., Hedges, J.I., Honjo, S., Wakeham, S.G., 2002. A new, mechanical model for organic carbon fluxes in the ocean based on the quantitative association of POC with ballast minerals. *Deep-Sea Research II* 49, 219-236.
- Armstrong, R.A., Peterson, M.L., Lee, C., Wakeham, S.G., 2009. Settling velocity spectra and the ballast ratio hypothesis. *Deep-Sea Research II* 56 (18), 1470-1478.
- Azam, F., 1998. Oceanography: Microbial Control of Carbon Flux: The Plot Thickens. *Science* 280 (5364), 694-696.
- Bishop, J.K.B., 1989. Regional extremes in particulate matter composition and flux: effects on the chemistry of the ocean interior. In: Berger, W.H., Smetacek, V., Wefer, G. (Eds.), *Dahlem Workshop Life Science Report - Productivity of the oceans: Present and Past*. John Wiley and Sons, New York, pp. 117-138.
- Bishop, J.K.B., Edmond, J.M., Ketten, D.R., Bacon, M.P., Silker, W.B., 1977. The chemistry, biology, and vertical flux of particulate matter from the upper 400 m of the equatorial Atlantic Ocean. *Deep-Sea Research* 24 (6), 511-548.
- Bishop, J.K.B., Stepien, J.C., Wiebe, P.H., 1987. Particulate matter distributions, chemistry and flux in the Panama basin: response to environment forcing. *Progress in Oceanography* 17 (1-2), 1-59.
- Blain, S., Quéguiner, B., Armand, L., Belviso, S., Bombled, B., Bopp, L., Bowie, A., Brunet, C., Brussaard, C., Carlotti, F., Christaki, U., Corbiere, A., Durand, I., Ebersbach, F., Fuda, J.-L., Garcia, N., Gerringa, L., Griffiths, B., Guige, C., Guillelm, C., Jacquet, S.H.M., Jeandel, C., Laan, P., Lefevre, D., Lo Monaco, C., Malits, A., Mosseri, J., Obernosterer, I., Park, Y.-H., Picheral, M., Pondaven, P., Remenyi, T., Sandroni, V., Sarthou, G., Savoye, N., Scouarnec, L., Souhaut, M., Thuiller, D., Timmermans, K., Trull, T., Uitz, J., van Beek, P., Veldhuis, M., Vincent, D., Viollier, E., Vong, L., Wagener, T., 2007. Effect of natural iron fertilization on carbon sequestration in the Southern Ocean. *Nature* 446, 1070-1075.
- Bowie, A.R., Lannuzel, D., Remenyi, T.A., Wagener, T., Lam, P.J., Boyd, P.W., Guieu, C., Townsend, A.T., Trull, T.W., 2009. Biogeochemical iron budgets of the Southern Ocean south of Australia demonstrate that summertime supply decouples iron and nutrient cycles in the subantarctic zone. *Global Biogeochemical Cycles* 23, GB4034, doi:10.1029/2009GB003500.
- Boyd, P., Newton, P., 1995. Evidence of the potential influence of planktonic community structure on the interannual variability of particulate organic carbon flux. *Deep-Sea Research I* 42 (5), 619-639.
- Boyd, P.W., Newton, P.P., 1999. Does planktonic community structure determine downward particulate organic carbon flux in different oceanic provinces? *Deep-Sea Research I*: 46 (1), 63-91.
- Boyd, P.W., Trull, T.W., 2007. Understanding the export of biogenic particles in oceanic waters: Is there consensus? *Progress in Oceanography* 72 (4), 276-312.
- Boyd, P.W., Watson, A.J., Law, C.S., Abraham, E.R., Trull, T., Murdoch, R., Bakker, D.C.E., Bowie, A.R., Buesseler, K.O., Chang, H., Charette, M., Croot, P., Downing, K., Frew, R., Gall, M., Hadfield, M., Hall, J., Harvey, M., Jameson, G., LaRoche, J., Liddicoat, M., Ling, R., Maldonado, M.T., McKay, R.M., Nodder, S., Pickmere, S., Pridmore, R., Rintoul, S., Safi, K., Sutton, P., Strzepek,

III. Manuscript 2

- R., Tanneberger, K., Turner, S., Waite, A., Zeldis, J., 2000. A mesoscale phytoplankton bloom in the polar Southern Ocean stimulated by iron fertilization. *Nature* 407 (6805), 695-702.
- Buesseler, K.O., 1991. Do upper-ocean sediment traps provide an accurate record of particle flux? *Nature* 353, 420-423.
- Buesseler, K.O., Boyd, P.W., 2009. Shedding light on processes that control particle export and flux attenuation in the twilight zone of the open ocean. *Limnology and Oceanography* 54 (4), 1210-1232.
- Buesseler, K.O., Lamborg, C., Boyd, P.W., Lam, P.J., Trull, T.W., Bidigare, R.R., Bishop, J.K.B., Casciotti, K.L., Dehairs, F., Elskens, M., Honda, M., Karl, D.M., Siegel, D.A., Silver, M.W., Steinberg, D.K., Valdes, J., Van Mooy, B., Wilson, S., 2007a. Revisiting Carbon Flux Through the Ocean's Twilight Zone. *Science* 316, 567-570.
- Buesseler, K.O., Antia, A.V., Chen, M., Fowler, S.W., Gardner, W.D., Gustafsson, O., Harada, K., Michaels, A.F., van der Loef, M.R., Sarin, M., Steinberg, D.K., Trull, T., 2007b, An assessment of the use of sediment traps for estimating upper ocean particle fluxes. *Journal of Marine Research* 65, 345-416.
- Cardinal, D., Savoye, N., Trull, T.W., Andre, L., Kopczynska, E.E., Dehairs, F., 2005. Variations of carbon remineralisation in the Southern Ocean illustrated by the Ba_{xs} proxy. *Deep-Sea Research I* 52, 355-370.
- Cassar, N., DiFiore, P., Barnett, B.A., Bender, M.L., Bowie, A.R., Tilbrook, B., Petrou, K., Westwood, K.J., Wright, S.W., Lefevre, D., 2010. The influence of iron and light on carbon export production in the subantarctic and polar frontal zones, submitted to *Biogeosciences*.
- Cavagna, A.-J., Elskens, M., Griffiths, F. B., Fripiat, F., Jacquet, S.H.M., Westwood, K.J., Dehairs, F., 2010. Contrasting regimes of productivity and potential for carbon export in the Sub-Antarctic Zone and Polar Frontal Zone south of Tasmania. *Deep-Sea Research II*, this issue.
- Cheah, W., McMin, A., Griffiths, F.B., Westwood, K., Webb, J., Molina, E., Wright S.W., van den Enden R., 2010. Assessing Sub-Antarctic Zone primary productivity from fast repetition rate fluorometry. *Deep-Sea Research II*, this issue.
- Cullen, J.J., 1995. Status of the iron hypothesis after the Open-Ocean Enrichment Experiment. *Limnology and Oceanography* 40 (7), 1336-1343.
- De La Rocha, C., Passow, U., 2007. Factors influencing the sinking of POC and the efficiency of the biological carbon pump. *Deep-Sea Research II* 54, 639-658.
- de Salas, M.F., Eriksen, R., Davidson, A.T., Wright, S., 2010. Protistan communities in the Australian sector of the subantarctic zone during SAZ-Sense, *Deep-Sea Research II*, this issue.
- Dilling, L., Alldredge, A.L., 2000. Fragmentation of marine snow by swimming macrozooplankton: A new process impacting carbon cycling in the sea. *Deep-Sea Research I* 47 (7), 1227-1245.
- Doblin M.A., Ralph P.J., Petrou K.L., Shelly K., Westwood K., van den Enden R, Wright S.W., Griffiths F.B., 2010 Diel variation of chl-a fluorescence, phytoplankton pigments and productivity in the Sub-Antarctic Zone. *Deep-Sea Research II*, this issue.
- Ebersbach, F., Trull, T., 2008. Sinking particle properties from polyacrylamide gels during the Kerguelen Ocean and Plateau compared Study (KEOPS): Zooplankton control of carbon export in an area of persistent natural iron inputs in the Southern Ocean. *Limnology and Oceanography* 53 (1), 212-224.
- Evans, C., Thomson, P.G., Davidson, A.T., Bowie, A.R., van den Enden, R., Witte, H., Brussaard, C.P.D., 2010. Potential implications of climate change-induced shifts in microbial distribution for carbon cycling in the Australian Southern Ocean. *Deep-Sea Research II*, this issue.
- Falkowski, P.G., Scholes, R.J., Boyle, E.A., Canadell, J., Canfield, D., Elser, J., Gruber, N., Hibbard, K., Hogberg, P., Linder, S., Mackenzie, F.T., Moore, B.I., Pedersen, T., Rosenthal, Y., Seitzinger, S., Smetacek, V., Steffen, W., 2000. The global carbon cycle: a test of our knowledge of Earth as a system. *Science* 290, 291-296.
- Fowler, S.W., Knauer, G.A., 1986. Role of large particles in the transport of elements and organic compounds through the oceanic water column. *Progress in Oceanography* 16 (3), 147-194.
- Francois, R., Honjo, S., Krishfield, R., Mangani, S., 2002. Factors controlling the flux of the organic carbon to the bathypelagic zone of the ocean. *Global Biogeochemical Cycles* 16 (4), 1087, 34 1-20, doi:10.1029/2001GB001722.

III. Manuscript 2

- Gonzalez, H.E., 1992. The distribution and abundance of krill faecal material and oval pellets in the Scotia and Weddell Seas (Antarctica) and their role in particulate flux. *Polar Biology* 12, 81-91.
- Gonzalez, H.E., Smetacek, V., 1994. The possible role of the cyclopoid copepod *Oithona* in retarding vertical flux of zooplankton faecal material. *Marine Ecology Progress Series* 113, 233-246.
- Griffiths, F.B., Bowie, A.R., Dehairs, F., Trull, T.W., 2010. Oceanographic setting of the Sub-Antarctic zone south of Australia. *Deep-Sea Research II*, this issue.
- Guidi, L., Jackson, G.A., Stemann, L., Carlos Miquel, J., Picheral, M., Gorsky, G., 2008. Relationship between particle size distribution and flux in the mesopelagic zone. *Deep-Sea Research I* 55, 1364-1374.
- Gust, G., Kozerski, H.-P., 2000. In situ sinking-particle flux from collection rates of cylindrical traps. *Marine Ecology Progress Series* 208, 93-106.
- Hill, K.S., Rintoul, S.R., Coleman, R., Ridgeway, K.R., 2008. Wind forced low frequency variability of the East Australia Current. *Geophysical Research Letters* 35 (L08602), doi:10.1029/2007GL032912.
- Honjo, S., 1996. Fluxes of particles to the interior of the open ocean. In: Ittekkot, V., Aschauer, P., Honjo, S., Depetris, P. (Eds.), *Particle Flux in the Oceans*. SCOPE 57, Wiley, New York, 91-154.
- Jackson, G.A., Waite, A.M., Boyd, P.W., 2005. Role of algal aggregation in vertical carbon export during SOIREE and in other low biomass environments. *Geophysical Research Letters* 32 (L13507), 1-4, doi:10.1029/2005GL023180.
- Jacquet, S.H.M., P. Lam, T. Trull, K. Buesseler, Dehairs, F., 2010. Carbon export production in the Polar Front Zone and Subantarctic Zone south of Tasmania. *Deep-Sea Research II*, this issue.
- Jouandet, M.-P., Trull, T.W., Picharel, M., Guidi, L., Ebersbach, F., Stemann, L., Blain, S., 2010. Optical imaging of mesopelagic particles indicated deep carbon flux beneath a natural iron fertilized bloom in the Southern Ocean, submitted to *Limnology and Oceanography*.
- Klaas, C., Archer, D.E., 2002. Association of sinking organic matter with various types of mineral ballast in the deep sea: Implication for the rain ratio. *Global Biogeochemical Cycles* 16 (4), 63 61-14, doi:10.1029/2001GB001765.
- Kwon, E.Y., Primeau, F., Sarmiento, J.L., 2009. The impact of remineralization depth on the air-sea carbon balance. *Nature Geoscience* 2, 630-635.
- Lam, P.J., Bishop, J.K.B., 2007. High biomass, low export regimes in the Southern Ocean. *Deep-Sea Research II* 54, 601-638.
- Lampitt, R.S., Antia, A.N., 1997. Particle flux in the deep seas: regional characteristics and temporal variability. *Deep-Sea Research I* 44 (8), 1377-1403.
- Lannuzel, D., Remenyi, T., Lam, P.J., Townsend, A., Ibisani, E., Butler, E., Wagener, T., Schoemann, V., Bowie, A.R., 2010. Distribution of dissolved and particulate iron in the sub-Antarctic and Polar Frontal Southern Ocean (Australian sector). *Deep-Sea Research II*, this issue.
- Lutz, M., Dunbar, R., Caldeira, K., 2002. Regional variability in the vertical flux of particulate organic carbon in the ocean interior. *Global Biogeochemical Cycles* 16 (3), 1037, 11 11-18, doi:10.1029/2000GB001383.
- Lutz, M.J., Caldeira, K., Dunbar, R.B., Behrenfeld, M.J., 2007. Seasonal rhythms of net primary production and particulate organic carbon flux to depth describe the efficiency of biological pump in the global ocean. *Journal of Geophysical Research* 112 (C10011), 1-26, doi:10.1029/2006JC003706.
- Martin, J.H., Knauer, G.A., Karl, D.M., Broenkow, W.W., 1987. VERTEX: carbon cycling in the northeast Pacific. *Deep-Sea Research* 34 (2), 267-285.
- Matear, R., Hirst, A.C., 1999. Climate change feedback on the future oceanic CO₂ uptake. *Tellus* 51 (3), 722-733.
- Menden-Deuer, S., Lessard, E.J., 2000. Carbon to volume relationship for dinoflagellates, diatoms, and other protist plankton. *Limnology and Oceanography* 45 (3), 569-579.
- Michaels, A.F., Silver, M.W., 1988. Primary production, sinking fluxes and the microbial food web. *Deep-Sea Research A* 35 (4), 473-490.
- Mongin, M., Matear, R., Chamberlain, M., 2010. Seasonal and spatial variability of remotely sensed chlorophyll and physical fields in the SAZ-Sense region. *Deep-Sea Research II*, this issue.

III. Manuscript 2

Noji, T.T., Estep, K.W., MacIntyre, F., Norrrbin, F., 1991. Image analysis of faecal material grazed upon by three species of copepods: Evidence for coprorhexy, coprophagy, and coprochaly. *Journal of the Marine Biological Association of the United Kingdom* 71 (2), 465-480.

Morel, F.M.M., Rueter, J.G., Price, N.M., 1991. Iron nutrition of phytoplankton and its possible importance in the ecology of ocean regions with high nutrients and low biomass. *Oceanography* 4 (2), 56-61.

Passow, U., 2004. Switching perspectives: Do mineral fluxes determine particulate organic carbon or vice versa? *Geochemistry Geophysics Geosystems* 5 (4), 1-5, doi:10.1029/2003GC000670.

Passow, U., Alldredge, A.L., Logan, B.E., 1994. The role of particulate carbohydrate exudates in the flocculation of diatom blooms. *Deep-Sea Research I* 42 (2), 335-357.

Pearce I., Davidson A., Thomson P., Wright S., van den Enden R., 2010. Marine microbial ecology in the Subantarctic Zone: rates of bacterial and phytoplankton growth and grazing by heterotrophic protists. *Deep-Sea Research II*, this issue.

Peterson, M.L., Wakeham, S.G., Lee, C., Askea, M.A., Miquel, J.C., 2005. Novel techniques for collection of sinking particles in the ocean and determining their settling rates. *Limnology and Oceanography Methods* 3, 520-532.

Peterson, M.L., Fabres, J., Wakeham, S.G., Lee, C., Miquel, J.C., 2009. Sampling the vertical particle flux in the upper water column using a large diameter free-drifting Net-Trap adapted to an Indented Rotating Sphere sediment trap. *Deep-Sea Research II* 56, 1547-1557.

Petrou K., Hassler C.S, Doblin M.A., Shelly K., Schoemann V., van den Enden R., Wright S.W., Ralph P.J., 2010. Iron limitation and high light stress on phytoplankton populations from the Australian sub-Antarctic zone (SAZ). *Deep-Sea Research II*, this issue.

Ploug, H., Iversen, M.H., Fischer, G., 2008. Ballast, sinking velocity, and apparent diffusivity within marine snow and zooplankton fecal pellets: Implications for substrate turnover by attached bacteria. *Limnology and Oceanography* 52 (5), 1878-1886.

Pollard, R., Sanders, R., Lucas, M., Statham, P., 2007. The Crozet Natural Iron Bloom and Export Experiment (CROZEX). *Deep-Sea Research II* 54 (18-20), 1905-1914.

Reigstad, M., Wexel Riser, C., Wassmann, P., Ratkova, T., 2008. Vertical export of particulate organic carbon: Attenuation, composition and loss rates in the northern Barents Sea, *Deep-Sea Research II* 55, 2308-2319.

Rintoul, S., Trull, T.W., 2001. Seasonal evolution of the mixed layer in the Subantarctic Zone south of Australia. *Journal of Geophysical Research* 106 (C12), 31 447-462, doi:10.1029/2000JC000329.

Salter, I., Lampitt, R.S., Sanders, S., Poulton, A.J., Kemp, A.E.S., Boorman, B., Saw, K., Pearce, R., 2007. Estimating carbon, silica and diatom export from a naturally fertilised phytoplankton bloom in the Southern Ocean using PELAGRA: a novel drifting sediment trap. *Deep-Sea Research II* 54, 2223-2259.

Sarmiento, J.L., Le Quéré, C., 1996. Oceanic Carbon Dioxide Uptake in a Model of Century-Scale Global Warming. *Science* 274, 1346-1350.

Sedwick, P.N., DiTullio, G.R., Hutchins, D.A., Boyd, P.W., Griffiths, B.F., Crossley, A.C., Trull, T.W., Quéguiner, B., 1999. Limitation of algal growth by iron deficiency in the Australian Subantarctic region. *Geophysical Research Letters* 26 (18), 2865-2868, doi:10.1029/1998GL002284.

Sedwick, P.N., Bowie, A., Trull, T.W., 2008. Dissolved iron in the Australian sector of the Southern Ocean (CLIVAR SR3 section): Meridional and seasonal trends. *Deep-Sea Research I* 55, 911-925.

Stemmann, L., Jackson, G.A., Ianson, D., 2004. A vertical model of particle size distributions and fluxes in the midwater column that includes biological and physical processes - Part I: model formulation. *Deep-Sea Research I* 51, 865-884.

Stemmann, L., Eloire, D., Sciandra, A., Jackson, G.A., Guidi, L., Picheral, M., Gorsky, G., 2008. Volume distribution for particles between 3.5 and 2000 μm in the upper 200 m region of the South Pacific Gyre. *Biogeosciences* 5, 299-310.

Turner, J.T., 2002. Zooplankton fecal pellets, marine snow and sinking phytoplankton blooms. *Aquatic Microbial Ecology* 27, 57-102.

Trull, T.W., Bray, S.G., Buesseler, K.O., Lamborg, C.H., Manganini, S., Moy, C., Valdes, J., 2008. In situ measurement of mesopelagic particle sinking rates and the control of carbon transfer to

III. Manuscript 2

the ocean interior during the Vertical Flux in the Global Ocean (VERTIGO) voyages in the North Pacific. *Deep-Sea Research II* 55 (14-15), 1684-1695.

Trull, T.W., Sedwick, P.N., Griffiths, B.F., Rintoul, S.S., 2001a. Introduction to special section: SAZ project. *Journal of Geophysical Research* 106 (C12), 31/425-429, doi:10.1029/2001JC001008.

Trull, T.W., Bray, S.G., Manganini, S.J., Honjo, S., Francois, R., 2001b. Moored sediment trap measurements of carbon export in the Subantarctic and Polar Frontal Zones of the Southern Ocean, south of Australia. *Journal of Geophysical Research* 106 (C12), 31/489-509, doi:10.1029/2000JC000308.

Turner, J.T., 2002. Zooplankton fecal pellets, marine snow and sinking phytoplankton blooms. *Aquatic Microbial Ecology* 27 (1), 57-102.

Volck, T., Hoffert, M.I., 1985. Ocean carbon pumps: analysis of relative strengths and efficiencies in ocean-driven atmospheric CO₂ changes. *Geophysical Monographs* 32, 99-110.

Waite, A.M., Gustafsson, Ö., Lindahl, O., Tiselius, P., 2005. Linking ecosystem dynamics and biogeochemistry: Sinking fractionation of organic carbon in a Swedish fjord. *Limnology and Oceanography* 50 (2), 658-671.

Waite, A.M., Nodder, S.D., 2001. The effect of in situ iron addition on the sinking rates and export flux of Southern Ocean diatoms. *Deep-Sea Research II* 48, 2635-2654.

Wang, X., Matear, R., Trull, T.W., 2003. Nutrient utilization ratios in the Polar Frontal Zone in the Australian sector of the Southern Ocean: a model. *Global Biogeochemical Cycles* 17 (1), 1009, doi:10.1029/2002GB001938.

Wassmann, P., 1990. Relationship between primary and export production in the boreal coastal zone of the North Atlantic. *Limnology and Oceanography* 35 (2), 464-471.

Wassmann, P., Carroll, J., Bellerby, R.G.J., 2008. Carbon flux and ecosystem feedback in the northern Barents Sea in an area of climate change: An introduction. *Deep-Sea Research II* 55, 2143-2153.

Westwood, K.J., Griffiths, F.B., Webb, J., 2010. Primary productivity in the Sub-Antarctic and Polar Frontal zones south of Tasmania, Australia; SAZ-Sense survey, 2007. *Deep-Sea Research II*, this issue.

Wexels Riser, C., Wassmann, P., Reigstad, M., Seuthe, L., 2008. Vertical flux regulation by zooplankton in the northern Barents Sea during Arctic spring. *Deep-Sea Research II* 55, 2320-2329.

Wilson, S.E., Steinberg, D.K., Buesseler, K.O., 2008. Changes in fecal pellet characteristics with depth as indicators of zooplankton repackaging of particles in the mesopelagic zone of the subtropical and subarctic North Pacific Ocean. *Deep-Sea Research II* 55 (14-15), 1636-1647.

Figure captions

Fig. 1.

Map of SAZ-Sense cruise track and station locations, superimposed on the surface chlorophyll distribution (MERIS ocean colour 1-km resolution composite image for 5-11 Feb. 2007 courtesy of the Plymouth Marine Laboratory Remote Sensing Group; colour-scale is logarithmic from 0.01 to 60 $\mu\text{g Chla L}^{-1}$). Process Station P1, west of Tasmania in low-biomass Subantarctic waters was visited first, followed by P2 in the Polar Frontal Zone, and finally P3 in the high biomass SAZ east of Tasmania. Each Process Station was occupied for approximately 6 days. The image corresponds to the time of the transect from P2 to P3.

Fig. 2.

Biomass distributions at P1, P2 and P3 based on (upper panel) the particulate contribution to beam attenuation, at 660 nm using a Wetlabs C-Star transmissometer and (lower panel) chlorophyll fluorescence, at 695 nm from excitation at 470 nm using a Wetlabs ECO-FI fluorometer. The lower values of near-surface fluorescence were obtained during daylight, and reflect insolation quenching.

Fig. 3.

Particle categories as defined from photo-microscopy of particles collected by the 24 hour deployments of the free-drifting gel traps: Fluff-aggregates (c and k), faecal-aggregates (b, g, and m) cylindrical faecal pellets (a, f and j), ovoid faecal pellets (e, h, and i), and phyto-cells (d and l). While the fluff-aggregates resemble phyto-detritus (k) or feeding-structures (large particles in c), the faecal-aggregates appear to be composed of relatively compact material (b), and sometimes even have distinct shapes similar to a pellet (upper left particle in g) or they can be made of somewhat more degraded faecal material (upper particle in m). The large cylindrical faecal pellets are likely to originate from euphausiids (a and left pellet in j), whereas the smaller pellets presumably are of copepod origin (f, and upper and right pellet in j). The ovoid faecal pellets show two size classes, the larger pellets (i and left pellet in e) versus the smaller ones (h and right pellet in e). Phyto-cells are in general the smallest particles found.

Fig. 4.

Images of the gels (grid cells: 12.5x14 mm) from the gel traps showing the difference among the sites. The SAZ stations are shown at top (images A and B from station P1; images C and D from station P3) and the PFZ station at bottom (images E and F from station P2). The dominance of larger particles in the SAZ (A – D) in contrast to small particles in the PFZ (E, F) is clear. Particle variations with depth were complex (see text), but abundance generally decreased from the shallowest to the deepest trap at

III. Manuscript 2

each station, as shown here from left to right (images A, C, E from 140 m; images B, D, F from 290 m).

Fig. 5.

Detailed photos of individual particles collected with the gel traps are reflecting the difference in particles size: the SAZ (upper panel) is dominated by large particles, while in the PFZ (lower panel) phyto-cells and small aggregates are more abundant. SAZ-particles represent (from left to right in the upper panel): intact ovoid and cylindrical faecal pellet, degrading cylindrical faecal pellet and faecal-aggregate. PFZ-particles are mainly phyto-cells (distributed over all images in the lower panel) and small fluff-aggregates and fluffy faecal-aggregates (lower left image). Scale bar for all photos: 1 mm.

Fig. 6.

Number flux spectra from the Gel-traps, indicating the variations with depth (140, 190, 240 and 290 m).

Fig. 7.

Size fractioned volume flux spectra showing the greater importance of large particles to the volume flux than to the numerical flux (compare Fig. 6).

Fig. 8.

Estimated POC flux spectra from the piece-wise volume to POC conversion function that incorporates carbon content estimates for phytoplankton, faecal pellets, and aggregates (see 2.3.2). This function shifts the peak carbon flux to somewhat smaller particle sizes than the peak volume flux (because of the increasing porosity of large aggregates as modelled by fractal geometry).

Fig. 9.

Cumulative POC flux as a function of cumulative numerical flux indicating that more than half the flux is delivered by the largest 10% of the particles, even at the P2 site where small particles were abundant (see Fig. 4).

Fig. 1.

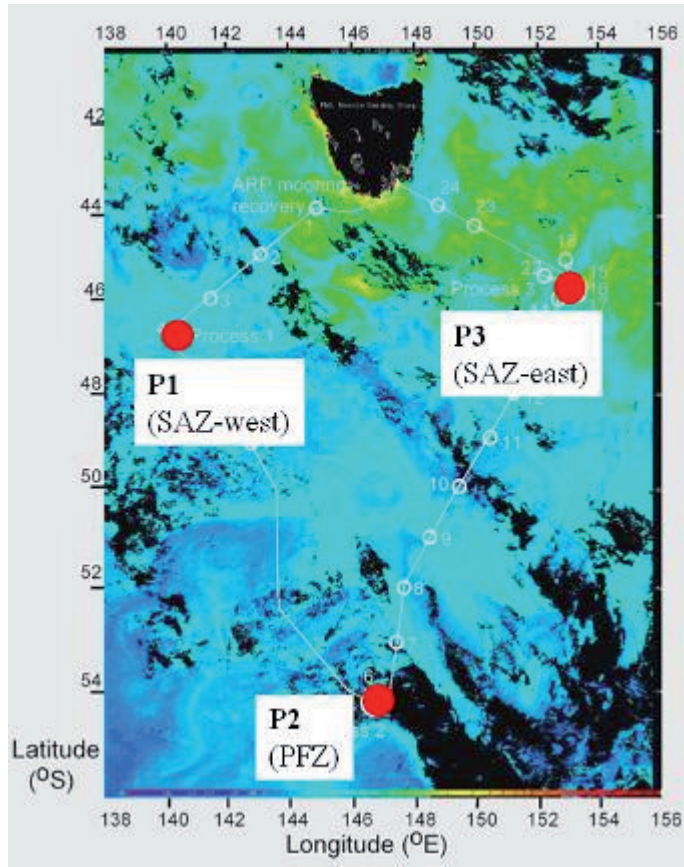


Fig. 2.

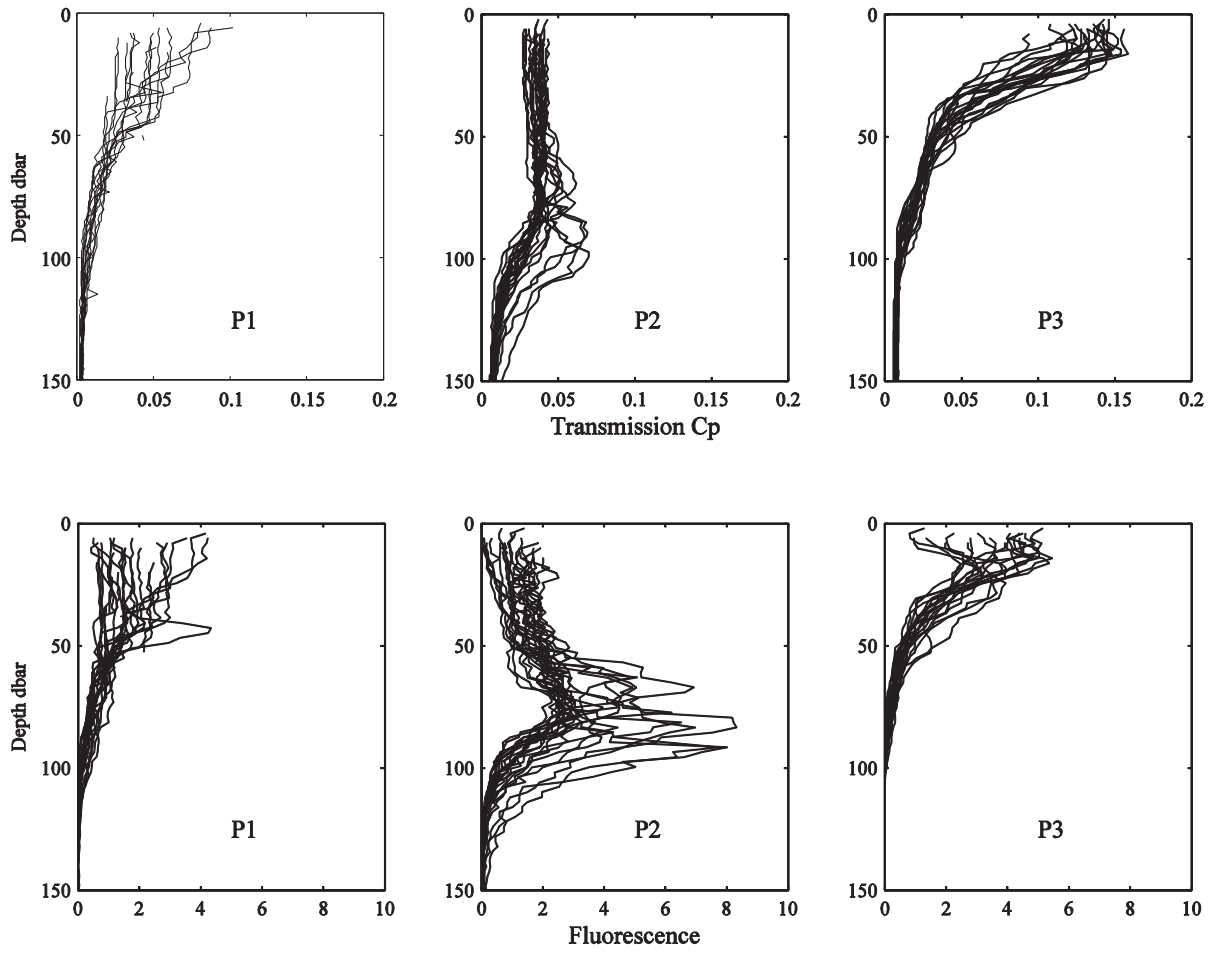


Fig. 3.

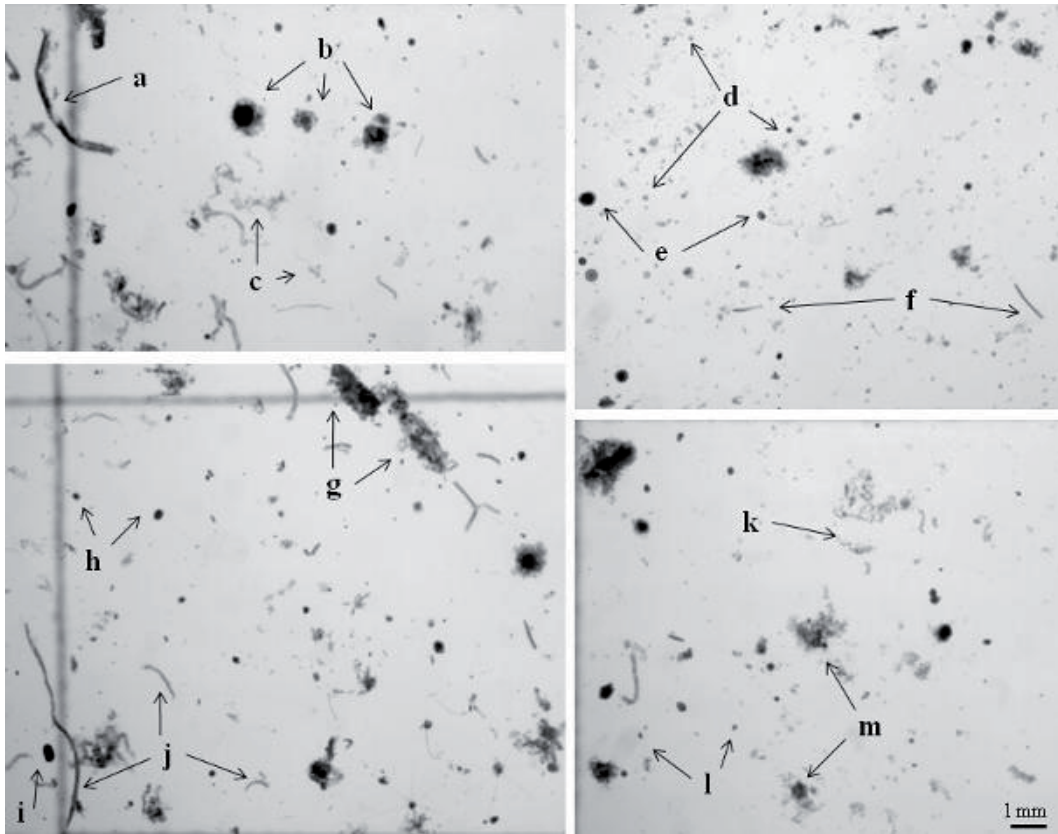


Fig. 4.

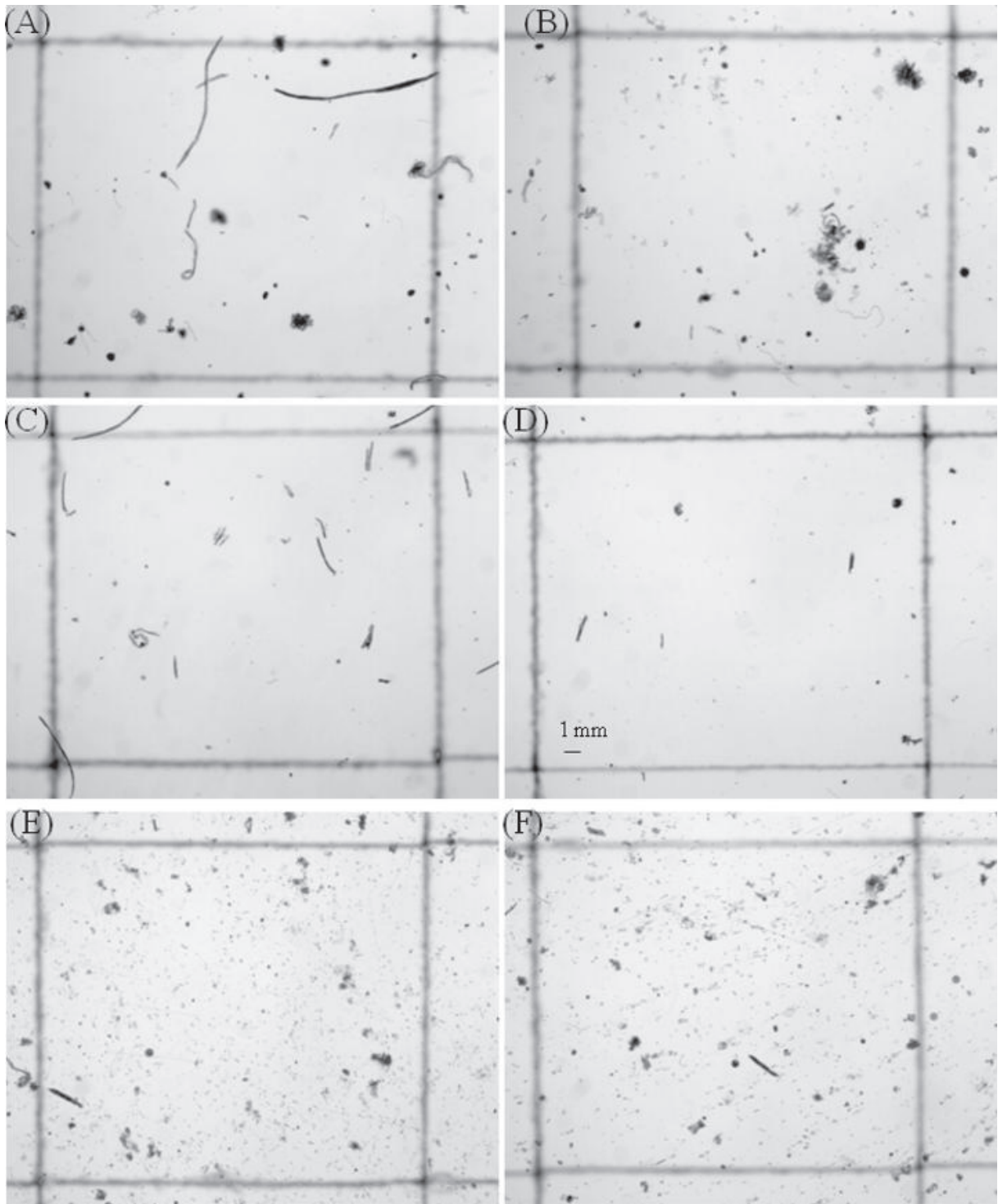


Fig. 5.

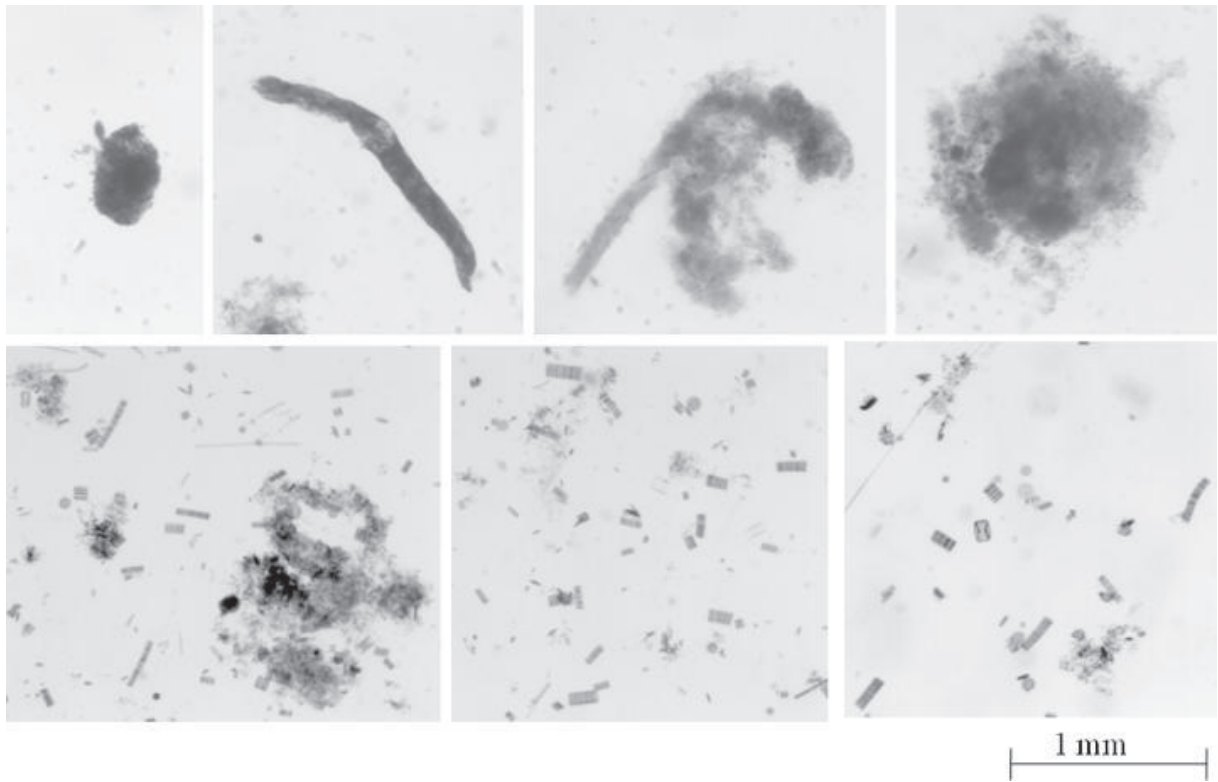


Fig. 6.

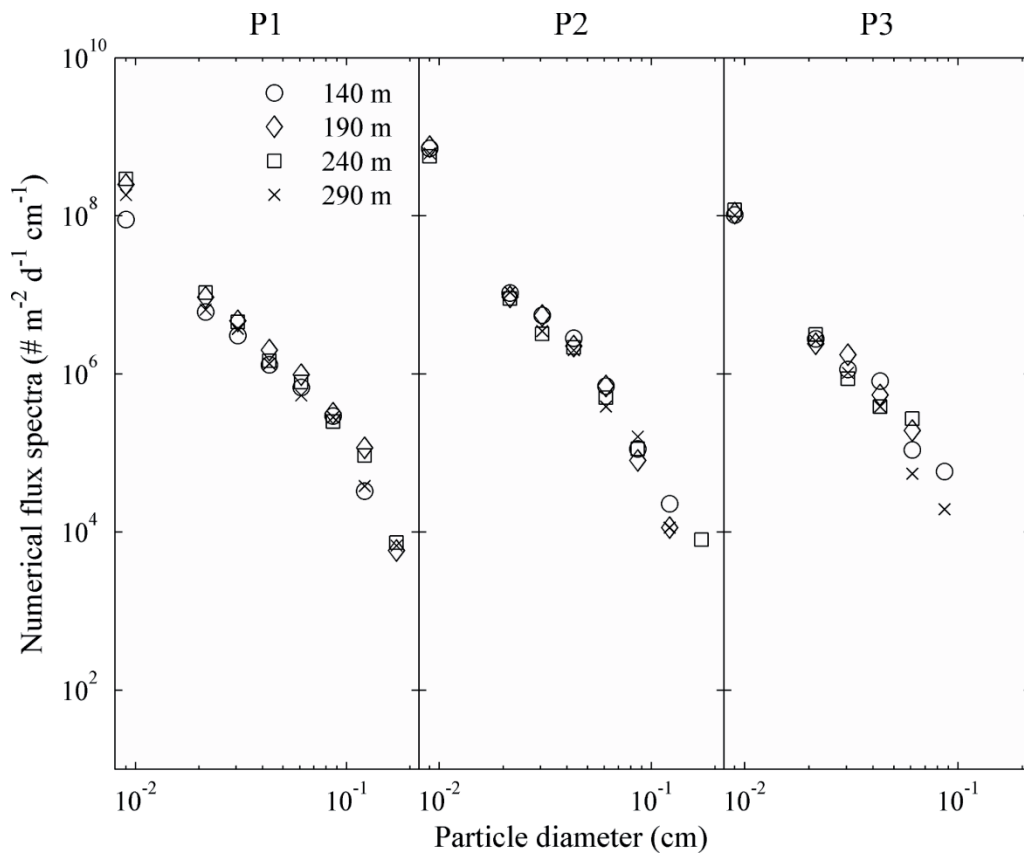


Fig. 7.

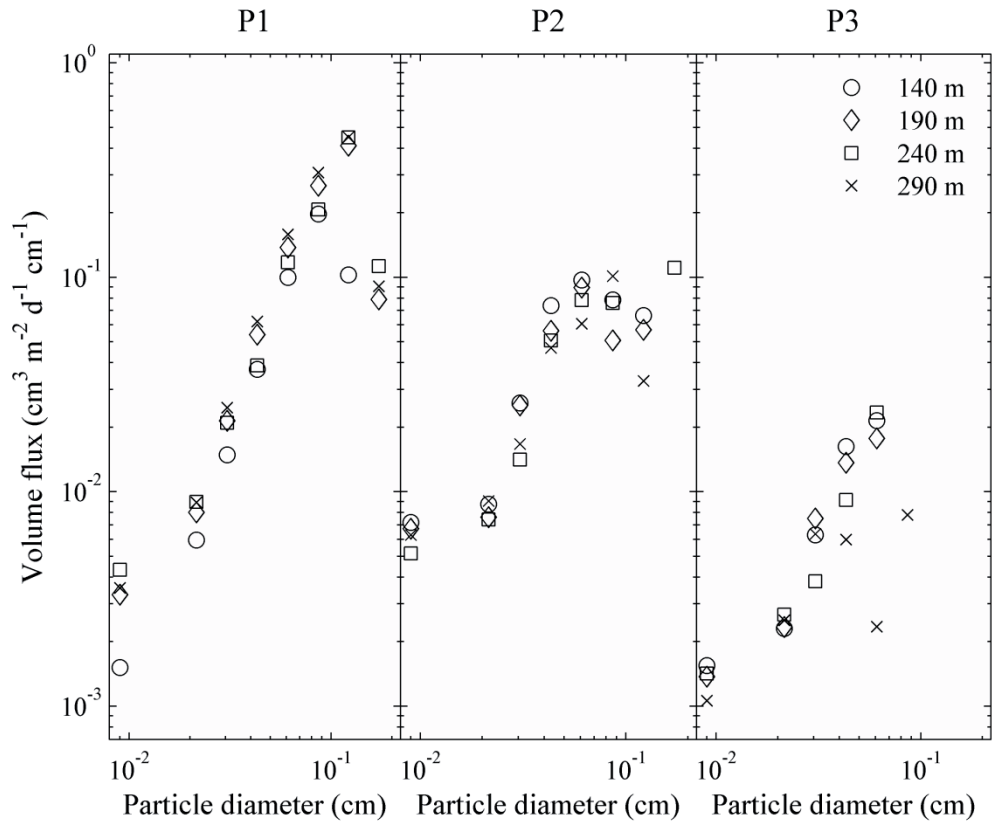


Fig. 8.

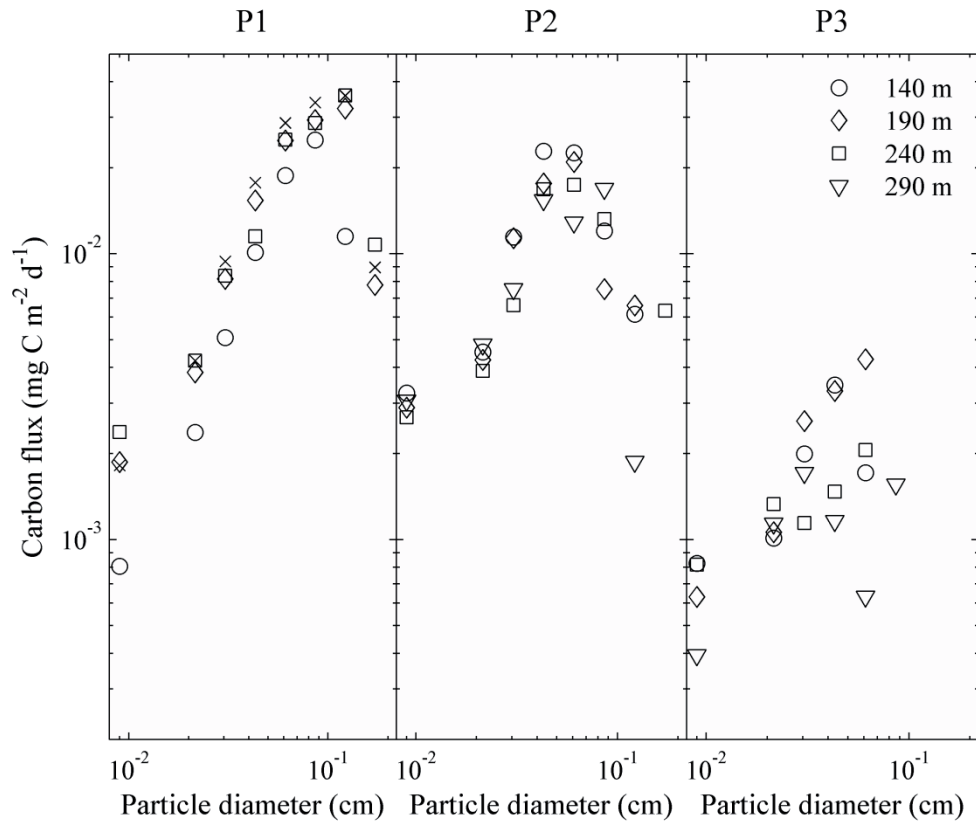


Fig. 9.

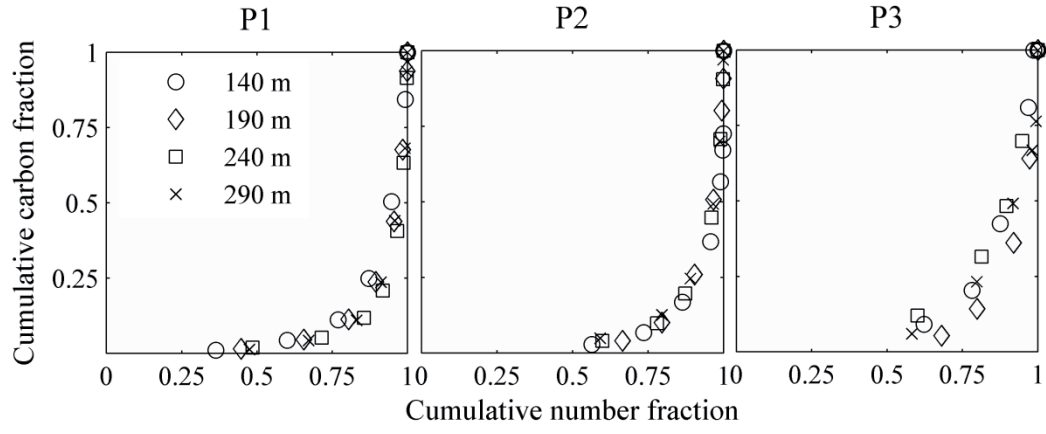


Table 1. Water column properties at the process stations

Site i.d.	Mixed layer depth (m)	Euphotic Layer		Surface		Integrated (0-150 m)		Surface		Integrated (0-100 m)		Primary production	
		Layer Depth (m)	Chl a ($\mu\text{g L}^{-1}$)	Chl a (mg m^{-2})	Chl a (mg m^{-2})	POC ($\text{mmolC m}^{-2} \text{d}^{-1}$)	POC ($\text{mmolC m}^{-2} \text{d}^{-1}$)	POC ($\text{mmolC m}^{-2} \text{d}^{-1}$)	POC ($\text{mmolC m}^{-2} \text{d}^{-1}$)	GPP ($\text{mmolC m}^{-2} \text{d}^{-1}$)	f-ratio	NPP ($\text{mmolC m}^{-2} \text{d}^{-1}$)	
P1	41 \pm 18	61 \pm 5	1.1 \pm 0.5	46.0 \pm 11.5	5.2 \pm 0.9	353.2 \pm 12.2	93 \pm 49	0.28 \pm 0.19	31 \pm 39				
P2	53 \pm 6	76 \pm 14	0.3 \pm 0.1	58.8 \pm 2.9	3.8 \pm 1.9	422.6 \pm 61.2	37 \pm 7	0.25 \pm 0.05	9 \pm 2				
P3	16 \pm 2, 79 \pm 2	47 \pm 13	1.9 \pm 0.3	62.4 \pm 20.0	13.7 \pm 1.1	580.5 \pm 14.0	60 \pm 29	0.21 \pm 0.05	12 \pm 1				

1. mixed layer depth calculated after Rintoul and Trull, 2001; see Mongin et al. this issue for discussion of 2 mixed layers at P3
2. euphotic depth and integrated Chla from Westwood et al., this issue
3. Chla measurements at 10 m from Pearce et. al, this issue
4. surface POC concentrations from Niskin bottle samples (Trull and Davies, unpublished)
5. primary production estimates as discussed in detail in Cavagna et al., this issue; large stdev. at P1 is due to different water masses
6. f-ratio=nitrate uptake/N-uptake, NPP=C-uptake x f-ratio

Table 2. Deployment schedules for the free-drifting sediment trap arrays

Site	Array	Trap Depths (m)	Event	Time (UTC)	Latitude	Longitude	Duration (d)	Drift (km)
P1	Gel traps	140, 190, 240, 290	Deploy	22-Jan-07 04:30	46° 20.50' S	140° 34.60' E	1.08	13
			Recover	23-Jan-07 06:29	46° 27.35' S	140° 32.23' E		
	PPS3/3 trap	150	Deploy	22-Jan-07 00:57	46° 25.38' S	140° 29.67' E	6.34	22
			Recover	28-Jan-07 21:15	46° 36.80' S	140° 25.65' E		
P2	Gel traps	140, 190, 240, 290	technical problems					
			precluded deployment					
	PPS3/3 trap	150	Deploy	31-Jan-07 16:15	54° 59.90' S	145° 56.90' E	1.14	16
			Recover	1-Feb-07 19:37	54° 03.45' S	146° 10.44' E		
P3	Gel traps	140, 190, 240, 290	Deploy	31-Jan-07 14:48	54° 00.03' S	145° 58.05' E	6.13	121
			Recover	5-Feb-07 22:40	54° 34.96' S	147° 32.94' E		
	PPS3/3 trap	150	Deploy	31-Jan-07 19:33	53° 59.85' S	145° 54.50' E	5.75	93
			Recover	6-Feb-04 04:24	54° 26.60' S	147° 06.62' E		
P3	Gel traps	140, 190, 240, 290	Deploy	10-Feb-07 23:26	45° 32.10' S	153° 11.48' E	0.97	9
			Recover	11-Feb-07 22:45	45° 29.44' S	153° 17.52' E		
	PPS3/3 trap	150	Deploy	10-Feb-07 20:01	45° 29.99' S	153° 11.94' E	6.06	49
			Recover	16-Feb-07 23:39	45° 24.52' S	153° 48.82' E		
IRS traps	170, 320	Deploy	10-Feb-07 21:41	45° 31.04' S	153° 11.87' E	5.89	47	
		Recover	16-Feb-07 15:21	45° 35.34' S	153° 47.09' E			

1. trap depths were constant within the 4 m depth and 5' time resolutions of the sensor on the deepest trap on each array.

Table 3. Particle fluxes at 150 m depth from the 6-day free-drifting deployments of the 12-cup-carousel cylindrical PPS3/3-trap.

Cup i.d. #	Cup opening date	Cup opening time	Cup duration hours	Cup poison type	POC flux per cup $\mu\text{mol m}^{-2} \text{d}^{-1}$	PON flux per cup $\mu\text{mol m}^{-2} \text{d}^{-1}$	BSi flux per cup $\mu\text{mol m}^{-2} \text{d}^{-1}$	PIC flux per cup $\mu\text{mol m}^{-2} \text{d}^{-1}$	POC/PON ratio	POC/BSi ratio	POC/PIC ratio
P 1											
3	23. Jan	07:00	12	none	1921	269	141	109	7.1	14	18
4	23. Jan	19:00	12	none	2589	380	108	138	6.8	24	19
5	24. Jan	07:00	12	merc. chlor.	1842	301	98	80	6.1	19	23
6	24. Jan	19:00	12	merc. chlor.	1648	227	56	95	7.3	29	17
9	26. Jan	07:00	12	none	4201	603	267	410	7.0	16	10
10	26. Jan	19:00	12	none	6145	959	662	1318	6.4	9	5
11	27. Jan	07:00	12	merc. chlor.	2587	382	169	301	6.8	15	9
12	27. Jan	19:00	12	merc. chlor.	5777	2219	128	423	2.6	45	14
				mean	3339	667	204	359	5.0	16	9
				std.dev.	1805	671	196	412	1.5	11	6
P 2											
3	23. Jan	07:00	12	none	2385	378	3154	360	6.3	0.76	7
4	23. Jan	19:00	12	none	1897	281	1945	165	6.7	0.98	11
5	24. Jan	07:00	12	merc. chlor.	1238	187	2220	223	6.6	0.56	6
6	24. Jan	19:00	12	merc. chlor.	1765	253	2516	260	7.0	0.70	7
9	26. Jan	07:00	12	none	3751	535	1866	436	7.0	2.01	9
10	26. Jan	19:00	12	merc. chlor.	1649	240	2299	266	6.9	0.72	6
				mean	2114	312	2333	285	6.8	0.91	7
				std.dev.	884	126	467	98	0.3	0.53	2
P 3											
3	23. Jan	07:00	12	merc. chlor.	1708	296	25	105	5.8	69	16
4	23. Jan	19:00	12	merc. chlor.	685	132	18	44	5.2	39	15
5	24. Jan	07:00	12	none	553	86	14	23	6.4	40	24
6	24. Jan	19:00	12	none	680	119	13	43	5.7	52	16
9	26. Jan	07:00	12	merc. chlor.	880	127	19	43	6.9	47	20
10	26. Jan	19:00	12	merc. chlor.	688	104	11	44	6.6	61	15
11	27. Jan	07:00	12	none	1073	153	13	65	7.0	81	16
12	27. Jan	19:00	12	none	594	86	11	33	6.9	53	18
				mean	858	138	15	50	6.2	55	17
				std.dev.	382	68	5	25	1	14	3

1. times are UTC, local time was UTC+11h, and thus cups ran dusk to dawn (18:00 to 06:00) and dawn to dusk (06:00 to 18:00) daily
2. particles were washed through a 350 μm screen to remove zooplankton and collected on a 1 mm silver filter
3. trace metal fluxes were measured in cups # 1, 2, 7 and 8 for each trap, respectively, and additionally in cups 11 and 12 at P2 (and are reported in Bowie et al., 2009)

III. Manuscript 2

Table 4. Particle fluxes separated by sinking rate from the 5-day free-drifting deployments of the IRS traps at 170 and 320 m depth.

Trap Depth m	Cup i.d. #	Sinking Rate $m\ d^{-1}$	Cup Duration minutes	POC flux per cup $\mu mol\ m^{-2}\ d^{-1}$	POC flux per cup dur. $\mu mol\ m^{-2}\ d^{-1}\ min^{-1}$	POC flux fraction %	POC flux cumulative %	corr-POC flux fraction %	corr-POC flux cumulative %	BSi flux per cup $\mu mol\ m^{-2}\ d^{-1}$	BSi flux per cup dur. $\mu mol\ m^{-2}\ d^{-1}\ min^{-1}$	BSi flux fraction %	BSi flux cumulative %	POC/BSi ratio mol/mol
P2				Begin Collection:	31-Jan-07 21:00	End Collection:	4-Feb-07 21:00							
170	1	>850	1	54	54	3	3	0	0	14	14	1	1	4.0
	2	410	1	318	318	17	20	21	21	372	372	27	28	0.9
	3	205	2	106	53	6	26	4	26	40	20	3	30	2.7
	4	137	2	85	42	5	31	3	29	39	20	3	33	2.2
	5	102	2	85	42	5	35	3	31	34	17	2	36	2.5
	6	51	8	108	13	6	41	5	36	96	12	7	43	1.1
	7	26	16	188	12	10	52	11	47	151	9.4	11	53	1.2
	8	13	32	176	5.5	10	61	10	57	158	4.9	11	65	1.1
	9	6	64	152	2.4	8	70	8	65	115	1.8	8	73	1.3
	10	2.3	231	504	2.2	28	97	35	100	377	1.6	27	100	1.3
	11	2.3	1	49	49	3	100	0	100	1	0.7	0	100	74
	Total			1826						1395				1.3
320														
	1	>850	1	77	77	7	7	4	4	3	2.8	0	0	28
	2	410	1	106	106	9	16	10	13	36	36	6	6	3.0
	3	205	2	138	69	12	28	16	29	68	34	11	18	2.0
	4	137	2	76	38	7	35	4	33	18	9.1	3	21	4.2
	5	102	2	94	47	8	43	7	40	40	20	7	27	2.3
	6	51	8	93	12	8	51	7	47	87	11	14	42	1.1
	7	26	16	118	7.4	10	61	12	59	57	3.5	9	51	2.1
	8	13	32	85	2.7	7	69	5	64	57	1.8	9	60	1.5
	9	6	64	128	2.0	11	80	14	78	68	1.1	11	72	1.9
	10	2.3	231	170	0.7	15	95	22	100	166	0.7	27	99	1.0
	11	2.3	1	58	58	5	100	0	100	7	6.6	1	100	8.7
	Total			1144						607				1.9
P3				Begin Collection:	10-Feb-07 23:00	End Collection:	15-Feb-07 23:00							
170	1-11	>2.3	360	864	2.4	100	100			11	0.03	100	100	76
	Total			864						11				76

III. Manuscript 2

320	1	>850	1	95	95	51	51	<1	<1	0	0	>95
		2.3-										
	2-11	850	359	90	0.3	49	100	5	0.01	100	100	20
	Total			185				5				37

1. times are UTC, local time was UTC+11h

2. all particles were collected on 1 mm silver filters, and the very few zooplankton present in a few fractions were removed manually.

3. corr-POC flux and corr-POC cumulative flux are values corrected for possible carry-over of slow-sinking particles from one IRS cycle to the next - see text for discussion.

Table 5. Particle categories based on microscopic observations of the polyacrylamide gels

Category	Appearance	Size range (μm^3)
Aggregates		
fluff-aggregate	(flu) amorphous shapes, fluffy, brownish in colour	1 – 5400
faecal-aggregate	(fae) composed of distinctly shaped smaller particles, especially faecal pellets. brownish in colour	0.07 – 1000
Phytoplankton cells		
phyto-cell	(phy) diatom chains or individual diatom cells	0.07 – 1
Faecal pellets		
cylindrical pellet	(cyl) intact cylindrically formed faecal pellet, brown colour	0.04 – 1600
ovoid pellet	(ovo) intact faecal pellet of oval form, dark brown/black	0.06 – 100

Table 6. Particle number and volume fluxes and fractional contributions from different particle types

Site	Depth	Numerical Flux	Fractional contributions (in %)				Volume Flux	Fractional contributions (in %)					
m	# m ⁻² d ⁻¹	flu	fae	cyl	ovo	phy	cm ³ m ⁻² d ⁻¹	flu	fae	cyl	ovo	phy	
P1	140	32	2	36	5	15	40	0.46	0	82	17	2	0
	190	73	4	28	1	11	55	0.98	0	95	4	1	0
	240	82	0	29	1	12	58	0.96	0	98	1	1	0
	290	53	0	28	2	17	54	0.94	0	93	4	2	0
P2	140	177	0	17	2	7	74	0.92	0	93	6	0	0
	190	183	-	15	5	9	71	0.29	-	91	7	1	0
	240	139	1	16	2	7	74	0.34	0	65	32	2	0
	290	151	0	17	1	7	74	0.27	0	81	17	1	0
P3	140	27	-	21	7	18	53	0.05	-	37	60	2	0
	190	29	-	20	5	27	47	0.04	-	81	16	1	0
	240	31	-	18	7	11	64	0.04	-	30	67	2	0
	290	26	-	15	4	16	65	0.03	-	70	24	5	0

1. - indicates no particle of this type observed.

2. particle types as defined in Table 5.

Table 7. POC fluxes and fractional contributions from identified particle types, as estimated from imaged areas

Site i.d.	Depth m	Total		flu		fae		cyl		ovo		phy	
		POC flux $\mu\text{mol m}^{-2} \text{d}^{-1}$	fraction %	POC flux $\mu\text{mol m}^{-2} \text{d}^{-1}$	fraction %	POC flux $\mu\text{mol m}^{-2} \text{d}^{-1}$	fraction %	POC flux $\mu\text{mol m}^{-2} \text{d}^{-1}$	fraction %	POC flux $\mu\text{mol m}^{-2} \text{d}^{-1}$	fraction %	POC flux $\mu\text{mol m}^{-2} \text{d}^{-1}$	fraction %
P1	140	6141.9	0	8.9	0	5731.7	93	363.9	6	37.1	1	0.4	0
	190	10280.9	0	38.6	0	9991.6	97	187.8	2	61.9	1	1.0	0
	240	10567.2	0	5.1	0	10482.0	99	33.0	0	45.5	1	1.3	0
P2	290	8103.2	0	0.0	0	7907.0	97	133.0	2	62.1	1	0.8	0
	140	9508.2	0	2.5	0	9219.8	97	266.9	3	15.7	0	3.2	0
	190	5928.5	-	-	-	5815.1	98	96.9	2	13.7	0	2.9	0
P3	240	5578.3	0	11.0	0	5008.3	90	528.5	9	28.3	1	2.2	0
	290	5196.5	0	16.9	0	4936.1	95	226.3	5	14.5	0	2.7	0
	140	752.3	-	-	-	611.1	81	136.5	18	4.2	1	0.5	0
	190	988.9	-	-	-	951.9	96	33.7	4	2.9	0	0.4	0
	240	568.0	-	-	-	434.7	77	128.5	23	4.3	1	0.5	0
	290	549.1	-	-	-	513.1	94	29.5	5	5.9	1	0.5	0

1. - indicates no particle of this type observed.
2. particle types as defined in Table 5.

Table 8. Median characteristics of the particle types

Site i.d.	Depth m	flu		fae		esd		cyl		ovo		l		ar		phy	
		vol μm^3	esd mm	ar %	vol μm^3	esd mm	ar %	vol μm^3	l mm	ar %	vol μm^3	l mm	ar %	vol μm^3	esd mm	ar %	
P1	140	0.6	1.1	60	8.4	2.5	5.3	58	0.60	19	3.5	0.2	76	0.1	62		
	190	0.6	1.1	56	7.4	2.4	5.9	56	0.62	22	2.1	0.2	76	0.1	62		
	240	0.6	1.1	65	4.5	2.1	4.9	59	0.54	23	1.9	0.2	78	0.1	61		
P2	290	-	-	-	6.2	2.3	5.3	59	0.64	17	2.5	0.2	98	0.1	61		
	140	1.0	1.2	50	4.1	2.0	0.5	63	0.23	24	1.4	0.1	77	0.1	59		
	190	-	-	-	4.3	2.0	0.2	60	0.15	28	0.9	0.1	76	0.1	59		
P3	240	0.6	1.1	56	3.9	2.0	0.3	62	0.17	27	1.1	0.1	76	0.1	59		
	290	0.8	1.1	54	3.5	1.9	0.3	62	0.18	25	1.4	0.1	77	0.1	60		
	140	-	-	-	2.8	1.8	13.9	56	0.90	13	0.6	0.1	79	0.1	63		
P4	190	-	-	-	4.3	2.0	7.9	57	0.76	14	0.5	0.1	79	0.1	64		
	240	-	-	-	3.0	1.8	9.1	54	0.73	14	1.1	0.1	78	0.1	63		
	290	-	-	-	4.9	2.1	11.4	56	0.81	16	1.0	0.1	77	0.1	65		

1. - indicates no particle of this type observed.

2. particle types as defined in Table 5.

3. volumes (vol), equivalent spherical diameters (esd), lengths (l), aspect ratios (ar) = width/length

Table 9. Comparison of POC fluxes and e-ratios

Site	PPS3/3 trap		e-ratio	IRS trap		Gel trap Depth	Ebersbach et al algorithm		Guidi algorithm		Ebersbach-Guidi	
	depth	POC flux		depth	POC flux		POC flux	e-ratio	POC flux	e-ratio	POC flux	POC flux ratio
i.d.	m	mmolC m ⁻² d ⁻¹	m	mmolC m ⁻² d ⁻¹	m	M	mmolC m ⁻² d ⁻¹	mmolC m ⁻² d ⁻¹	mmolC m ⁻² d ⁻¹	mmolC m ⁻² d ⁻¹	mmolC m ⁻² d ⁻¹	POC flux ratio
P1	150	3.3 ± 1.8	-	-	-	140	6.1	6.1	5.1	0.09	5.1	1.2
			-	-	-	190	10.3	10.3	8.7	0.16	8.7	1.2
			-	-	-	240	10.6	10.6	6.3	0.16	6.3	1.7
P2	150	2.1 ± 0.9	0.06 ± 0.04	170	1.8	140	9.5	9.5	7.2	0.12	4.9	1.6
				320	1.1	190	5.9	5.9	5.3	0.27	7.2	1.3
						240	5.6	5.6	4.7	0.17	5.3	1.1
P3	150	0.9 ± 0.4	0.01 ± 0.1	170	0.9	140	0.8	0.8	4.6	0.16	4.6	1.1
				320	0.2	190	1	1	1.4	0.15	1.4	0.6
						240	0.6	0.6	1.2	0.02	1.2	0.9
					290	0.6	0.6	0.8	0.02	0.8	0.5	
						290	0.6	0.6	0.8	0.01	0.8	0.8

1. e-ratio=POC flux/GPP (GPP in Table 1; data from Cavagna et al., this issue)
2. see Methods section for discussion of algorithms for POC content of particles

Manuscript 3

Optical imaging of mesopelagic particles indicates deep carbon flux beneath a natural iron fertilized bloom in the Southern Ocean.

Marie-Paule Jouandet¹, Thomas W. Trull^{1,2}, Lionel Guidi³, Marc Picheral⁴, Friederike Ebersbach⁵, Lars Stemann³, Stéphane Blain^{6,7}

¹Antarctic Climate and Ecosystems CRC, Institute for Marine and Antarctic Studies, University of Tasmania, Hobart, 7001, Australia.

²CSIRO Marine and Atmospheric Research, Hobart, 7001, Australia.

³Department of Oceanography, University of Hawaii, 1000 Pope Road, MSB205, Honolulu, HI 96822

⁴Laboratoire d'Océanographie de Villefranche, Université Pierre et Marie Curie-Paris 6, 06230 Villefranche-sur-Mer, France..

⁵International Graduate School for Marine Science (GLOMAR), University of Bremen, and Alfred Wegener Institute for Polar and Marine Research, Bremerhaven, Germany.

⁶UMPC Univ Paris 06, UMR 7621, LOMIC, Observatoire Océanologique, F-66650 Banyuls sur mer France.

⁷CNRS, UMR 7621, LOMIC, Observatoire Océanologique, 66650 Banyuls sur mer France.

Acknowledgements

Thanks to the KEOPS shipboard science team and the officers and crew of RV Marion Dufresne for their efforts. Australian involvement in KEOPS and this post-voyage project received support from the Australian Commonwealth Cooperative Research Centre Program and Australian Antarctic Sciences Award 1156. L.G. contribution was partly supported by the Center for Microbial Oceanography, Research and Education (C-MORE) (NSF grant EF-0424599) and the Gordon and Betty Moore foundation. We also thank two anonymous referees for their valuable comments.

Abstract

We recorded vertical profiles of size distributions of particles (ranging from 0.052 to several mm in equivalent spherical diameter) in the natural iron fertilized bloom southeast of Kerguelen Island (Southern Ocean) and in surrounding High Nutrient Low Chlorophyll (HNLC) waters with an Under Water Video Profiler (UVP) during the KEOPS cruise (Jan.-Feb 2005). Total particle numerical abundance (TPN) and total particle volume (TPV) in the 0-200 m layer were respectively 3-fold and 20-fold higher in the bloom, and integrated TPV was correlated to integrated chlorophyll concentration. The difference persisted well into the ocean interior with a 10-fold higher TPV at 400 m depth beneath the natural iron fertilized bloom. Below 400 m, increases in TPV values at the bloom stations reflect the suspension of bottom sediments. Bloom waters had a greater proportion of large particles from the surface to 400 m and also exhibited an increase of this proportion with depth compared to HNLC waters. Multiple visits to the bloom reference station, A3, suggest preferential removal of large particles as the bloom declined. Comparing our particle abundance size spectra with those observed previously in polyacrylamide gel filled sediment traps allows us to estimate mesopelagic particle sinking rates. These results suggest that particles sink faster in the HNLC waters than beneath the bloom. The fact that sinking speeds were not a simple monotonic function of particle size and varied spatially highlights the need to go beyond parameterisations of sinking rate as a function of size alone.

Introduction

The biological carbon pump is a key process influencing the atmospheric carbon dioxide (CO₂) concentration (Volk and Hoffert, 1985), and depends on both the magnitude of primary production (PP) in the surface mixed layer and the fraction of this organic matter that is exported to depth. Artificial iron fertilization experiments have demonstrated an enhancement of primary production associated with a shift in the structure of the phytoplankton community toward larger diatoms (de Baar et al., 2005), but the extent of carbon export to the ocean interior remains difficult to quantify (Boyd et al., 2007). The issue of carbon export has also been addressed in natural iron fertilization studies, which have observed an increase in shallow export compared to High Nutrient Low Chlorophyll (HNLC) surrounding waters (Blain et al., 2007; Pollard et al., 2007).

The amount of POC produced in the euphotic zone that is transferred through the mesopelagic zone by sinking particles depends on their sinking velocities and the rate at which they decompose or are consumed. The specific shape of the resultant POC flux profile is usually described as an empirical function of shallow export (Martin et al., 1987), but has been shown to vary from place to place (Berelson et al., 2002; Buesseler et al., 2007; Guidi et al., 2009). Flux attenuation has mainly been investigated using sediment traps, although this approach can only provide sparse observations, and may be biased by swimmer contamination, sample degradation, and hydrodynamic effects (Buesseler et al., 2007). These limitations underscore the utility of indirect methods to obtain estimates of flux, such as optical observations of in situ particle concentrations (Gorsky et al., 2000) associated to the use of empirical relationship, and this is the primary approach applied in this study.

The Kerguelen Ocean and Plateau compared Study (KEOPS) investigated a naturally iron-fertilized portion of the Southern Ocean, which is the largest HNLC region in the global ocean. The study area was located to the south-east of the Kerguelen Islands in the Indian sector of the Southern Ocean where a well-developed bloom is observed every summer in satellite chlorophyll images (Blain et al., 2007; Mongin et al., 2008). The bloom was found to be sustained by the supply of iron and major nutrients to surface waters from iron-rich deep water by vertical winter and diapycnal mixing (Blain et al., 2007). Export estimated from the seasonal surface mixed layer carbon budget and from the ²³⁴Th deficit method at 100 m suggested that the carbon export was more than two-fold higher over the plateau than in adjacent HNLC waters (Jouandet et al., 2008; Savoye et al., 2008) but that the efficiency, defined as the ²³⁴Th based export production to primary production ratio, was higher in the HNLC waters (Savoye et al., 2008). The difference appeared to be due to a higher bacterial activity in the iron fertilized waters (Obernosterer et al., 2008). The effect of iron on the biological carbon pump in the mesopelagic zone was inferred from the distribution of excess, non-lithogenic particulate barium, which indicated lower remineralisation between 125 and 400 m beneath the bloom than in the HNLC waters (Jacquet et al., 2008). Deployment of surface-tethered free-drifting sediment traps indicated higher export from the centre of the bloom than in surrounding HNLC waters, at 200 m depth (Trull et

III. Manuscript 3

al., 2008), and optical examination of particles trapped in polyacrylamide gels suggested export was dominated by fecal pellets and fecal aggregates within the bloom (Ebersbach and Trull, 2008).

These previous studies at the KEOPS site only examined export in the upper ~200 m. Only 3 free-drifting trap deployments were successful and one of these experienced technical problems (Ebersbach and Trull, 2008), and thus could not fully assess carbon export to the ocean interior. In this paper we examine in-situ particle concentrations and size spectra obtained from 25 vertical profiles using an Underwater Video Profiler (UVP). The objectives of the present study are three-fold. Firstly, to estimate to what extent the Kerguelen natural iron fertilization increases the abundance of particles in the water column, in and below the surface mixed layer. Secondly, to see if particle size spectra evolve with depth in the bloom and in the surrounding HNLC waters in order to estimate the processes controlling the export. Finally to investigate the response of particle sinking speeds to iron inputs, by comparison of the UVP particle abundances to those obtained from polyacrylamide gel filled sediment traps (Ebersbach and Trull, 2008).

Materials and methods

Site description – The KEOPS project has been summarized in an overview article and detailed in a special volume (Blain et al., 2007; 2008). In brief, the KEOPS cruise took place from 19 January to 13 February 2005. Satellite images (composite of MODIS and MERIS images provided by ACRI Co.) were used to determine the position of the stations and indicated that the phytoplankton bloom started in November, peaked in late December, and was in decline by the time of the voyage, reaching background levels by the end of February (Blain et al., 2007; Mongin et al., 2008). Three transects (A, B, C) of 11 stations each were carried out crossing the Kerguelen Plateau and extending into the off-shelf deep waters (deep being defined as water >1000 m; Figure 1). These transects crossed distinct biogeochemical provinces with stations A1-A5 and B1-B5 in the heart of the iron natural fertilized bloom (Figure 1), characterized by high Chl a and low nutrient concentrations (Blain et al., 2007; Mosseri et al., 2008) and the off shore stations (A9-A11, B9-B11, C9-C11) characterized by HNLC conditions. A3 and C11 were considered to be reference stations for the bloom and HNLC conditions, respectively (Blain et al., 2007), and were visited multiple times to examine temporal changes. Station A3 (50°38'S, 72°05' E) was sampled twice early in the voyage (A3-1: 22/01/05, A3-2: 23/01/05) and again near the end (A3-3: 12/02/2005), and station C11 (51 ° 39'S, 78 ° 00'E) was visited twice (C11-1: 26/01/2005 and C11-2: 05/02/2005).

As indicated in Figure 1, the eastward flowing Antarctic Circumpolar Current is divided by the Kerguelen plateau, with some flow transiting the plateau in association with the Polar Front just south of the Kerguelen islands, and the majority flowing around the southern edge of the plateau in the Fawn Trough (Park et al., 2008a). This southern branch turns northward along the eastern edge of the plateau before continuing on its circumpolar path. These flows influence the intensity of the phytoplankton bloom. Stations A1-A5 and B1-B5 on the central plateau were characterized by weak

III. Manuscript 3

geostrophic currents ($3\text{--}5\text{ cm s}^{-1}$) and an anticyclonic flow and exhibited the highest biomass. Stations C1, C3, and C5 were influenced by the relatively strong (up to 18 cm s^{-1}) northerly flow bringing HNLC waters onto this southern border of the plateau, and exhibited relatively low chlorophyll. The stations to the east of the plateau (A9-11, B9-11, C9-11) were generally in HNLC conditions, but with somewhat higher biomass downstream of the plateau along the A and B transects than on the C transect.

All the bloom stations were dominated by the micro-phytoplankton size class, primarily composed of diatoms. The HNLC stations exhibited similar community structure, but with a greater contribution from the nano-phytoplankton size class (Uitz et al., 2009). The decline of the bloom during the study period was associated with a change in diatom community structure shifting from an initial bloom of *Chaetoceros hyalochoete* species to a quite monospecific bloom of *Eucampia antarctica* (Armand et al., 2008). In contrast, only small changes were observed between the two visits to the HNLC station, where *Fragilariopsis pseudonana* was the most abundant diatom and the larger open-ocean species *Fragilariopsis kerguelensis* dominated the diatom carbon biomass. Zooplankton communities were dominated by copepods, particularly by large- and medium-size calanoid species, at all stations but with a 4 fold higher depth integrated (0-200 m) biomass in the bloom compared to outside (Carlotti et al., 2008).

Underwater Video Profiler (UVP) deployments - During the KEOPS A, B, and C transects, 25 vertical profiles, from the surface to 500 m for the plateau stations and to 1000 m for the off-shelf stations, were carried out with the Underwater Video Profiler (UVP) constructed in the Laboratoire d’Oceanographie of Villefranche sur Mer. The UVP measured objects illuminated in a slab of water of known volume of 10.53 L. The number of pixels was converted to surface areas, using the results of size and volume calibrations conducted in a seawater tank using natural particles of different types to determine the conversion between pixels to metric units (Picheral et al., unpubl.). The equivalent spherical diameter (ESD) of particles larger than 0.052 mm was calculated from the particle’s projected area in the image, assuming spherical shape. Images were recorded digitally by two cameras (the second camera with a higher magnification observes a portion of the illuminated volume) at a rate of 12 images per second and processed with custom made image analysis software (Gorsky et al., 2000).

The resulting particles sizes were binned into 27 ESD intervals (from 0.052 mm to 27 mm, spaced geometrically), and concentrations were averaged over 5 m depth intervals referenced to simultaneously acquired CTD bio-optical data. The UVP was equipped with sensors for temperature, salinity, fluorescence, and turbidity (backscattered red light). We examined size spectra showing a minimum of 5 particles per bin and depth interval (this criterion eliminated bins greater than 3.34 mm, Table 1) and divided each spectrum into small particles ($0.0052\text{ mm} < \text{ESD} \leq 0.527\text{ mm}$) and large particles ($0.527\text{ mm} < \text{ESD} < 3.34\text{ mm}$). The particle results are presented in terms of their number and volume concentration within each size, N ($\# \text{ L}^{-1}$) and V ($\text{mm}^3 \text{ L}^{-1}$), respectively. The CTD and sensor

data allow the particle image statistics to be compared to physical water column structure. We estimated surface mixed layer depth defined as the depth where the potential density differs by 2% from the surface value (Price, 1978). These ranged from ~50 to ~110 m depth, and are shown in Figure 2.

Results

Total Particle concentration and volume distributions along the A, B and C transects – The individual profiles of Total Particle Number (TPN), Total Particle Volume (TPV), and fluorescence are shown in Figure 2, arranged according to their longitudes along the A, B, and C transects to provide a picture of the overall spatial distribution. Several broad characteristics emerge from this picture: i) surface waters have the highest values of TPN and TPV, and these are higher over the plateau than outside, ii) TPN and TPV values decrease rapidly beneath the mixed layer, iii) values at mid-depths (200-400 m) are very low at all the stations (with the exception of C3), and iv) many stations over the plateau show near-bottom TPN enrichments (below 400 m). In the following paragraphs we examine these characteristics in more detail.

In the surface mixed layer, the maximum TPN and TPV at the bloom stations (A1, A3, A5, B1, B3, B5) averaged $1.4 \times 10^3 \pm 0.2 \times 10^3 \text{ \# L}^{-1}$ and $183 \pm 34 \text{ mm}^3 \text{ L}^{-1}$, respectively. In contrast, the HNLC stations were characterized by at least 3-fold lower values with TPN under 500 \# L^{-1} and TPV under $50 \text{ mm}^3 \text{ L}^{-1}$. The smallest TPN ($73 \pm 15 \text{ \# L}^{-1}$) and TPV ($1.8 \pm 0.5 \text{ mm}^3 \text{ L}^{-1}$) occurred at HNLC stations C5 and C11. The overall spatial distribution of the surface mixed layer TPN and TPV values is similar to that for phytoplankton fluorescence (Figure 2), and this leads to a correlation of TPV and Chl a when integrated over the top 200 m (Figure 3). The correlation is largely defined by two end-members - the highest values in the bloom over the plateau including the first two visits to the A3 bloom reference station, and the lowest values at the off-plateau stations including the C11 HNLC reference station (Figure 3). Within the subset of the bloom stations, there is less correlation, with varying Chl a levels accompanied by relatively constant TPV values. One possible explanation is an increase in Chl a levels per cell in response to self-shading in the bloom, but data to test this are not available.

Below the mixed layer, TPN and TPV both decreased very rapidly from the surface values, by a factor of 10 (TPN = $128 \pm 33 \text{ \# L}^{-1}$ and TPV = $17 \pm 10 \text{ \# L}^{-1}$ at 200 m depth) at the bloom stations. Broadly similar vertical profiles occurred at the HNLC stations (Figure 2). These strong decreases with depth also occurred in phytoplankton fluorescence (Figure 2), suggesting that the profiles below the mixed layer (down to 200 m) are controlled by active exchange of surface and subsurface waters (as mediated by energetic internal waves and reflected in high estimates for the vertical eddy diffusivity, Park et al. (2008b)).

Below 200 m depth, phytoplankton fluorescence is minimal, and the TPN and TPV values decrease relatively slowly, only a factor of 1.7 from 200 to 400 m in contrast to the 10-fold decrease

III. Manuscript 3

from surface maxima to 200 m depth. Vertical mixing is much less active at these depths, which are below the remnant temperature minimum layer at ~200 m depth that reflects the maximum depth of winter mixing (Blain et al., 2007). In this layer, particle populations may be controlled primarily by biological processes.

Within about 100 m from the bottom, many on-plateau stations exhibit sharp increases in TPN values, and less strongly in TPV values (Figure 2). This presumably represents resuspension of bottom sediments, as has also been suggested based on particulate iron measurements (Chever et al, 2010). This explanation may also apply to the somewhat elevated TPN and TPV between 200 and 400 m that was observed only at station C3 (TPN ranging between 220 and 502 # L⁻¹, and TPV between 23 and 125 mm³ L⁻¹), with the particles possibly derived from the shelf near Heard Island. There is no evidence of TPN or TPV increases at similar depths in any of the off-plateau stations, including stations A9 and B9 which are directly downstream from the plateau, suggesting that the resuspended particles are not transported far laterally.

In the sections that follow we discuss the 0-200 m and 200-400 m depth bands separately. Phytoplankton dominates TPN in the first band, and these waters exhibit strong decreases in particle number and volume with depth. Extant phytoplankton is essentially absent in the second band, and changes in particle numbers with depth are smaller and steadier. We refer to these two bands as the surface and mesopelagic layers.

For the surface layer we focus on temporal changes related to bloom and particle formation dynamics, and for the mesopelagic layer we emphasize the estimation of the changes in particle abundances and sizes with depth to demonstrate biological or/and physical controls on material transfer to the ocean interior. We focus on stations A3 and C11 which are respectively reference stations for the bloom and the HNLC area (Blain et al., 2007) and also examine HNLC station C5 where particle size distributions were also determined from polyacrylamide-gel filled sediment traps (Ebersbach and Trull, 2008).

Vertical distributions of small and large particles in the 0-200 m surface layer at the bloom and HNLC reference stations - The vertical distributions of the small particle volumes (0.052 mm <ESD ≤ 0.527 mm; SPV) and large particle volumes (0.527 mm <ESD < 3.34 mm; LPV) for the A3 bloom reference station (A3-1: 22/01/05, A3-2: 23/01/05, A3-3: 12/02/05), and the HNLC stations C11 (C11-1: 26/01/05 ; C11-2: 05/02/05) and C5 are shown in Figure 4. This set of sites and profiles lets us examine differences between the bloom and HNLC waters, variations with depth, and changes with time. As noted above in discussing Figure 2, the A3 bloom station has higher TPV than the HNLC stations. Figure 4 shows that this higher TPV is accompanied by a greater proportion of large particles, throughout the water column.

Vertical distributions of SPV and LPV differed between the bloom and HNLC sites. At the A3 bloom station, LPV showed high values from the surface to ~150 m depth before decreasing strongly. At the HNLC sites the near surface particle abundances did not extend as deeply, dropping to low

III. Manuscript 3

values at ~120 m. This difference does not appear to be driven by the differences in the depth of the mixed layers, because mixed layer depths were similar or slightly deeper at the HNLC sites (Figure 4 and 5), and generally shallower than the depths at which particle volumes decreased strongly (Figure 4). The bloom sites exhibited double maxima in LPV values, the first one around 50 m and the second one between 100 and 140 m, but no structure in SPV profiles. In contrast, the HNLC sites exhibited profiles with single maxima in LPV, which were echoed by SPV values, at much shallower depth (60-70 m). LPV and SPV values in these maxima were more than six-fold lower than at the bloom stations.

These interesting features in the LPV and SPV distributions were correlated to the profiles of phytoplankton fluorescence and turbidity (Figure 5). In the bloom, fluorescence profiles were also characterized by first maxima around 50 m and second maxima at 120 m although these features were not as strong as in the LPV profiles (Figure 4). Weak maxima in fluorescence corresponding to the SPV/LPV maxima were also present for the HNLC stations. Turbidity exhibits a maximum only at the depth of the deeper LPV feature at A3. Taken together, these observations suggest that the LPV, and to a lesser degree the SPV, distributions correspond with those of phytoplankton for both the bloom and HNLC environments in surface waters.

Changes over time were minimal at the C11 HNLC reference site, but dramatic at the A3 bloom reference site between the first two visits (A3-1 and A3-2 just one day apart) and the last visit 20 days later (A3-3). By the time of the last A3-3 visit the LPV values had decreased more than 5-fold in comparison to the A3-1 and A3-2 visits, yet the double maxima persisted. This makes it clear that the lower values were not the result of HNLC waters arriving at the bloom site, but of temporal evolution of the bloom, a perspective consistent with the slow circulation in this region (as detailed in the Methods section). The intensity of the shallow sub-surface maximum at 50 m decreased with time from $160 \text{ mm}^3 \text{ L}^{-1}$ (A3-1) to $27 \text{ mm}^3 \text{ L}^{-1}$ (A3-3) and the deeper maximum at 100-140 m from $108 \text{ mm}^3 \text{ L}^{-1}$ (A3-1) to $20 \text{ mm}^3 \text{ L}^{-1}$ (A3-3). The volume of small particles also decreased three-fold from $7.4 \pm 0.7 \text{ mm}^3 \text{ L}^{-1}$ to $2.2 \pm 0.3 \text{ mm}^3 \text{ L}^{-1}$.

Vertical distributions of the large and small particle volumes in the mesopelagic layer (depth > 200 m) at the bloom and HNLC reference stations – Figure 6 focuses on the profiles between 200 and 400 m depth. As noted for surface waters in the previous section, large particles dominated at all sites, and contributed more strongly to total particle volume TPV, the sum of SPV and LPV, at the bloom stations. The first two visits to the A3 bloom site exhibited monotonic decreases in all particle volume parameters with depth, with the steepest decrease of the LPV at A3-1. Most of the difference between A3-1 and A3-2 comes from lower LPV ($12 \text{ mm}^3 \text{ L}^{-1}$) at 200 m while LPV values were similar at 400 m depth, equal to an average of $5.4 \pm 0.8 \text{ mm}^3 \text{ L}^{-1}$ (n=2). These profiles contrast with the C11 HNLC reference site, which exhibited fairly constant values with depth, and the C5 site at which LPV increased with depth. The last visit to A3 (A3-3), when particle concentrations were greatly

III. Manuscript 3

diminished, showed a profile similar to the HNLC sites, with an LPV increase by 40 % between 200 m and 400 m at A3-3, though still an SPV decrease with depth.

Variations in particle size spectra – So far we have discussed the results by binning the particle properties into two classes: small and large. In this section we discuss the continuum of particle sizes observed by the UVP, using particle size distributions. Particle number distributions (n) were calculated by dividing the abundance of particles (N) within a given bin by the width of the equivalent spherical diameter (ESD) bin, and are thus in units of $\# \text{ cm}^{-4}$. The size distributions for each stations are shown for 3 depth layers : i) at 5m intervals between 30 and 70 m, where the first maximum in LPV occurs, ii) between 100 and 140 m, where the second LPV maximum occurs, and iii) in the mesopelagic layer from 200 m to 400 m (Figure 7). The general pattern for all stations is a decrease of abundance with increasing size (the small “zig-zags” in the spectra are an artifact of the binning procedure, but this does not affect the total values of TPN or the slopes in the spectra). This pattern, expected from coagulation models (Jackson et al., 2005), has also been observed in previous studies (Mc Cave, 1984; Jackson et al., 1997; Stemmann et al., 2008c).

Changes with depth in the shape of the particle number size distributions were observed for each station. To investigate these changes in detail we followed the approach of Guidi et al. (2009) and computed the slope (m) of the particle number size distributions according to the equation $\ln(n) = m \ln(\text{ESD}) + c$. The slope m is negative (because all sites have more small than large particles), and more negative values of m correspond to steeper particle distributions that have a smaller proportion of large particles.

As seen on Figure 7 (D), the particles during the two first visits of A3 were larger than in the HNLC environment and demonstrate the effect of iron on the particle size spectra. Previous study had shown an increase of size of particle in response to iron addition during SOIREE (Jackson et al., 2005). Two m maxima were observed at 50 m and 120 m at A3-1 and A3-2, corresponding to an increase of the proportion of large particles. These features correspond to the LPV maxima pointed out in Figure 4.

Profiles of m below 200 m at A3-2, A3-3, C11-1, and C5 were characterized by a slight increase of m with depth, while the m profile at A3-1 was quite flat, and C11-2 was characterized by a decrease in m with depth. Similar values of m , and similar variations with depth, have been observed at many other sites, and those observed for the bloom stations over the Kerguelen plateau fit within the cluster-6 classification for productive waters in the classification scheme developed for a globally distributed set of observations by Guidi et al. (2009).

Carbon export flux – The particulate organic carbon export flux (F_{POC}) can be estimated from the size spectra using the empirical relationship:

$$F_{\text{POC}} = A d^b$$

where A (12.5) and b (3.81) were estimated by Guidi et al. (2008) by comparison of size spectra to deep ocean moored and free floating sediment trap POC fluxes for sites distributed around

III. Manuscript 3

the global ocean. The value of b is lower than the value of 5 that would be expected for spherical constant density particles (for which mass increases as d^3 , and sinking speed as d^2), and this is consistent with increasing porosity with size for marine aggregates (Alldredge and Gotschalk, 1988). We estimated fluxes in this way for the same depth and sites where free-drifting sediment traps were deployed (Ebersbach and Trull, 2008; Trull et al., 2008). The resulting fluxes at 200, 330 and 400 m were highest at the first visit of A3 and decreased from 869 to 57 $\text{mg m}^{-2} \text{d}^{-1}$ at 200 m, from 325 to 65 $\text{mg m}^{-2} \text{d}^{-1}$ at 330 m and from 259 to 95 $\text{mg m}^{-2} \text{d}^{-1}$ at 400 m by the time of the last visit (Table 2). Considering the HNLC environment, POC fluxes were quite similar at 200 m between the different visits of C11 and C5 ($32 \pm 3 \text{ mg m}^{-2} \text{d}^{-1}$, $n=3$). More variability was observed at 330 m (400 m) with values ranging from 24 $\text{mg m}^{-2} \text{d}^{-1}$ (40 $\text{mg m}^{-2} \text{d}^{-1}$) at C11-1 to 52 $\text{mg m}^{-2} \text{d}^{-1}$ (67 $\text{mg m}^{-2} \text{d}^{-1}$) at C5. These fluxes were still more than 3-fold lower than fluxes in productive iron fertilized bloom waters.

POC flux at 200 m, 330 m, and 400 m were also derived from the size of particles recorded in polyacrylamide-gel sediment traps using an empirical algorithm between the carbon content and the volume of particles (Ebersbach and Trull, 2008). These values are compared to the POC flux derived from the algorithm of Guidi et al. (2008) at the last visit of A3 and C5 (Table 2). A good agreement is observed between both methods for both stations except at 330 m for A3. The difference observed could result from the parameterization from Guidi et al. (2008) which assumes constant values of A and b for all depths.

As for the POC fluxes derived from the gel traps (Ebersbach and Trull, 2008), POC fluxes derived from UVP particle sizes are more than two fold higher than the POC flux measured in a drifting cylindrical sediment trap (Trull et al., 2008), suggesting that POC flux estimation from optical images tends to overestimate the flux. Nevertheless all methods show an increase of the POC flux in the bloom at 200 m in comparison to the HNLC waters. The UVP data provide new results at depth; specifically the inferred flux is still higher at 400 m depth beneath the bloom in comparison to the surrounding HNLC waters. These results emphasize an increase of the intensity of the biological pump in a natural iron fertilized bloom.

Particle sinking speed estimation – The average particle velocity (w_i) for each size class, i , can be estimated by dividing the number flux spectra (F_i in $\# \text{m}^{-2} \text{d}^{-1} \text{cm}^{-1}$) estimated from gel traps by simultaneous measurements of the number spectra (n_i in $\# \text{m}^{-3} \text{cm}^{-1}$) derived from the UVP according to:

$$w_i(\text{ESD}) = F_i(\text{ESD}) \times (n_i(\text{ESD}))^{-1} \quad \text{with } i \text{ referring to the size class}$$

Simultaneous measurements of F_i and n_i were only realised at A3-3 and C5 at 200 m and 330 m, and 430 m. We didn't compute sinking speed at 430 m as particle abundances was affected by resuspension at this depth (cf Figure 2). F_i was derived from the microscopic image analyses of the gel trap cups over the 0.155 to 2.855 mm particle size interval, binning into nine size classes (Table 1) (Ebersbach and Trull, 2008). The 17 bins used for the number spectra determination with the UVP

III. Manuscript 3

were combined to compare to these 9 bins (gathering bins 5-6, 6-8, 8-9, 9-11, 11-12, 12-14, 14-15, 15-17, 17-18). The resulting sinking velocities are shown in Figure 8.

These results suggest particles sink faster in the HNLC environment compared to the bloom. This difference is driven by the higher trap flux number spectrum at C5 compared to A3 with the greatest difference occurring at 330 m, and is thus subject to the possibility that it results from differences in the efficiency of particle collection by the traps at the two sites, although deployment conditions were similar (Ebersbach and Trull, 2008).

The general pattern of sinking speeds as a function of size was remarkably similar for the two depths (200 and 330 m) and two sites (A3 and C5) where direct comparison of gel-traps and UVP results was possible. - a decrease of w_i from the first size class to the second one followed by an increase to reach a maximum for the 0.5-0.7 mm size class, except at A3-330 m where a continuous decrease with size was observed. The fastest w_i was computed at C5 with value of 1400 m d^{-1} , seven fold higher than the maxima at A3. This high value results from a high number flux recorded by the gel trap while the UVP number spectrum was low. In contrast, the high values for the size class 0.5-0.7 mm at A3-200 m, C5-200 m and C5-300 m results from a sharp decrease of n_i for a similar F_i . The w_i for particles with ESD up to 0.7 mm decrease with increasing ESD. No sinking speeds could be computed for the 2 largest size classes (ESD > 1.4 mm) at A3-200 and 330 m and C5-330 m as no particles this large were recorded by the gel trap. Concerning the variation of the sinking speed with depth, w_i was characterized by a decrease from 200 m to 330 m with the largest decrease noticed at A3-330 m. This decrease is due to the diminution of F_i (Figure 8 A).

Discussion

Comparison of bloom and HNLC environments – The overall objective of this work was to assess the impact of iron on the intensity of the biological carbon pump. The UVP images clearly show that more and larger particles are present beneath the bloom than in surrounding waters, and that this extends deep into the mesopelagic ocean (to 400 m depth). Figures 2, 3, 4, and 5 reveal that the higher production of particles in the natural iron fertilized bloom is linked to the stronger surface phytoplankton production. Figures 6 and 7 indicate that differences in particle processing also occur at mesopelagic depths. The analysis of the gel traps showed that the sinking material was dominated by fecal material at 100, 200 and 330 m depth demonstrating that the formation of large particles results mainly from grazing rather than diatom aggregation (Ebersbach and Trull, 2008).

At the time of the bloom (A3-1 and A3-2) F_{POC} and LPV in the mesopelagic waters were characterized by decreases with depth associated with an increase of the proportion of large particles. Several mechanisms could account for this pattern, among them the most likely are particle alteration processes such as fragmentation and/or remineralisation and/or zooplankton grazing. No increase of small particle volume was observed in the mesopelagic layer and thus fragmentation seems unlikely. Microbial consumption of particles is also known to affect particle geometry and to decrease particle

III. Manuscript 3

volume (Stemmann et al., 2004) but this process is unlikely to promote an increase of the fraction of large particles and remineralisation rate based on excess barium concentrations was low in the mesopelagic zone (Jacquet et al., 2008). Consumption by zooplankton appears most likely to be responsible for the decrease of LPV and for the increase of the proportion of larger particles by repackaging through the excretion of larger fecal pellets. Of course, the shift towards a greater proportion of larger particles with depth could also reflect temporal change in the delivery of particles produced at the surface, with production of fewer smaller particles at the end of the bloom as seen on Figure 7 at the last visit of A3.

The last visit at A3 was characterized by an increase of TPV with depth in the mesopelagic layer, which could reflect the decline in particle delivery from the bloom above, or temporal variability between the timing of production in surface and export at depth as previously described in Savoye et al. (2008). Another contributing explanation could come from the decrease of sinking speed with depth (shown in Figure 8), since a slowdown in particle settling would lead to an accumulation with depth proportional to the diminution of the settling rate.

Sinking speed – The sinking speed computed using gel trap and UVP data was lower in the natural iron fertilized bloom compared to the HNLC waters for the whole size spectrum. Phytoplankton community was dominated by diatoms in the bloom and in the HNLC waters but with difference in silicification degree (Mosseri et al., 2008). The stronger silicification in the HNLC waters could contribute to the high sinking speed in the HNLC waters, via an increase of ballast. Higher porosity in the bloom derived particles, as a result of differing grazing and aggregation processes could also contribute to this result.

The fact that the sinking speed is not a simple monotonic function of particle size was a surprising result and was also observed by McDonnell and Buesseler (2010) in the Southern Ocean (West Antarctic Peninsula) using the same computational method. Nevertheless the variation of sinking speed observed in this study is different from the one reported in McDonnell and Buesseler (2010). The sinking speed was maximal for the middle size class (0.5-0.7 mm) in our study whereas they computed maximal sinking speeds for the smallest and largest size classes, dominated by diatom aggregates and krill fecal pellets, respectively. These results, in addition to comparison with sinking speeds from the literature (Figure 9) highlight the need to go beyond parameterisations of sinking rate as a function of size alone, as derived previously from in-situ studies (Alldredge and Gotschalk, 1989; Syvitski et al., 1995) and models (Stokes law, Stemmann et al., 2004b) .

Comparison between the study of McDonnell and Buesseler (2010) and our results shows also discrepancy in the variation of sinking speed with depth. Sinking speed was characterized by an increase with depth in waters of the Antarctic Peninsula while our study demonstrated a decrease of the sinking speed with depth, by more than a factor of 2. This decrease was unexpected considering the study of Berelson et al. (2002) that argued for increasing sinking rates with depth based on deep ocean moored traps. This finding is of crucial importance, as parameterisations consistent with

III. Manuscript 3

increasing sinking speed (Najjar et al., 1992; Maier Reimer, 1993; Sarmiento et al., 1993; Schmitter et al., 2005) or constant sinking speed (Gregg et al., 2003) for flux attenuation have been used in large scale biogeochemical models to explain regional variations in the biological pump. The decrease of the sinking speed in the present study is associated to an increase of the proportion of larger particles (cf Figure 7) which would be consistent with a decrease of porosity in large particles (Ploug et al., 2008). Overall, the observed sinking speed variability with environment and depth indicates that global relationships between particle concentrations and flux are oversimplifications for the estimation of POC flux.

Our sinking speed estimation approach is admittedly indirect, and it is perhaps possible that the complex relationships between the size of the particles and their sinking speed results from low efficiency of the gel trap to collect large particles or/and the fact that some unknown fraction of the larger particles seen by the UVP is not sinking (e.g. zooplankton). These estimations of sinking rate also assume that no sorting or particle size conversions occur during trapping, which is debateable (Buesseler et al., 2007), although the fine and complex structures observed in the gel traps favour relatively undisturbed collection. Focusing only on the small size classes (ESD < 0.5 mm), where UVP and gel trap are most likely to sample the same material, also shows no correlation between sinking speed and size.

References:

- Allredge, A.L., and C. Gotschalk. 1988. In situ settling behavior of marine snow. *Limnol. Oceanogr.* **33**: 339–351.
- Allredge, A.L., and C. Gotschalk. 1989. Direct observations of the mass flocculation of diatom blooms: characteristics, settling velocities and formation of diatom aggregates. *Deep-Sea Res.* **36**: 159–171.
- Azetsu-Scott, K., B.D. Johnson. 1992. Measuring physical characteristics of particles: a new method of simultaneous measurement for size, settling velocity and density of constituent matter. *Deep-Sea Res. I* **39**: 1057–1066.
- Armand, L.K., V. Cornet-Barthaux, J. Mosseri, B. Quéguiner. 2008. Late summer diatom biomass and community structure on and around the naturally iron-fertilized Kerguelen Plateau in the Southern Ocean. *Deep-Sea Res. II* **55**: 653–676.
- Berelson, W. M. 2002. Particle settling rates increase with depth in the ocean. *Deep-Sea Res. II* **49**: 237–251.
- Blain, S., B. Quéguiner, L. Armand, S. Belviso, B. Bombled, L. Bopp, A. Bowie, C. Brunet, K. Brussaard, F. Carlotti, U. Christaki, A. Corbière, I. Durand, F. Ebersbach, J. L. Fuda, N. Garcia, L. J. A. Gerringa, F. B. Griffiths, C. Guigue, C. Guillermin, S. Jacquet, C. Jeandel, P. Laan, D. Lefèvre, C. Lomonaco, A. Malits, J. Mosseri, I. Obernosterer, Y. H. Park, M. Picheral, P. Pondaven, T. Remenyi, V. Sandroni, G. Sarthou, N. Savoye, L. Scouarnec, M. Souhault, D. Thuillers, K. R. Timmermans, T. Trull, J. Uitz, P. Van-Beek, M. J. W. Veldhuis, D. Vincent, E. Viollier, L. Vong, et T. Wagener. 2007. Impacts of natural iron fertilisation on carbon sequestration in the Southern Ocean. *Nature* **446**: 1070–1074.
- Blain S., B. Quéguiner, T. W. Trull. 2008. The natural iron fertilization experiment KEOPS (Kerguelen Ocean and Plateau compared Study): an overview. *Deep Sea Res. II* **55**: 559–565.
- Boyd, P. W., T. Jickells, C. S. Law, S. Blain, E. A. Boyle, K. O. Buesseler, K. H. Coale, J. J. Cullen, H. J. W. de Baar, M. Follows, M. Harvey, C. Lancelot, M. Levasseur, N. P. J. Owens, R. Pollard, R. B. Rivkin, J. Sarmiento, V. Schoemann, V. Smetacek, S. Takeda, A. Tsuda, S. Turner, A. J. Watson. 2007. Mesoscale Iron Enrichment Experiments 1993-2005: Synthesis and Future Directions. *Science* **315**: 612 – 617.
- Buesseler, K., C. Lamborg, P.W. Boyd, P. Lam, T. Trull, B. T. Bidigare, R. Bishop, C. James, F. Dehairs, M. Elskens, M. Honda, D. Karl, D. Siegel, M. Silver, D. Steinberg, J. Valdes, B. Mooy, S. Wilson. 2007. Revisiting Carbon Flux Through the Ocean's Twilight Zone. *Sciences* **316**: 567–570.
- Buesseler, K. O., A.N. Antia, M. Chen, S.W. Fowler, W.D. Gardner, O. Gustafsson, K. Harada, A.F. Michaels, M. Rutgers van der Loeff, M. Sarin, D.K. Steinberg, T. Trull. 2007. An assessment of the use of sediment traps for estimating upper ocean particle fluxes. *J. Mar. Res.* **65**: 345–416.
- Carder, K.L., R.G. Steward, P. R. Betzer. 1982. In situ holographic measurements of the sizes and settling rates of oceanic particulates. *J. Geophys. Res.* **87** : 5681–5685.
- Carlotti, F., D. Thibault-Botha, A. Nowaczyk, and D. Lefèvre. 2008. Zooplankton community structure, biomass and role in carbon fluxes during the second half of a phytoplankton bloom in the Eastern sector of the Kerguelen shelf (January - February 2005). *Deep-Sea Res. II* **55**: 720–733.
- Chever, F., G. Sarthou, E. Bucciarelli, S. Blain, and A. R. Bowie. 2010. An iron budget during the natural iron fertilisation experiment KEOPS (Kerguelen Islands, Southern Ocean). *Biogeosci.* **7**: 455–468.
- De Baar, H.J.W., P.W. Boyd, K.H. Coale, M.R. Landry, A. Tsuda, P. Assmy, D.C.E. Bakker, Y. Bozec, R.T. Barber, M.A. Brzezinski, K.O., Buesseler, E. Boye, P.L. Croot, F. Gervais, M.Y., Gorbunov, P.J., Harrison, W.T., Hiscock, P., Laan, C., Lancelot, C.S., Law, M. Levasseur, A. Marchetti, F.J. Millero, J. Nishioka, Y. Nojiri, T. van Oijen, U. Riebesell, M.J.A. Rijkenberg, H. Saito, S. Takeda, K.R. Timmermans, M.J.W. Veldhuis, A.M. Waite, C-H. Wong. 2005. Synthesis of iron fertilization experiments. *J. Geophys. Res.-Oceans.* **110**: C09S16, doi:10.1029/2004JC002601.

III. Manuscript 3

- Diercks, A.R., V.L. Asper. 1997. In situ settling speeds of marine snow aggregates below the mixed layer: Black Sea and Gulf of Mexico. *Deep-Sea Res. I* **44**: 385–398.
- Ebersbach, F., and T.W. Trull. 2008. Sinking particle properties from polyacrylamide gels during KEOPS : controls on carbon export in an area of persistent natural iron inputs in the Southern Ocean. *Limnol. Oceanogr.* **53**: 212–224.
- Gorsky, G., M. Picheral, and L. Stemann. 2000. Use of the underwater video profiler for the study of aggregate dynamics in the North Mediterranean. *Estuar. Coast. Shelf Sci.* **50**:121–128.
- Gregg, W., P. Ginoux, P. Schopf, and N. Casey. 2003. Phytoplankton and iron: validation of a global three-dimensional ocean biogeochemical model. *Deep-Sea Res. II* **50**: 3143–3169.
- Guidi, L., A.G. Jackson, L. Stemann, J. C. Miquel, M. Picheral, G. Gorsky. 2008. Relationship between particle size distribution and flux in the mesopelagic zone. *Deep-Sea Res.* **55**: 1364–1374.
- Guidi, L., L. Stemann, G. A. Jackson, F. Ibanez, H. Claustre, L. Legendre, M. Picheral, G. Gorsky. 2009. Effects of phytoplankton community on production, size and export of large aggregates: A world-ocean analysis. *Limnol. Oceanogr.* **54**: 1951–1963.
- Jackson, G.A., R. Maffione, D.K. Costello, A.L. Alldredge, B.E. Logan, H.G. Dam. 1997. Particle size spectra between 1 μm and 1 cm at Monterey Bay determined using multiple instruments. *Deep-Sea Res. I* **44**: 1739–1767.
- Jackson, G.A., A.M. Waite, P.W. Boyd. 2005. Role of algal aggregation in vertical carbon export during SOIREE and in other low biomass environments. *Geophys. Res. Lett.* **32**: doi:10.1029/2005GL023180.
- Jacquet, S. H. M., F. Dehairs, N. Savoye, I. Obernosterer, U. Christaki, C. Monnin, D. Cardinal. 2008. Mesopelagic organic carbon behaviour station in the Kerguelen Plateau region tracked by biogenic particulate Ba. *Deep-Sea Res. II* **55**: 868–879.
- Jouandet, M.P., S. Blain, N. Metzl., C. Brunet, T. W. Trull, I. Obernosterer. 2008. A seasonal carbon budget for a naturally iron-fertilized bloom over the Kerguelen Plateau in the Southern Ocean. *Deep-Sea Res. II* **55**:856–867.
- Maier-Reimer, E. 1993. Geochemical cycles in an ocean general circulation model. Preindustrial tracer distributions. *Glob. Biogeochem. Cyc.* **7**: 645–677.
- Martin, J.H., G.A. Knauer, D.M. Karl, W.W. Broenkow. 1987. VERTEX: carbon cycling in the northeast Pacific. *Deep-Sea Res.* **43**: 267–285.
- McCave, I.N. 1983. Particulate size spectra, behaviour, and origin of nepheloid layers over the Nova Scotian continental rise. *J. Geophys. Res- Oceans* **88**: 7647–7666.
- McDonnell A. M. P., and K. O. Buesseler. 2010. Variability in the average sinking velocity of marine particles. *Limnol. Oceanogr.* **55**: 2085–2096.
- Mongin M., E. Molina, T. W. Trull. 2008. Seasonality and scale of the Kerguelen plateau phytoplankton bloom: a remote sensing and modeling analysis of the influence of natural iron fertilization in the Southern Ocean. *Deep Sea Res. II* **55**: 880–892.
- Mosseri J., B. Quéguiner, L. Armand, and V. Cornet-Barthaux. 2008. Impact of iron on silicon utilization by diatoms in the Southern Ocean: a case study of the Si/N cycle decoupling in a naturally iron-enriched area. *Deep Sea Res. II* **55**: 801–819.
- Najjar, R., J. Sarmiento, and J. Toggweiler. 1992. Downward transport and fate of organic matter in the ocean: simulations with a general circulation model. *Glob. Biogeochem. Cyc.* **6**: 45–76.
- Obernosterer, I., U. Christaki, D. Lefèvre, P. Catala, F. Van Wambeke, and P. Lebaron. 2008. Rapid bacterial mineralization of organic carbon produced during a phytoplankton bloom induced by natural iron fertilization in the Southern Ocean. *Deep-Sea Res. II* **55**: 777–789.
- Park, Y. H., F. Roquet, J.L. Fuda, I. Durand. 2008a. Large scale circulation over and around the Kerguelen Plateau. *Deep-Sea Res. II* **55**: 566–581.
- Park Y.H., J.L. Fuda, I. Durand, and A. C. Naveira Garabato. 2008b. Internal tides and vertical mixing over the Kerguelen Plateau. *Deep Sea Res. II.* **55**: 583–593
- Ploug, H., M.H. Iversen, G. Fischer. 2008. Ballast, sinking velocity, and apparent diffusivity within marine snow and zooplankton fecal pellets: Implications for substrate turnover by attached bacteria. *Limnol. Oceanogr.* **53**: 1878–1886.

III. Manuscript 3

- Pollard, R. T., H. J. Venables, J. F. Read, and J. T. Allen. 2007. Large-scale circulation around the Crozet Plateau controls an annual phytoplankton bloom in the Crozet Basin. *Deep-Sea Res. II* **54**: 1915–1929.
- Price, J.F., C.N.K. Mooers, J.C. Van Leer. 1978. Observation and simulation of storm-induced mixed-layer deepening. *J. Phys. Oceanogr.* **8**, 582–599.
- Sarmiento, J., R. Slater, M. Fasham, H. Ducklow, J. Toggweiler, and G. Evans. 1993. A seasonal three-dimensional ecosystem model of nitrogen cycling in the North Atlantic euphotic zone. *Glob. Biogeochem. Cyc.* **7** : 417–450.
- Savoie, N., T. W. Trull, S. H. M. Jacquet, J. Navez, and F. Dehairs. 2008. ²³⁴Th-based export fluxes during a natural iron fertilization experiment in the Southern Ocean (KEOPS). *Deep-Sea Res. II* **55**: 841–855.
- Shanks, A.L., and J.D. Trent. 1980. Marine snow-sinking rates and potential role in vertical flux. *Deep-Sea Res. I* **27**: 137–143.
- Smayda, T.J. 1970. The suspension and sinking of phytoplankton in the sea (RV). *Oceanogr. and Mar. Biol.* **8**, 353–414.
- Stemmann, L., G. Gorsky, J. C. Marty, M. Picheral, and J. C. Miquel. 2002. Four-year study of large-particle vertical distribution (0–1000 m) in the NW Mediterranean in relation to hydrology, phytoplankton, and vertical flux. *Deep-Sea Res. II* **49**: 2143–2162.
- Stemmann, L., G. A. Jackson, and G. Gorsky. 2004. A vertical model of particle size distributions and fluxes in the midwater column that includes biological and physical processes—part II: Application to a three-year survey in the NW Mediterranean Sea. *Deep-Sea Res. I* **51**: 885–908.
- Stemmann, L., D. Eloire, A. Sciandra, G. A. Jackson, L. Guidi, M. Picheral, and G. Gorsky. 2008c. Volume distribution for particles between 3.5 to 2000 μm in the upper 200 m region of the South Pacific Gyre. *Biogeosc.* **5**: 299–310.
- Syvitski, J.P.M., K.W. Asprey, K.W.G. Leblanc. 1995. In-situ characteristics of particles settling within a deep-water estuary. *Deep-Sea Res. II* **42**: 223–256.
- Trull, T. W., D. Davies, K. Casciotti. 2008. Insights into nutrient assimilation and export in naturally iron-fertilized waters of the Southern Ocean from nitrogen, carbon and oxygen isotopes. *Deep-Sea Res. II* **55**: 820–840.
- Uitz, J., H. Claustre, B. Griffiths, J. Ras, and V. Sandroni. 2009. A phytoplankton class-specific primary production model applied to the Kerguelen Islands region (Southern Ocean). *Deep Sea Research I* **56**: 541–560.
- Volk, T., and M.I. Hoffert. 1985. Ocean carbon pumps: Analysis of relative strengths and efficiencies in ocean-driven atmospheric CO₂ changes. **In:** E.T. Sundquist and W.S. Broecker (eds) *The Carbon Cycle and Atmospheric CO₂: Natural Variations Archean to Present*. *Geophys. Monogr. Ser.* **32**: 99–110.

III. Manuscript 3

Table 1: Particles were divided into 17 size bins according to their computed ESD from the UVP and into 9 from the gel analysis. Only size bins with a minimum of 5 particles were conserved for the analyses therefore decreasing the total number of bins from 27 to 17. Small particles range from 0.052 to 0.527 mm and large particles from 0.527 to 3.34 mm.

ESD bin	ESD (mm) (UVP)	ESD (mm) (gel trap)
1	0.052	
2	0.066	
3	0.083	
4	0.105	
5	0.132	0.155
6	0.166	0.178
7	0.209	
8	0.264	0.252
9	0.332	0.357
10	0.419	
11	0.527	0.505
12	0.665	0.714
13	0.837	
14	1.055	1.009
15	1.329	1.427
16	1.674	
17	2.11	2.019
18	3.34	2.855

III. Manuscript 3

Table 2: Comparison of the POC fluxes (F_{POC} in $\text{mg m}^{-2} \text{d}^{-1}$) derived from particle size distributions from the UVP, particle distributions from gel-filled sediment traps (Ebersbach and Trull, 2008), and direct F_{POC} measurements on sediment traps in the bloom and HNLC waters (Trull et al., 2008).

		F_{POC}		
		F= Ad ^b	Gel trap	PPS3
A3-1				
200 m		869		
330 m		326		
400 m		259		
A3-2				
200 m		357		
330 m		322		
400 m		191		
A3-3				
200 m		58	62	44-48
330 m		67	8	
400 m		95		
C11-1				
200 m		34		
330 m		30		
400 m		40		
C11-2				
200 m		27		
330 m		25		
400 m		19		
C5				
200 m		32	49	18-20
330 m		53	41	
400 m		67		

Figure caption

Figure 1: Monthly mean chlorophyll concentration for January 2005 from MODIS data. The currents and fronts are from Park et al. (2008a). Plateau bathymetry is shown by black contours (at 500, 1000, 2000 m). The three transects A, B, and C, each with 11 stations, are shown in black. A3 was designated as the bloom reference station and C11 as the HNLC reference station (Blain et al., 2007). C5 also exhibited HNLC characteristics, and was the site of the HNLC sediment trap deployment (Ebersbach and Trull, 2008).

Figure 2: Near surface vertical distribution of the total particle number (TPN), volume (TPV) and fluorescence for transects A (A), B (B), and C (C) in the water column. The black lines show the mixed layer depth.

Figure 3: Comparison of the total particle volume, TPV, to phytoplankton fluorescence integrated on the 0-200 m surface layer for all KEOPS stations.

Figure 4: Vertical profiles of small (SPV), large (LPV) and total (TPV) particle volumes in the water column (0-550 m) for the 3 visits at A3, two visits at C11, and single visit at C5. Mixed layer depth is indicated by a black line.

Figure 5: Density (A), fluorescence (B) and turbidity (C) vertical distributions for the 3 visits at A3, two visits at C11 and single visit at C5 in the water column (0-550 m).

Figure 6: Vertical profiles of SPV, LPV, and TPV for the 3 visits at A3, two visits at C11 and single visit at C5 in the mesopelagic layer (200-400 m).

Figure 7: A-Compilation of the particle size distributions for the layers 50-90 m (A), 100-140 m (B), and 200-400 m (C) for the 3 visits at A3, two visits at C11 and single visit at C5. (D) Vertical profiles of the slopes (m) of the particle size distributions at these sites. Grey line is the m (-4) value for the global ocean from Guidi et al. (2009).

Figure 8: Number flux spectra from the polyacrylamide-gel filled traps as calculated from the data of Ebersbach and Trull (2008) (A) and number spectra for water column particles at the trap depths from the UVP images (B) at A3 and C5. Settling velocities as a function of size (ESD) in the natural iron enriched bloom (A3) and in HNLC waters (C5) at 200 m (C) and 330 m (D) estimated by comparing the gel-trap and UVP data.

III. Manuscript 3

Figure 9: Comparison of particle sinking velocities estimated here with previous results using the same approach from McDonnell and Buesseler, 2010 (PS1, PS2, PS3) and other approaches (from Guidi et al., 2008; Circle: Smayda, 1970; triangle: Shanks and Trent, 1980; cross: Carder et al., 1982; plus sign: Azetsu-Scott and Johnson, 1992; Empirical relationships: 1—Alldredge and Gotschalk, 1988; 2—Alldredge and Gotschalk, 1989; 3—Syvitski et al., 1995). Settling velocities calculated using the coagulation model (Stemmann et al., 2004b) with different parameter values (5— $Dr^{1/4} = 0.08$, $D^{1/4} = 2.33$; 6— $Dr^{1/4} = 0.01$, $D^{1/4} = 1.79$) are also reported. The regression line 7 is the settling speed predicted by Stokes Law. The dashed line 8 is the settling speed calculated in Guidi et al. (2008).

Fig. 1.

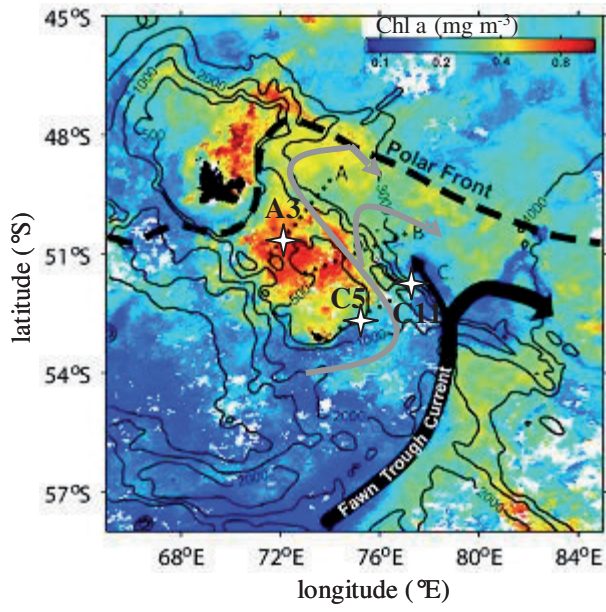


Fig2.

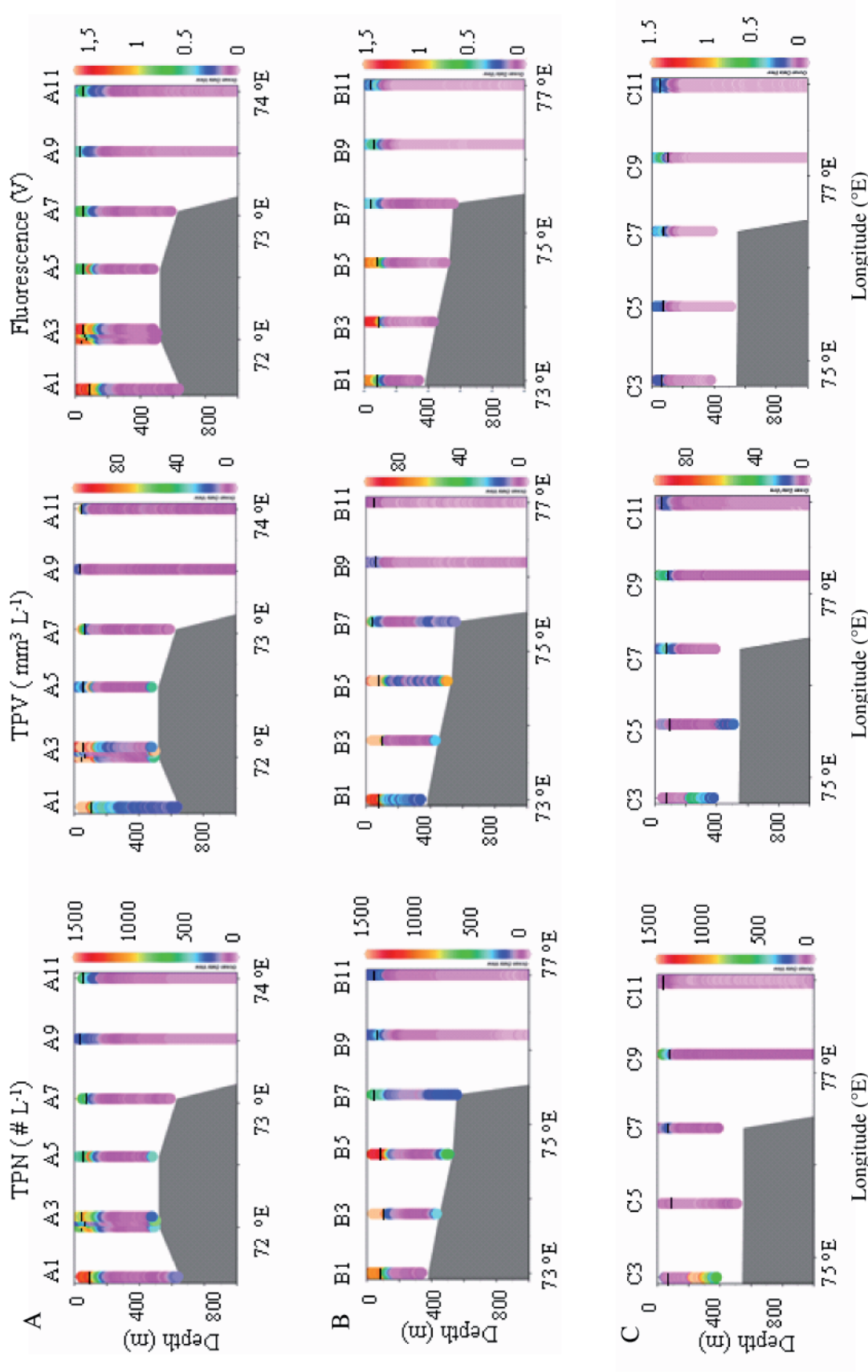


Fig. 3.

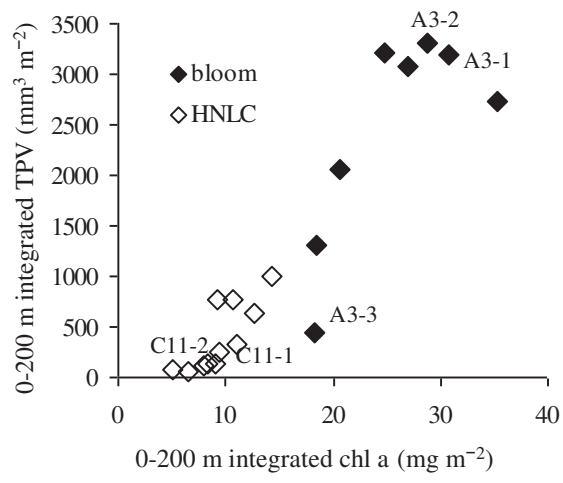


Fig.4

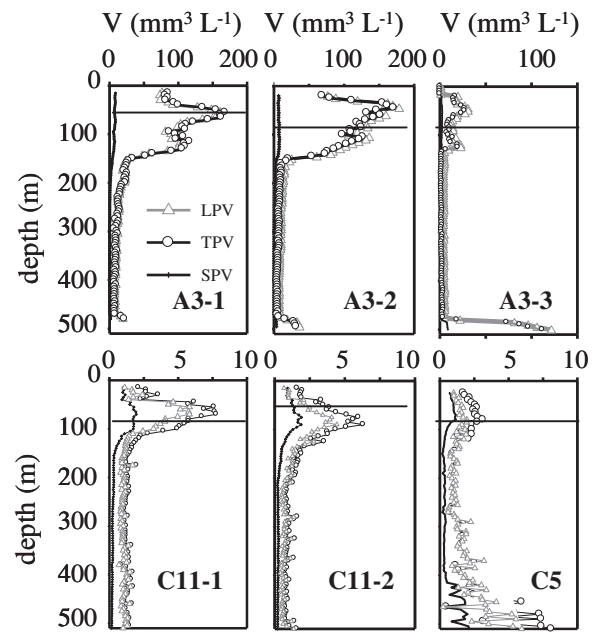


Fig. 5

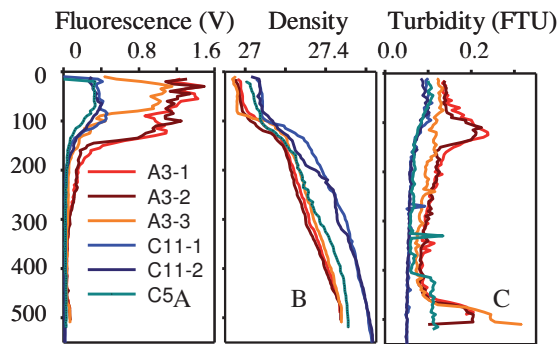


Fig. 6

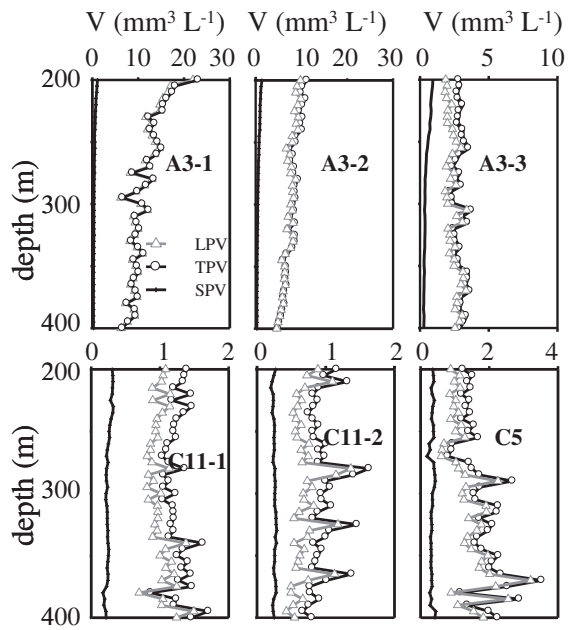


Fig. 7.

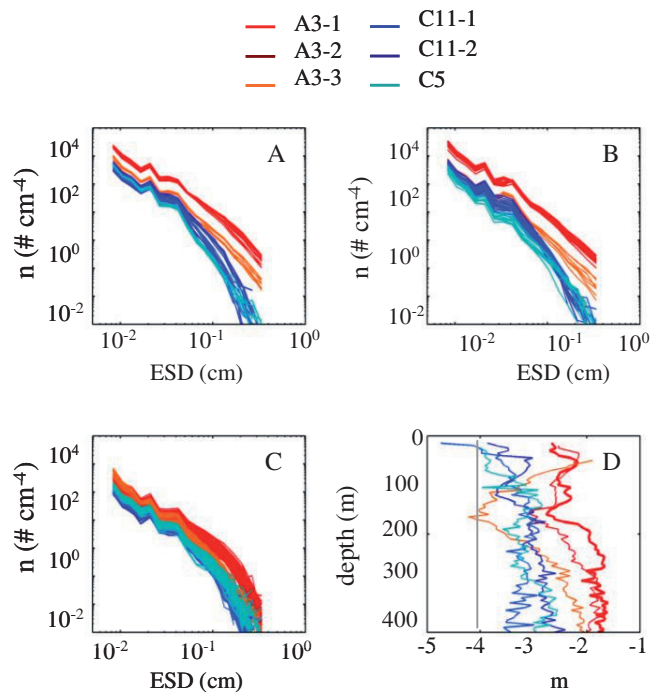


Figure 8

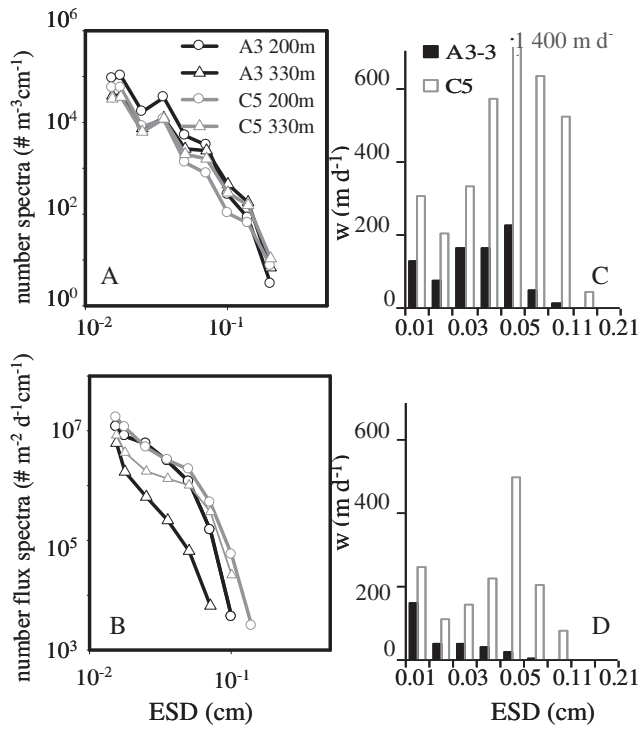
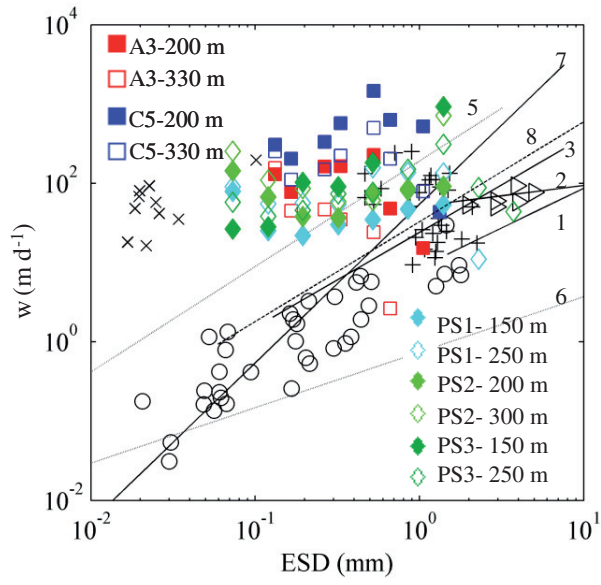


Fig. 9



III. Manuscript 3

Manuscript 4

Sedimentation patterns of phyto- and protozooplankton during the iron fertilisation experiment LOHAFEX in the Southern Ocean

Friederike Ebersbach^{1,2}, Philipp Assmy^{1,2}, Eva-Maria Nöthig¹

1 Alfred Wegener Institute for Polar and Marine Research, Am Handelshafen 12, 27570 Bremerhaven, Germany

2 International Graduate School for Marine Science (GLOMAR), University of Bremen, Germany

(Draft 28 October 2010 in preparation for Journal of Marine Systems)

Abstract

The LOHAFEX project, a meso-scale iron fertilisation experiment that was conducted in the Atlantic Sector of the Southern Ocean during austral summer (January – March 2009), examined the response of the plankton community to iron addition. Furthermore, the fate of the iron induced phytoplankton bloom (IN stations) was studied and compared to surrounding waters (OUT stations). Sinking particles were collected using i) bulk samples of neutrally buoyant sediment traps (NBSTs) for biogeochemical fluxes and microscopic investigations, and ii) polyacrylamide gel equipped NBSTs in order to visualise shape and structure of intact particles.

Small flagellates, in particular *Phaeocystis antarctica*, and unidentified Prasinophytes dominated the iron stimulated phytoplankton bloom. Diatom build-up was limited due to very low silicic acid concentrations ($<2 \mu\text{mol L}^{-1}$) at the surface. Although the surface plankton community showed an increase at IN in comparison to OUT stations, the export fluxes responded only with a slight increase. The sinking particle assemblage indicated no detectable difference between IN and OUT stations. Biogenic particles mainly consisted of faecal matter. Overall, it is evident that the ecosystem structure prevailing during LOHAFEX was characterised through recycling.

1. Introduction

Particulate organic carbon (POC) is built up in the sunlit surface ocean, and is transported downwards via the biological pump (Volk and Hoffert 1985; De La Rocha 2007). The mesopelagic (depth range of 100 – 1000 m) and the deep ocean (>1000 m depth) are coupled to processes in the euphotic zone (e.g. primary production (PP)) via sinking particles (e.g. Boyd and Trull 2007). Particle formation largely depends on the phytoplankton community prevailing at the surface and food web structure in the mesopelagic zone (Boyd and Trull 2007; Buesseler and Boyd 2009), resulting in various forms of particles, such as marine snow or faecal pellets (Turner 2002). Transparent Exopolymer Particles (TEP) are known to play an important role in the sedimentation of particulate matter (Passow et al. 2001; Passow 2002) since they stimulate formation of marine snow and facilitate incorporation of small particles into larger aggregates that would otherwise be too small to sink on their own (Passow et al. 2001). High TEP production and subsequent sinking of phytoplankton blooms has been widely observed in several regions (see Passow (2002) for a recent review).

Particle formation and flux in the world oceans have been a matter of intense discussion because of the ability of the surface ocean to take up CO₂ from the atmosphere and sequester it at depth. The Southern Ocean, which acts as large sink for atmospheric CO₂, is therefore of particular interest. Large parts of the Southern Ocean are characterised as High-Nitrate-Low-Chlorophyll (HNLC) areas, where PP is low despite high nitrate and phosphate concentrations. Martin (1990) postulated with the ‘iron-hypothesis’ that the trace metal iron (Fe) might be a limiting factor for phytoplankton growth. So far, 11 scientific in situ iron fertilisation experiments have univocally confirmed Martin’s iron hypothesis and stimulated phytoplankton blooms in HNLC areas (see Boyd et al. (2007) for a recent review) and the fertilisation of oceanic waters can be seen as one possibility to sequester parts of anthropogenic CO₂ concentrations in the atmosphere (Smetacek and Naqvi 2008).

In the Southern Ocean four iron fertilisation experiments were carried out in the last decade: the Southern Ocean Iron RElease Experiment (SOIREE) in the Pacific sector (Boyd et al. 2000), the Southern Ocean Iron Experiment North and South (SOFeX-N and -S) in the Australian sector (Coale et al. 2004), and the Iron Experiment (EisenEx) (Assmy et al. 2007) and the European Iron Fertilisation Experiment (EIFEX) (Bathmann 2005) in the Atlantic sector. So far, EIFEX was the only iron fertilisation experiment, where an export event subsequent to the collapse of the iron-induced bloom could be followed through the deep water column (Smetacek et al. in prep.). During SOFeX a shallow carbon export (< 200 m) was reported (Coale et al. 2004). Unfortunately, the fate of the EIFEX bloom could not be studied in detail due to ship time constraints. That’s why the latest iron fertilisation experiment LOHAFEX (‘loha’ is the Hindi word for iron) was designed in consideration of having enough time to allow examining the build-up and demise of the iron-induced bloom and minimise the effects of dilution with unfertilised waters respectively. Therefore, the duration of the experiment and the size of the fertilised patch were maximized as far as ship time and logistics permitted (Smetacek and Naqvi 2008).

This manuscript is focussed on studying the contribution of phytoplankton and protozooplankton to POC export fluxes by using neutrally buoyant sediment traps, of which some were equipped with polyacrylamide (PA) gels in order to preserve intact sinking particles. Species composition was determined microscopically, converted into C fluxes, and compared with the particle assemblage as collected with the PA gels. The combination of both approaches provides insights into particle dynamics that regulated export flux during LOHAFEX. In addition, the analysed distribution of TEP in the water column as well as in the trap material allows speculation on particle formation.

2. Material and Methods

2.1 Study area

The meso-scale iron fertilisation experiment LOHAFEX was carried out in the Atlantic Sector of the Southern Ocean (Fig. 1). It took place during austral summer within a meso-scale eddy in the south-western Atlantic Sector of the Antarctic Circumpolar Current (ACC). Over the course of the experiment, mixed layer depth ranged from 50-75 m, and the chosen eddy provided a coherent water mass (Murty et al. 2010). LOHAFEX was conducted over a period of 39 days (26 January to 5 March 2009), being the longest iron enrichment experiment to date. The centre of the eddy was fertilised with 10 t dissolved ferrous sulphate (FeSO_4) on January 26 (d0) creating a patch of approximately 300 km² (Smetacek and Naqvi 2010). A second fertilisation followed after 3 weeks on February 17 (d21), where another 10 t FeSO_4 were added. For tracking the fertilised patch, it was marked by two floating surface buoys (Mazzocchi et al. 2009). In order to compare fertilised with un-fertilised waters, throughout the experiment it was distinguished between stations inside and outside the patch, referred to as IN- and OUT-stations, respectively. The stations were allocated (as IN or OUT) on the basis of several parameters, such as Fv/Fm ratios, and concentrations of chlorophyll, pCO₂, and the tracer SF₆ (Smetacek and Naqvi 2010).

2.2 Sampling procedure onboard

2.2.1 Sinking material

To collect sinking particles, PELAGRA-traps, funnel shaped neutrally buoyant sediment traps (Lampitt et al. 2008) were deployed. Trap deployments were successful at 200 and 450 m for several distinct time intervals inside and outside the fertilised patch (Table 1), but a complete coverage over the course of the experiment was not achieved due to technical problems and weather conditions.

Bulk samples were preserved with formalin (2%), split on board using a rotary splitter identical to that described by Lamborg et al. (2008) and stored at 4° C until processing in the laboratory on shore.

PA gels were prepared onshore prior to the cruise following the method of Ebersbach et al. (in prep.). Unfortunately, some of the PELAGRA traps equipped with a PA gel, suffered from technical problems (Table 1). For this reason PA gels samples are only available from the beginning and the end

of the experiment (Table 1). Successful PA gels were photographed on board as described in Ebersbach and Trull (2008) in order to document the state of the fresh material.

2.2.2 Water column

For TEP measurements within the water column (as opposed to sinking particulate material) water samples of 250 ml were collected with Niskin bottles attached to a conductivity temperature depth (CTD) rosette at discrete depth in the upper 500 m (Table 2).

2.3 Microscopic analyses and data processing

The planktonic composition of the material collected with the PELAGRA traps was examined using inverted light and epifluorescence microscopy (Axiovert 135, 200; Zeiss, Oberkochen, Germany) following the method of Utermöhl (1958). 10 or 50 mL of each split were settled in 10 or 50 mL sedimentation chambers (Hydrobios; Kiel, Germany) for 48 h. Unicellular organisms were identified and counted at three magnifications, 100, 200, and 400 ×, respectively, according to the size of the respective organisms. Dependent on their abundance, unicellular organisms were counted in transects, quarter, half or whole chambers, and identified down to the species level.

In order to determine species-specific biovolumes 10-20 individuals per species/group were measured with 400 × magnification and biovolumes estimated according to Hillebrand et al. (1999). Using equation (1) these biovolumes were converted into carbon content after Menden-Deuer and Lessard (2000), with a and b being defined in their Table 4, $C \text{ cell}^{-1}$ in pg and V in μm^3 .

$$\log C \text{ cell}^{-1} = \log a + b * \log V \quad (1)$$

This calculation distinguishes between different types of protists and two size classes of diatoms (smaller or larger than $3000 \mu\text{m}^3$), which is displayed in different a and b values (Menden-Deuer and Lessard 2000). Based on abundance of the protists and their corresponding carbon content per unicellular organism, the vertical carbon flux ($\text{mg C m}^{-2} \text{d}^{-1}$) was determined and will be referred to as unicellular plankton carbon (UPC) flux. Thus, UPC accounts for phytoplankton carbon (PPC) as well as for protozooplankton biomass.

2.4 TEP analyses

Water samples were processed on board a few hours off collection following the protocol of Passow and Alldredge (1995). Each sample was split into half to receive duplicates of 100 mL. After being stained with alcian blue (Passow and Alldredge 1995), the samples were frozen at -20°C in sealed polycarbonate tubes until further processing in the laboratory on shore.

Staining of TEP particles from the PELAGRA-splits was performed according to an adapted method as described in detail in Passow et al. (2001) was applied.

TEP measurements were conducted with the colorimetric method (Pharma Spec UV-1700; Shimadzu) according to Passow and Alldredge (1995). For calibrating the TEP measurement, a calibration curve for the alcian blue solution was prepared with gum xanthan and the factor f_x estimated (Passow and Alldredge 1995). TEP concentration (C_{TEP}) is then expressed as gum xanthan

equivalent ($\mu\text{g L}^{-1}$) and can be estimated with equation (2), where E_{787} is the absorption of the sample at a wavelength of 787 nm, C_{787} the absorption of the blank at the same wavelength, and V_f the filtered volume (L).

$$C_{TEP} = (E_{787} - C_{787}) \times (V_f)^{-1} \times f_x \quad (2)$$

For the concentration of TEP in the water column, depth integrated values were estimated over 100, 200 and 500 m, respectively. C_{TEP} flux of the trap samples are referred to as TEP flux

3. Results

3.1 Flux characteristics from PA gels

During the LOHAHEX iron fertilisation experiment flux at 450 m predominantly consisted of large and relatively compact particles (Fig. 2). The sinking particles preserved in the PA gels suggest that the material was heavily processed before entering the trap as evidenced by the low abundance of fragile phyto-detritus aggregates. The temporal resolution is unfortunately very coarse because PA gel samples are only available from d0-d3, d26-d27 and d34 (Table 1) and thus temporal trends are not shown in detail. However, only small differences in regard to flux composition are detectable between the gels of the beginning and the end of the experiment, except the considerable number of large metazoan in the initial gels (Fig. 3). Towards the end, slightly more compact aggregates were present (Fig. 3b), but due to the low temporal resolution and the probability of a strong bias of the sinking particles during collecting (compare 4.1.1) this observation is not representative for the vertical flux.

3.2 Magnitude of unicellular plankton carbon (UPC) fluxes

UPC flux rates at IN and OUT stations were low throughout the first half of the LOHAFEX study and did not differ significantly from each other, after three weeks IN-fluxes were somewhat higher than OUT-fluxes (Fig. 4). Due to the limited number of deployments at 200 m (Table 1), flux dynamics over the course of the experiment were not well captured and are therefore not considered in detail.

At 450 m, UPC flux from the PELAGRA trap was very low throughout the experiment (IN and OUT) with some temporal variation (Table 3). The IN-trap in the period d29-d33 had somewhat lower fluxes in comparison to that of d23-d28 and d34-d37. The three traps were deployed directly one after another (Table 1), but there was no indication for a mal-functioning of any of these traps.

3.3 Composition of UPC fluxes

The collected plankton was divided into different groups of phytoplankton and protozooplankton based on microscopic investigations (compare 2.3). Phytoplankton was distinguished into diatoms, flagellates, silicoflagellates, coccoid cells, and autotrophic dinoflagellates. Within the flagellates *Phaeocystis antarctica* was considered separately, and within autotrophic dinoflagellates *Ceratium pentagonum*, because they were important constituents of the phytoplankton

assemblage at the surface. For diatoms also the C flux equivalent of intact empty and broken frustules was considered, in order to allow direct comparison with full cells and estimate the amount of carbon that was lost due to mortality. Protozooplankton was divided into heterotrophic dinoflagellates, ciliates (here only tintinnid ciliates were found), foraminifera, radiolaria, and heliozoa. Among the protozoa only dinoflagellates accounted for carbon transport to depth. To avoid confusion, it is important to remember that dinoflagellate flux was provided by both, autotrophic (e.g. *C. pentagonum*) and heterotrophic species. Apart from heterotrophic dinoflagellates, the protozoa consisted either almost entirely of empty or broken individuals or their abundance was very low (see below for details). According to the fact that the empty/broken or rare individuals of a species didn't account for carbon flux, these species were not accounted for UPC estimates. UPC flux was carried by diatoms, flagellates, coccoid cells and dinoflagellates in variable fractions (Fig. 5). The species are listed in Table 4, and it is indicated, whether they were found at IN and/or OUT stations and at which depth, and whether they contributed to UPC flux.

3.3.1 Phytoplankton

3.3.1.1 Diatoms

Generally, C flux of diatoms was very low (Fig. 6a). In the beginning, diatom C flux was comparably high inside the patch, decreased by 50% in the following three weeks, increased to the highest diatom C flux in the fourth week, but was halved afterwards (Table 3). Outside the patch, diatom C fluxes were very similar (Table 3). Overall contribution of diatom C flux to the UPC flux was just under a quarter at the most and in most cases less than 10% (Fig. 5).

The vast majority of sinking diatom frustules was empty and/or broken (Fig. 6b), whereas the ratio of full to empty and broken frustules (F:EB) was slightly higher at 200 m than at 450 m (Table 3). At 450 m the F:EB ratio was in most cases less than 0.5 (Table 3). Exceptions of 0.59 and 1.03 F:EB were detected in the beginning (Table 3), which coincides with higher diatom C fluxes (Fig. 6a). Moreover, it is striking that the flux of *Fragilariopsis kerguelensis* after 11 days showed a strong increase in empty and broken frustules, which is more than one order of magnitude higher than prior to iron addition (Fig. 6c).

In terms of C flux, the weekly silicified diatom *Ephemera cf. planamembranacea* played the most important role, followed by *F. kerguelensis* and *Thalassionema nitzschioides* (Fig. 7a-c). Notable, the large cylindrical diatoms (*Corethron pennatum*, *Corethron inerme*, *Proboscia alata*, *Rhizosolenia* spp.) vanished from the 450 m flux after 10 days and only returned as a few empty and/or broken frustules later in the experiment (Fig. 6d). Generally, most diatoms encountered during LOHAFEX were present in the lower size range reported in the literature for the respective species.

3.3.1.2 Flagellates

The C flux of flagellates at 450 m differed largely between IN and OUT stations: Inside the patch flagellate C fluxes increased with time, while they remained at the initial level outside the patch

(Table 3). Although absolute flagellate fluxes at 200 m were not variable (Table 3), their contribution to overall UPC flux increased with time (Fig. 5).

Most abundant at any time and depth were the smallest flagellates (up to 5 μm in size), and the large flagellates (>10 μm) were rarest, but the C flux was predominantly carried by the mid-sized (5-10 μm) and large flagellates (Fig. 8). At 450 m inside the patch, the flux of small flagellates increased in the first two weeks, showed a similar distribution in terms of size classes in the period of d23-d28 as in the beginning and then followed again a shift towards small flagellates (Fig. 8).

Phaeocystis antarctica, which was not present in C flux (at 200 m) or had low numbers (450 m) inside the patch in the beginning, showed an increase with time (Table 3). No regular trend was detected (Fig. 9), and they provided between 6 and 19% of flagellate C flux at 450 m and up to of 27% at 200 m depth (Fig. 8, Table 3). Outside the patch, the contribution of *Phaeocystis antarctica* decreased towards the end (Table 3, Fig. 8, 9).

The coccolithophore *Emiliana huxleyi* continuously contributed to the flux. But its abundance could not be determined due to many broken individuals that were not countable.

The Silicoflagellate *Dictyocha speculum* (Table 4) showed very low abundances in the UPC flux (<0.1%) throughout the experiment. Moreover, only empty or broken individuals were present and therefore *Dictyocha speculum* was not followed further.

3.3.1.3 Coccoid cells

The carbon flux of coccoid cells (2 μm in diameter) at 200 m was relatively low at any time and site during the experiment, and showed a slight decrease towards the end (d26/d27). Despite the decline of absolute coccoid cell flux, its contribution to total UPC flux increased due to a decrease of the other components, such as diatoms, flagellates and dinoflagellates (Table 3; Fig. 5).

At 450 m inside the patch, coccoid cell C flux increased by one order of magnitude after three weeks (Table 3) and hence provided 4% of total UPC flux at the end (Fig. 5). Outside the patch, the absolute C flux of coccoid cells at 450 m remained as low as in the beginning (Table 3), but their relative importance increased up to 3% (Fig. 5).

3.3.1.4 Autotrophic dinoflagellates

See 3.3.2.1.

3.3.2 Protozoa

3.3.2.1 Dinoflagellates

Although autotrophic and heterotrophic dinoflagellates were counted separately, they are here combined to simplify matters because they were not divided into autotrophic and heterotrophic species when considering C flux. During the experiment, dinoflagellates at 450 m inside the patch accounted for half or more of the UPC flux, except the low fluxes in the second week (Table 3, Fig. 5). Afterwards, their contribution increased enormously by one order of magnitude (Table 3) and dominated the UPC flux (Fig. 5). The strongest contribution of dinoflagellates to C flux was detected at 200 m in the first two weeks, but it strongly decreased towards the end (Fig. 5, Table 3). Outside the

patch dinoflagellates showed a decrease of C flux by one half towards the end of the fourth week (Table 3, Fig. 5).

As one example for development with time, the magnitude of the (autotrophic) dinoflagellate *C. pentagonum* is given (Fig. 10). However, it was present as individual specimen as well as incorporated in aggregates and faecal pellets (Fig. 11).

3.3.2.2 Ciliates

Within the group of ciliates, only tintinnid ciliates were present (Table 4) and the flux consisted entirely of empty and/or crashed loricae (Fig. 11). The abundance of tintinnid loricae increased strongly inside the patch at 200 m and at 450 m, with *Acanthostomella norvegica* being the dominant species (Table 5). Outside the patch, tintinnid ciliate abundance was always somewhat lower, and also showed an increase at 450 m (Table 5). The highest abundance occurred three weeks within the experiment inside the patch at 450 m (Table 5). All loricae collected between d6 and d10 were crashed, which was the case for the majority in the other samples as well, but not as pronounced (Table 5).

Among the tintinnid ciliates collected, *A. norvegica* was dominant at IN and OUT stations and it is notable that those counted as “other tintinnid ciliates” (hyaline loricae in the size range of *A. norvegica*) very likely also belong to this species but were crashed beyond recognition – adding to the already high fraction of *A. norvegica* (Table 5). Second most important were *Stenosonella avellana*, especially outside the patch, and *Cymatocyclis antarctica* (Table 5).

3.3.2.3 Foraminifera

The vast majority of the collected foraminifera was empty; in all samples, except one, not more than 6% of them were full; only between d6 and d10 18% were full (Table 6). Some of the empty individuals were also broken and showed explicit signs/traces of grazing, such as broken spines and/or tests (Fig. 11). The ratio of full to empty and broken tests did not show a tendency, but indicates low ratios or even total absence of full houses towards to end in 450 m depth (Table 6).

Among the total number of foraminifera the non-spinos species *Neogloboquadrina* sp. accounted for most of the individuals (Table 6). Due to heavily fractured houses and broken spines, the spinos foraminifers could not always be determined to species level. Thus, *Globigerina bulloides* and *Turborotalita quinqueloba* were not distinguished, but counted as spinos foraminifera.

3.3.2.4 Radiolaria

Radiolaria played a minor role in the protozoan flux. A few *Nasselaria* and *Spumellaria* were present whereas *Phaeodaria* were completely absent (Table 4). Inside the patch, only empty and/or broken individuals were found and no trend with depth or time was recognisable (Table 7). Those very few individuals that were full occurred outside the patch (at 200 m in #5, and at 450 m in #8 and #10), where abundances in general were slightly higher than inside (Table 7).

Heliozoa flux was very small (<0.1‰ of UPC) and did not differ between 200 and 450 m, thus they are not considered in detail for this study. The dominant species was *Sticholonche zanclea* (Table 4).

3.4 TEP concentration

3.4.1 Water column TEP

Throughout the experiment TEP concentrations were highest in the surface layer (upper 20 m) and decreased with increasing depth by approximately one third from the surface to 500 m (Fig. 12a, b). The strongest decrease was detected within the upper 100 m. This is the case for both, IN and OUT stations. In the beginning, TEP concentrations were comparably low, especially below 100 m (Fig. 12a; Table 8). Inside the patch, TEP values were highest at all depths after approximately two weeks, remained at that high level from d12 until d24, and decreased towards to end of the experiment (Fig. 12a; Table 8). Unfortunately, TEP profiles outside the patch are only available for the second half of the experiment (Table 2). The first two TEP profiles (d16 and d22) resemble each other, but a decrease at the end (d35) is also detectable (Fig. 12b).

Depth integrated TEP also represented a muted increase from d0 until d24, followed by a slight decrease towards the end (Fig. 12c). The increasing tendency of TEP in 500 m is somewhat slower than that in 200 m. The total amount of TEP in the water column is very similar inside and outside the patch (Fig. 12a-c).

TEP and Chla in the surface layer (at 10 m depth) are not correlated (Fig. 12d). Surface TEP varied between 86 and 95 $\mu\text{g L}^{-1}$ (Table 8) and did not follow a trend with time, while Chla increased towards highest values at d24 and then decreased again (Fig. 12d).

3.4.1 TEP flux

TEP flux at 200 m was highest two weeks after iron addition, where it accounted for 34% d^{-1} of water column TEP (Table 8). At 450 m, TEP flux constituted 12% d^{-1} or less of the TEP in stock in the water column (Table 8). TEP flux at 450 m strongly increased from 0 to 4.26 $\text{mg m}^{-2} \text{d}^{-1}$ in the fourth week, followed by a decrease (Table 8). Difference between IN and OUT-station were small (Fig. 13a).

4. Discussion

4.1 Trap accuracy

The successful PELAGRA trap deployments considered for this study (Table 1) allow studying flux dynamics based on biogeochemical fluxes (Table 3), because over- or undersampling was not evident. However, particles collected with PA gels deployed with the PELAGRA traps are not preserved as undisturbed as anticipated (Fig. 2, 3 and 4.1.2 for details). This suggests that the sinking particles were heavily biased as they settled into the collection funnel (Ebersbach et al. in prep.) and have to be regarded with suspicion when drawing conclusions on flux composition.

4.1.1 Biogeochemical fluxes

Although sinking fluxes intercepted with PELAGRA traps have been reported in previous studies (e.g. Lampitt et al. 2008), the daily flux rates have to be viewed with caution, because export events may occur in pulses. Given the fact that during LOHAFEX most PELAGRA traps were deployed for several days (Table 1) and between successive deployments large difference in average daily fluxes of UPC were collected (Fig. 4), non continuous fluxes of sinking material is suggested. This seemed to have been the case in the second half of the experiment in particular (Fig. 4; Table 3).

4.1.1 PA gels

The particle assemblage in the PA gels from the first 2 days as compared to those that were collected well after iron enrichment during the phase of biomass build-up at the surface, are very similar in appearance (Fig. 3). One reason for this similarity might be that flux characteristics were not influenced by iron fertilisation (see 4.5.2). Another reason could have been the impact of the PELAGRA trap design on the sampling procedure and the subsequent destruction of the collected particles. Possibly, structure and form of the particles were altered in the trap funnel before they settled into the PA gel (Ebersbach et al. in prep.). This makes the identification of individual particles in these gels very difficult (Fig. 3), especially those that appear to be heavily reworked and may be attributed to faecal aggregates (compare 4.3).

4.2 Magnitude of flux

The small difference in the UPC flux between the fertilised patch and surrounding waters (Table 3; Fig. 4) suggests that the iron-induced increase in primary production did not result in an increased export signal at depth. In comparison to total POC flux, UPC accounted for less than 10% in most cases, and for even less than 5% in the second half of the LOHAFEX study, where total UPC fluxes had increased (Table 3). The conspicuously higher contribution of UPC of 28 and 45% to POC at the beginning of the experiment indicates that UPC flux was more important to overall export before iron was added to the system, and might have resulted from a previous natural bloom that occurred in this region prior to our arrival. This is supported by additional evidences, such as the very low silicic acid (Si(OH)_4) concentrations in the upper 100 m (0.5-2 μM) at d0 (Pratihary et al. 2010) and the ^{234}Th -profiles, which implied that an export of particles from the surface waters had occurred in the past approximately two months (Rengarajan et al. 2010). Thus, the LOHAFEX eddy had probably experienced a diatom bloom prior to the experiment that had depleted surface silicic acid concentrations and accounted for the surface deficit in the ^{234}Th signal (Mazzocchi et al. 2009). Whereas the decline of UPC flux over the first three weeks (Fig. 4) probably depicts the fading of the previous bloom, the noticeable high UPC flux in the fourth week of the LOHAFEX experiment might mirror the settling of the bloom induced by iron addition. However, UPC flux was still very low and more or less within the variability of the data.

The low fluxes collected with the PELAGRA traps agree with vertical particle profiles recorded with the Underwater Video Profiler (UVP), the transmissometer profiles, and ^{234}Th

measurements (Mazzocchi et al. 2009). This suggests that only a small fraction of the algal biomass that was built up at the surface settled out of the mixed layer. Instead, it must have been maintained in the surface layer. This is in contrast to EIFEX, where a massive sinking event of the senescent bloom was observed at the end of the experiment (Smetacek et al. in prep.). During LOHAFEX, on the contrary, UPC played a minor role for export flux.

4.3 Composition of the flux

First of all, it stands out that full diatoms were very rare in the UPC flux during LOHAFEX, which contradicts findings of previous iron fertilisation experiments in the Southern Ocean (compare Boyd et al. 2007 and references therein). However, UPC flux depicts the phytoplankton composition of the surface layer. The iron induced bloom was dominated by small flagellates, in particular *Phaeocystis antarctica* and unidentified Prasinophytes (Assmy et al. 2010), which agrees with their consistent presence in the UPC flux following the evolving bloom (Table 3; Fig. 5, 8 and 9). Especially, the highest *Phaeocystis antarctica* flux in the third week (Fig. 9) coincides with high *Phaeocystis antarctica* abundances at the surface a few days before (P. Assmy pers. comm.). In coincidence with the surface community, flux was dominated by small flagellates, although the fewer but larger individuals were carrying the C flux (Fig. 8).

The observation that with time the size spectrum of flagellates at 450 m shifted towards smaller individuals and the abundance of the even smaller coccoid cells also increased (Fig. 8, Table 3), suggests selective grazing. Due to heavy grazing pressure by large copepods in the surface waters, only small individuals escaped, which would also explain the increasing relative importance of coccoid cells at 200 m, in spite of decreasing absolute numbers (Table 3).

In regard to diatom flux, the large increase of empty and broken frustules in response to iron addition (Fig. 6) confirms strong grazing at the surface. This is in agreement with many broken diatom frustules showing traces of handling by copepods and being incorporated into faecal aggregates (Fig. 11). The flux of empty and broken diatom frustules is also depicted in an increasing BSi flux at the same time (P. Martin, unpubl. data). Despite low SiOH_4^{4-} levels during LOHAFEX, diatoms showed high in-situ growth rates in the surface layer but did not accumulate biomass (pers. comm. P. Assmy), indicative of high grazing pressure. Moreover, the shift within the diatom community in the trap material from large cylindrical diatoms, such as *Corethron pennatum*, *C. inerme*, *Proboscia alata*, and *Rhizosilenia* spp., at the beginning of the experiment (Fig. 6d), towards smaller and partly heavily silicified pennate diatoms indicates a shift in the surface community which is supported by water column observations (P. Assmy, unpubl. data). While the former species likely constituted a signal from a previous bloom, the latter species contributed a relatively constant but low flux of mainly empty frustules to the deep water column for the remainder of the experiment.

While phyto-detritus did not contribute to C flux to a large extent, particulate transport was dominated by heavily processed material as demonstrated in the PA gels (Fig. 2 and 3). Most of these particles appear to be of faecal origin, which supports the finding of grazing playing the most

important role for export flux of organic material. Besides the obvious presence of faecal matter, traces of grazing also become evident by the striking dominance of empty and/or broken individuals of diatoms, radiolaria, silicoflagellates, and foraminifera in the flux (Table 6 and 7).

Moreover, cells of *C. pentagonum* as well as empty loricae of tintinnid ciliates were frequently found in faecal material (Fig. 11). Tintinnids are efficient grazers of small flagellates that dominated the iron induced bloom and responded to the enhanced food supply at the surface with increasing abundances (Mazzocchi et al. 2009). However they were themselves kept in check by copepod grazers as evidenced by the increase in empty or even crashed loricae of tintinnid ciliates that contributed to the flux (Table 5). The strong decrease of *C. pentagonum* and their incorporation in faecal material towards the end of the experiment is further evidence of heavy copepod grazing pressure (Mazzocchi et al. 2009). Thus trophic cascades played an important role in channelling carbon through the pelagic food web and eventually led to an export flux dominated by faecal material as evidenced by the PA gels (Fig. 2 and 3).

The presence of copepods is also mirrored in their grazing traces, for instance in forms of bitten spines of foraminifera, the large abundance of broken diatom frustules, and *C. pentagonum* and tintinnid loricae being incorporated in faecal aggregates (Fig. 11).

4.4. The role of TEP for export processes

The distribution of TEP in the water column (Fig. 12) resembled typical TEP profiles (Passow 2002). Compared to other Southern Ocean studies, TEP did not play an important role during LOHAFEX, where TEP concentrations were about one order of magnitude lower than previously determined (Passow et al. 1995; Hong et al. 1997).

In regard to the development of TEP production with time, the negligible differences between IN and OUT stations and the small changes within TEP profiles down to 500 m over the course of the experiment (Fig. 12a and b) support the low importance of TEP for particle aggregation in this ecosystem. Several studies have shown, that diverse phytoplankton communities are positively correlated to TEP production (Passow (2002) and references therein). This was also observed for flagellate dominated blooms and in particular for *Phaeocystis*. However, during LOHAFEX TEP at depths had increased slightly (Fig. 12a), and TEP integrated over the water column only showed minor variation with time (Fig. 12c). If at all, a small increase two weeks after the initial fertilisation could be detected (Fig. 12a-c). Furthermore, no positive correlation between TEP and Chla was detected at the surface (10 m depth) (Fig. 12d), suggesting that the production of TEP did not respond to iron addition.

In contrast, TEP flux at 450 m shows a strong increase from the first week to the maximal TEP concentrations four weeks after iron release (Fig. 13a). This finding stands in opposite to the more or less invariant TEP profiles in the upper 500 m (Fig. 12) and raises the question whether water column sampling was not conducted appropriate (detailed discussion below). Apart from the 12% d⁻¹ TEP that arrived at 450 m in the third week, TEP fluxes accounted for 8% d⁻¹ at the most (Table 8).

Although only a small fraction of TEP was recovered at depth, it was still more than the nearly 2% d⁻¹ that were measured in the only other TEP flux study available (Passow et al. 2001). Considering the different environmental conditions (Santa Barbara Channel with much higher TEP concentration in the water column (Passow et al. 2001)), a comparison to the LOHAFEX site does not make sense.

The observation that TEP flux seems to be totally unrelated to UPC flux (Fig. 13b), but shows a positive correlation with POC flux (at 450 m inside the patch; Fig. 13c) indicates that neither TEP production nor UPC flux responded to iron addition with a simple increase. In contrast, it is an evidence for export being not driven by phyto-detritus aggregates (which would have been displayed in UPC flux), but through a different pathway such as formation of faecal matter aggregates. It has been observed that zooplankton, especially copepods, may also contribute to TEP production (Prieto et al. 2001), although the mechanisms are not clear. The high abundance of copepods during LOHAFEX (Mazzocchi et al. 2009) could be one explanation for the positive relation between TEP flux and POC flux (Fig. 13c), assuming that TEP is incorporated into faecal aggregates produced by copepods. This would agree with the findings of (Passow et al. 2001), who proposed grazing as a possible sink for TEP loss.

It is likely that the sampling protocol for TEP in the water column was not sufficient to capturing TEP distribution representatively. Possibly, faecal aggregates, which appeared to have carried TEP to depths, might not have been collected adequately with this technique. Moreover, the spontaneous and short sinking events (compare also 4.1.1) might not have been collected in a representative way with our sampling frequency (Table 2). As each TEP profile only represents a snapshot of the overall picture (Fig. 12), a higher resolution with time and depths might have provided more inside into TEP dynamics and its role for export. Nonetheless, it has to be taken into account that only a very small fraction of the integrated TEP was exported (Table 8) and thus, uncertainties within the data might be large.

4.5 Comparison to previous iron fertilisation experiments

With respect to the composition of the surface phytoplankton community as well as the sinking material, the LOHAFEX iron enrichment study differs considerably from comparable studies conducted in the Southern Ocean. This might be due to several reasons. First of all, LOHAFEX was carried out in the northern part of the ACC in waters strongly depleted in silicic acid and thus dominated by phytoflagellates. Previous iron fertilisation experiments were conducted in silicic acid enriched waters and thus dominated by diatoms. (Boyd et al. (2007) and references therein), except SOFeX-North, where silicic acid concentrations were <3 $\mu\text{mol L}^{-1}$ (Coale et al. 2004). SOFeX investigated the response of iron addition to waters, that are only limited by iron (SOFeX-South) and those that are co-limited by iron and silicic acid (SOFeX-North; Coale et al. 2004). Despite low silicic acid concentrations, enhanced export fluxes were detected in the fertilised area of SOFeX-North, but data on rates are not available (Coale et al. 2004). However, export fluxes during SOFeX-North were probably regulated through phyto-detritus (Bishop et al. 2004; Coale et al. 2004). This result stands in

opposite to LOHAFEX, where the sinking particle assemblage predominantly consisted of faecal material (compare 4.3). In respect to flux composition, LOHAFEX might have resembled CROZEX, a naturally iron fertilisation experiment conducted in the Indian Sector of the Southern Ocean (Pollard et al. 2007). During CROZEX, parts of the iron fertilised bloom was provided by flagellates due to insufficient silicic acid concentrations for diatom growth (Poulton et al. 2007) and nonetheless translated into enhanced export rates in comparison to HNLC waters (Pollard et al. 2007).

5. Conclusions

The sinking particle assemblage during LOHAFEX reveals no detectable difference between fertilised and unfertilised waters. Despite a positive response of the surface plankton community to iron addition, export flux seems to have reacted to the changing conditions in the euphotic zone with only a slight increase. Our results indicate that fertilising the ecosystem of the Si-limited northern band of the ACC will not result in an enhanced export of carbon to the deep water column but in a retention system that will recycle most of the iron-induced biomass build-up in the surface mixed layer.

Considering the sparse resolution of data points and the uncertainties (compare 4.1 and 4.4) the results suggest that the sampling resolution was probably too coarse in regard to time and space. A higher spatial and temporal resolution might have shed more light on flux dynamics. Furthermore, it is possible that more insights into export processes would have been gained if moored deep sea traps were deployed in addition. One trap could have been positioned directly under the fertilised patch and a second trap mooring could have been deployed outside the patch. This would have provided some means to compare IN and OUT deep fluxes, although finding a good position for the IN trap would not have been an easy task because the patch was moving with the eddy field (Fig. 1). However, examining deep fluxes (close to the sea floor) could have been useful to prove the observation that iron fertilisation appeared to have only little effect on export flux during the LOHAFEX study.

References

- Assmy, P., J. Henjes, C. Klaas, and V. Smetacek. 2007. Mechanisms determining species dominance in a phytoplankton bloom induced by the iron fertilization experiment EisenEx in the Southern Ocean. *Deep Sea Research I* **54**: 340-362.
- Assmy, P., F. Ebersbach, N. Fuchs, C. Klaas, M. Montresor, and V. Smetacek. 2010. Phyto- and Protozooplankton, p. 81-86. In H. Bornemann and B. Chiaventone [eds.], Reports on Polar and Marine Research. The expedition of the Research Vessel "Polarstern" to the Antarctic on 2009 (ANT-XXV/3-LOHAFEX). Alfred Wegener Institute.
- Bathmann, U. 2005. Ecological and Biogeochemical Response of Antarctic Ecosystems to Iron Fertilization and Implications on Global Carbon Cycle. *Ocean and Polar Research* **27**: 231-235.
- Bishop, J. K. B., T. J. Wood, R. E. Davis, and J. T. Sherman. 2004. Robotic Observations of Enhanced Biomass and Export at 55°S During SOFex. *Science* **304**: 417-420.
- Boyd, P. W. and others 2007. Mesoscale Iron Enrichment Experiments 1993-2005: Synthesis and Future Directions. *Science* **315**: 612-617.
- Boyd, P. W., and T. W. Trull. 2007. Understanding the export of biogenic particles in oceanic waters: Is there consensus? *Progress In Oceanography* **72**: 276-312.
- Boyd, P. W. and others 2000. A mesoscale phytoplankton bloom in the polar Southern Ocean stimulated by iron fertilization. *Nature* **407**: 695-702.
- Buesseler, K. O., and P. W. Boyd. 2009. Shedding light on processes that control particle export and flux attenuation in the twilight zone of the open ocean. *Limnology and Oceanography* **54**: 1210-1232.
- Coale, K. H. and others 2004. Southern Ocean Iron Enrichment Experiment: Carbon Cycling on High- and Low-Si Waters. *Science* **304**: 408-414.
- De La Rocha, C. L. 2007. The Biological Pump, p. 1-29. In D. H. Heinrich and K. T. Karl [eds.], *Treatise on Geochemistry*. Pergamon.
- Ebersbach, F., and T. Trull. 2008. Sinking particle properties from polyacrylamide gels during the Kerguelen Ocean and Plateau compared Study (KEOPS): Zooplankton control of carbon export in an area of persistent natural iron inputs in the Southern Ocean. *Limnology and Oceanography* **53**: 212-224.
- Ebersbach, F., T. W. Trull, D. M. Diana, and C. Moy. 2010. A unique opportunity to study intact sinking particles: The combination of Polyacrylamide gels and sediment traps. *Limnology and Oceanography: Methods* **in prep.**
- Hillebrand, H., C.-D. Dürselen, D. Kirschtel, U. Pollinger, and Z. Tamar. 1999. Biovolume calculation for pelagic and benthic microalgae. *J. Phycol.* **35**: 403-424.
- Hong, Y., W. O. J. Smith, and A.-M. White. 1997. Studies on transparent exopolymers (TEP) produced in the Ross Sea (Antarctica) and by *Phaeocystis Antarctica* (Prymnesiophyceae). *Journal of Phycology* **33**: 368-376.
- Lamborg, C. H. and others 2008. The flux of bio- and lithogenic material associated with sinking particles in the mesopelagic 'twilight zone' of the northwest and North Central Pacific Ocean. *Deep Sea Research II* **55**: 1540-1562.
- Lampitt, R. S. and others 2008. Particle export from the euphotic zone: Estimates using a novel drifting sediment trap, 234Th and new production. *Deep Sea Research Part I: Oceanographic Research Papers* **55**: 1484-1502.
- Martin, J. H. 1990. Glacial-Interglacial CO₂ Change: The Iron Hypothesis. *Paleoceanography* **5**: 1-13.
- Mazzocchi, M. G. and others 2009. A non-diatom plankton bloom controlled by copepod grazing and amphipod predation: Preliminary results from the LOHAFEX iron-fertilisation experiment. *Globec International Newsletter*: 3-6.
- Menden-Deuer, S., and E. J. Lessard. 2000. Carbon to volume relationship for dinoflagellates, diatoms, and other protist plankton. *Limnology and Oceanography* **45**: 569-579.
- Murty, V. S. N. and others 2010. Physical Oceanography, p. 16-26. In H. Bornemann and B. Chiaventone [eds.], Reports on Polar and Marine Research. The expedition of the Research Vessel "Polarstern" to the Antarctic on 2009 (ANT-XXV/3-LOHAFEX). Alfred Wegener Institute.

III. Manuscript 4

- Passow, U. 2002. Transparent exopolymer particles (TEP) in aquatic environments. *Progress in Oceanography* **55**: 287-333.
- Passow, U., and A. L. Alldredge. 1995. A dye-binding assay for the spectrophotometric measurement of transparent exoplomer particles (TEP). *Limnology and Oceanography* **40**: 1326-1335.
- Passow, U., W. Kozlowski, and M. Vernet. 1995. Palmer LTER: Temporal variability of transparent exoplomymmer particles in Arthur Harbor during the 1994-1995 growth season. *Antartic Journal of the United States* **30**: 265-266.
- Passow, U., R. F. Shipe, A. Murray, D. K. Pak, M. A. Brzezinski, and A. L. Alldredge. 2001. The origin of transparent exopolymer particles (TEP) and their role in the sedimentation of particulate matter. *Continental Shelf Research* **21**: 327-346.
- Pollard, R., R. Sanders, M. Lucas, and P. Statham. 2007. The Crozet Natural Iron Bloom and Export Experiment (CROZEX). *Deep Sea Research II* **54**: 1905-1914.
- Poulton, A. J., C. M. Moore, S. Seeyave, M. I. Lucas, S. Fielding, and P. Ward. 2007. Phytoplankton community composition around the Crozet Plateau, with emphasise on diatoms and Phaeococysis. *Deep-Sea Research II* **54**: 1905-1914.
- Pratihary, A. K., D. Baraniya, and S. W. A. Naqvi. 2010. Macro nutrients, p. 29-30. In H. Bornemann and B. Chiaventone [eds.], *Reports on Polar and Marine Research. The expedition of the Research Vessel "Polarstern" to the Antarctic on 2009 (ANT-XXV/3-LOHAFEX)*. Alfred Wegener Institute.
- Prieto, L., F. Sommer, H. Stibor, and W. Koeve. 2001. Effects of planktonic copepods on transparent exopolymeric particles (TEP) abundance and size spectra. *Journal of Plankton Research* **23**: 515-525.
- Rengarajan, R., M. Soares, and M. M. Rutgers Van Der Loeff. 2010. Natural Rasionuclides and Radium Isotopes, p. 48-53. In H. Bornemann and B. Chiaventone [eds.], *Reports of Polar and Marine Research. The expedition of the Research Vessel "Polarstern" to the Antarctic on 2009 (ANT-XXV/3-LOHAFEX)*. Alfred Wegener Institute.
- Smetacek, V., and S. W. A. Naqvi. 2008. The next generation of iron fertiisation experiments in the Southern Ocean. *Philosophical Transactions of the Royal Society London A*. **366**: 3947-3967.
- Smetacek, V., and S. W. A. Naqvi. 2010. Summery and Iternary, p. 9-12. In H. Bornemann and B. Chiaventone [eds.], *Reports on Polar and Marine Research. The expedition of the Research Vessel "Polarstern" to the Antarctic on 2009 (ANT-XXV/3-LOHAFEX)*. Alfred Wegener Institute.
- Smetacek, V. and others 2010. Massive carbon flux to the deep sea from an iron-fertilized phytoplankton bloom in the Southern Ocean. *Nature* **in prep**.
- Turner, J. T. 2002. Zooplankton fecal pellets, marine snow and sinking phytoplankton blooms. *Aquatic Microbial Ecology* **27**: 57-102.
- Utermöhl, H. 1958. Zur Vervollkommnung der quantitativen Phytoplankton-Methodik. *Mitteilungen/Internationale Vereinigung für Theoretische und Angewandte Limnologie* **9**: 1-13.
- Volk, T., and M. I. Hoffert. 1985. Ocean carbon pumps: analysis of relative strengths and efficiencies in ocean-driven atmospheric CO₂ changes. *Geophysical Monographs* **32**: 99-110.

Figures

Fig. 1. MODIS image of the LOHAFEX study area showing Chla surface concentrations in the period 12 to 14 February. The iron induced bloom is encircled and its elongated form is recognisable. Note the size of the much larger phytoplankton blooms in the northeast of the (artificial) LOHAFEX bloom for comparison. (Source: <http://modis.gsfc.nasa.gov/>)

Fig. 2. Image of entire PA gel (Gel 10; see Table 1 for deployment time), in which particulate flux of a 24 h sampling period from the second half of the LOHAFEX study is preserved. The uneven distribution of the particulate matter points to a strong impact of the trap design on the collection procedure (see 4.1.1 for a detailed discussion).

Fig. 3. Detailed images of PA gels as they were obtained during LOHAFEX: a) Gel 1-3 (beginning of the experiment), b) Gel 10-12 (end of the experiment). See Table 1 for deployment details. No considerable difference of flux composition between beginning and end of the experiment is evident and the majority of the collected particles appear to be of faecal origin. (Scale bar: 1 mm)

Fig. 4. Total Unicellular Planktonic Carbon (UPC) flux determined from PELAGRA trap samples: Development of IN and OUT fluxes at 200 and 450 m, respectively.

Fig. 5. Relative Unicellular Plankton Carbon (UPC) flux of the C flux carrying groups i) diatoms, ii) flagellates, iii) dinoflagellates, and iv) coccoid cells: Development over the course of the experiment a) at 200 m (IN and OUT), b) at 450 m IN, and c) at 450 m OUT.

Fig. 6. Contribution of diatoms to the flux at 450 m inside the patch: Development over the course of the experiment. (Note the different scales on the y-axis) a) total diatom C flux (only full frustules), b) total diatom C flux (full frustules) and C flux equivalent (empty and broken frustules), c) full, empty and broken of *F. kerguelensis*, d) full, empty and broken frustules of large cylindrical diatoms (*C. pennatum*, *C. inerme*, *Proboscia alata*, *Rhizosilenia* spp.).

Fig. 7. C flux and ratio of full to empty and broken frustules of some selected abundant diatoms species: a) and d) *F. kerguelensis*, b) and e) *T. nitzschioides* and c) and f) *Ephemera* cf. *planamembranacea*.

Fig. 8. Relative fluxes of different sizes classes (2.5-5 μm , 5-10 μm , >10 μm) and the separate contribution of *Phaeocystis antarctica* within the flagellates C flux: Development over the course of the experiment a) at 200 m (IN and OUT), b) at 450 m IN, and c) at 450 m OUT.

Fig. 9. C flux of the flagellate *Phaeocystis antarctica* that was amongst the important primary producers in the surface community: Development of IN and OUT fluxes at 200 and 450 m, respectively.

Fig. 10. C flux of the surface autotrophic dinoflagellate *Ceratium pentagonum*: Development of IN and OUT fluxes at 200 and 450 m, respectively.

Fig. 11. Images showing the flux composition as examined with the microscope (from bulk sediment trap samples; a, b, c, f: 450 m; e, d: 200 m): a) dinoflagellate *Gyrodinium* spec. and faecal material, b) broken radiolaria embedded in faecal matter, c) shells of protozoan origin (for instance empty tintinnid loricae) integrated in faecal material, d) empty foraminifera with broken spines and *C. pentagonum* incorporated in faecal material, e) broken *Proboscia alata*, *C. pentagonum*, and faecal matter, f) faecal material containing empty tintinnid loricae, *C. pentagonum* as well as recognisable individual faecal pellets.

Fig. 12. TEP distribution in the upper 500 m of the water column: profiles a) inside, and b) profiles outside the patch, c) integrated TEP over the water column. d) relation of surface TEP (at 10 m) to Chla. (See Table 2 for sampling details of water column TEP.)

Fig. 13. TEP flux at 200 m and 450 m over the course of the experiment: a) absolute TEP flux, b) relation between TEP and UPC flux, and c) relation between TEP and POC flux.

Fig. 1.

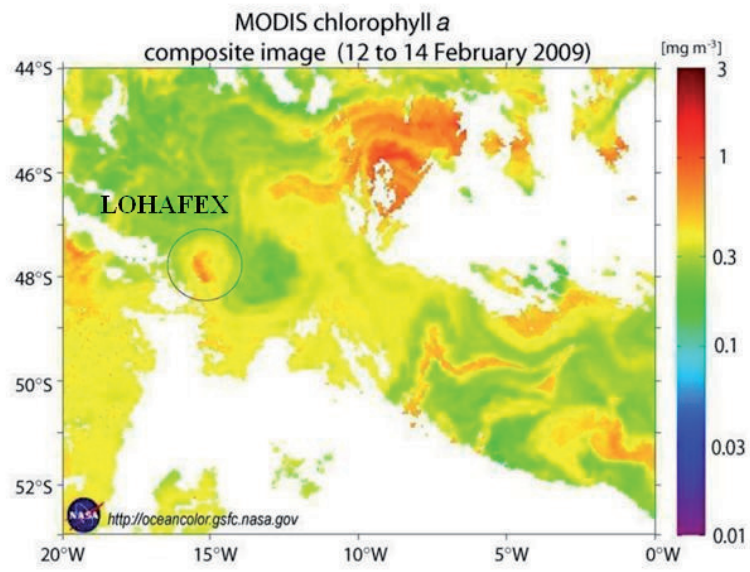


Fig. 2.

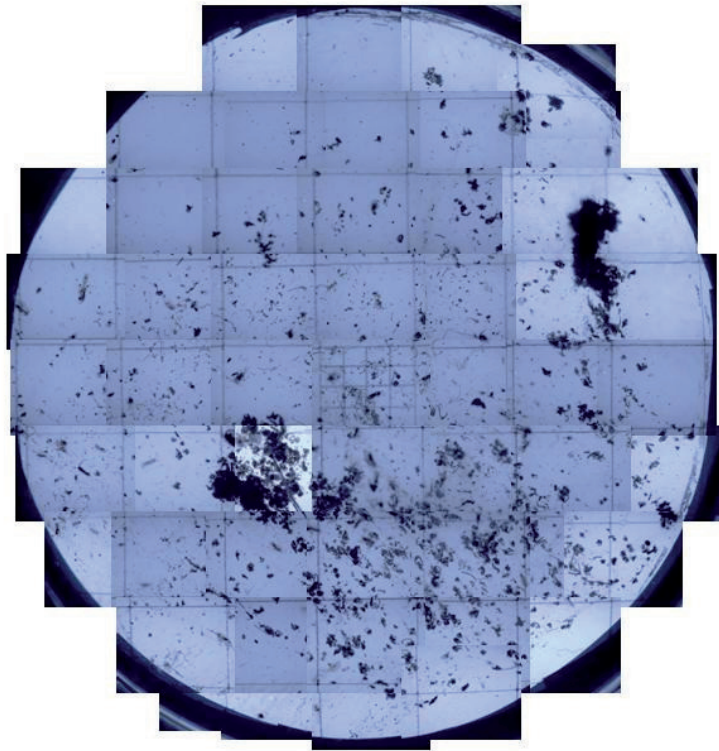


Fig. 3.

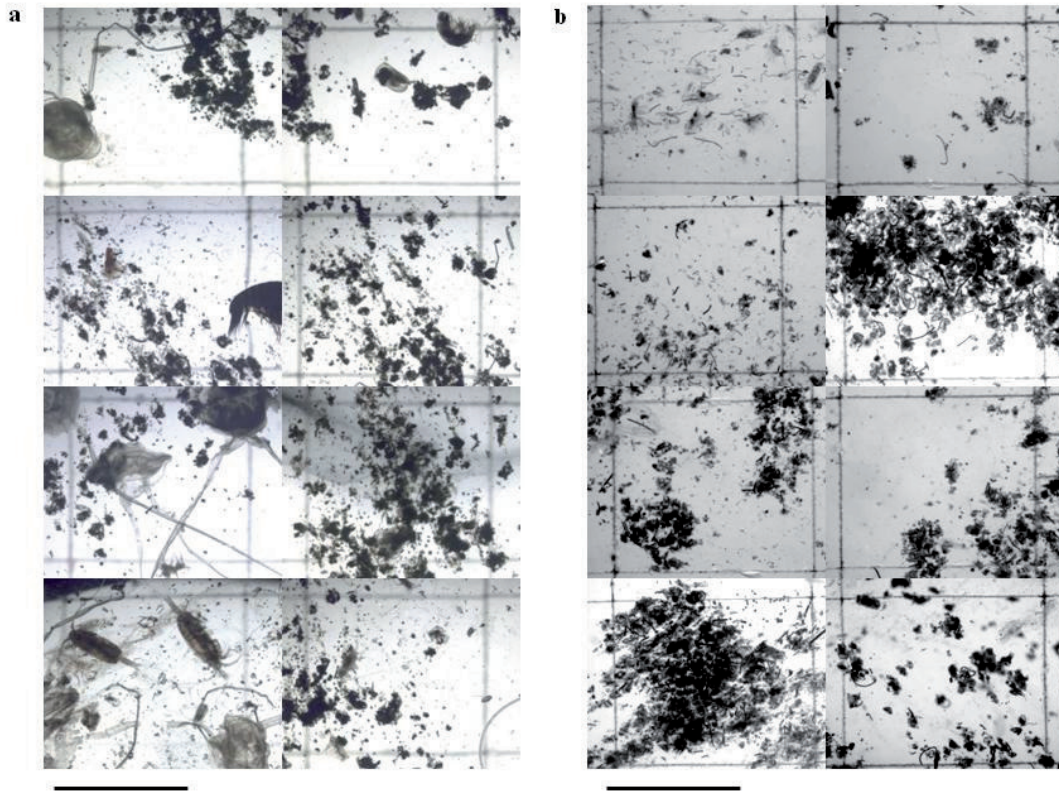


Fig. 4.

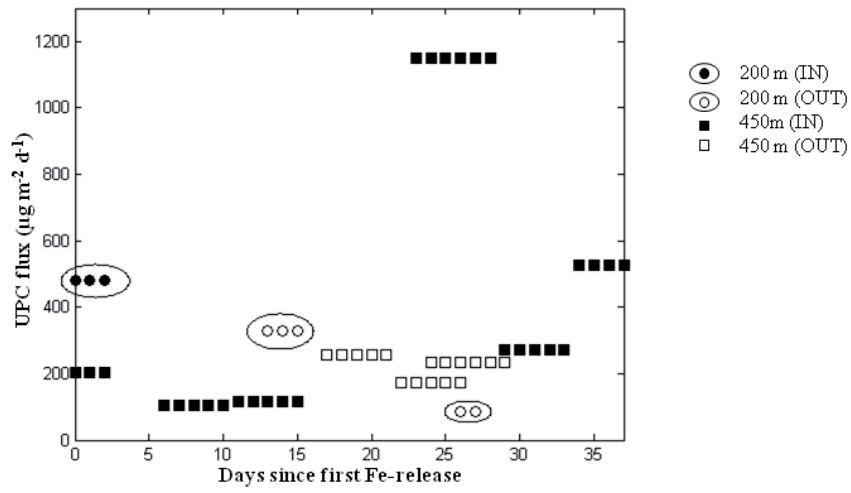


Fig. 5.

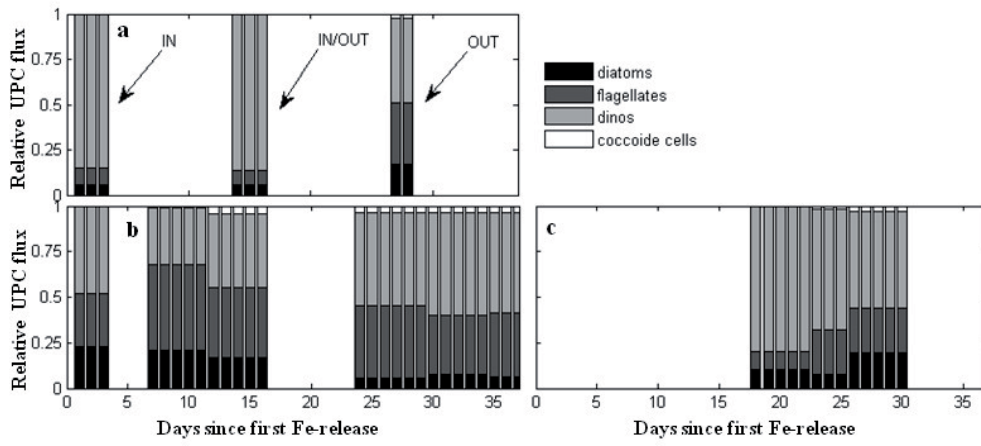


Fig. 6.

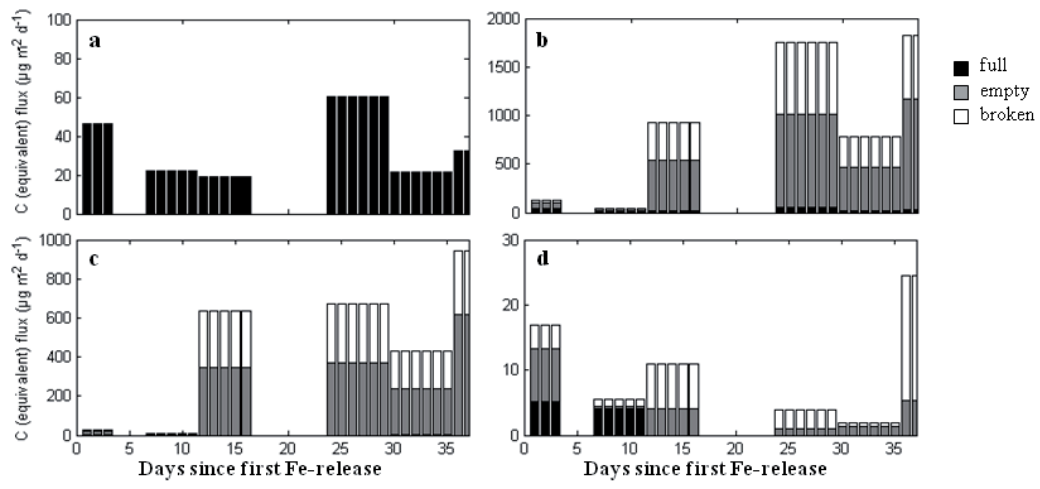


Fig. 7.

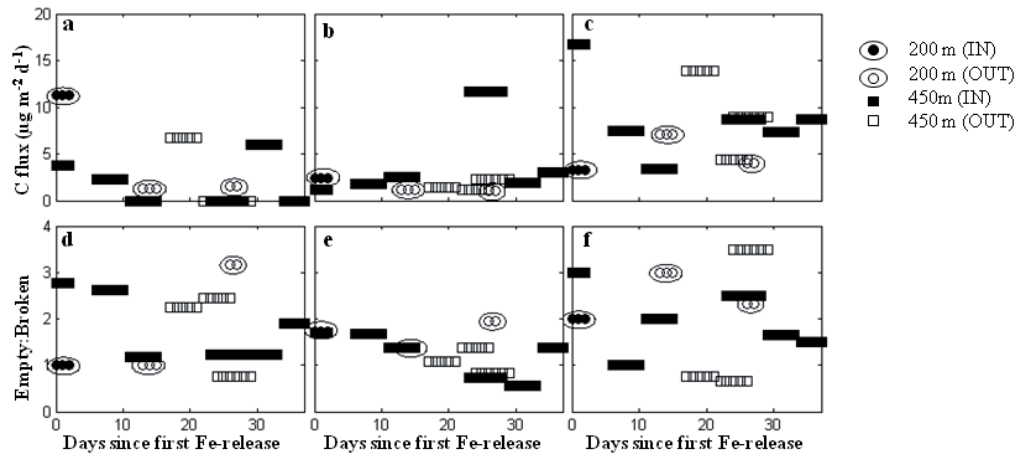


Fig. 8.

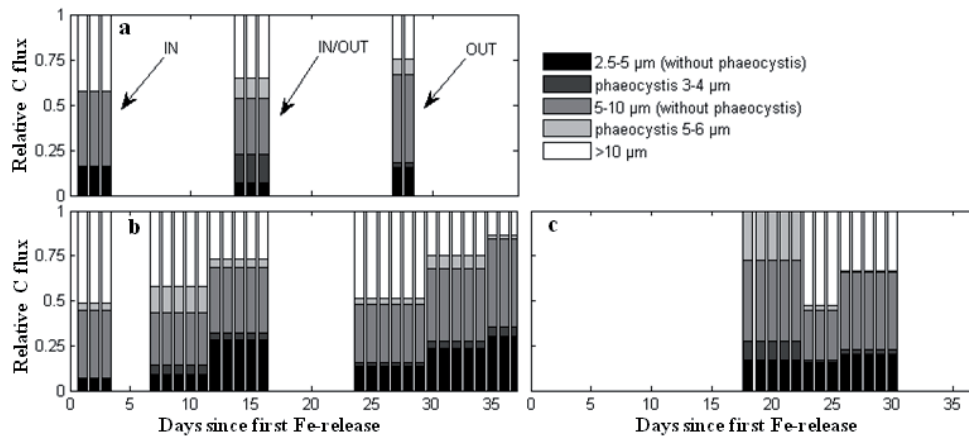


Fig. 9.

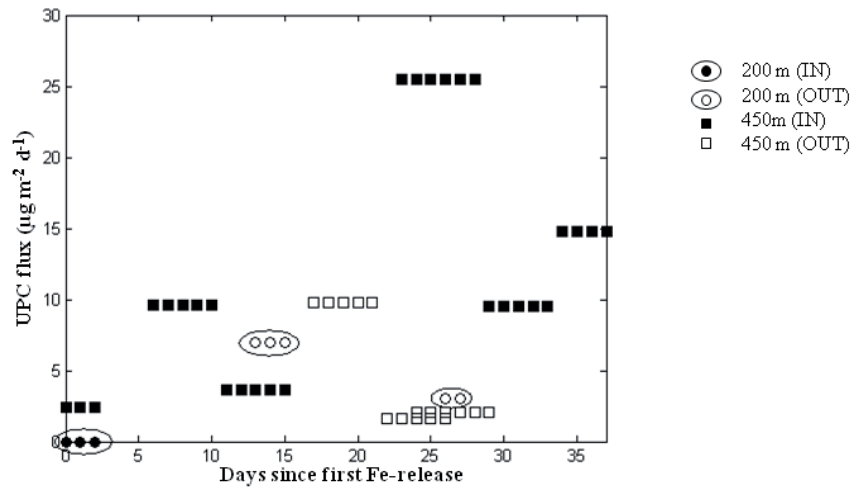


Fig. 11.

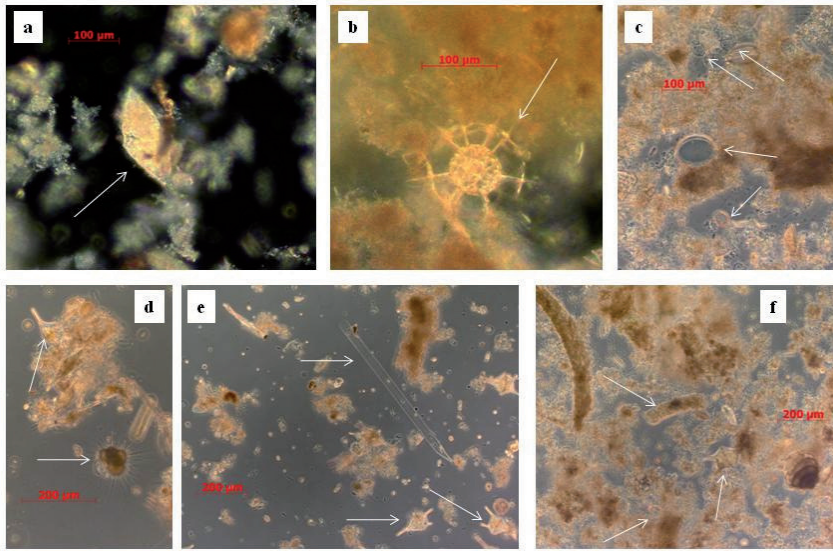


Fig. 12.

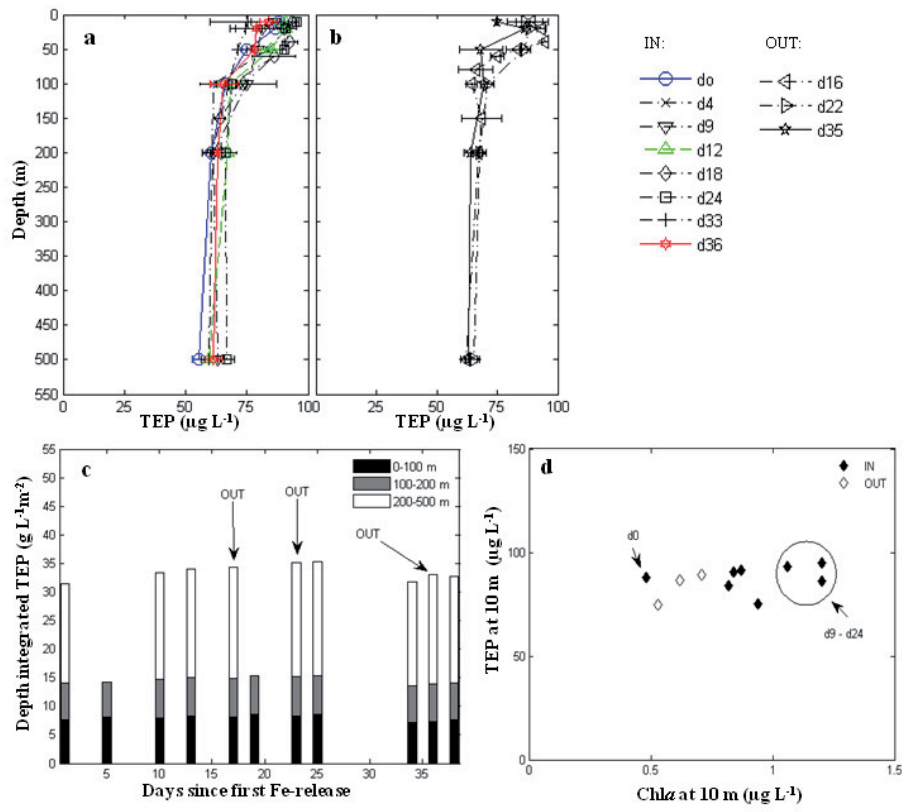


Fig. 13.

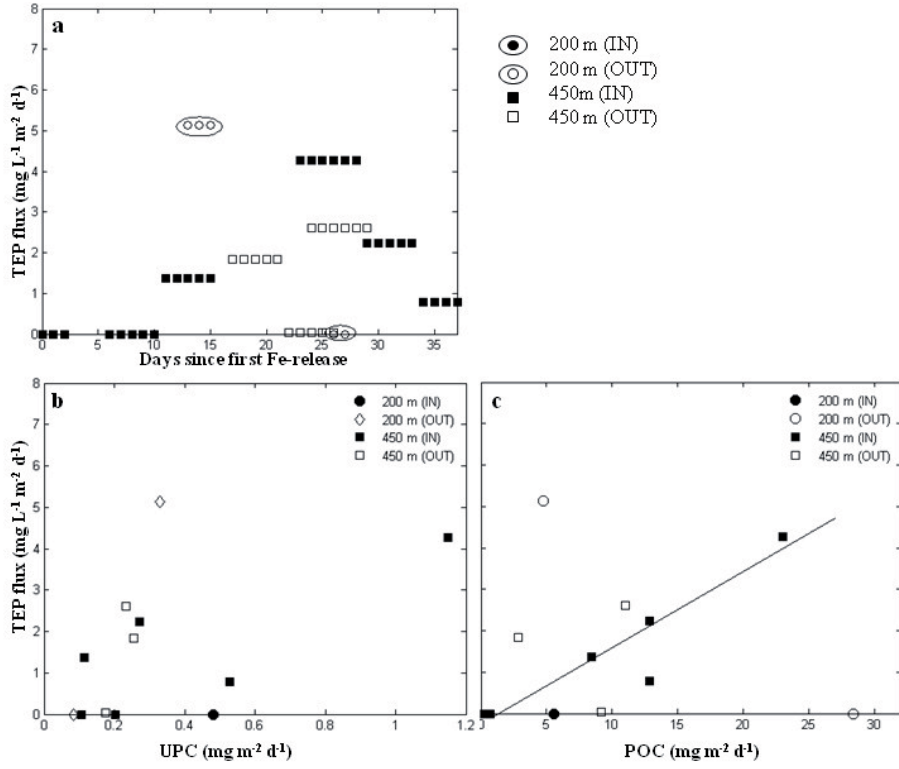


Table 1. PELAGRA trap deployments.

#	Days	Time* (h)	Depth (m)	Patch	Application	Start position	End position
1	d0 - d2	48	210	IN	biogeochemical fluxes	48°02.39'S, 15°81.07'W	47°87.17'S, 15°88.06'W
2	d0 - d2	48	450	IN	biogeochemical fluxes	48°02.96'S, 15°79.55'W	47°89.00'S, 15°85.89'W
3	d0 - d2	48	450	IN	Gel 1 - 3	48°02.74'S, 15°80.20'W	47°88.45'S, 15°88.42'W
4	d6 - d10	107	490	IN	biogeochemical fluxes	47°57.20'S, 15°67.03'W	47°51.05'S, 15°14.50'W
5	d13 - d15	48	200	IN/OUT	biogeochemical fluxes	47°89.45'S, 15°26.48'W	47°79.95'S, 15°51.89'W
6	d13	-	450	IN	Gel 4, 5	47°89.77'S, 15°27.48'W	-**
7	d11 - d15	121	440	IN/OUT	biogeochemical fluxes	47°73.20'S, 15°12.53'W	47°84.89'S, 15°46.95'W
8	d17 - d21	99	470	OUT	biogeochemical fluxes	47°50.27'S, 15°44.10'W	47°47.90'S, 14°88.60'W
9	d19	-	450	IN	Gel 6, 7	47°82.00'S, 15°12.60'W	-**
10	d22 - d26	123	440	OUT	biogeochemical fluxes	47°65.52'S, 15°59.53'W	47°58.60'S, 14°56.11'W
11	d22	-	450	IN	Gel 8, 9	47°35.10'S, 15°41.68'W	-**
12	d26 - d27	24	230	IN/OUT	biogeochemical fluxes Gel 10, 11	47°51.38'S, 15°45.07'W	48°37.31'S, 14°75.42'W
13	d24 - d29	132	430	OUT***	biogeochemical fluxes	47°30.00'S, 15°55.60'W	48°38.47'S, 14°62.64'W
14	d23 - d28	126	440	IN	biogeochemical fluxes	47°35.10'S, 15°41.68'W	47°89.36'S, 14°42.47'W
15	d29 - d33	120	460	IN	biogeochemical fluxes	48°08.60'S, 14°46.70'W	48°97.89'S, 15°13.47'W
16	d34 - d37	86	440	IN	biogeochemical fluxes Gel 12	48°79.57'S, 15°23.70'W	49°04.06'S, 15°28.53'W

* Collection time (Cups open)

** Deployment was not successful due to technical problems

*** close to IN

Table 2. CTD stations, where TEP samples were taken

Station	Day	Depth (m)	Patch	Position
St. 114	d0	10, 20, 50, 100, 200, 500	IN	48°00.18'S, 15°80.83'W
St. 132	d4	20, 50, 100, 200	IN	47°64.34'S, 15°72.56'W
St. 135	d9	10, 20, 50, 100, 200, 500	IN	47°70.03'S, 15°11.49'W
St. 137	d12	10, 20, 50, 100, 200, 500	IN	47°85.45'S, 15°24.39'W
St. 146	d16	10, 20, 40, 50, 60, 80, 100, 150, 200, 500	OUT	47°49.09'S, 15°42.00'W
St. 147	d18	10, 20, 40, 60, 100, 150, 200	IN	48°04.13'S, 15°24.65'W
St. 160	d22	10, 20, 50, 100, 200, 500	OUT	47°34.30'S, 15°66.28'W
St. 162	d24	10, 20, 50, 100, 200, 500	IN	47°35.54'S, 14°71.56'W
St. 192	d33	10, 20, 50, 100, 200, 500	IN	48°79.59'S, 15°24.67'W
St. 199	d35	10, 20, 50, 100, 200, 500	OUT	48°06.13'S, 15°23.19'W
St. 204	d36	10, 20, 50, 100, 200, 500	IN	48°97.48'S, 15°23.41'W

III. Manuscript 4

Table 3. UPC flux, separated into diatoms, flagellates, coccoid cells and dinoflagellates.

PELAGRA trap	Days after Fe addition	diatoms $\mu\text{g C m}^{-2} \text{d}^{-1}$	(F:EB)*	flagellates $\mu\text{g C m}^{-2} \text{d}^{-1}$	P.a.** (%)	coccoide cells $\mu\text{g C m}^{-2} \text{d}^{-1}$	dinoflagellates $\mu\text{g C m}^{-2} \text{d}^{-1}$	C. p.*** (%)	total PPC $\mu\text{g C m}^{-2} \text{d}^{-1}$	POC**** $\text{mg C m}^{-2} \text{d}^{-1}$	PPC of POC (%)
200 m											
# 1 (IN)	d0 - d2	28.23	(0.11)	42.92	(0)	3.23	408.22	(0.68)	482.60	5.56	8.7
# 5 (IN/OUT)	d13 - d15	17.93	(0.20)	26.31	(27)	0.82	283.36	(0.66)	328.42	4.78	6.9
# 12 (OUT)	d26 - d27	14.24	(0.13)	28.65	(10)	1.75	39.86	(0.14)	84.50	28.39	0.3
450 m (IN)											
# 2	d0 - d2	46.21	(0.59)	58.95	(4)	1.41	96.26	(0.31)	202.83	0.73	28
# 4	d6 - d10	21.96	(1.03)	49.51	(19)	0.78	33.34	(0.16)	105.58	0.24	45
# 7 (IN/OUT)	d11 - d15	19.33	(0.02)	43.84	(8)	4.81	46.26	(0.14)	114.24	8.44	14
# 14	d23 - d28	60.76	(0.04)	457.47	(6)	39.73	591.05	(0.09)	1149.01	22.96	5
# 15	d29 - d33	21.33	(0.03)	87.54	(11)	10.62	150.94	(0.10)	270.43	12.82	2.1
# 16	d34 - d37	32.18	(0.02)	187.05	(8)	19.56	288.84	(0.16)	527.63	12.85	4.1
450 m (OUT)											
# 8	d17 - d21	26.95	(0.05)	25.71	(38)	1.53	202.14	(0.08)	256.34	2.83	9.1
# 10	d22 - d26	13.84	(0.03)	42.72	4)	2.57	115.05	(0.09)	174.19	9.18	1.9
# 13 (close to IN)	d24 - d29	45.23	(0.03)	58.48	(4)	7.11	123.47	(0.35)	234.29	10.97	2.1

* ratio of full (F) to empty (E) and broken (B) frustules

** POC flux of *Phaeocystis antarctica* as fraction of flagellate POC flux

*** POC flux of *Ceratium petagonum* as fraction of dinoflagellate POC flux

**** total POC flux from PELAGRA traps (unpubl. data P. Martin)

Table 4. Plankton groups present in the PELAGRA traps

Group	200 m (IN)	200 m (OUT)	450 m (IN)	450 m (OUT)
Diatoms				
pennate diatoms				
Fragilariopsis kerguelensis	++	++	++	++
Fragilariopsis rhombica/seperanda	++	++	++	++
Thalassionema nitzschioides	++	++	++	++
Thalassionema n. var. lanceolatum	+	+	++	+
Ephemera cf. planamembranacea	++	++	++	++
Haslea sp.	++	++	++	++
Pseudo-nitzschia linola	++	++	++	+
Pseudo-nitzschia turgidula	++	++	++	++
Pseudo-nitzschia heimii	+	+	+	++
Lennoxia	++	++	++	++
Ceratoneis closterium	-	-	+	-
centric diatoms				
Thalassiosira gracilis	+	+	+	+
Thalassiosira oestrupii	+	+	+	+
Thalassiosira lentiginosa	++	++	++	++
Thalassiosira spp.	++	++	++	++
Asteromphalus hyalines	-	-	++	+
Asteromphalus hookeri/parvulus	+	+	++	++
Azpeitia sp.	+	+	+	+
Actinocyclus sp.	++	+	+	+
Eucampia antarctica	+	+	+	+
Corethron pennatum (small)	++	++	++	++
Chaetoceros convulata	-	+	+	-
Chaetoceros spore	++	++	++	++
Corethron pennatum (large)	+	+	+	++
Corethron inerme	+	+	++	+
Proboscia alata	+	+	++	++
Rhizosolenia curvata	-	-	++	+
Rhizosolenia sp.	-	-	+	+
Flagellates				
Phaeocystis	++	++	++	++
'Nose'-flagellate	++	++	++	++
'Trunk'-flagellat	-	-	++	++
Choanoflagellate	++	++	++	++
Flagellate sp.	++	++	++	++
Emiliana huxleyi	++	++	++	++

III. Manuscript 4

Dinoflagellates

Ceratium pentagonum	++	++	++	++
Gyrodinium	++	++	++	++
Nematodium	-	-	++	-
Prorocentrum spp.	++	++	++	++
Protoperdinium spp.	++	++	++	++
Podolampas sp.	++	++	++	++
'Cone'-flagellate	++	++	++	++
naked dinoflagellate	++	++	++	++
thecate dinoflagellate	++	++	++	++

Coccolid cells

	++	++	++	++
--	----	----	----	----

Ciliates (tintinnid ciliates)

Acanthostomella norvegica	+	+	+	+
Stenosemella avellana	+	+	+	+
Cymatocyclis antarctica	+	+	+	+
Cymatocyclis vanhoeffeni	+	+	+	+
Codonellopsis pusilla	+	-	+	-
Codonellopsis gausii	+	-	+	-

Foraminifera

Neogloboquadrina sp.	++	++	++	++
Globigerina buloides /	++	++	++	++
Turborotalita quinqueloba*				

Radiolaria

Nasselaria spp.	+	+	+	+
Spumellaria spp.	+	+	+	+

Heliozoa

Sticholonche zanclea	++	++	++	++
----------------------	----	----	----	----

Silicoflagellates

Dictyocha	+	+	+	+
-----------	---	---	---	---

-: nothing

+: empty and/or broken

++: full and empty/broken

* were not distinguished and together referred to as spinos foraminifera

III. Manuscript 4

Table 5. Abundance of tintinnid ciliates from PELAGRA traps: abundance of empty and crashed loricae together is presented (and the crashed loricea as a fraction thereof is given in brackets). Note: no full tintinnids were present.

PELAGRA trap	Acanthostomella		Stenosemella		Cymatocyclus		Cymatocyclus		Codonellopsis		Codonellopsis		other		total	
	norvegica	avellana	antarctica	vanhoffeni	pusilla	gausii	tin. ciliates	tin. ciliates	tin. ciliates	tin. ciliates	tin. ciliates	tin. ciliates	tin. ciliates	tin. ciliates	tin. ciliates	tin. ciliates
	# 10 ³ m ⁻² d ⁻¹	# 10 ³ m ⁻² d ⁻¹	# 10 ³ m ⁻² d ⁻¹	# 10 ³ m ⁻² d ⁻¹	# 10 ³ m ⁻² d ⁻¹	# 10 ³ m ⁻² d ⁻¹	# 10 ³ m ⁻² d ⁻¹	# 10 ³ m ⁻² d ⁻¹	# 10 ³ m ⁻² d ⁻¹	# 10 ³ m ⁻² d ⁻¹	# 10 ³ m ⁻² d ⁻¹	# 10 ³ m ⁻² d ⁻¹	# 10 ³ m ⁻² d ⁻¹	# 10 ³ m ⁻² d ⁻¹	# 10 ³ m ⁻² d ⁻¹	# 10 ³ m ⁻² d ⁻¹
200 m																
# 1 (IN)	148.8	1	17.5 (1.00)	0 -	0.3 (0.50)	0 -	8.8 (1.00)	87.5	262.9							
# 5 (IN/OUT)	70.5 (0.93)		16.3 (0.67)	2.7 (1.00)	0 -	0 -	0 -	73.2	162.7							
# 12 (OUT)	475.9 (0.96)		59.4 (0.79)	33.9 (1.00)	0.2 (0.00)	0 -	0 -	100.7	670.1							
450 m (IN)																
# 2	63.1 (0.71)		11.1 (0.33)	0 -	0 -	0 -	0 -	59.4	133.6							
# 4	11.1 (1.00)		0 -	0 -	0 -	0 -	0 -	2.8	13.9							
# 7 (IN/OUT)	348.4 (0.87)		312.7 (0.97)	0 -	0.7 (0.38)	0 -	0.1 (0.00)	160.8	822.6							
# 14	4867.2 (1.00)		413.2 (1.00)	137.7 (1.00)	0.4 (1.00)	0 -	0 -	3076.4	8495.0							
# 15	1371.4 (1.00)		222.0 (1.00)	26.1 (1.00)	0.4 (0.33)	0 -	0 -	509.4	2129.3							
# 16	1578.5 (0.94)		1067.8 (1.00)	0 -	1.3 (0.67)	0 -	0 -	603.6	3251.2							
450 m (OUT)																
# 8	147.7 (1.00)		64.6 (0.43)	0 -	0.3 (0.33)	9.2 (0.00)	0 -	387.6	609.4							
# 10	337.0 (0.93)		199.1 (1.00)	15.3 (1.00)	0 -	0 -	0 -	650.9	1202.3							
# 13(close to IN)	1383.7 (0.95)		739.6 (1.00)	23.9 (1.00)	0.7 (0.33)	0 -	0 -	107.4	2255.2							

Table 6. Abundances of foraminifera: distinction between full, empty and broken individuals ($10^3 \# \text{ m}^{-2} \text{ d}^{-1}$). For the total abundance fractions are given in brackets.

PELAGRA trap	non-spinos			spinous			sum			f:eb*			
	full	empty	broken	full	empty	broken	full	empty	broken				
200 m													
# 1 (IN)	0	4.07	0.34	0	1.53	0	0	(0)	5.60	(0.94)	0.34	(0.06)	-
# 5 (IN/OUT)	0.15	3.09	0.23	0.08	0.70	0	0.30	(0.06)	3.79	(0.89)	0.23	(0.05)	1:17
# 12 (OUT)	0.08	1.29	0	0	0.16	0	0.08	(0.05)	1.45	(0.95)	0	(0)	1:18
450 m (IN)													
# 2	0	2.82	0	0.09	0.97	0	0.09	(0.02)	3.79	(0.98)	0	(0)	1:43
# 4	0.11	0.77	0.06	0.11	0.22	0	0.22	(0.18)	0.99	(0.78)	0.06	(0.04)	1:5
# 7(IN/OUT)	0	0	0	0	0.51	0.08	0	(0)	0.51	(0.86)	0.08	(0.14)	-
# 17	0.89	38.29	4.01	0	0.89	0	0.89	(0.02)	39.18	(0.89)	4.01	(0.09)	1:49
# 15	0.25	10.64	1.39	0	0.38	0.1	0.25	(0.02)	11.02	(0.86)	1.52	(0.12)	1:50
# 16	0	19.19	4.41	0	1.10	0	0	(0)	20.29	(0.82)	4.41	(0.18)	-
450 m (OUT)													
# 8	0.27	9.13	0.81	0.09	0.45	0.09	0.36	(0.03)	9.58	(0.89)	0.89	(0.08)	1:29
# 10	0.58	8.08	1.67	0	0.51	0.22	0.58	(0.05)	8.59	(0.78)	1.89	(0.17)	1:18
# 13 (close to IN)	0.45	28.22	4.19	0	1.02	0.34	0.45	(0.01)	29.24	(0.86)	4.53	(0.13)	1:75

*: ratio of full to empty and broken individuals of all foraminifers

III. Manuscript 4

Table 7. Abundance of Radiolaria ($10^3 \# \text{ m}^{-2} \text{ d}^{-1}$).

PELAGRA trap	Nasselaria			Spumellaria		
	full	empty	broken	full	empty	broken
200 m						
# 1 (IN)	0	0.17	0.17	0	0.17	0
# 5 (IN/OUT)	0.08	0	0.23	0	0	0
# 12 (OUT)	0	0.24	0	0	0	0
450 m (IN)						
# 2	0	0	0.09	0	0	0
# 4	0	0	0	0	0	0
# 7 (IN/OUT)	0	0.42	0	0	0	0
# 14	0	0	0	0	0	45.92
# 15	0	0.13	0	0	0	0
# 16	0	0.44	0	0	0	0
450 m (OUT)						
# 8	0.27	0	0	0	0	0
# 10	0.07	0.07	0.07	0	0	0
# 13 (close to IN)	0	0.45	0.45	0	0.34	0.11

Table 8. TEP concentration in the water column and TEP flux.

Day	Chla*		TEP in the water column				TEP flux		fraction of int. TEP (% d ⁻¹)
	surface (10 m) µg L ⁻¹	10 m mg m ⁻³	100 m mg m ⁻³	500 m mg m ⁻³	200 m (int.)* g m ⁻³	500 m (int.)* g m ⁻³	200 m mg m ⁻² d ⁻¹	450 m mg m ⁻² d ⁻¹	
IN									
d0	0.48	88.06 ± 0.73	66.38 ± 4.40	55.30 ± 2.72	14.04	31.38			
d0-d2							0	0	0
d4	0.87	91.49 ± 3.88*	61.25 ± 5.24	-	14.18	-			0
d6-									
d10									
d9	1.20	86.29 ± 9.76	74.93 ± 12.17	62.92 ± 3.02	14.78	33.44			
d11-									
d15	0.84	90.77 ± 4.08	68.20 ± 5.01	59.42 ± 0.39	15.04	34.02		1.358	0.04
d12									
d13-									
d15	1.06	93.31 ± 1.34	73.62 ± 1.85	-	15.31	-	5.135		0.34
d18									
d23-									
d28	1.20	95.14	69.09 ± 1.22	66.81 ± 2.97	15.35	35.30		4.260	0.12
d24									
d29-									
d33	0.94	75.13 ± 15.08	67.73 ± 1.41	59.56 ± 3.35	13.60	31.68		2.237	0.07
d33									
d34-									
d37	0.82	83.95 ± 3.76	65.58 ± 5.47	61.32 ± 3.40	14.02	32.68		0.784	<0.001
d36									
OUT									
d16	0.71	89.38 ± 6.76	64.44 ± 2.23	62.36 ± 0.51	14.82	34.27			

IV. Synthesis and future perspectives

IV. Synthesis and future perspectives

IV.1 Synthesis

The objective of this thesis was to investigate the mechanisms that influence particle fluxes and modification in the mesopelagic zone. This was done by successfully applying a novel technique – gel equipped free-floating sediment traps –and using the obtained results to relate to data received with other sampling procedures such as ‘normal’ sediment traps, NBSTs and camera systems. This new method was then used in three field studies in the Southern Ocean within the framework of climate change and iron fertilisation experiments in a HNLC domain.

A comparison of the three export flux studies presented in this thesis reveals that flux dynamics are highly variable within the investigated regions and in different areas of the Southern Ocean (**Manuscript 2, 3 and 4, and Appendix 1**). This is in good agreement with previous studies (e.g. Berelson 2001; Fischer et al. 2000; Honjo et al. 2000; Nelson et al. 2002) and once more emphasises the need to investigate flux-determining processes. The composition of the export flux examined in these three field studies shows strong similarities by being mainly due to faecal material, highlighting the importance of grazing in the studied areas. Evidence for grazer-regulated ecosystems can also be determined through parameters such as zooplankton community or the biogeochemical composition of the sinking material as has been done routinely in previous studies (e.g. Steinberg et al. 2008; Kobari et al. 2008). Nevertheless, a detailed investigation of sinking particles will help to advance our understanding on the variations in flux dynamics.

In the following, I will recapitulate the specific questions of my thesis (II.5) and provide answers as well as directions for further research areas.

Can polyacrylamide gels capture the forms of individual sinking particles in a way that allows conclusions to be drawn on flux dynamics? I showed that sediment traps perform reasonable well to determine POC flux in a qualitative manner (**Manuscript 1-4, Appendix 1**). Since their first deployment in the 1970s techniques improved substantially (as described in the recent review by Buesseler et al. (2007)). Above all, it was the understanding of the functioning of sediment traps and the ability to consider biases (and correct for them) that helped to improve their technical reliability. Despite all limitations (Buesseler et al. (2007) and references therein), sediment traps offer the possibility to examine in-situ flux. Bearing in mind that ‘bulk samples’

IV. Synthesis and future perspectives

lack the prospect to investigate undisturbed particulate flux, the improvement of the methodology described in **Manuscript 1** provides great potential to look at “intact” particles (**Fig. 6 and 7**). The physical properties of the material are almost unaffected when it is captured by such means and the collected sinking particles are therefore representative for the composition of fluxes as they occur in the water column. In this work, I introduced the combination of free-floating sediment traps and polyacrylamide (PA) gels to collect intact individual particles and preserve them for several months (**Manuscript 1**).

The idea to equip sediment traps with gels is not new. Jannasch et al. (1980) used PA gels in a multiple-sampling sequential sediment trap in an attempt to obtain flux time-series. Although perspectives of this approach appeared promising, it was not until 15 years later. Lundsgaard (1995) suggested deploying sediment traps with PA gels to study flux characteristics by keeping particles separated as they settle into the gel. This slightly modified technique according to Lundsgaard (1995) was applied successfully in order to investigate structure and composition of individual sinking particles in both coastal (e.g. Kiorboe et al. 1994; Lundsgaard et al. 1999; Waite et al. 2005) and open ocean settings (e.g. **Appendix 1**; Waite et al. 2000; Waite and Nodder 2001) or to validate model estimates (e.g. Boyd et al. 2002; Jackson et al. 2005). Here we modified the approach of Lundsgaard (1995) to allow quantitative flux estimates in addition to collecting intact and preserved individual sinking particles (**Manuscript 1 and 2**, and **Appendix 1**).

With respect to sediment traps, the greatest improvement since JGOFS was the development of neutrally buoyant sediment traps (NBSTs). These sediment traps float freely in the water column and are therefore least biased by hydrodynamics (Lampitt et al. 2008; Valdes and Price 2000). Because of the opportunities offered by PA gels, NBSTs were also equipped with gels recently. In 2009, both available types of NBSTs, the cylindrical trap as introduced by Valdes and Price (2000) and the funnel-shaped PELAGRA traps as described in Lampitt et al. (2008) were deployed in combination with PA gels. This study shows that the design of the traps largely affects the success of deploying PA gels and that PELAGRA traps and gels are incompatible, mainly due to their funnel design (**Manuscript 1**). However, McDonnell and Buesseler (2010) demonstrated that cylindrical NBSTs and PA gels work together perfectly, making it a promising approach for future studies.

One disadvantage of relying on sediment traps is the fact that some impact on collecting material caused by hydrodynamics will always remain, even for NBSTs (Gardner 2000). Using

IV. Synthesis and future perspectives

an optical technique in combination with a sediment trap would therefore offer the possibility to receive impressions of the entire flux spectrum in-situ, in its natural environment. Modern camera systems, such as the UVP (Guidi et al. 2008; Stemmann et al. 2008) deliver particle flux spectra of a high resolution and allow for the collecting of large data sets. **Manuscript 3** demonstrates the advantages of comparing flux data received from PA gels (deployed with a free-floating sediment trap) and the UVP (mounted on a CDT) during the KEOPS study (see below and **Appendix 1** for details). This approach could be used in further studies, preferably with a camera mounted directly on top of the gel trap. This would provide valuable insights on the particles settling into the gel. Sediment traps have been equipped with camera systems in the very beginning of the trap era (e.g. Asper 1987), but somehow this combined application seems to have fallen into oblivion. Especially considering how particles are preserved within the PA gels, an additional tool such as the combination with a camera would be powerful. A camera system could for instance be used to determine sinking velocities of particles afterwards collected and thus help to understand flux dynamics.

The advantage of using PA gels in free floating sediment traps is that the collected material is maintained as intact and individual particles in the gels (**Manuscript 1**). Using advanced microscopic investigations such as scanning electron microscopy (SEM) would provide insights into structures on the fine scale, e.g. through high-resolution images of phytoplankton composition of the respective particles. Another possibility to analyse particles preserved in the gels in more detail is the use of dyes. Laboratory tests showed that Alcian Blue, which is staining TEPs, Transparent Exopolymer Particles, (Passow and Alldredge 1995), is not compatible with PA gels. However, other stains, such as the viability stain FDA (Garvey et al. 2007), need to be tested to show whether it is possible to differentiate fresh and vital sinking material from sinking material which was already processed repeatedly on its journey through the water column.

In conclusion, collecting sinking particles in PA gels provide a great opportunity to improve our knowledge on the appearance and formation of sinking particles and can give a more realistic picture about their modification in the water column. This technique possesses several possibilities to further improve our understanding of modification processes in sinking material along the ideas proposed in this thesis.

IV. Synthesis and future perspectives

How do particle fluxes differ between two regions of the Southern Ocean south of Australia, where different surface plankton communities are present? SAZ-Sense, which is one of the three studies that are subject of this thesis, was focussing on three sites in the Southern Ocean south of Tasmania (**Manuscript 2**). The two sites in the Subantarctic Zone (SAZ), P1 and P3, were characterised by non-silicious phytoplankton communities and the site P2 in the Polar Frontal Zone (PFZ) was dominated by diatoms (de Salas et al. 2010). Of the two sites in the SAZ, P1 showed low PP and biomass accumulation at the surface, but the highest POC export flux (**Manuscript 2**). Whereas at P3 biomass levels were high due to enhanced iron input (Bowie et al. 2009), but POC export flux was lowest (**Manuscript 2**). P2 was characterised by HNLC conditions and showed intermediate POC but highest BSi export flux (**Manuscript 2**).

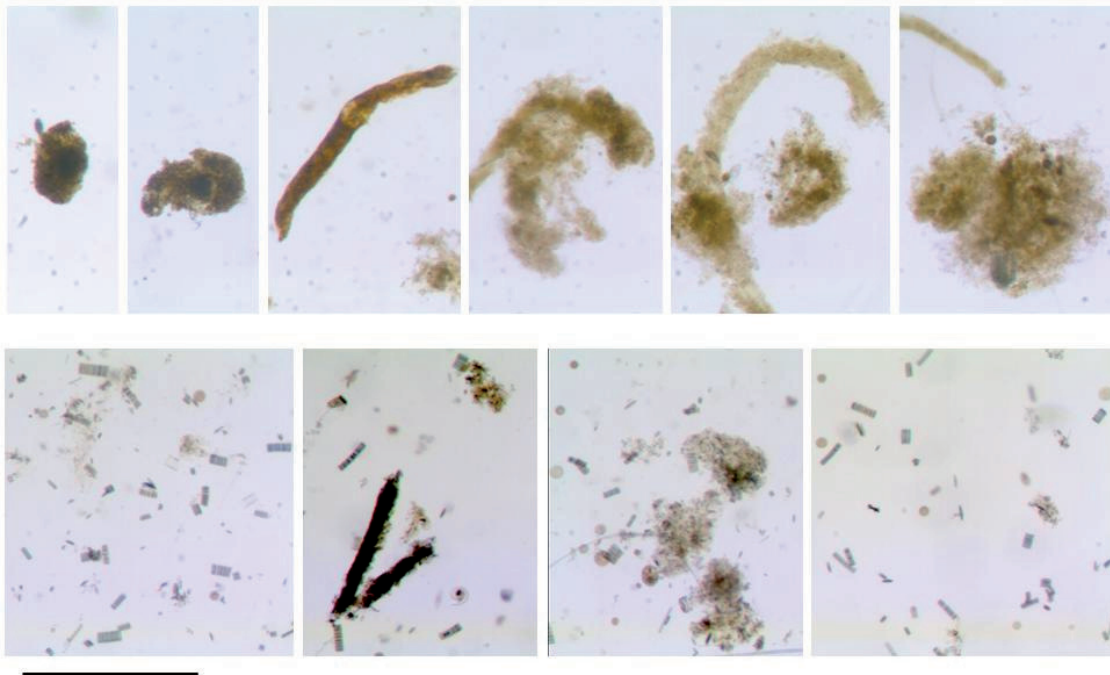


Fig. 6. Detailed images of sinking particles preserved in PA gels during SAZ-Sense. The upper row shows particles collected in the SAZ: intact ovoid faecal pellets, degrading ovoid pellet, intact cylindrical faecal pellets and different stages of degradation of faecal material (from left to right). In the lower row particles collected in the PFZ are depicted: mainly chains of diatoms or individual frustules (mainly *F. kerguelensis* and relatively large centric diatoms), degrading cylindrical faecal pellets and loose faecal material. Scale bar: 1 mm for all graphs.

The different flux regimes are mirrored in particle assemblages collected in PA gels: both SAZ sites were regulated by relatively large faecal-aggregate fluxes and in the PFZ small faecal-aggregates and phytoplankton-cells (mainly chains or single cells of heavily silicified diatoms,

IV. Synthesis and future perspectives

like *Fragilariopsis kerguelensis*; **Fig. 6**). These detailed observations of sinking particles were only possible by using PA gels (as described in **Manuscript 1**) for examining particulate flux, because microscopic investigations of these PA gels were the basis to determine POC flux (which was validated by biogeochemical analyses of bulk sediment trap samples; **Manuscript 2**). This method facilitates the characterisation of the entire flux spectrum, given that the entirety of sinking particles is accounted for and converted into POC flux.

The high contribution of faecal pellets to POC flux at P2 and P3 is evidence for grazing being more pronounced than at P1, where somewhat more fluffy sinking material is determining export fluxes. This proves that within the SAZ, flux characteristics differ considerably – and that surface PP alone is not sufficient to predict POC flux. The PFZ P2 shows yet another particle assemblage, which is not surprising considering the different surface phytoplankton community.

The clear response of the zooplankton community to enhanced PP fuelled by iron input (P3) indicates that phytoplankton biomass increase might rather lead to efficient recycling than to enhanced export rates. This has also been observed by previous studies of natural iron fertilisation, such as KEOPS (Blain et al. 2007; **Manuscript 3, Appendix 1**) and CROZEX (Pollard et al. 2007).

Are the processes in naturally iron fertilised waters on the Kerguelen Plateau in the Indian Sector of the Southern Ocean mirrored in sizes and forms of the sinking particle assemblage in comparison to surrounding waters? During KEOPS, a bloom in a naturally iron fertilised area was compared with the surrounding HNLC-waters (Blain et al. 2007). Export fluxes in both areas were investigated by using sediment traps, of which some were equipped with PA gels (**Appendix 1**) and the Underwater Video Profiler (UVP; **Manuscript 3**). Within the bloom (over the Kerguelen plateau), particulate volume flux and POC flux were larger than in HNLC-waters (off the plateau) and the flux was predominately carried by large particles (>0.5 mm) in both environments (**Manuscript 3, Appendix 1**). The overall POC flux of large particles decreased with depth and the largest changes, as observed with the UVP, occurred between 200 and 300 m (**Manuscript 3**). This decrease was very likely due to biological impact, such as repackaging through grazing (**Manuscript 3**). During KEOPS, mesozooplankton, which was dominated by copepods, showed high abundance and biomass (Carlotti et al. 2008) favouring grazing as an important mechanism. Over the plateau, net community production (NCP) furthermore indicated that a large fraction of photosynthetically fixed carbon was

IV. Synthesis and future perspectives

available for mesozooplankton grazing and export into the ocean interior (Lefèvre et al. 2008). In agreement with the overall decline in POC flux below 200 m, which might result from high grazing activities as indicated by the high abundance of faecal matter collected in PA gels (**Fig. 7**), the absence of particle accumulation at 200 m (Park et al. 2008) supports the view of biological mediated particle modification. Grazer-initiated repackaging at depth probably scavenged small particles and transferred them into larger faecal material, which coincides with a relative increase of large particles at depth as detected by the UVP (**Manuscript 3**). Moreover, it is in agreement with the particulate flux being dominated by faecal material (**Fig. 7**) as was shown by particles studies of PA gels (**Appendix 1**).

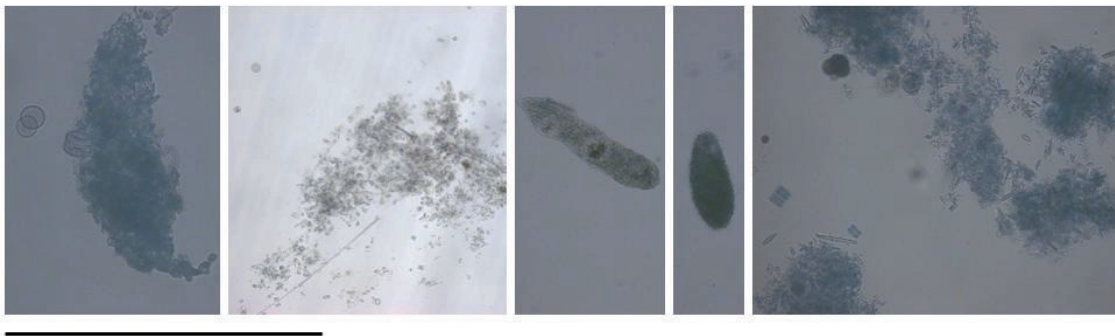


Fig. 7. High resolution images of sinking particles collected in PA during KEOPS: degraded faecal pellet, fluffy faecal material, cylindrical faecal pellet, ovoid faecal pellet, degraded faecal material (from left to right). Scale bar: 1 mm for all graphs.

These findings indicate that during KEOPS both environments (independent on iron supply) are characterised as recycling systems and export flux is regulated by particle repackaging through grazing at depths – as opposed to sinking of phyto-detritus aggregates. The differences between flux characteristics above and off the plateau reveal that natural iron fertilisation has nonetheless an impact on export POC flux. On the one hand, the magnitude of the flux above the plateau was about three times higher than in HNLC-waters (Blain et al. 2007). On the other hand, the POC transfer efficiency was highest in HNLC-waters, which indicates less efficient recycling (probably due to the less pronounced grazer community and/or different functioning of the microbial food web). The higher Chla standing stock in the KEOPS bloom ($\sim 3 \mu\text{g Chla L}^{-1}$ above, and $0.5 \mu\text{g Chla L}^{-1}$ off the plateau, respectively; Blain et al. (2007))

IV. Synthesis and future perspectives

nonetheless resulted in a POC export flux of $85\pm 33 \text{ mmol C m}^{-2} \text{ d}^{-1}$, which is one of the highest export estimates in the Southern Ocean (Jouandet et al. 2008).

One aim of artificial iron fertilisation experiments has been to study the possibility of sequestering carbon (Chisholm et al. 2001). During the natural iron fertilisation experiment KEOPS and the artificial iron enrichment experiments SOIREE and EisenEx similarly high daily NCP was obtained, but during KEOPS POC export was higher by at least a factor of 2.5 (Jouandet et al. 2008). However, it has to be taken into account that blooms induced by natural iron fertilisation last much longer (the KEOPS bloom was recorded by satellite images over a period of 3 months; Blain et al. 2007) than those stimulated by artificial iron addition experiments, which only last several weeks (see Boyd et al. (2007) for a recent review). The higher POC export in combination with the lower iron supply during the natural iron fertilisation study KEOPS (Blain et al. 2008) leads to a higher efficiency for carbon sequestration in comparison to artificial blooms (Blain et al. 2007). With respect to the KEOPS blooms and the surrounding HNLC-waters, the different export mechanisms are mirrored in the particle assemblage: Although export efficiency above the plateau is lower than off the plateau, the export flux is much higher above the plateau, which is in coincidence with more large particles that showed signs of heavy re-working processes such as grazing (**Manuscript 3, Appendix 1**).

What is the fate of unicellular plankton during an iron fertilisation experiment in the Atlantic Sector of the Southern Ocean – recycling or sinking? The iron enrichment experiment LOHAFEX evoked a phytoplankton bloom that predominantly consisted of small flagellates (Assmy et al. 2010). The accumulated phytoplankton biomass provided sufficient food supply for protozoan grazers, such as heterotrophic dinoflagellates and tintinnid ciliates, which in turn attracted copepods (Mazzocchi et al. 2009). The low fraction of unicellular plankton carbon (UPC) and heavily reworked organic material that contributed to the export flux at 450 m supports the view of a recycling system (**Manuscript 4**). The detailed microscopic examination of the particulate flux during LOHAFEX was primarily based on bulk samples (because PA gel deployment was only partially successful). Thus, only UPC, such as phytoplankton cells and protozooplankton was identified and converted into C flux, but the remaining ‘unidentifiable’ particles were not investigated as accurately. Although intact sinking faecal pellets were analysed (H. Gonzalez, pers. comm.), there is still a large amount of material consisting mainly of faecal material (**Manuscript 4**) that was not examined in detail (but accounted for in the

IV. Synthesis and future perspectives

biogeochemical flux measurement). Considering the fact that most of the sinking material was of faecal origin, the investigation of individual particles, as preserved in PA gels, would have provided further insights into the structure of the particle assemblage. This would have allowed for estimations of particle specific C fluxes. Due to the fact that studying UCP (which contributed only to a small fraction of total POC) offers the possibility to gain detailed information on one part of the flux, the combination of this approach (**Manuscript 4**) together with using PA gels as described in **Manuscript 1** would be useful for future studies.

LOHAFEX was an iron fertilisation experiment conducted in the Southern Ocean that was faced with silicic acid depleted ($<2 \mu\text{M}$) surface waters. In contrast, most previous iron addition experiments generated diatom blooms and it was found that iron enrichment favours diatoms (Coale et al. 1996a). The Southern Ocean Iron Experiment, SOFeX, however, examined two areas: SOFeX-S (in the South, 66°S) with high nitrate, high silicic acid concentrations and SOFeX-N (in the North, 55°S) with high nitrate, low silicic acid ($<3 \mu\text{M}$) concentrations (Coale et al. 2004). The iron induced bloom of SOFeX-N consisted of flagellated phytoplankton groups and *Pseudo-Nitzschia* spp. (Coale et al. 2004). Diatoms provided half of the phytoplankton biomass at the most (Coale et al. 2004). This shows that the surface phytoplankton community that was present during LOHAFEX somehow resembles that of the SOFeX-N bloom. The observation of higher PP rates in the iron induced SOFeX-N bloom compared to SOFeX-S led Coale et al. (2004) to conclude that low silicic acid concentrations do not necessarily limit PP or POC accumulations. This is in agreement with the biomass accumulation during LOHAFEX that followed iron addition (Mazzocchi et al. 2009). Due to insufficient export measures of SOFeX-N the fate of the bloom can only be speculated on (Coale et al. 2004). The presence of phyto-detritus aggregates towards the end of the bloom (Coale et al. 2004) support the indications of a large flux event within the SOFeX-N area that was detected by an autonomous drifter (Bishop et al. 2004). Although these observations are somewhat vague, they suggest that the bloom of non-silicous phytoplankton (flagellated phytoplankton groups) translated into POC export flux. In general, LOHAFEX and SOFeX-N display similarities: they both showed enhanced POC export flux. More specific, the particles assemblages that determined the flux were very different. While LOHAFEX flux was dominated by faecal aggregates (**Manuscript 4**), during SOFeX-N phyto-detritus was probably responsible for export (Bishop et al. 2004; Coale et al. 2004). That means that LOHAFEX was regulated through recycling, i.e. grazing, whereas SOFeX-N export fluxes

IV. Synthesis and future perspectives

consisted of material that was not reworked. This shows once again that export flux driving processes are highly variable, even under apparently similar conditions.

The only iron fertilisation experiment conducted in the Southern Ocean that showed enhanced export flux as a response to iron addition was the European Iron Fertilisation Experiment EIFEX (Peeken et al. 2006; Smetacek et al. in prep.). EIFEX was also situated in the Atlantic Sector, but surface waters were not depleted in silicic acid and thus the build-up of a diatom bloom was induced by adding iron (Bathmann 2005). Towards the decline of the EIFEX bloom the sinking out of phyto-detritus material was observed in the deep water column (Peeken et al. 2006). Unfortunately the fate of this sinking matter could not be studied in detail due to ship time constrains. Because the composition of the export flux during EIFEX probably resembled the structure of that detected during SOFeX-N, it appears that these two communities were regulated through similar processes but differed considerably from LOHAFEX. During LOHAFEX, in contrast, the sinking of the iron-stimulated bloom might have been impeded through the prevailing recycling system, which seemed to control the LOHAFEX community.

IV. Synthesis and future perspectives

Table 3. Compilation of the export flux results from the three Southern Ocean studies that are presented in this thesis: POC flux and characteristics of the sinking particulate material is given (including methods used to obtain these data).

Study	Site	Depth m	POC flux mg C m ⁻² d ⁻¹	Particle assemblage	Methods	Reference
SAZ-Sense	P1 (SAZ)	140, 190, 240, 290	73-127	faecal aggregates	Gel trap	Mansucript 2
		150	18-61		PPS3/3 trap	
	P2 (PFZ)	140, 190, 240, 290	62-144	small faecal aggregates, phytoplankton-cells	Gel trap	
		150	14-36		PPS3/3 trap	
	P3 (SAZ)	170, 320	13-22		IRS trap	
		140, 190, 240, 290	7-12	faecal aggregates, faecl pellets	Gel trap	
KEOPS	A3	100, 200, 330, 430	15-56	faecal pellets, faecal aggregates	Gel trap	Appendix 1
		100, 200, 330, 430	8-63	faecal pellets, faecal aggregates	Gel trap	
	A3	200-300	57-869	more large particles (>0.5 mm)	UVP	Mansucript 3
	C11	200-300	19-40	more small particles (<0.5 mm)	UVP	
	C5		32-67	more large particles (>0.5 mm)	UVP	
	LOHAFEX	IN	200, 450	5-23		PELAGRA (bulk)
				faecal material	PELAGRA (PA gels)	
OUT		200, 450	3-28	faecal material	PELAGRA (bulk) PELAGRA (PA gels)	

IV. Synthesis and future perspectives

IV.2 Conclusions

This thesis aims to contribute to understanding of the mechanisms that are relevant for modification processes of sinking particles in the mesopelagic zone, with emphasis on the Southern Ocean. By way of a conclusion, I will now reconsider the hypotheses put forward in the introduction (II.5) in the light of the study's results.

I. Structure and composition of sinking particles provide information on the mechanisms of particle flux and modification.

Within the three field studies presented in this thesis, I showed that the examination of individual sinking particles reveal valuable information on export determining processes, such as grazing and particle repackaging at depth (**Manuscript 2, 3, 4, Appendix 1**). The different particle assemblages mirror the varying ecosystems in the respective parts of the Southern Ocean (**Table 3**). The identification of faecal material (intact faecal pellets and/or faecal aggregates) clearly indicates grazing as important mechanism for export flux, while the occurrence of phyto-detritus aggregates is evident for the sinking of relatively fresh unprocessed material. Despite the gained knowledge on the particle assemblage, the formation pathways of sinking particles still remain unknown. For example, since marine snow captures surrounding particles as it is travelling through the water column, the identification of the collected material cannot necessarily identify the ecological pathways that initiated vertical export. Thus, even the recognition of individual sinking particles is not able to entirely explain the unknowns of particulate flux modification. Moreover, the sinking particles collected during the presented studies (**Manuscript 2, 3, 4, Appendix 1**) have already left the euphotic zone, where a critical fraction of the flux alteration occurred. For this reason, I would recommend a higher depth resolution for sample collection, particularly in the euphotic layer and upper mesopelagic zone.

II. Free-floating gel traps are sufficient to collect intact sinking particles.

The combination of free-floating sediment traps and PA gels for collection and preservation of sinking particles is a powerful tool to examine fluxes of intact particles (**Manuscript 1, 2, 3, 4, Appendix 1**). I have shown that this method is a very reliable technique once important requirements in terms of design (e.g. fitting of trap sampling devices and gel container) are met (**Manuscript 1**). Several successful deployments proved that PA gels can

IV. Synthesis and future perspectives

provide valuable additional information on structure and composition of sinking particles (**Manuscript 2, 3, Appendix 1**). The application of PA gels for studying particulate flux therefore offers the possibility to improve our understanding on the base of intact individual sinking particles

III. Different magnitude and composition of biogenic particle fluxes in different regions of the Southern Ocean can be categorised as biogeochemical provinces.

The three field studies presented in this thesis were each located in different regions of the Southern Ocean: SAZ-Sense in the Australian Sector (**Manuscript 2**), KEOPS in the Indian Sector (**Manuscript 3, Appendix 1**), and LOHAHEX in the Atlantic Sector (**Manuscript 4**). Although these field studies were carried out in similar latitudes (between 45° S and 55° S), the export flux showed considerable differences in terms of magnitude and sinking particle assemblage (**Table 3**).

According to Longhurst (1998), who separated the ocean basins into different biogeochemical provinces, SAZ-Sense, KEOPS and LOHAFEX altogether belong to Subantarctic Water Ring Province (SANT). These biogeochemical provinces are established based on regional characteristics such as oceanic fronts (Longhurst 1998). The SANT occupies a zone between ~35° S and the Antarctic Polar Front at ~55° S, with several regimes distinguished in this area. The fact that the iron induced phytoplankton bloom during LOHAFEX was mainly provided by small flagellates assigns this (iron-limited) region to the oligotrophic regime, which is typically controlled through grazing (of predominantly copepods). This is consistent with the comparably low flux and the predominance of faecal material (**Table 3**). The KEOPS bloom occurred in Fe-replete waters within the oligotrophic regime and is depicted in intermediate export fluxes, which mainly consists of intact faecal pellets and faecal aggregates (**Table 3**). During SAZ-Sense, three different regimes were investigated, P1 in Fe-replete oligotrophic waters, P3 in Fe-limited oligotrophic waters and P2 in the frontal regime (**Table 3**). At P2 even frustules of diatoms (large centric diatoms or chains of *F. kerguelensis*) were collected separately and not integrated into marine snow implying single cell and/or diatom chain sinking. Although the mechanisms behind this observation are not clear it is evidence for a decoupling of POC and biogenic silica flux.

IV. Synthesis and future perspectives

By using PA gel equipped free-floating sediment traps (**Manuscript 1**), I could demonstrate that grazing and the resultant flux of predominantly faecal matter was driving export fluxes in large areas of the SAZ-Sense study, during KEOPS and during LOHAFEX (**Table 3**). Considering the good preservation of fragile particles in PA gels, the absence of fluffy phyto-detritus within the sinking particulate matter collected in most cases during the presented studies indicates that sinking of marine snow was not important in any of these export regimes. Due to the finding of export flux being dominated by faecal material – as opposed to marine snow – I suggest that faecal material is much more relevant to POC flux than is marine snow.

To sum up, therefore, I can state that the findings of my thesis verify all three hypotheses.

IV. Synthesis and future perspectives

IV.3 Future perspectives

This thesis is based upon three export flux studies in different parts of the Southern Ocean and I concluded that POC flux to depth is regulated through grazing followed by the production of faecal material. Seasonal variability was not investigated, since all of these studies were conducted in austral summer. A comparison with flux regimes during autumn, winter or early spring, when surface PP is much lower, should be assessed in the future. Due to the lower abundance of protozooplankton in the beginning of the growth season, different export regimes (e.g. marine snow driven flux) might be prevailing. With the deployment of PA gels, it would be feasible to collect these possibly very fragile and fluffy aggregates.

Additionally, I would like to use PA gel based particulate fluxes for studying other ocean areas, in particular the Arctic Ocean, which, like the Southern Ocean, is highly sensitive to climate change (e.g. ice cover and water temperature). Even though the Southern Ocean and the Arctic Ocean are similar in many respects, there are significant differences regarding, for example, the mixed layer depth, seasonal mixing, and influence of landmasses (and the subsequent input of lithogenic material).

One possible framework for using PA gels in the Arctic is the long-term study HAUSGARTEN that was established in 1999 by the AWI in Fram Strait (Soltwedel et al. 2005). Flux samples from 15 permanent sampling sites (1000-5500 m depth) obtained by annually moored sediment traps showed that the settling material is of quite variable composition (Soltwedel et al. 2005) and the seasonal patterns show large variation (Bauerfeind et al. 2009). Hence, the composition and structure of the particulate flux is of high interest. Therefore, the deployment of PA gels might provide additional insights into export driving processes.

I very much appreciate the opportunity of looking at intact in-situ particle fluxes (as the PA gels allow it) as it reveals a great amount of details about flux characteristic. Respect goes to scuba divers in the 1970s and 80s who first realised that such a thing as marine snow exists in the water column. Today, autonomous underwater vehicle (AUV) can dive down to thousands of meters and are able to take detailed images and we still do not completely understand the modification processes of sinking particles during their transit to depth. Nonetheless, I recommend using the sense of sight more, as it might tell much more than laboratory analyses in some respects. If it was not so difficult for practical reason I would suggest more direct

IV. Synthesis and future perspectives

observations of sinking particles, either by scuba diving or by relying on AUVs. Keeping in mind that little is known about the fate of sinking particles in the mesopelagic, this would contribute to shedding more light into the ‘twilight zone’.

References

References

- Abramson, L., C. Lee, Z. Liu, S. G. Wakeham, and J. Szlosek. 2010. Exchange between suspended and sinking particles in the northwest Mediterranean as inferred from the organic composition of in situ pump and sediment trap samples. *Limnology and Oceanography* **55**: 752-739.
- Allredge, A. L. 1992. Marine Snow in Oceanic Cycling, p. 139-147. In W. Nierenberg [ed.], *Encyclopedia of Earth System Science*. Academic Press.
- Allredge, A. L., and C. Gotschalk. 1989. Direct observations of the mass flocculation of diatom blooms: characteristics, settling velocities and formation of diatom aggregates. *Deep Sea Research* **36**: 159-171.
- Allredge, A. L., and M. W. Silver. 1988. Characteristics, Dynamics and Significance of Marine Snow. *Progress Oceanography* **20**: 41-82.
- Allredge, A. L., and M. L. Youngbluth. 1985. The significance of macroscopic aggregates (marine snow) as sites of heterotrophic bacterial production in the mesopelagic zone at the subtropical Atlantic. *Deep Sea Research* **32**: 1445-1456.
- Allison, D. B., D. Stramski, and G. Mitchell. 2010. Seasonal and interannual variability of particulate organic carbon within the Southern Ocean from satellite ocean color observation. *Journal of Geophysical Research* **115**: 1-18.
- Andersson, J. H., J. W. M. Wijsman, P. J. Herman, J. J. Middelburg, K. Soetaert, and K. Heip. 2004. Respiration patterns in the deep sea. *Geophysical Research Letter* **31**: 1-4.
- Antia, A. N. and others 2001. Basin-wide particulate carbon flux in the Atlantic Ocean: Regional export patterns and potential for atmospheric CO₂ sequestration. *Global Biogeochemical Cycles* **15**: 845-862.
- Armand, L. K., V. Cornet-Barthaux, J. Mosseri, and B. Quéguiner. 2008. Late summer diatom biomass and community structure on and around the naturally iron-fertilised Kerguelen Plateau in the Southern Ocean. *Deep Sea Research Part II: Topical Studies in Oceanography* **55**: 653-676.
- Armstrong, R. A., C. Lee, J. I. Hedges, S. Honjo, and S. G. Wakeham. 2002. A new, mechanical model for organic carbon fluxes in the ocean based on the quantitative association of POC with ballast minerals. *Deep-Sea Research II* **49**: 219-236.
- Asper, V. L. 1987. Measuring the flux and sinking speed of marine snow aggregates. *Deep Sea Research* **34**: 1-17.
- Assmy, P., F. Ebersbach, N. Fuchs, C. Klaas, M. Montresor, and V. Smetacek. 2010. Phyto- and Protozooplankton, p. 81-86. In H. Bornemann and B. Chiaventone [eds.], *Reports on Polar and Marine Research. The expedition of the Research Vessel "Polarstern" to the Antarctic on 2009 (ANT-XXV/3-LOHAFEX)*. Alfred Wegener Institute.
- Assmy, P., J. Henjes, C. Klaas, and V. Smetacek. 2007. Mechanisms determining species dominance in a phytoplankton bloom induced by the iron fertilization experiment EisenEx in the Southern Ocean. *Deep Sea Research I* **54**: 340-362.
- Bathmann, U. 2005. Ecological and Biogeochemical Response of Antarctic Ecosystems to Iron Fertilization and Implications on Global Carbon Cycle. *Ocean and Polar Research* **27**: 231-235.
- Bathmann, U., J. Priddle, P. Tréguer, M. I. Lucas, J. Hall, and J. Parslow. 2000. Plankton ecology and biogeochemistry in the Southern Ocean: A review of the Southern Ocean JGOFS, p. 300-337. In R. B. Hanson, H. W. Ducklow and J. G. Field [eds.], *The Changing Ocean*

References

- Carbon Cycle, A midterm synthesis of the Joint Global Ocean Flux Study. International Geosphere-Biosphere Programme Book Series. Cambridge University Press.
- Bauerfeind, E. and others 2009. Particle sedimentation patterns in the eastern Fram Strait during 2000-2005: Results from the Arctic long-term observatory HAUSGARTEN. *Deep-Sea Research I* **56**: 1471-1487.
- Beaulieu, S. E. 2002. Accumulation and fate of phytodetritus on the sea floor. *Oceanography and Marine Biology: an Annual Review* **40**: 171-232.
- Berelson, W. M. 2001. The Flux of Particulate Organic Carbon Into the Ocean Interior: A comparison of Four U.S. JGOFS Regional Studies. *Oceanography* **14**: 59-67.
- Bishop, J. K. B. 1989. Regional extremes in particulate matter composition and flux: effects on the chemistry of the ocean interior, p. 117-138. In W. H. Berger, V. Smetacek and G. Wefer [eds.], *Dahlem Workshop Life Science Report - Productivity of the oceans: Present and Past*. John Wiley and Sons.
- Bishop, J. K. B., R. E. Davis, and J. T. Sherman. 2002. Robotic Observations of Dust Storm Enhancement of Carbon Biomass in the North Pacific. *Science* **298**: 817-821.
- Bishop, J. K. B., D. Schupack, R. M. Sherrell, and M. Conte. 1985. A multiple-unit large-volume in-situ filtration system for sampling oceanic particulate matter in mesoscale environments. *Advances in Chemistry Series* **9**: 155-175.
- Bishop, J. K. B., T. J. Wood, R. E. Davis, and J. T. Sherman. 2004. Robotic Observations of Enhanced Biomass and Export at 55°S During SOFex. *Science* **304**: 417-420.
- Blain, S. and others 2007. Effect of natural iron fertilization on carbon sequestration in the Southern Ocean. *Nature* **446**: 1070-1075.
- Blain, S., G. Sarthou, and P. Laan. 2008. Distribution of dissolved iron during the natural iron-fertilization experiment KEOPS (Kerguelen Plateau, Southern Ocean). *Deep Sea Research Part II: Topical Studies in Oceanography* **55**: 594-605.
- Bowie, A. R. and others 2009. Biogeochemical iron budgets of the Southern Ocean south of Australia demonstrate that summertime supply decouples iron and nutrient cycles in the subantarctic zone. *Global Biogeochemical Cycles* **GB4034**.
- Boyd, P. W., G. A. Jackson, and A. M. Waite. 2002. Are mesoscale perturbation experiments in polar waters prone to physical artefacts? Evidence from algal aggregation modelling studies. *Geophysical Research Letters* **29**: 36 31-34.
- Boyd, P. W. and others 2007. Mesoscale Iron Enrichment Experiments 1993-2005: Synthesis and Future Directions. *Science* **315**: 612-617.
- Boyd, P. W., and P. Newton. 1995. Evidence of the potential influence of planktonic community structure on the interannual variability of particulate organic carbon flux. *Deep Sea Research Part I: Oceanographic Research Papers* **42**: 619-639.
- Boyd, P. W., and P. P. Newton. 1999. Does planktonic community structure determine downward particulate organic carbon flux in different oceanic provinces? *Deep Sea Research Part I: Oceanographic Research Papers* **46**: 63-91.
- Boyd, P. W., and T. W. Trull. 2007. Understanding the export of biogenic particles in oceanic waters: Is there consensus? *Progress In Oceanography* **72**: 276-312.
- Boyd, P. W. and others 2000. A mesoscale phytoplankton bloom in the polar Southern Ocean stimulated by iron fertilization. *Nature* **407**: 695-702.
- Buesseler, K. O. 1998. The decoupling of production and particulate export in the surface ocean. *Global Biogeochemical Cycles* **12**: 297-310.
- Buesseler, K. O., J. E. Andrews, S. M. Pike, and M. A. Charette. 2004. The effect of iron fertilization on carbon sequestration in the Southern Ocean. *Science* **304**: 414-417.

References

- Buesseler, K. O. and others 2007. An assessment of the use of sediment traps for estimating upper ocean particle fluxes. *Journal of Marine Research* **65**: 345-416.
- . 2001. Upper ocean export of particulate organic carbon and biogenic silica in the Southern Ocean along 170°W. *Deep-Sea Research II* **48**: 4275-4297.
- Buesseler, K. O., and P. W. Boyd. 2009. Shedding light on processes that control particle export and flux attenuation in the twilight zone of the open ocean. *Limnology and Oceanography* **54**: 1210-1232.
- Buesseler, K. O. and others 2008. Ocean Iron Fertilisation-Moving Forward in a Sea of Uncertainty. *Science* **319**: 162.
- . 2000. A comparison of the quantity and quality of material caught in a neutrally buoyant versus a surface-tethered sediment trap. *Deep-Sea Research I* **47**: 227-294.
- Carlotti, F., D. Thibault-Botha, A. Nowaczyk, and D. Lefèvre. 2008. Zooplankton community structure, biomass and role in carbon fluxes during the second half of a phytoplankton bloom in the eastern sector of the Kerguelen Shelf (January-February 2005). *Deep Sea Research Part II: Topical Studies in Oceanography* **55**: 720-733.
- Chrisholm, S. W., P. G. Falkowski, and J. J. Cullen. 2001. Dis-Crediting Ocean Fertilization. *Science* **294**: 309-310.
- Coale, K. H., S. E. Fitzwater, R. M. Gordon, K. S. Johnson, and R. T. Barber. 1996b. Control of community growth and export production by upwelled iron in the equatorial Pacific Ocean. *Nature* **379**: 621-624.
- Coale, K. H. and others 2004. Southern Ocean Iron Enrichment Experiment: Carbon Cycling on High- and Low-Si Waters. *Science* **304**: 408-414.
- Coale, K. H., K. S. Johnson, S. E. Fitzwater, S. P. G. Blain, T. P. Stanton, and T. L. Coley. 1998. IronEx-I, an in situ iron-enrichment experiment: Experimental design, implementation and results. *Deep Sea Research Part II: Topical Studies in Oceanography* **45**: 919-945.
- Coale, K. H. and others 1996a. A massive phytoplankton bloom induced by an ecosystem-scale iron fertilisation experiment in the equatorial Pacific Ocean. *Nature* **383**: 495-501.
- de Baar, H. J. W. and others 2005. Synthesis of iron fertilisation experiments: From the Iron Age in the Age of Enlightenment. *Journal of Geophysical Research* **110**: 1-24.
- De La Rocha, C., and U. Passow. 2007. Factors influencing the sinking of POC and the efficiency of the biological carbon pump. *Deep Sea Research II* **54**: 639-658.
- De La Rocha, C. L. 2007. The Biological Pump, p. 1-29. In D. H. Heinrich and K. T. Karl [eds.], *Treatise on Geochemistry*. Pergamon.
- de Salas, M. F., R. Eriksen, A. T. Davidson, and S. Wright. 2010. Protistan communities in the Australian sector of the subantarctic zone during SAZ-Sense. *Deep-Sea Research II* **in press**.
- Dilling, L., and A. L. Alldredge. 2000. Fragmentation of marine snow by swimming macrozooplankton: A new process impacting carbon cycling in the sea. *Deep Sea Research Part I: Oceanographic Research Papers* **47**: 1227-1245.
- Dubischar, C. D., and U. Bathmann. 2002. The occurrence of faecal material in relation to different pelagic systems in the Southern Ocean and its importance for vertical flux. *Deep-Sea Research II* **49**: 3229-3242.
- Ducklow, H. W., D. K. Steinberg, and K. O. Buesseler. 2001. Upper Ocean Carbon Export and the Biological Pump. *Oceanography* **14**: 50-58.
- Dugdale, R. C., and J. J. Goering. 1967. Uptake of new and regenerated forms of nitrogen in primary productivity. *Limnology and Oceanography* **12**: 196-206.

References

- Fischer, G., V. Ratmeyer, and G. Wefer. 2000. Organic carbon fluxes in the Atlantic and the Southern Ocean: relationship to primary production compiled from satellite radiometer data. *Deep-Sea Research I* **47**: 1961-1997.
- Francois, R., S. Honjo, R. Krishfield, and S. Manganini. 2002. Factors controlling the flux of the organic carbon to the bathypelagic zone of the ocean. *Global Biogeochemical Cycles* **16**: 34, 31-20.
- Gardner, W. D. 1980a. Field calibration of sediment traps. *Journal of Marine Research* **38**: 41-52.
- . 1980b. Sediment trap dynamics and calibration: a laboratory evaluation. *Journal of Marine Research* **38**: 17-39.
- . 1985. The effect of tilt on sediment trap efficiency. *Deep-Sea Research* **32**: 349-361.
- . 2000. Sediment trap sampling in surface waters, p. 240-280. In R. B. Hanson, H. W. Ducklow and J. G. Field [eds.], *The Changing Ocean Carbon Cycle, A midterm synthesis of the Joint Global Ocean Flux Study*. International Geosphere-Biosphere Programme Book Series. Cambridge University Press.
- Garvey, M., B. Moriceau, and U. Passow. 2007. Applicability of the FDA assay to determine the viability of marine phytoplankton under different environmental conditions. *Marine Ecology Progress Series* **352**: 17-26.
- Goldthwait, S. A., J. Yen, J. Brown, and A. L. Alldredge. 2004. Quantification of marine snow fragmentation by swimming euphausiids. *Limnology and Oceanography* **49**.
- Gorsky, G., C. Aldorf, M. Kage, M. Picheral, C. M. Garcia, and Y. Favole. 1992. Vertical distribution of suspended aggregates determined by a new underwater video profiler, p. 275-280. In P. Nival, J. Boucher and M. Bhaud [eds.], *3eme Colloque du Programme National sur le Determinisme du Recrutement*. Annales de l'Institut oceanographic, Paris, Nantes (France).
- Gorsky, G., M. Picheral, and L. Stemmann. 2000. Use of the Underwater Video Profiler for the study of aggregate dynamics in the North Mediterranean. *Estuarine Coastal and Shelf Science* **50**: 121-128.
- Guidi, L., G. A. Jackson, L. Stemmann, J. C. Miquel, M. Picheral, and G. Gorsky. 2008. Relationship between particle size distribution and flux in the mesopelagic zone. *Deep Sea Research Part I: Oceanographic Research Papers* **55**: 1364-1374.
- Griffiths, F.B., Bowie, A.R., Dehairs, F., Trull, T.W., 2010. Oceanographic setting of the Sub-Antarctic zone south of Australia. *Deep-Sea Research II*, submitted.
- Hargrave, B. T., and N. M. Burns. 1979. Assessment of sediment trap collection efficiency. *Limnology and Oceanography* **24**: 1124-1136.
- Hill, P. S. 1998. Controls on Floc Size in the Sea. *Oceanography* **11**: 13-18.
- Hoffmann, L. J., I. Peeken, K. Lochte, P. Assmy, and M. Veldhuis. 2006. Different reactions of Southern Ocean phytoplankton size classes to iron fertilization. *Limnology and Oceanography* **51**: 1217-1229.
- Honjo, S. 1982. Seasonality and interaction of biogenic and lithogenic particulate flux at the Panama Basin. *Science* **218**: 883-884.
- . 1996. Fluxes of particles to the interior of the open ocean. In V. Ittekkot, P. Aschauffer, S. Honjo and P. Depetris [eds.], *Particle Flux in the Ocean*. Wileys.
- Honjo, S., A. L. Doherty, Y. C. Agrawal, and V. L. Asper. 1984. Direct optical assessment of large amorphous aggregates (marine snow) in the deep ocean. *Deep-Sea Research* **31**: 61-76.

References

- Honjo, S., R. Francois, S. Manganini, J. Dymond, and R. Collier. 2000. Particle fluxes to the interior of the Southern Ocean in the Western Pacific sector along 170°W. *Deep-Sea Research II* **47**: 3521-3548.
- Ishii, M., H. Y. Inoue, H. Matsueda, and E. Tanoue. 1998. Close coupling between seasonal biological production and dynamics of dissolved inorganic carbon in the Indian Ocean sector and the western Pacific Ocean sector of the Antarctic Ocean. *Deep-Sea Research I* **45**: 1187-1209.
- Iversen, M. H., N. Nowald, H. Ploug, G. A. Jackson, and G. Fischer. 2010. High resolution profiles of vertical particulate organic matter export off Cape Blanc, Mauritania: Degradation processes and ballasting effects. *Deep-Sea Research I* **57**: 771-784.
- Iversen, M. H., and H. Ploug. 2010. Ballast minerals and the sinking carbon flux in the ocean: carbon-specific respiration rates and sinking velocity of marine snow aggregates. *Biogeosciences* **7**: 2613-2624.
- Jackson, G. A., A. M. Waite, and P. W. Boyd. 2005. Role of algal aggregation in vertical carbon export during SOIREE and in other low biomass environments. *Geophysical Research Letters* **32**: 1-4.
- Jannasch, H. W., O. C. Zafiriou, and J. W. Farrington. 1980. A sequencing sediment trap for time-series studies of fragile particles. *Limnology and Oceanography* **25**: 939-943.
- Jouandet, M. P., S. Blain, N. Metzl, C. Brunet, T. W. Trull, and I. Obernosterer. 2008. A seasonal carbon budget for a naturally iron-fertilized bloom over the Kerguelen Plateau in the Southern Ocean. *Deep Sea Research Part II: Topical Studies in Oceanography* **55**: 856-867.
- Karl, D. M., B. Tilbrock, and D. Tien. 1991. Seasonal coupling of organic matter production and particle flux in the western Bransfield Strait, Antarctica. *Deep-Sea Research* **38**: 1097-1126.
- Kiorboe, T. 2001. Formation and fate of marine snow: small-scale processes with large-scale implications. *Scientia Marina* **65**: 57-71.
- Kiorboe, T., C. Lundsgaard, M. Olesen, and J. L. S. Hansen. 1994. Aggregation and sedimentation processes during a spring phytoplankton bloom: A field experiment to test coagulation theory. *Journal of Marine Research* **52**: 297-323.
- Klaas, C., and D. E. Archer. 2002. Association of sinking organic matter with various types of mineral ballast in the deep sea: Implication for the rain ratio. *Global Biogeochemical Cycles* **16**: 63 61-14.
- Kobari, T., D. K. Steinberg, A. Ueda, A. Tsuda, M. W. Silver, and M. Kitamura. 2008. Impacts of ontogenetically migrating copepods on downward carbon flux in the western subarctic Pacific Ocean. *Deep Sea Research Part II: Topical Studies in Oceanography* **55**: 1648-1660.
- Lam, P. J., and J. K. B. Bishop. 2007. High biomass, low export regimes in the Southern Ocean. *Deep Sea Research II* **54**: 601-638.
- Lampitt, R. S., and A. N. Antia. 1997. Particle flux in the deep seas: regional characteristics and temporal variability. *Deep Sea Research I* **44**: 1377-1403.
- Lampitt, R. S. and others 2008. Particle export from the euphotic zone: Estimates using a novel drifting sediment trap, ²³⁴Th and new production. *Deep Sea Research Part I: Oceanographic Research Papers* **55**: 1484-1502.
- Lampitt, R. S., K. F. Wishner, C. M. Turley, and M. V. Angel. 1993. Marine snow studies in the Northwest Atlantic Ocean: distribution, composition and role as a food source for migrating plankton. *Marine Biology* **116**: 689-702.

References

- Lee, C., S. G. Wakeham, and J. I. Hedges. 1988. The measurement of oceanic flux - are 'swimmers' a problem? *Oceanography*: 34-36.
- Lefèvre, D., C. Guigue, and I. Obernosterer. 2008. The metabolic balance at two contrasting sites in the Southern Ocean: The iron-fertilized Kerguelen area and HNLC waters. *Deep Sea Research Part II: Topical Studies in Oceanography* **55**: 766-776.
- Longhurst, A. 1998. *Ecological Geography of the Sea*. Academic Press.
- Longhurst, A., S. Sathyendranath, T. Platt, and C. Caverhill. 1995. An estimate of global primary production in the ocean from satellite radiometer data. *Journal of Plankton Research* **17**: 1245-1271.
- Lundsgaard, C. 1995. Use of high viscosity medium in studies of aggregates. In S. Floderus, A.-S. Heiskanen, M. Oleson and P. Wassmann [eds.], *Sediment trap studies in the Nordic Countries*, 3. Proceeding of the Symposium on Seasonal Dynamics of Planktonic Ecosystems and Sedimentation in Coastal Nordic Waters. Numi Print.
- Lundsgaard, C., M. Olesen, M. Reigstad, and K. Olli. 1999. Sources of settling material: aggregation and zooplankton mediated fluxes in the Gulf of Riga. *Journal of Marine Systems* **23**: 197-210.
- Lutz, M., R. Dunbar, and K. Caldeira. 2002. Regional variability in the vertical flux of particulate organic carbon in the ocean interior. *Global Biogeochemical Cycles* **16**: 11/11-18.
- Marsh, R., R. A. Mills, D. R. H. Green, I. Salter, and S. Taylor. 2007. Controls on sediment geochemistry in the Crozet Region. *Deep-Sea Research II* **54**.
- Martin, J. H. 1990. Glacial-Interglacial CO₂ Change: The Iron Hypothesis. *Paleoceanography* **5**: 1-13.
- Martin, J. H. and others 1994. Testing the iron hypothesis in ecosystems of the equatorial Pacific Ocean. *Nature* **371**: 123-129.
- Martin, J. H., and R. M. Gordon. 1988. Northeast Pacific iron distribution in relation phytoplankton productivity. *Deep-Sea Research* **35**: 177-196.
- Martin, J. H., R. M. Gordon, and S. E. Fitzwater. 1991. Iron limitation? *Limnology and Oceanography* **36**: 1793-1802.
- Martin, J. H., R. M. Gordon, S. E. Fitzwater, and W. W. Broenkow. 1989. VERTEX: Phytoplankton/iron studies in the Gulf of Alaska. *Deep-Sea Research* **36**: 649-680.
- Martin, J. H., G. A. Knauer, D. M. Karl, and W. W. Broenkow. 1987. VERTEX: carbon cycling in the northeast Pacific. *Deep Sea Research* **34**: 267-285.
- Mazzocchi, M. G. and others 2009. A non-diatom plankton bloom controlled by copepod grazing and amphipod predation: Preliminary results from the LOHAFEX iron-fertilisation experiment. *Globec International Newsletter*: 3-6.
- McDonnell, A. M. P., and K. O. Buesseler. 2010. Variability in the average sinking velocities of marine particles. *Limnology and Oceanography*.
- Nelson, D. M. and others 2002. Vertical budgets for organic carbon and biogenic silica in the Pacific sector of the Southern Ocean, 1996-1998. *Deep Sea Research Part II: Topical Studies in Oceanography* **49**: 1645-1674.
- O'Reilly, J. E. and others 1998. Ocean color chlorophyll algorithms for SeaWiFS. *Journal of Geophysical Research* **103**: 937-953.
- Park, Y.-H., F. Roquet, I. Durand, and J.-L. Fuda. 2008. Large-scale circulation over and around the Northern Kerguelen Plateau. *Deep Sea Research Part II: Topical Studies in Oceanography* **55**: 566-581.
- Passow, U. 2004. Switching perspectives: Do mineral fluxes determine particulate organic carbon or vice versa? *Gechemistry Geophysics Geosystems* **5**: 1-5.

References

- Passow, U., and A. L. Alldredge. 1995. A dye-binding assay for the spectrophotometric measurement of transparent exoplomer particles (TEP). *Limnology and Oceanography* **40**: 1326-1335.
- Passow, U., and C. De La Rocha. 2006. Accumulation of mineral ballast on organic aggregates. *Global Biogeochemical Cycles* **20**: 1-7.
- Peeken, I. and others 2006. Effects of in situ iron fertilisation during contrasting seasons - comparison between EisenEx and EIFEX. ALSO-TOS-AGU Ocean Science meeting abstract **OS32A-06**.
- Peterson, M. L., P. J. Hernes, D. S. Thoreson, J. I. Hedges, C. Lee, and S. G. Wakeham. 1993. Field evaluation of a valved sediment trap designed to minimize collection of swimming animals. *Limnology and Oceanography* **38**: 1741-1761.
- Peterson, M. L., S. G. Wakeham, C. Lee, M. A. Askea, and J. C. Miquel. 2005. Novel techniques for collection of sinking particles in the ocean and determining their settling rates. *Limnology and Oceanography Methods* **3**: 520-532.
- Pollard, R., R. Sanders, M. Lucas, and P. Statham. 2007. The Crozet Natural Iron Bloom and Export Experiment (CROZEX). *Deep Sea Research II* **54**: 1905-1914.
- Pomeroy, L. R., and D. Deibel. 1980. Aggregation of organic matter by pelagic tunicates. *Limnology and Oceanography* **25**: 643-652.
- Pondaven, P., D. Ruiz-Pino, C. Fravallo, P. Treguer, and C. Jaendel. 2000. Interannual variability of Si and N cycles at the time-series station KERFIX between 1990 and 1995 - a 1-D modelling study. *Deep-Sea Research I* **47**: 223-257.
- Poulton, A. J., C. M. Moore, S. Seeyave, M. I. Lucas, S. Fielding, and P. Ward. 2007. Phytoplankton community composition around the Crozet Plateau, with emphasis on diatoms and Phaeocystis. *Deep-Sea Research II* **54**: 2085-2105.
- Ratmeyer, V., and G. Wefer. 1996. A high resolution camera system (ParCa) for imaging particles in the ocean: system design and results from profiles and a three-month deployment. *Journal of Marine Research* **54**: 589-603.
- Report, I. 2007. Climate Change 2007: The physical science basis, p. 996. In S. Solomon et al. [eds.], Contribution of Working Group I to the Fourth Assessment Report of the Intergovernmental Panel on Climate Change.
- Robison, B. H., K. R. Reisenbichler, and R. E. Sherlock. 2005. Giant Larvacean Houses: Rapid Carbon Transport to the Deep Sea Floor. *Science* **308**: 1609-1611.
- Rutgers Van Der Loeff, M. M., K. O. Buesseler, U. Bathmann, I. Hense, and I. Andrews. 2002. Comparison of carbon and opal export rates between summer and spring bloom periods in the region of the Antarctic Polar Front, SE Atlantic. *Deep-Sea Research II* **49**: 3849-3869.
- Rutgers Van Der Loeff, M. M., J. Friedrich, and U. Bathmann. 1997. Carbon export during the Spring Bloom at the Antarctic Polar Front, determined with the natural tracer ²³⁴Th. *Deep-Sea Research II* **44**: 457-478.
- Sabine, C. L. and others 2004. The Oceanic Sink for Anthropogenic CO₂. *Science* **305**: 367-371.
- Sarmiento, J. L., and N. Gruber. 2006. *Ocean Biogeochemical Dynamics*. Princeton University Press.
- SCOR. 1990. JGOFS science plan. JGOFS Report No. 5.
- Shanks, A. L., and J. D. Trent. 1980. Marine snow: sinking rates and potential role in vertical flux. *Deep Sea Research* **27**: 137-143.
- Silver, M. W., and M. M. Gowing. 1991. The 'Particle' Flux: Origins and biological components. *Progress Oceanography* **26**: 75-113.

References

- Smetacek, V., and S. W. A. Naqvi. 2008. The next generation of iron fertilisation experiments in the Southern Ocean. *Philosophical Transactions of the Royal Society London A* **366**: 3947-3967.
- Smetacek, V. and others 2010. Massive carbon flux to the deep sea from an iron-fertilized phytoplankton bloom in the Southern Ocean. *Nature* **in prep**.
- Smith, W. O., R. F. Anderson, J. Keith Moore, L. A. Codispoti, and J. M. Morrison. 2000. The US Southern Ocean Joint Global Ocean Flux Study: an introduction to AESOPS. *Deep Sea Research Part II: Topical Studies in Oceanography* **47**: 3073-3093.
- Soltwedel, T. and others 2005. HAUSGARTEN Multidisciplinary Investigations at a Deep-Sea, Long-Term Observatory in the Arctic Ocean. *Oceanography* **18**: 46-61.
- Stanley, R. H. R., K. O. Buesseler, S. Manganini, D. K. Steinberg, and J. R. Valdes. 2004. A comparison of major and minor elemental fluxes collected using neutrally buoyant and surface-tethered traps. *Deep-Sea Research I* **51**: 1387-1395.
- Staresinic, N., G. Rowe, D. Shaughnessy, and A. J. Williams Iii. 1978. Measurement of the vertical flux of particulate organic matter with a free-drifting sediment trap. *Limnology and Oceanography* **23**: 559-563.
- Steinberg, D. K., J. S. Cope, S. E. Wilson, and T. Kobari. 2008. A comparison of mesopelagic mesozooplankton community structure in the subtropical and subarctic North Pacific Ocean. *Deep Sea Research Part II: Topical Studies in Oceanography* **55**: 1615-1635.
- Stemmann, L. and others 2008. Volume distribution for particles between 3.5 to 2000 μ m in the upper 200 m region of the South Pacific Gyre. *Biogeosciences* **5**: 299-310.
- Suess, E. 1980. Particulate organic carbon flux in the oceans - surface productivity and oxygen utilization. *Nature* **288**: 260-263.
- Sullivan, C. W., K. R. Arrigo, C. R. McClain, J. C. Comiso, and J. Firestone. 1993. Distributions of Phytoplankton Blooms in the Southern Ocean. *Science* **262**.
- Trull, T., and L. Armand. 2001. Insights into Southern Ocean carbon export from the $\delta^{13}C$ of particles and dissolved inorganic carbon during the SOIREE iron release experiment. *Deep Sea Research II* **48**: 2655-2680.
- Trull, T. W., S. G. Bray, S. J. Manganini, S. Honjo, and R. Francois. 2001. Moored sediment trap measurements of carbon export in the Subantarctic and Polar Frontal Zones of the Southern Ocean, south of Australia. *Journal of Geophysical Research* **106**: 31/489-509.
- Turner, J. T. 2002. Zooplankton fecal pellets, marine snow and sinking phytoplankton blooms. *Aquatic Microbial Ecology* **27**: 57-102.
- Tyrell, T., A. Merico, J. J. Waniek, C.-S. Wong, N. Metzl, and F. Whitney. 2005. Effect of seafloor depth and phytoplankton blooms in high nitrate low chlorophyll (HNLC) regions. *Journal of Geophysical Research* **110**: 1-12.
- Valdes, J. R., and J. F. Price. 2000. A neutrally buoyant, upper ocean sediment trap. *Atmospheric and Oceanographic Technology* **17**: 62-68.
- Volk, T., and M. I. Hoffert. 1985. Ocean carbon pumps: analysis of relative strengths and efficiencies in ocean-driven atmospheric CO₂ changes. *Geophysical Monographs* **32**: 99-110.
- Waite, A. M., Ö. Gustafsson, O. Lindahl, and P. Tiselius. 2005. Linking ecosystem dynamics and biogeochemistry: Sinking fractionation of organic carbon in a Swedish fjord. *Limnology and Oceanography* **50**: 658-671.
- Waite, A. M., and S. D. Nodder. 2001. The effect of in situ iron addition on the sinking rates and export flux of Southern Ocean diatoms. *Deep-Sea Research II* **48**: 2635-2654.

References

Waite, A. M., K. A. Safi, J. A. Hall, and S. D. Nodder. 2000. Mass sedimentation of picoplankton embedded in organic aggregates. *Limnology and Oceanography* **45**: 87-97.

Websites:

<http://cafethorium.whoi.edu/website/projects/tzex.html>

<http://www.awi.de/en/home/lohafex/>

<http://modis.gsfc.nasa.gov/>

<http://www-argo.ucsd.edu/>

<http://www.ifm-geomar.de/index.php?id=1241&L=1>

Eidesstattliche Erklärung

Gemäß §6(5) Nr. 1-3 der Promotionsordnung des Fachbereichs 2

Hiermit erkläre ich, dass ich die vorliegende Arbeit ohne unerlaubte fremde Hilfe angefertigt habe, keine anderen als die angegebenen Quellen und Hilfsmittel benutzt und die den benutzten Werken wörtlich oder inhaltlich entnommenen Stellen als solche kenntlich gemacht habe.

Bremen, den

Appendix 1

Sinking particle properties from polyacrylamide gels during the Kerguelen Ocean and Plateau compared Study (KEOPS): Zooplankton control of carbon export in an area of persistent natural iron inputs in the Southern Ocean

F. Ebersbach¹

Antarctic Climate and Ecosystems (ACE) Cooperative Research Centre, Institute of Antarctic and Southern Ocean Studies (IASOS), University of Tasmania, Hobart, 7001, Australia; Carl von Ossietzky University, Oldenburg, Germany

T. W. Trull

Antarctic Climate and Ecosystems (ACE) Cooperative Research Centre, Institute of Antarctic and Southern Ocean Studies (IASOS), University of Tasmania, Hobart, 7001, Australia; Commonwealth Scientific and Industrial Research Organization (CSIRO) Marine and Atmospheric Research, Hobart, 7001, Australia

Abstract

The Kerguelen ocean and plateau compared study (KEOPS) examined the origin of elevated phytoplankton biomass in naturally iron-fertilized waters over the Kerguelen plateau during midsummer (January–February 2005). We report sinking particle characteristics determined from image analysis of thousands of individual particles collected in viscous polyacrylamide gels placed in free-drifting sediment traps at two sites: a high phytoplankton biomass site over the central plateau (A3) and a moderate biomass site at its periphery (C5). The particles were divided into three types (1) oval fecal pellets, (2) cylindrical fecal pellets, and (3) aggregates. The aggregates were most abundant and mainly consisted of agglomerations of the cylindrical fecal pellets. Conversion of the pellet and aggregate volumes to carbon contents suggests export fluxes of 50–60 mg C m⁻² d⁻¹ at 100-m depth, in reasonable agreement with independent estimates from carbon and ²³⁴Th measurements. Our observation that the majority of the particle flux was processed through the heterotrophic foodweb contrasts with the results of artificial iron-fertilization experiments and with models for export from productive diatom-dominated waters that emphasize direct export of phytoplankton detritus. The KEOPS results may offer more appropriate scaling for the response of ecosystem structure and carbon export to persistent iron fertilization in the Southern Ocean.

The Kerguelen Ocean and Plateau compared Study (KEOPS) program carried out a survey of biogeochemical processes over the Kerguelen plateau in the Southern Ocean. The primary objective was to determine the cause of

¹Present address: Alfred Wegener Institute for Marine and Polar Research (AWI), Am Handelshafen 12, 27570 Bremerhaven, Germany.

Acknowledgments

We thank KEOPS chief scientists Stephane Blain and Bernard Queguiner (Université de Marseille) for inviting our participation, Dan McLaughlin Commonwealth Scientific and Industrial Research Organization (CSIRO) and Stephen Bray Antarctic Climate and Ecosystems (ACE) for trap preparation, Clodagh Moy (ACE) for gel preparation, and Tom Remenyi (ACE), Pierre Sangiardi, and Christophe Guillerm for onboard preparation of replacement trap arrays. Ron Thresher, Rob Guerne, and Jawahar Patil provided access and aid in the CSIRO microscopy laboratory, and Karin Beaumont (Institute of Antarctic and Southern Ocean Studies) and Stephanie Wilson (Virginia Institute of Marine Sciences) gave advice on fecal pellet identification and carbon content estimation. Funding was provided by the Australian Commonwealth Cooperative Research Centre Program, the French-Australian Science and Technology Cooperation (A. Bowie, T. Trull et al. award FR040170), the Australian Antarctic Science Program (T. Trull et al. AAS1156), and loan of equipment from the U.S. National Science Foundation (K. Buesseler, T. Trull et al. award 0301139). We are grateful for constructive reviews and editorial input that significantly improved this paper.

persistently high phytoplankton biomass in this region, as seen in *SeaWiFS* and *MODIS* satellite images of ocean color. Enhanced iron supply from plateau sediments appears to play the key role (Blain et al. 2007). The iron input increases phytoplankton growth rates and draws down surface carbon dioxide partial pressure by more than 700 Pa (70 μ atm) although full use of macronutrients (phosphate, nitrate, silicate) is still not achieved (Blain et al. 2007). Thus the Kerguelen plateau offers an opportunity to examine the influence of iron on ocean biogeochemistry and carbon sequestration beyond what can be achieved with short-term iron “fertilization” experiments (Buesseler and Boyd 2003).

The carbon sequestration accompanying the iron inputs over the Kerguelen plateau depends on the transfer of carbon from surface waters to the ocean interior in sinking particles. The magnitude of this export production is generally linked to primary production, although the relationship can be complex and strongly dependent on ecosystem structure (Michaels and Silver 1988; Boyd and Newton 1999). Export estimates from the ²³⁴Th deficit method during KEOPS suggest that particulate organic carbon (POC) export over the plateau was approximately twice that in adjacent high-nutrient low-chlorophyll (HNLC) waters but that the efficiency of export as a fraction of primary production was lower over the plateau (~16% to 28%) than in the HNLC waters where it reached nearly 60% (Savoye et al. 2006).

A first step in determining the ecosystem processes responsible for POC export is to characterize the sinking particles, often by their collection in sediment traps. This has significant compromises because the particles can disaggregate or form new agglomerations within the trap. An improvement is the use of polyacrylamide gels within sediment traps (Lundsgaard 1995; Waite and Nodder 2001). With viscosity similar to honey, these chemically inert gels provide a slow deceleration of sinking particles and isolate the particles from each other in their original forms.

Here we report sinking particle characteristics determined from polyacrylamide gels in short-term free-drifting sediment trap deployments during KEOPS. The observations suggest that export was dominated by zooplankton fecal pellets—sinking both individually and in larger aggregates, and that the sinking flux decreased rapidly with depth. This situation is in considerable contrast to the results of Southern Ocean short-term iron-fertilization experiments, in which zooplankton responses have generally (Boyd et al. 2000; Coale et al. 2004) but not always (Peeken et al. 2006) been muted.

Materials and methods

Site description—The KEOPS voyage occupied three east–west transects over and to the east of the Kerguelen plateau (Fig. 1), and singled out two “reference” stations for repeat visits—A3 at the epicenter of the high, chlorophyll *a* (Chl *a*) region, and C11 at the southeast extreme of the study region in low-Chl *a* waters. Deployment of free-drifting sediment traps was originally planned for these sites, but loss of equipment required these plans to be modified, and samples were collected twice at A3 and once at a moderate Chl *a* concentration site (C5) along the southern periphery of the plateau. As summarized in Table 1, the traps were deployed at four depths below the mixed layer (which was relatively constant at 70 ± 10 m throughout the region; Blain et al. 2007).

The pattern of regional chlorophyll accumulation was relatively constant during the KEOPS study period (18 January to 13 February 2005) in terms of its major features of elevated biomass over the plateau and low biomass off the plateau to the south and east. Placed in a seasonal context, the Chl *a* over the plateau increased strongly in October and November, reached maximum levels of $\sim 2.5 \mu\text{g L}^{-1}$ in December and January, and then slowly declined through the shipboard study period to less than $0.5 \mu\text{g L}^{-1}$ by early March (Blain et al. 2007). In keeping with the biomass distributions, surface mixed layer nutrient levels were lower over the plateau than at the C11 HNLC site (Blain et al. 2007). Primary production estimated from small-bottle short-term ^{14}C incubations during the shipboard observations was moderate at the A3-plateau and C5-bloom periphery sites and lower at the C11-HNLC site ($\sim 300, 200,$ and $100 \text{ mg C m}^{-2} \text{ d}^{-1}$, respectively, Griffiths and Uitz 2006).

All three trap deployment sites exhibited similar phytoplankton communities dominated by large diatoms, although pigment analyses suggested that the C5 site had

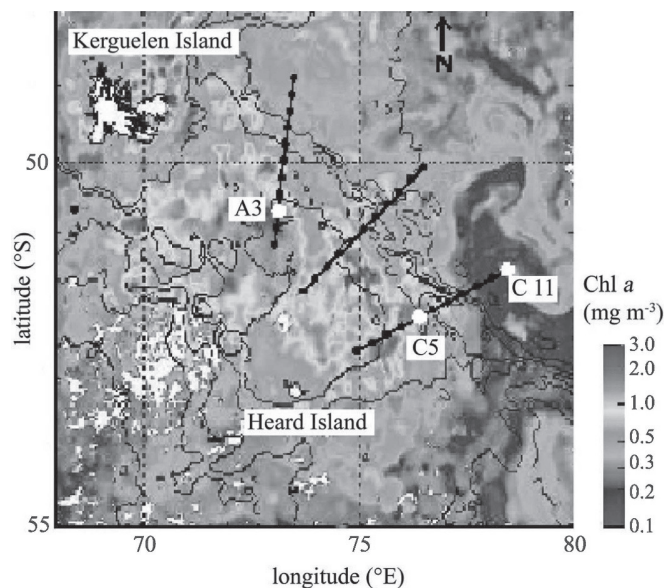


Fig. 1. Map of KEOPS cruise track, bathymetry, MODIS Chl *a*, and sediment trap deployment locations. In white are Kerguelen Island at the top left and Heard Island at the lower center (near $53^{\circ}\text{S}, 74^{\circ}\text{E}$). Bathymetric contours are at 500-m intervals. Eleven stations were carried out along each of three east–west transects—referred to as A, B, C from north to south. Sta. A3 was at the epicenter of the biomass-rich region and served as the reference high-biomass site. Gels were deployed and recovered there twice, and once at Sta. C5 near the 1,000-m contour at the southeast periphery of the plateau in the presence of low to moderate biomass. Sta. C11 at the eastern extreme provided the HNLC reference site, but no traps were deployed there because of earlier equipment failures. Table 1 provides more details of the gel deployments.

a somewhat larger proportion of nondiatom phytoplankton than either the A3 or C11 sites (Griffiths and Uitz 2006). Total ^{234}Th inventories observed in the water column, combined with C: ^{234}Th ratio estimates from sediment trap and large volume filtrations, suggest relatively high POC export from all three of these sites (Savoie et al. 2006). At the A3 bloom site, POC export at 100-m depth varied in the range $120\text{--}480 \text{ mg m}^{-2} \text{ d}^{-1}$ over three visits, and was $240\text{--}300 \text{ mg m}^{-2} \text{ d}^{-1}$ during the A3f trap deployment, equivalent to $\sim 28\%$ of primary production. At the C11 HNLC site, this export was $\sim 144 \text{ mg m}^{-2} \text{ d}^{-1}$, which was $\sim 58\%$ of the primary production. At the bloom periphery site C5, the export was $\sim 108 \text{ mg m}^{-2} \text{ d}^{-1}$, but this was only $\sim 21\%$ of the primary production. Thus, the traps were deployed in central and peripheral regions of the elevated biomass region over the Kerguelen plateau, under conditions of moderate production and export toward the end of the annual diatom-dominated phytoplankton “bloom.”

Sediment trap deployments—The gels were prepared following the method of Lundsgaard (1995), with slight modifications. Prior to the expedition, Southern Ocean nutrient replete seawater was filtered through a glass fiber filter (nominal $0.8\text{-}\mu\text{m}$ pore size) and 20 g L^{-1} NaCl was

Table 1. Sediment trap deployments.

Site	Depths (m)	Start date	End date	Duration	Start position	End position	Drift (km)
A3i	200	03 Feb 2005 21:36 h	04 Feb 2005 17:11 h	18 h 35 min	50°37.80'S, 72°04.80'E	50°15.60'S, 72°34.00'E	32
C5	100, 200, 330, 430	07 Feb 2005 07:21 h	08 Feb 2005 06:55 h	23 h 34 min	52°27.43'S, 75°36.06'E	52°13.87'S, 75°43.67'E	16
A3f	100, 200, 330, 430	12 Feb 2005 08:09 h	13 Feb 2005 08:19 h	24 h 10 min	50°37.73'S, 72°00.01'E	50°35.62'S, 72°11.22'E	8

added to increase its density. Acrylamide (16 weight percent) was dissolved in this solution and polymerized to form ~4-cm thick gels in containers with optically clear polycarbonate bottoms. No poisons, stains, or buffers were used.

A layer of filtered seawater amended with 10 g L⁻¹ NaCl was placed over the gels several days before deployment to allow a viscosity gradient of ~1-cm thickness to develop to ensure slow deceleration of sinking particles entering the gel. This ensures that particles enter the gel without contacting an interface that might alter their forms. Our concentration of acrylamide was twice that used in many previous studies (Waite and Nodder 2001; Whiteley 2003; Waite et al. 2005). This prevents flow of the gel during recovery and slows particle sinking rates sufficiently that they accumulate at ~1-cm depth within the gel where they are easily photographed in a single field of view. The particles then take several weeks to months to settle to the bottom of the containers. During this period they exhibit some degradation (loss of color, minor disaggregation that spreads their shapes isotropically) but show little sign of changes in form attributable to deformation by the gel (little or no flattening of the shapes in the vertical direction).

The gels were deployed in cylindrical traps (12-cm diameter by 60-cm long), fitted with slightly conical bottoms with a central drain valve. The gels completely covered the bottom of the tubes, preventing particles from settling outside the gel and potentially being resuspended and entering the gel in altered form. This is an advance from previous approaches that placed small Petri dishes in the center of trap tubes (Waite and Nodder 2001; Whiteley 2003; Waite et al. 2005). To minimize possible alteration of sinking particles, no baffles were used. Brine (filtered seawater amended with 10 g L⁻¹ NaCl) was carefully added to cover the gel to a depth of one trap diameter and was overlain with filtered seawater to fill the trap tube.

The individual trap tubes were spaced along a low-drag (5-mm diameter) plastic-jacketed wire (with a 20-kg weight at the end) beneath a surface float equipped with a flashing light and an Argos/global positioning system beacon, and released to drift freely for ~24 h (further details are given in Table 1). The trap at 200 m was configured differently than the others. It was attached with its top level with a larger cylindrical trap (2-m long, 60-cm diameter PPS3/3 trap, Technicap, France) used to collect particles for separate chemical studies (Savoye et al. 2006; Trull unpubl. data).

The trap deployments at site C5 and during the final deployment at site A3 were carried out in moderate winds (5–10 m s⁻¹) and seas (2–3 m) with little difficulty. The two deeper tubes were successfully and rapidly deployed and

recovered with essentially no loss of trap fluid, with little tilting of the traps and without any significant time spent in the mixed layer (a few minutes at most). Conditions for the 200-m tubes attached to the PPS3 sediment trap were also relatively benign but did involve considerable tilting of the tubes during deployment when slow filling and sinking of the PPS3 trap kept the tubes close to horizontal for several minutes. Fortunately, recovery showed that the gels did not flow out during this period and still covered the full expanse of the sediment trap bases. Recovery also involved greater tilting of the 100-m traps because of the higher drag of the PPS3 trap (up to 30 degrees from the vertical for up to 10 min), and the gel-brine interface for these traps was ~10 degrees from horizontal on recovery but showed no significant signs of flow within the gel having disturbed the particle distributions.

In contrast, the initial deployment at site A3 (on 03–04 February 2005, referred to as A3i) experienced difficulties during recovery in higher winds (10–13 m s⁻¹) and seas (4–5 m) as the array became snagged under the hull and was dragged for ~30 min. On recovery the two gel tubes mounted on the PPS3 trap at 200 m were found to have flowed to angles of approximately 30 and 45 degrees from horizontal. The more disturbed gel showed signs of slumping that happened as seawater poured from the tube during recovery; therefore, it was not examined further. The other gel was in reasonable condition but showed a much greater amount of individual algal cells than those from the A3f and C5 deployments, suggesting they may have entered the trap as it was dragged near the surface. For this reason we focus primarily on the results of the C5 and final A3 (12–13 February 2005, referred to as A3f) deployments in the discussion below. We do present the A3i results, but they must be viewed with considerable caution.

Immediately on recovery the overlying seawater in the gel cups was carefully removed with a 50-ml plastic syringe equipped with a short length of fine-bore tubing (which allows seawater but not the viscous gel to be removed), and the cups were sealed and stored at 4°C. This rapid removal of overlying seawater limits the collection of particles that entered the tube during its passage through the mixed layer on recovery, without removing particles that settled into the gel during deployment.

Gel microscopy and image analysis—The gels were examined onboard the ship within a few hours of recovery using low magnification stereomicroscopy (6.5 to ×50) and again in the laboratory 4 months after collection, using high magnification stereomicroscopy (Leica MZ 16 FA at

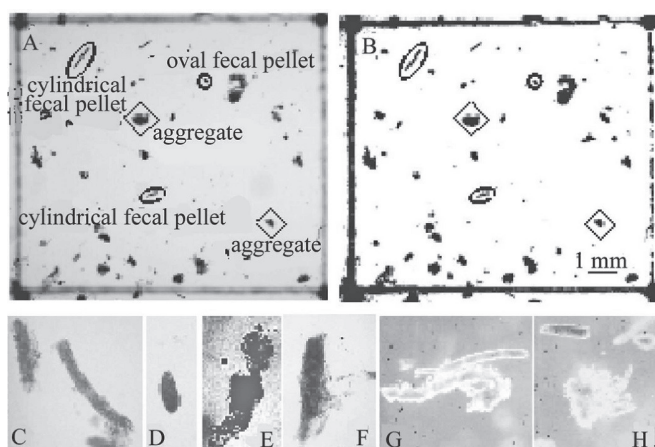


Fig. 2. Images of particles in the gels. (A) One of the ~ 30 grid cells (14 mm across) examined for each gel, with different particle types indicated. (B) The same image after thresholding to produce a binary image for particle analysis. The three classified particle types are shown: (C) cylindrical pellet, (D) oval pellet, (E) aggregate, followed by images illustrating fecal pellet transformations: (F) fecal material loosening up, (G) pellets sticking together (lower one in the process of degradation), (H) an aggregate of fecal pellets and other material. Panels C–H are ~ 1 mm across.

up to $\times 115$) and inverted compound microscopy (Leica DM IRB at up to $\times 400$). Whereas all of the quantitative results presented here are based on the shipboard analyses, the laboratory analyses confirmed the shipboard result that most aggregates were formed from degraded, agglomerated fecal pellets. The significantly advanced particle degradation prior to laboratory analysis helped in some aspects of particle identification, e.g., the removal of organic matter increased the transparency of pellets and aggregates allowing their contents to be examined in greater detail, but hindered other aspects, e.g., fecal pellets lost some of their structural integrity.

To obtain particle statistics, the entire gel was photographed against an etched-glass grid of 36 cells (each 14 mm \times 12.5 mm) at a magnification of $\times 6.5$, using light-field transmitted illumination and a Zeiss Stemi 2000 CS stereo microscope coupled to a Leica DFC280 1.5 million pixel digital camera and Leica Firecam software on an Apple G4 computer. These 32-bit grayscale images were converted into binary images using the U.S. National Institutes of Health free software package ImageJ. Iterative exploration of lighting conditions and image acquisition parameters was used to optimize the process of automated thresholding to ensure that the binary particle images well represented the original sizes and shapes (Fig. 2).

As summarized in the Results section, we chose to classify the particles into three types: cylindrical fecal pellets, ovoid fecal pellets, and aggregates. All of these particles in each gel (thousands) were classified individually by us by comparing the binary and original images, and the image analysis routine was applied to obtain their areas, lengths, and aspect ratios (by fitting ellipses to their areas). This individual assessment allowed us to verify particle boundaries and rectify any misidentifications of particle

areas caused by overlap in the images. Because particles less than 150 μm in size were uncommon (*see Results*), we chose to ignore particles smaller than 100 pixels in area (0.00019 cm^2) in the analysis procedure, and thus were also able to avoid spurious “particles” arising from small variations in optical density associated with gel thickness, glass-grid and optical path cleanliness, etc. Based on test processing without this size cutoff, we estimate that this procedure omitted hundreds of “particles” but less than 5% of the total particle area, and therefore introduced negligible bias in our overall conclusions. Of course, transparent or nearly transparent particles or portions of them are not directly imaged. Inspection at higher magnification ($\times 50$ shipboard and $\times 400$ in Hobart) suggests that nearly transparent materials were often present within aggregates, but because the three-dimensional aggregate structures caused the visible and transparent portions to overlies each other in the two-dimensional images, much of this material was effectively measured.

Conversion of the imaged areas to volumes required some assumptions. For the aggregates and oval fecal pellets we estimated ellipsoidal volumes by assuming the third axis to be equal to the minor axis of the imaged ellipse. Since these shapes were close to isotropic this introduces minor errors. For the cylindrical pellets we estimated cylindrical volumes using the imaged length and width as the length and diameter, respectively. Because the cylindrical pellets had relatively high aspect ratios (long, thin shapes) their imaged areas will underestimate their volumes unless they lie horizontally in the gel. Inspection of the gels from the side revealed that many particles were arranged randomly in terms of their angles to the vertical, although some tendency toward longer fecal pellets lying more horizontally was observed. Assuming random orientation suggests that the areas of the long cylindrical fecal pellets could be underestimated by up to $\sim 36\%$ (integrating the random distribution over the $\pi/2$ angles from horizontal to vertical implies a mean imaged length of $2/\pi$ of the true length). Given the tendency for the cylindrical pellets to lie horizontally, this is a maximum bias and we did not correct for it.

Conversion from particle volume to organic carbon content was the most uncertain step in our estimation of carbon fluxes. Removing particles from the gel was not practical, and attempts to estimate aggregate carbon contents from optical density were not successful because of varying illumination and the lack of a means to calibrate the optical observations. Therefore we relied on published carbon content analyses. For the fecal pellets, we used a value of 0.057 mg C mm^{-3} (Gonzalez and Smetacek 1994). This is a midrange value based on estimates for copepod fecal pellets that range from 0.05 to 0.11 mg C mm^{-3} (Silver and Gowing 1991; Gonzalez and Smetacek 1994; Carroll et al. 1998). For the aggregates, we used a more complex relation between size and carbon content. For large aggregates (greater than 0.004 mm^3 in volume; or an equivalent spherical diameter [esd] of ~ 0.02 cm), we used a fractal relationship (Alldredge 1998) of $\text{POC} = 0.99V^{0.52}$ (POC in μg and volume in mm^3). For smaller aggregates (< 0.004 mm^3 in volume), we used a linear (i.e.,

Table 2. Particle characteristics and bins for aggregates (agg), cylindrical (cyl), and ovoid (ova) fecal pellets.

Characteristics Name	Unit										Definition
Area	cm ²										pixel area of the particle image
Volume	cm ³										volume calculated from area (<i>see Methods</i>)
Equivalent spherical diameter (esd)	cm										diameter of a sphere with the same imaged area
Perimeter	cm										sum of pixel lengths at particle edge
Length	cm										major axis of ellipse fit to particle
Aspect ratio	none										major/minor axis ratio of fitted ellipse
Roughness	none										ratio of perimeter to ellipse perimeter
Number flux	m ⁻² d ⁻¹										number flux of sinking particles
Volume flux	cm ³ m ⁻² d ⁻¹										volume flux of sinking particles
Carbon flux	mg C m ⁻² d ⁻¹										organic carbon flux in sinking particles
Number flux size spectrum	cm ⁻¹ m ⁻² d ⁻¹										number flux per unit esd size interval
Volume flux size spectrum	cm ³ cm ⁻¹ m ⁻² d ⁻¹										volume flux per unit esd size interval
Number flux fraction	none										number flux of particle type as a fraction of total
Volume flux fraction	none										volume flux of particle type as a fraction of total
Carbon flux fraction	none										carbon flux of particle type as a fraction of total
Bins											
Bin limit	0	1	2	3	4	5	6	7	8	9	
esd	0.0155	0.0178	0.0252	0.0357	0.0505	0.0714	0.1009	0.1427	0.2019	0.2855	

solid geometry) dependence on size and a carbon content of 0.25 times that of the fecal pellets.

We chose this piece-wise relation between aggregate size and carbon content for several reasons: (1) for our large aggregates, the fractal power law that parameterizes increasing porosity with increasing size (Alldredge 1998) was consistent with our microscopic observations of aggregate structures; (2) extending this relationship to smaller sizes (less than an esd of ~ 0.01 cm) was clearly not appropriate because it leads to carbon densities for small aggregates that greatly exceed those of phytoplankton and thus a change to a linear relation at smaller sizes is required (Kriest 2002); (3) a carbon content for the small aggregates of 0.25 times that of fecal pellets was consistent with our microscopic observations, suggesting that smaller aggregates were often formed from disaggregating single cylindrical fecal pellets that had approximately doubled in diameter; and (4) using an esd of ~ 0.02 cm for the transition from linear to fractal geometry is consistent with compiled mass-size relations (Kriest 2002) and was close to the median size of cylindrical fecal pellets in our samples and thus was appropriate for the transition from small aggregates consisting of disaggregating individual fecal pellets to large aggregates consisting of agglomerated fecal pellets.

While our chosen parameterization for aggregate carbon content is consistent with previous work (Alldredge 1998; Kriest 2002), we emphasize that it probably represents carbon flux to no better than an order of magnitude. This reflects the uncertainties in the published power law as derived from suspended aggregates at shallow Californian coastal waters (Alldredge 1998) and its uncertain applicability to sinking particles at mesopelagic depths in the Southern Ocean. More aggregate carbon measurements are very much needed to improve this situation.

Following the approach of previous studies (Jackson et al. 1997, 2005), we present the particle information as size

spectra in units of flux of particle numbers per unit particle size, using an equivalent spherical particle diameter for the size based on the imaged area of the particle (Jackson et al. 2005). Definitions and units for these terms are provided in Table 2, including the bin limits used to construct the spectra. The bins were spaced at a factor of two intervals in terms of the imaged area, with the lowest limit set to the 100 pixel cutoff in imaged area and the highest limit set to ensure several particles were present (i.e., to ensure statistically appropriate sampling; Jackson et al. 1997).

Results

The polyacrylamide-gel sediment traps deployed at the central KEOPS high-biomass Sta. A3 and at the peripheral moderate-biomass Sta. C5 (Fig. 1 and Table 1) performed very well in terms of collecting intact sinking particles as shown by the fragile forms preserved in the gels (Fig. 2). The short duration (~ 1 d) of the trap deployments avoided overloading the gels and facilitated the image processing. The particles were evenly distributed over the collection area of the gels, in contrast to some previous studies (Whiteley 2003), suggesting vertical deployments and a negligible flow of the gel within the trap.

The first notable aspect of the materials collected in the gel traps was the absence of significant numbers of zooplankton. There were at most one to two copepods per trap, and a single euphausiid in one trap, despite their high abundances and dominance of surface net collections (Carlotti et al. 2006). There were similarly small numbers of acantharia but slightly higher numbers of pelagic tunicates and especially foraminifera, which reached ~ 10 per gel. No further quantification or identification of zooplankton was pursued. The low numbers of copepods and euphausiids possibly reflect the absence of poisons in the traps but may also be due to the gels themselves discouraging zooplankton—since very low zooplankton numbers in gel traps in

comparison with unpoisoned traps were observed in a later study in the subarctic North Pacific (Trull, Ebersbach, and Buesseler, unpubl. data).

The second notable aspect was the absence of large numbers of individual phytoplankton, small fecal “mini-pellets” (<100 μ ; as derived from heterotrophic nanoflagellates and other small protists; Gonzalez 1992b; Gowing et al. 2001; Turner 2002), eggs, or other small particles. Some individual large diatom frustules were present (primarily large centric and pennate diatoms but also including a few 1–3 mm long *Thalassiothrix antarctica* needle-like frustules), but the total contribution of individual phytoplankton was estimated as less than 1% of the particle population. For this reason we used a cutoff of ~150 μ m equivalent spherical diameter (esd) for the smallest particles in our image processing and thus did not quantify this contribution further.

The third notable aspect was the presence of many large fecal pellets and aggregates of these pellets, examples of which are shown in Fig. 2. Cylindrical pellets were most common. These included (1) highly cylindrical pellets with very smooth borders and nearly invariant diameters that appeared to contain fine materials, these were commonly brown or tan in color; (2) pellets that tapered slightly over their length, these were often among the largest pellets, exhibited similar or slightly lighter colors, and did not appear to be as tightly packed as the former; (3) relatively short, only approximately cylindrical pellets with very rough edges that appeared to contain large diatom frustules. Of these three subtypes of cylindrical pellets, the first was by far the most common. In addition there were small numbers of distinctly ovoid fecal pellets, which were usually very black and tightly packed, similar to those reported in Antarctic waters (Gonzalez 1992a).

The highly cylindrical fecal pellets were probably derived from copepods, based on morphological similarity to previous identifications (Honjo and Roman 1978; Gonzalez and Smetacek 1994) and the observation that large copepods along with less abundant euphausiids dominated net samples during KEOPS (Carlotti et al. 2006). The rarer large, tapering, cylindrical, less tightly packed fecal pellets were probably from euphausiids, again based on morphological similarity to previously studied pellets (Gonzalez 1992a; Gonzalez et al. 1994; Waite et al. 2000). The origin of the ovoid fecal pellets in our study, as in previous work (Gonzalez 1992a), remains unknown. These ovoid pellets were almost always observed singly rather than within aggregates, suggesting that they do not readily stick to other particles.

Aggregates were the most abundant particle type. They were generally approximately isotropic in shape, commonly contained of the order of two to eight cylindrical pellets or pellet fractions and were brown in color (Fig. 2). There was little evidence for loose aggregates formed by direct flocculation of relatively undamaged phytoplankton, e.g., as observed in the Pacific by in situ examination of suspended particles (Alldredge and Gotschalk 1988), in gel traps in a Swedish fjord (Waite et al. 2005), and during the Southern Ocean iron enrichment experiment (SOIREE; Waite and Nodder 2001; Jackson et al. 2005). For example,

loose aggregates of the long (1–2 mm) needle-like diatom *T. antarctica*, large spiral-chain forms of *Eucampia antarctica*, or other large diatoms that were present in surface waters (Armand et al. 2006) were not observed. Loose amorphous aggregates without internal structure as observed during SOIREE (Waite and Nodder 2001), where they were attributed to physical aggregation, or in subantarctic waters (Waite et al. 2000), where they were thought to possibly derive from disaggregating salp fecal pellets, were not observed either.

The general internal structure of the aggregates seemed to be related to the agglomeration of cylindrical fecal pellets—often pairs of pellets were arranged in parallel, and others in crossing shapes. Pellets grouped around nearly transparent material including transparent exopolymeric particles or appendicularian molts were also observed, but were less common. Many of these pellets were in the process of disaggregating (Fig. 2), and exhibited loosening of material, opening out of their shapes, and spreading of their tightly packed contents in very similar ways to that observed for copepod pellets in the laboratory (Honjo and Roman 1978). Studies of the incorporation of radio-labeled compounds (Turley 1993; Bidle and Azam 1999; Turley and Stutt 2000) have demonstrated that this degradation is mediated by bacteria, and as reviewed by Turner (2002) includes activity internally as well as on external surfaces. Along with pellet disruption by physical processes and zooplankton feeding, this bacterial activity is an important contributor to the vertical flux (Lampitt et al. 1991; Noji et al. 1991; Silver and Gowing 1991). As disintegration proceeds, the fecal pellets become less identifiable and eventually indistinguishable from what might have been flocculated phytoplankton (as is evident from comparison to other studies of aggregates in gels, Waite et al. 2000; Waite and Nodder 2001). This means that we cannot rule out a role for physical aggregation of phytoplankton, although we consider it to have been a minor contributor to export.

Given the dominant abundance of the aggregates and the subjective nature of distinguishing the three subtypes of the cylindrical pellets, we chose to quantify three types of particles: (1) cylindrical fecal pellets, (2) oval fecal pellets, and (3) aggregates. In our classification, the term “aggregate” means that a particle was not distinctly recognizable as a single fecal pellet, an animal, or an individual phytoplankton cell. Based on low-power shipboard microscopy (up to $\times 50$) most of these aggregates were composed of agglomerated cylindrical fecal pellets (see Fig. 2). The higher magnification microscopy in Hobart 4 months later revealed the evolution of particle forms during their degradation and suggested that many of the smaller particles identified shipboard as aggregates may have formed from degraded individual fecal pellets. Thus our overall qualitative conclusion was that most of the flux was derived from copepod fecal pellets, sinking either individually as intact pellets, individually as degrading pellets, or most commonly as aggregates of pellets in various states of decay.

The image analysis procedure allowed us to classify the vast majority of collected particles into these three types (in

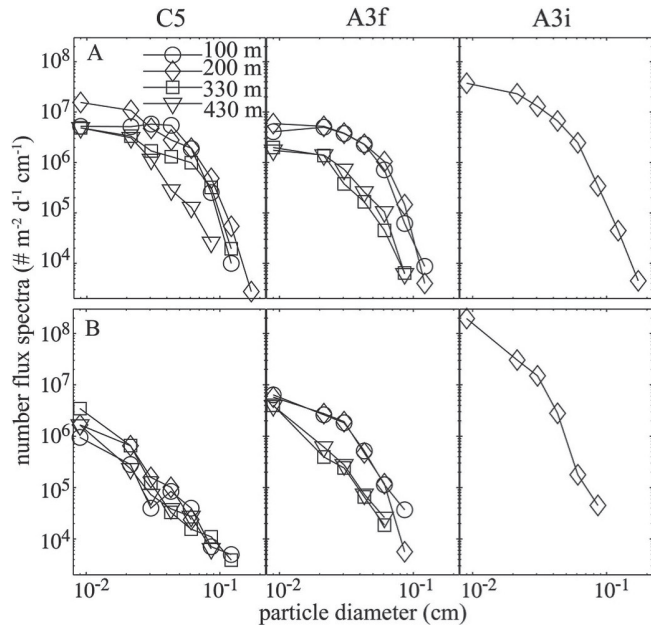


Fig. 3. Number flux spectra (A) aggregates, (B) cylindrical fecal pellets. Aggregates were in general larger than cylindrical fecal pellets. Both types decreased in size with depth in the water column.

excess of 90% and often 95% of the areas of the images occupied by particles) and to determine their total fluxes, sizes, shapes, and other characteristics (Table 2 provides a short summary of our particle measurement terminology and associated units). First we present the total fluxes of the particles across the three types, in terms of both numbers of particles and volumes of particles (in Tables 3, 4, and 5). Then we examine size distributions for the cylindrical fecal pellets and the aggregates in Figs. 3, 4, and 5 (but not for the oval fecal pellets because of the small numbers collected). Finally we consider the shapes of the cylindrical fecal pellets and aggregates (Fig. 6). We emphasize the results from C5 and the final visit to A3 (A3f), for which information was obtained at four depths (Table 1), but also provide results from the initial visit to A3 (A3i) for which results are available only from 200-m depth (and may have been compromised during trap recovery; see the *Methods* section).

Total number fluxes were highest in the C5 collections at 100- and 200-m depths (Table 3) and slightly exceeded the total number fluxes at A3f at these depths, by 29% and 6%, respectively. Deeper in the water column, total number fluxes decreased strongly at both sites—to approximately one third to one half of 100-m values at 330- and 430-m water depth. Aggregates were the dominant particle type, contributing at least 49% of the particles in the C5 and A3f collections at all depths, and generally much more, ranging up to 96% in the C5 100-m trap (Table 3). This dominance was stronger at C5 than at A3f and decreased with depth at both sites. After aggregates, cylindrical fecal pellets were the next most important particle type. Their importance was larger at A3f (27% to 37% of total numbers) than at C5 (3% to 12% of total numbers). This difference is

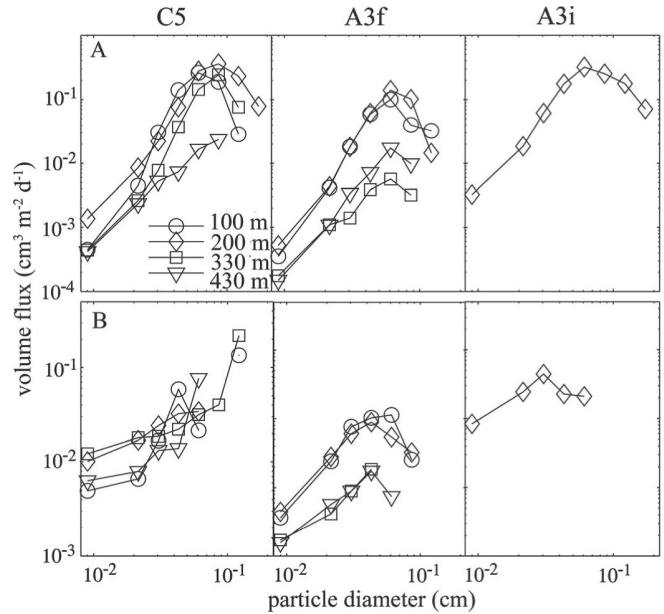


Fig. 4. Volume flux as a function of particle size. (A) Aggregates and (B) cylindrical fecal pellets. Medium-sized particles dominated the volume fluxes, in contrast to the dominance of number fluxes by small particles (Fig. 3).

emphasized by considering the ratio of aggregates to cylinders (which exceed 30 at C5 but was less than 3 at A3f). Oval pellets were the minor player in all collections except at C5 430 m, where they reached 17% of total numbers and exceeded the 10% contribution from cylindrical pellets. The compromised A3i 200-m trap was distinguished by a much higher flux than any other trap

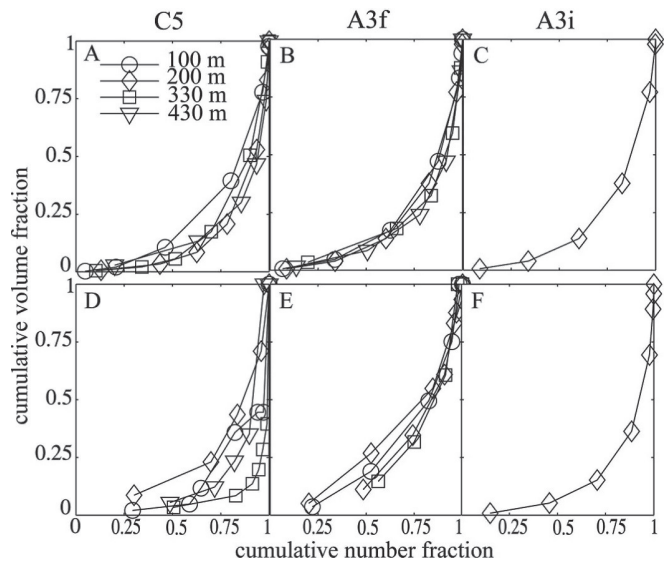


Fig. 5. Cumulative carbon flux as a function of cumulative number flux summed across increasing size classes. (A–C) Aggregates, (D–F) cylindrical fecal pellets. The largest 20% of the particles contributed more than 50% of the carbon flux at all sites and depths.

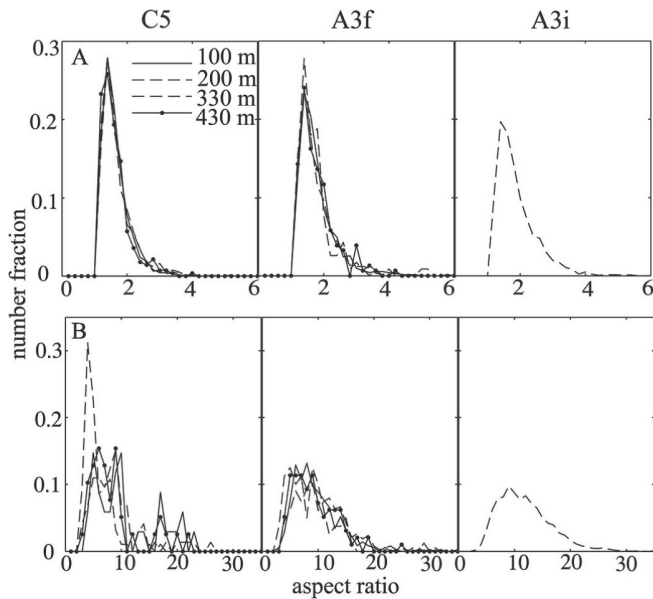


Fig. 6. Changes in particle shape with depth and among the sites. (A) Aggregate aspect ratios and (B) cylindrical fecal pellet aspect ratios. The aggregates had a narrow range of aspect ratios and very similar aspect ratio distributions in all the samples. In contrast, the cylindrical fecal pellet aspect ratios varied more than an order of magnitude.

(approximately four times higher) and a much greater contribution from cylindrical fecal pellets to the total flux (58%, Table 3).

Examining the particle fluxes in terms of volume fluxes underlines the trends observed in the particle number statistics. Volume fluxes were higher at C5 than A3f and decreased strongly with depth, with the results for 330- and 430-m representing as little as 10% of those at the surface (Table 4). Aggregates contributed more than 77% of the total volume flux in all traps (Table 4) in comparison with greater than 48% of the number flux, reflecting the larger size of the aggregates in comparison with the fecal pellets (as indicated by the median dimensions for the particles presented in Table 5).

The smallest particles (~ 0.01 cm) were most abundant at all the sites (Fig. 3). There was a strong decrease of more

than two orders of magnitude in terms of number flux per unit size (diameter) across the observed size range from 0.01 to 0.1 cm (see Table 2 for bin sizes used to construct Figs. 3, 4, and 5). For both aggregates and cylindrical fecal pellets, the general trend of decreasing size and number flux with depth (Fig. 3) was noted earlier by reference to median particles sizes (Table 5).

Although small particles dominated the aggregate and especially the cylindrical fecal pellet number flux spectra (Fig. 3), their contribution to the volume flux was not as important. Midrange particle sizes (in particular from 0.02 to 0.08 cm) were most important to the volume fluxes (Fig. 4). The trend toward a greater contribution from small particles at deeper depths noted for the number flux above was still discernable but much less pronounced. This is in part because the small particles contributed less importantly to the volume flux than the number flux, and in part because variations in the abundance of the largest size classes dominated the control of the volume flux variations (this latter effect is particularly evident in the results for aggregates at site C5 in Fig. 4). In general, a narrower range of aggregate sizes was important to the volume flux than for cylindrical fecal pellets. Although very large fecal pellets and large aggregates were rare, their presence was still important to the control of the volume and carbon fluxes, as is made clear in Fig. 5. For all the samples, 50% of the carbon flux comes from the large particles that make up less than 20% of the number flux, and conversely the small particles that make up more than 50% of the total number of particles contribute less than 20% of the carbon flux.

Aggregates contributed at least 77% of the total volume flux in all the traps, and often exceeded 95% (Table 4). In terms of carbon contents, their role was considerably reduced but still dominant at shallow depths (100 and 200 m) at site C5, where they made up 74% and 85% of the carbon flux. This influence decreased at depth (330 and 430 m) to 49% and 33%. At A3, the aggregate contribution to carbon flux was limited to 25% to 36% at all depths, again with a slight decrease in its importance with depth.

Particle shape variations for the cylindrical fecal pellets and the aggregates differed dramatically. Aspect ratios of the latter were in a narrow range (mostly between one and approximately four, none above eight) and their distribu-

Table 3. Contributions to the total number flux.

Site	Depth (m)	Aggregates		Cylinders		Ovals		Total flux
		Flux	Fraction	Flux	Fraction	Flux	Fraction	
C5	100	24	0.96	1	0.03	0.3	0.01	25
	200	26	0.94	1	0.04	0.6	0.02	28
	330	10	0.84	2	0.12	0.5	0.04	12
	430	5	0.72	1	0.10	1.3	0.18	7
A3f	100	14	0.68	6	0.32	0.0	0.00	20
	200	15	0.65	6	0.27	2.0	0.08	23
	330	2	0.51	2	0.36	0.5	0.12	4
	430	3	0.48	2	0.31	1.2	0.21	6
A3i	200	55	0.37	85	0.58	6.6	0.04	147

All fluxes in units of $10^{-4} \text{ m}^{-2} \text{ d}^{-1}$.

Table 4. Contributions to the total volume and carbon fluxes.

Site	Depth (m)	Volume flux	Fraction			Carbon flux	Fraction		
			Agg	Cyl	Ova		Agg	Cyl	Ova
C5	100	11.6	0.98	0.02	0.00	56	0.74	0.26	0.01
	200	14.3	0.99	0.01	0.00	49	0.85	0.14	0.01
	330	7.51	0.95	0.05	0.00	41	0.49	0.50	0.01
	430	1.20	0.85	0.10	0.05	15	0.33	0.44	0.23
A3f	100	5.36	0.86	0.14	0.00	63	0.30	0.70	0.00
	200	6.61	0.89	0.10	0.01	62	0.36	0.58	0.06
	330	0.44	0.77	0.21	0.03	8	0.25	0.66	0.09
	430	0.86	0.81	0.13	0.07	13	0.25	0.49	0.26
A3i	200	22.2	0.82	0.17	0.01	287	0.24	0.71	0.05

Volume fluxes in $\text{cm}^3 \text{m}^{-2} \text{d}^{-1}$, carbon fluxes in $\text{mg C m}^{-2} \text{d}^{-1}$

tions were very similar at all sites and depths (Fig. 6). In contrast, cylindrical pellet aspect ratios ranged much more broadly, up to almost a factor of 30. Variations with depth were subdued at A3f, but considerable at C5 (albeit without any systematic changes across the four depths). Fragmentation into shorter lengths would seem to be a likely process, but the aspect ratios did not show any systematic trend in this regard, and thus new pellet formation, pellet disaggregation, and other processes appear to also be important. This complexity of controls on fecal pellet types and their variation with depth has been observed in many environments, as reviewed recently by Turner (2002).

Discussion

The primary objective of this work was to assess the ecosystem processes controlling particulate carbon export in the iron-fueled high productivity region over the Kerguelen plateau and to compare these processes to those of the HNLC waters that prevail throughout the surrounding open Southern Ocean. Because difficult shipboard conditions precluded collection of HNLC sediment trap samples during KEOPS (originally planned for HNLC site C11), we examine the differences between the high-biomass (A3) and moderate-biomass (C5) sites as a guide to possible variations in the control of export as a function of biomass and production levels, and supplement this analysis by comparison with literature results from other Southern Ocean HNLC sites.

Comparison of the gel flux results to biogeochemical estimates—The carbon flux estimates (Table 4) compare reasonably well with two other estimates made during the KEOPS program, given the uncertainties of all these techniques. POC was measured on samples from the PPS3/3 cylindrical sediment trap suspended at 200 m on the same drifting trap arrays as the gel traps. At each site two cups from the PPS3/3 trap were sieved through a 350- μm screen to remove swimmers and filtered onto a 1- μm quartz fiber filter and yielded organic carbon fluxes of 18–20 $\text{mg C m}^{-2} \text{d}^{-1}$ for C5, 13–20 $\text{mg C m}^{-2} \text{d}^{-1}$ for A3f, and 44–48 $\text{mg C m}^{-2} \text{d}^{-1}$ for A3i (the ranges represent those obtained from two cups rotated beneath the PPS3/3 trap during the deployment, Trull unpubl. data). The approximately three to four times higher gel carbon fluxes suggest that our volume to carbon conversion relation overestimates carbon fluxes, assuming that the larger diameter PPS3/3 trap and the gel trap had similar collection efficiencies. Estimates of carbon flux at 100-m depth based on water-column ^{234}Th disequilibria combined with C: ^{234}Th ratios from the PPS3/3 trap and from size-fractionated particle samples obtained with a high-volume pump are approximately twice those obtained from the gels at C5 and A3f, but similar for A3i, with values of ~ 130 , 110, and 290 $\text{mg C m}^{-2} \text{d}^{-1}$ at C5, A3f, and A3i, respectively (Savoie et al. 2006). These differences could be accommodated by a choice of higher carbon contents for the aggregates (*see Method section*), or lower C/Th ratios for exported particles (Savoie et al. 2006). Alternatively, the flux measured punctually by the

Table 5. Median particle volumes and equivalent spherical diameters.

Site	Depth (m)	Aggregates		Cylinders		Ovals	
		Volume ($\times 10^{-6} \text{cm}^3$)	esd ($\times 10^{-1} \text{cm}$)	Volume ($\times 10^{-6} \text{cm}^3$)	esd ($\times 10^{-1} \text{cm}$)	Volume ($\times 10^{-6} \text{cm}^3$)	esd ($\times 10^{-1} \text{cm}$)
C5	100	26	0.37	3.6	0.21	0.9	0.13
	200	12	0.28	3.4	0.20	1.3	0.15
	330	21	0.34	2.8	0.17	1.6	0.15
	430	6	0.22	2.5	0.18	3.1	0.20
A3f	100	16	0.31	5.7	0.24	0.0	0.00
	200	15	0.30	5.4	0.24	2.5	0.18
	330	6	0.22	2.1	0.17	2.0	0.17
	430	8	0.25	2.7	0.19	3.1	0.20
A3i	200	0.9	0.26	1.9	0.18	2.8	0.19

gels in this period of a general decline in surface chlorophyll concentrations (*see the Introduction*) may have been lower than that held sway during the previous few weeks over which the ^{234}Th method integrates (Buesseler et al. 2006).

Comparison of the high (A3) and moderate (C5) biomass sites—The formation of fecal pellets and their aggregates was the key process responsible for particle export at A3 and C5. Direct export of large cylindrical fecal pellets was secondary in terms of volume flux but of similar importance in terms of carbon export (Table 4). Contributions from “minipellets” (<100 μm), single phytoplankton cells, or phytoplankton dominated aggregates (phytodetritus) were negligible. This suggests that the dominant control on export is biological aggregation of phytoplankton into fecal pellets by large zooplankton, followed by further agglomeration into large aggregates by either physical or biological processes.

At both sites, particle fluxes decreased strongly with depth, particularly between the two shallower traps (100 and 200 m) and the two deeper traps (330 and 430 m). For comparison with open ocean environments, we plotted the KEOPS carbon flux estimates against power-law curves used to parameterize observed open ocean flux attenuation with depth (Martin et al. 1987; Buesseler et al. 2007). Comparing the deepest (430 m) and shallowest (100 m) traps, the KEOPS carbon flux attenuation at both sites was very similar to open ocean observations (Fig. 7). At C5, the intermediate depth traps displayed higher carbon fluxes than expected from the open ocean power law, suggesting relatively little flux attenuation between 100 and 330 m. At A3, this behavior was observed only between 100- and 200-m depth, with the flux decreasing rapidly between the 200- and 330-m traps. The relatively large variations with depth, (approximately fivefold at A3f and approximately fourfold at C5) may be a real characteristic of the flux of large particles over these mesopelagic depths—a depth range for which very few data are available (Martin et al. 1987; Buesseler et al. 2007).

Comparing the A3 and C5 sites, the number and volume fluxes were somewhat larger at the moderate biomass site (C5) than at the high-biomass site (A3f) although carbon fluxes were similar, (Tables 3 and 4). Decreases with depth also differed in terms of both total fluxes (Fig. 7) and details of the changes in particle size distributions (Fig. 4). Other estimates of export or correlated properties suggest the probability of a greater flux at the A3 bloom site than at C5: approximately twofold higher primary production at A3f based on ^{14}C incubations (Griffiths and Uitz 2006) and approximately twofold higher export at A3f based on ^{234}Th deficits (Savoie et al. 2006).

It is possible that the two- to threefold uncertainties associated with the hydrodynamics of particle collection into drifting sediment traps (Gardner 2000) has biased the gel-trap results, but the temporal decoupling of export from primary production, from particle standing stocks, and from the longer timescales (several weeks) over which the ^{234}Th method integrates export (Buesseler et al. 2006) could also explain these differences. Given the uncertainties in all the methods and the similarity of the particle types

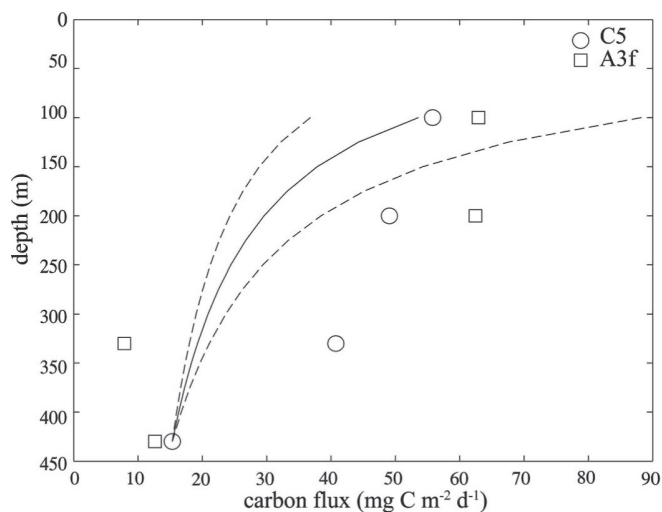


Fig. 7. Variations of KEOPS carbon fluxes with depth in comparison with commonly applied power-law parameterizations for flux attenuation, $\text{flux}(z) = \text{flux}(100\text{ m}) \times (z/100)^{-b}$, as estimated from drifting traps (solid curve from Martin et al. 1987 for $b = 0.858$) and moored traps (dotted curves indicate bounds for b of 0.6 and 1.2; Boyd and Trull 2006).

collected, the most robust conclusion is that the controls on export were similar at the epicenter (A3) and the periphery (C5) of the Kerguelen bloom.

Comparison to other Southern Ocean studies—Comparing the KEOPS particle characteristics to results from Southern Ocean HNLC sites is hampered by a lack of observations from drifting traps. The only other drifting gel-trap study in polar open ocean waters was carried out during the short-term SOIREE. During this 13-d experiment in HNLC waters of the Antarctic circumpolar current south of the Polar Front in February 1999 (Boyd et al. 2000), gel traps were deployed within and outside of the artificially iron-fertilized “patch” for several periods of 2 to 3 d (Waite and Nodder 2001). The in-patch and out-patch traps collected very similar total fluxes (Nodder et al. 2001), and carbon isotopic compositions suggested little increase in flux induced by the iron fertilization (Trull and Armand 2001), which was consistent with ^{234}Th results (Charette and Buesseler 2000). However, measurements of the size distribution of aggregates in the SOIREE gels suggested a small increase in particle size in the in-patch traps in comparison with the out-patch HNLC waters (Waite and Nodder 2001; Jackson et al. 2005). Thus the SOIREE gel-trap size distribution results (Jackson et al. 2005) offer the possibility to compare the KEOPS results with both export from Southern Ocean HNLC waters (the SOIREE out-patch results) and with export following an artificial iron fertilization (the SOIREE in-patch results).

During SOIREE the distribution of particle sizes (both in-patch and out-patch) was dominated by smaller particles than those dominating the KEOPS traps, including a large contribution from individual pennate and centric diatoms of a few hundred microns in size, along with diatom aggregates that were considered to have formed by

coagulation (Waite and Nodder 2001; Jackson et al. 2005). Fecal pellet statistics from the SOIREE gels have not been published, but their abundance was low (Waite and Nodder 2001; Jackson et al. 2005), and negligible mesozooplankton grazing was observed (Zeldis 2001). Interestingly, the particle number flux spectra from SOIREE (both in-patch and out-patch) exhibit values of 10^9 decreasing to 10^7 $\text{cm}^{-1} \text{m}^{-2} \text{d}^{-1}$ across the size interval from 0.01 to 0.1 cm (Jackson et al. 2005), for which the KEOPS number spectra exhibit a similar decrease but much lower values (10^7 decreasing to 10^5 $\text{cm}^{-1} \text{m}^{-2} \text{d}^{-1}$; Fig. 3). The 100-fold higher particle flux numbers were a surprise given that organic carbon fluxes estimated for SOIREE from free-drifting sediment traps and ^{234}Th disequilibria (~ 90 to 160 $\text{mg C m}^{-2} \text{d}^{-1}$; Charette and Buesseler 2000; Nodder and Waite 2001; Waite and Nodder 2001) were similar to those estimated for KEOPS using these methods (~ 20 – 50 $\text{mg C m}^{-2} \text{d}^{-1}$ from the traps, Trull unpubl. data, and 100 – 300 $\text{mg C m}^{-2} \text{d}^{-1}$ from ^{234}Th disequilibria, Savoye et al. 2006). This difference raises the importance of variability in the volume-carbon conversion relation for marine particles (see the *Methods* section). The SOIREE particles in this 0.01- to 0.1-cm size range were predominantly fluffy diatom aggregates (Waite and Nodder 2001; Jackson et al. 2005), while those during KEOPS were tightly compacted fecal pellets and aggregates of those pellets.

In comparison with the SOIREE results, the KEOPS results suggest that persistent natural iron inputs lead to a much greater fraction of export being derived from zooplankton fecal pellets and large aggregates than occurs in either Southern Ocean HNLC waters (SOIREE out-patch results) or following artificial iron fertilization of these waters (SOIREE in-patch results). This perspective needs to be tempered by the fact that coupling of phytoplankton production, zooplankton grazing, and the magnitude of particle export is highly variable seasonally (Wassmann 1998), and thus both the SOIREE and KEOPS results represent brief moments in possibly large-amplitude variability in this coupling.

The Kerguelen time series study (Kerfix) in HNLC waters to the west of Kerguelen Island offers another useful comparison for the KEOPS results. Direct studies of exported particle characteristics are not available, but synthesis of carbon budgets (Jeandel et al. 1998) and simulation of seasonal cycles is consistent with zooplankton grazing control of phytoplankton biomass, without a requirement for physical phytoplankton aggregation to enhance export (Mongin et al. 2006). Observations of zooplankton populations and feeding experiments also suggest that zooplankton are capable of removing all primary production in this Indian sector of the Southern Ocean (Mayzaud et al. 2002). Thus, in contrast to the comparison with the SOIREE results, it appears that zooplankton mediated removal of biomass may be similarly important in HNLC waters near the Kerguelen plateau as it is in the high-biomass waters over the plateau. This result is consistent with the observation of generally similar zooplankton population structures on-plateau and off-plateau during KEOPS, but with more of the largest class of zooplankton present on-plateau in the high-

biomass region (Carlotti et al. 2006). More detailed comparisons with other observations of particle export and its coupling to primary production and ecosystem structure are beyond the scope of this paper and hampered by the short period of the KEOPS export observations. Additional discussion of these issues is available in Dunne et al. (2005) and Boyd and Trull (2006).

Implications for the response of carbon export to persistent iron fertilization—Two aspects of our limited observations merit emphasis, in the context of attempting to understand the sensitivity of ecosystem structure and carbon export to natural and artificial iron fertilization: (1) direct export of phytoplankton or phytoplankton aggregates was negligible, (2) zooplankton grazing, large fecal pellet formation, and in particular agglomeration of large fecal pellets into large aggregates controlled export.

These results differ from those of Southern Ocean short-term iron-fertilization experiments, in which zooplankton responses have generally (Boyd et al. 2000; Coale et al. 2004) but not always (Peeken et al. 2006) been muted. Moreover, they differ from the view that nutrient-rich waters that develop high biomass usually export a significant fraction of it directly as phytoplankton aggregates rather than via fecal pellets from higher trophic levels (Boyd and Newton 1995, 1999; Turner 2002). Whether this difference simply reflects the short-term aspect of the KEOPS observations or a more fundamental aspect of persistently iron-fertilized Southern Ocean waters is not yet clear and will require more sustained observations of the mechanisms of export.

Possible reasons why zooplankton might have been more important during KEOPS than during artificial iron fertilizations include the predictability of the annually occurring Kerguelen plateau phytoplankton bloom and the relatively modest phytoplankton levels that develop within it (~ 3 $\mu\text{g Chl } a \text{ L}^{-1}$, Blain et al. 2007), which are close to those estimated to be sufficient to induce efficient aggregation (Jackson and Lochmann 1993; Boyd et al. 2005; Jackson et al. 2005). There is evidence for an important role for zooplankton in export from other recent gel-trap studies in polar waters. Euphausiid fecal pellets dominated export in subantarctic waters east of New Zealand (Waite et al. 2000) and in Antarctic coastal waters in Prydz Bay (Whiteley 2003). In contrast, phytodetrital aggregates were important in Antarctic waters during SOIREE, both in and outside the iron-fertilized waters (Waite and Nodder 2001; Boyd et al. 2002; Jackson et al. 2005), during the Subarctic Ecosystem Response to Iron Enrichment Study (SERIES) (Boyd et al. 2005), and in polar waters in a Swedish Fjord (Waite et al. 2005). These differences emphasize that site, season, and ecosystem specific controls on carbon export are likely to be the rule rather than the exception.

References

- ALLDREDGE, A. L. 1998. The carbon, nitrogen and mass content of marine snow as a function of aggregate size. *Deep-Sea Res. I* **45**: 529–541.

- , AND C. GOTSCHALK. 1988. In situ settling behavior of marine snow. *Limnol. Oceanogr.* **33**: 339–351.
- ARMAND, L. K., V. BARTHAUX, AND B. QUEGUINER. 2006. Phytoplankton responses within and peripheral to the naturally iron-fertilized Kerguelen region. ASLO-TOS-AGU Ocean Sciences meeting abstracts, OS35M–08.
- BIDLE, K. D., AND F. AZAM. 1999. Accelerated dissolution of diatom silica by marine bacterial assemblages. *Nature* **397**: 508–512.
- BLAIN, S., AND OTHERS. 2007. Impacts of natural iron fertilisation on the Southern Ocean. *Nature* **446**: 1070–1074. [doi:10.1038/nature05700].
- BOYD, P. W., G. A. JACKSON, AND A. WAITE. 2002. Are mesoscale perturbation experiments in polar waters prone to physical artefacts? Evidence from algal aggregation modeling studies. *Geophys. Res. Lett.* **29** [doi: 10.1029/2001GL014210].
- , AND P. NEWTON. 1995. Evidence of the potential influence of planktonic community structure on the interannual variability of particulate carbon flux. *Deep-Sea Res. I* **42**: 619–639.
- , AND ———. 1999. Does planktonic community structure determine downward particulate organic carbon flux in different oceanic provinces? *Deep-Sea Res. I* **46**: 63–91.
- , AND T. W. TRULL. 2006. Understanding the export of marine biogenic particles: Is there consensus? *Prog. Oceanogr.* **4**: 276–312. [doi:10.1016/j.pocean.2006.10.1007].
- , AND OTHERS. 2000. A mesoscale phytoplankton bloom in the Southern Ocean stimulated by iron fertilization. *Nature* **407**: 695–702.
- , AND ———. 2005. The evolution and termination of an iron-induced mesoscale bloom in the northeast subarctic Pacific. *Limnol. Oceanogr.* **50**: 1872–1886.
- BUESSELER, K. O., AND P. W. BOYD. 2003. Does ocean fertilization work? *Science* **300**: 67–68. [doi:10.1126/science.1082959].
- , AND OTHERS. 2006. An assessment of particulate organic carbon to thorium-234 ratios in the ocean and their impact on the application of ^{234}Th as a POC flux proxy. *Mar. Chem.* **100**: 213–233. [doi:10.1016/j.marchem.2005.10.013].
- , AND ———. 2007. Revisiting carbon flux through the ocean's twilight zone. *Science* **316**: 567–570. [doi:10.1126/science.1137959].
- CARLOTTI, F., D. BOTHA, D. LEFÈVRE, A. NOWACZYK, M. CLEMENT, AND D. VINCENT. 2006. Mesozooplankton size structure and biomass above the Kerguelen Plateau (Southern Ocean) during KEOPS: First results on two contrasted areas. ASLO-TOS-AGU Ocean Sciences meeting abstract, OS35M–13.
- CARROLL, M. L., J.-C. MIQUEL, AND S. W. FOWLER. 1998. Seasonal patterns and depths—specific trends of zooplankton fecal pellet fluxes in the northwest Mediterranean Sea. *Deep-Sea Res. I* **45**: 1303–1318.
- CHARETTE, M. A., AND K. O. BUESSELER. 2000. Does iron fertilization enhance carbon export in the Southern Ocean? *Geochem Geophys. Geosyst.* **1** [doi:2000GC000069].
- COALE, K. H., AND OTHERS. 2004. Southern Ocean iron enrichment experiment: Carbon cycling in high and low-Si waters. *Science* **304**: 408–414.
- DUNNE, J. P., R. A. ARMSTRONG, A. GNANADESIKAN, AND J. L. SARMIENTO. 2005. Empirical and mechanistic models for the particle export ratio. *Glob. Biogeochem. Cycles* **19**: GB4026 [doi:10.1029/2004GB002390, 002005].
- GARDNER, W. D. 2000. Sediment trap sampling in surface waters, p. 240–281. *In* R. B. Hanson, H. W. Ducklow and J. G. Field [eds.], *The changing ocean carbon cycle: A midterm synthesis of the Joint Global Ocean Flux Study*. International Geosphere-Biosphere Program Block Series. Cambridge Univ. Press.
- GONZALEZ, H. E. 1992a. The distribution and abundance of krill faecal material and oval pellets in the Scotia and Weddell Seas (Antarctica) and their role in particle flux. *Polar Biol.* **12**: 81–91.
- . 1992b. Distribution and abundance of minipellets around the Antarctic peninsula. Implications for protistan feeding behaviour. *Mar. Ecol. Prog. Ser.* **90**: 223–236.
- , F. K. KURBJEWIT, AND U. V. BATHMANN. 1994. Occurrence of cyclopoid copepods and faecal material in the Halley Bay region, Antarctica, during January–February 1991. *Polar Biol.* **14**: 331–342.
- , AND V. S. SMETACEK. 1994. The possible role of cyclopoid copepod *Oithona* in retarding vertical flux of zooplankton faecal material. *Mar. Ecol. Prog. Ser.* **113**: 233–246.
- GOWING, M. M., D. L. GARRISON, H. B. KUNZE, AND D. J. WINCHELL. 2001. Biological components of Ross Sea short-term particle fluxes in the austral summer of 1995–96. *Deep-Sea Res. I* **48**: 2645–2671.
- GRIFFITHS, F. B., AND J. UITZ. 2006. Photosynthetic parameters, size-fractionated chlorophyll and primary production during the KEOPS expedition East of Kerguelen Island January–February 2005. ASLO-TOS-AGU Ocean Sciences meeting abstract, OS35M–09.
- HONJO, S., AND M. R. ROMAN. 1978. Marine copepod fecal pellets: Production, preservation, and sedimentation. *J. Mar. Res.* **36**: 45–57.
- JACKSON, G. A., AND S. E. LOCHMANN. 1993. Modelling coagulation of algae in marine ecosystems, p. 387–414. *In* J. Buffle and H. P. van Leeuwen [eds.], *Environmental particles*. Lewis Publ., Ann Arbor, Michigan.
- , R. MAFFIONE, D. K. COSTELLO, A. L. ALLDREDGE, B. E. LOGAN, AND H. G. DAM. 1997. Particle size spectra between 1 μm and 1 cm at Monterey Bay determined using multiple instruments. *Deep-Sea Res. I* **44**: 1739–1767.
- , A. M. WAITE, AND P. W. BOYD. 2005. Role of algal aggregation in vertical carbon export during SOIREE and in other low biomass environments. *Geophys. Res. Lett.* **32** [doi: 10.1029/2005GL023180].
- JEANDEL, C., AND OTHERS. 1998. KERFIX, a time-series station in the Southern Ocean: A presentation. *J. Mar. Syst.* **17**: 555–570.
- KRIEST, I. 2002. Different parameterizations of marine snow in a 1D-model and their influence on representation of marine snow, nitrogen budget and sedimentation. *Deep-Sea Res. I* **49**: 2133–2162.
- LAMPITT, R. S., T. NOJI, AND B. V. BODUNGEN. 1991. What happens to zooplankton faecal pellets? Implications for material flux. *Mar. Biol.* **104**: 15–23.
- LUNDGAARD, C. 1995. Use of a high viscosity medium in studies of aggregates, p. 141–152. *In* S. Floderus, A.-S. Heiskanen, M. Oleson and P. Wassmann [eds.], *Sediment trap studies in the Nordic countries 3*. Proceeding of the Symposium on Seasonal Dynamics of Planktonic Ecosystems and Sedimentation in Coastal Nordic Waters. Numi Print, Oy.
- MARTIN, J. H., G. A. KNAUER, D. M. KARL, AND W. W. BROENKOW. 1987. VERTEX: Carbon cycling in the Northeast Pacific. *Deep-Sea Res.* **34**: 267–285.
- MAYZAUD, P., V. TIRELLI, A. ERRIFF, J. P. LABAT, S. RAZOULS, AND R. PERISSINOTTO. 2002. Carbon intake by zooplankton: Importance and role of zooplankton grazing in the Indian sector of the Southern Ocean. *Deep-Sea Res. II* **49**: 3169–3188.

- MICHAELS, A. F., AND M. W. SILVER. 1988. Primary production, sinking fluxes and the microbial food web. *Deep-Sea Res.* **35**: 473–490.
- MONGIN, M., D. M. NELSON, P. PONDAVEN, AND P. TREGUER. 2006. Simulation of upper-ocean biogeochemistry with a flexible-composition phytoplankton model: C, N and Si cycling and Fe limitation in the Southern Ocean. *Deep-Sea Res. II* **53**: 601–619.
- NODDER, S. D., M. A. CHARETTE, A. M. WAITE, T. W. TRULL, P. W. BOYD, J. ZELDIS, AND K. O. BUESSELER. 2001. Particle transformation and export flux during an in situ iron-stimulated bloom in the Southern Ocean. *Geophys. Res. Lett.* **28**: 2409–2412.
- , AND A. M. WAITE. 2001. Is carbon export in the Southern Ocean enhanced by iron-stimulated increases in biological production? Sediment trap results from an in situ iron enrichment experiment. *Deep-Sea Res. II* **48**: 2681–2702.
- NOJI, T. T., K. W. ESTEP, F. MACINTYRE, AND F. NORRIN. 1991. Image analysis of faecal material grazed upon by three species of copepods: Evidence for coprophagy, coprophagy, and coprochaly. *J. Mar. Biol. Assoc. U.K.* **71**: 46–48.
- PEEKEN, I., AND OTHERS. 2006. Effect of in situ iron fertilisation during contrasting seasons—comparison between EisenEx and EIFEX. ASLO-TOS-AGU Ocean Sciences meeting abstract, OS32A–06.
- SAVOYE, N., T. TRULL, S. JAQUET, AND F. DEHAIRS. 2006. ²³⁴Th-based export production during the KEOPS natural iron fertilization. ASLO-TOS-AGU Ocean Sciences meeting abstract, OS33F–04.
- SILVER, M. W., AND M. M. GOWING. 1991. The 'particle' flux: Origins and biological components. *Prog. Oceanogr.* **26**: 75–113.
- TRULL, T. W., AND L. ARMAND. 2001. Insights into Southern Ocean carbon export from the $\delta^{13}\text{C}$ of particles and dissolved inorganic carbon during the SOIREE iron fertilisation experiment. *Deep-Sea Res. II* **48**: 2655–2680.
- TURLEY, C. M. 1993. The effect of pressure on leucine and thymidine incorporation by free-living bacteria attached to sinking oceanic particles. *Deep-Sea Res. I* **40**: 2193–2206.
- , AND E. D. STUTT. 2000. Depth-related cell-specific bacterial leucine incorporation rates on particles and its biogeochemical significance in the Northwest Mediterranean. *Limnol. Oceanogr.* **45**: 419–425.
- TURNER, J. T. 2002. Zooplankton fecal pellets, marine snow and sinking phytoplankton blooms. *Aquat. Microb. Ecol.* **27**: 57–102.
- WAITE, A. M., O. GUSTAFSSON, O. LINDAHL, AND P. TISELIUS. 2005. Linking ecosystem dynamics and biogeochemistry: Sinking fractionation of organic carbon in a Swedish fjord. *Limnol. Oceanogr.* **50**: 658–671.
- , AND S. D. NODDER. 2001. The effect of in situ iron addition on the sinking rates and export flux of Southern Ocean diatoms. *Deep-Sea Res. II* **48**: 2635–2654.
- , K. A. SAFI, J. A. HALL, AND S. D. NODDER. 2000. Mass sedimentation of picoplankton embedded in organic aggregates. *Limnol. Oceanogr.* **45**: 87–97.
- WASSMANN, P. 1998. Retention versus export food chains: Processes controlling sinking loss from marine pelagic systems. *Hydrobiologica* **363**: 29–57.
- WHITELEY, M. 2003. The influence of Antarctic krill (*Euphausia superba*) on carbon fluxes in the Southern Ocean. Honours thesis, Univ. of Western Australia.
- ZELDIS, J. 2001. Mesozooplankton community composition, grazing, nutrition, and export production at the SOIREE site. *Deep-Sea Res. II* **48**: 2615–2634.

Received: 26 July 2006
 Accepted: 21 June 2007
 Amended: 31 July 2007